

AN ANALYSIS OF SAPPI SAICCOR'S EFFLUENT STREAMS

By

Fathima Ismail
BSc., BSc. (HONS) (Natal)

Submitted in fulfilment of the requirements for the degree of
Master of Science
in the
School of Pure and Applied Chemistry,
University of Natal,
Durban

2003

*To my dear family,
Dad, mum, Araff & Naseem*

*Acquire knowledge, it enables us to distinguish right from wrong, it lights the way to heaven.
It is our friend in the desert, our company in solitude and companion when friendless.
It guides us to happiness, it sustains us in misery.
It is an ornament amongst friends and an armour against enemies.*

(The Holy Prophet Mohammad S.A.W.)

PREFACE

The experimental work described in this dissertation was carried out in the School of Pure and Applied Chemistry, at the University of Natal, Durban, South Africa, under the supervision of Professor J.J. Marsh and Professor D.A. Mulholland.

This study represents original work by the author and has not been submitted in any other form to another university. Where use was made of the work of others, it has been duly acknowledged in the text.

Signed:



Fathima Ismail
B.Sc. Hons (Natal)

I hereby certify that the above statement is correct.

Signed:



Professor J.J. Marsh
Ph.D. (RAU)
Professor of Applied Chemistry
University of Natal, Durban



Professor D.A. Mulholland
Ph.D. (Natal)
Professor of Organic Chemistry
University of Natal, Durban

ACKNOWLEDGEMENTS

Firstly, and most importantly, all praise and gratitude belong to the Lord Almighty who has bestowed me with the moral, intellectual and spiritual strength to accomplish this work.

I am indebted to my supervisor, Professor Dulcie Mulholland for her continuous support and encouragement throughout this project. Thank you for never being too busy to offer your advice and assistance with any problems encountered. It has truly been a great honour to be a part of your research group.

I would also like to thank my second supervisor, Professor Jeremy Marsh, for sparing his valuable time to organize the numerous trips to SAPPI SAICCOR. Thank you also for your assistance and for your constant words of encouragement especially through the tough times.

I express my sincere gratitude to SAPPI SAICCOR for their generous funding of this project. In particular, I would like to thank John Thubron and Tracy Pohl from SAPPI SAICCOR for their help in collecting the necessary samples during this study. Thank you John for your informative tours through the plant and for providing me with all the information needed regarding the plant's process.

Many thanks must go to both the academic and technical staff in the School of Pure and Applied Chemistry who has assisted me in some way through the course of this project. Specifically, I would like to thank Dilip Jagjivan for the efficient and professional running of the NMR spectra and Bret Parel for his technical assistance in the laboratory and for aiding me with any computer – related problems that I encountered. Thank you also to Ernest Makhaza for always providing a clean and tidy working environment in the laboratory.

I would also like to thank Dashnie Naidoo and the staff from the Department of Medicinal Chemistry at the University of Utrecht, namely, Professor A.J.J. van den Berg, C.J. Beukelman, S.B.A. Halkes and H.C. Quarles van Ufford for their assistance in carrying out the chemiluminescence and DPPH bioassays as well as the toxicity tests.

I wish to thank all my friends and colleagues in the Natural Products Research Group, especially Dashnie Naidoo, Raylene Kemm and Taryn Toach for making this an enjoyable and memorable experience. Thank you to Phil Coombes for helping me keep my sanity intact and for always finding the time to offer his advice. A special thank you goes to my best friend Ursulla. Your encouragement and confidence in me has been constant and unconditional and for this I shall be eternally grateful.

Finally, I would like to dedicate this thesis to my wonderful family, daddy, mummy, and brothers Araff and Naseem. I express my sincere gratitude to you all for your patience, tolerance and for your selfless support during the process of my research. Without your love and goodwill, this task would not have come to fruition.

LIST OF ABBREVIATIONS

| | | |
|----------------------------------|---|--|
| ^1H NMR spectroscopy | - | proton nuclear magnetic resonance spectroscopy |
| ^{13}C NMR spectroscopy | - | carbon-13 nuclear magnetic resonance spectroscopy |
| COSY | - | correlated spectroscopy |
| NOESY | - | nuclear Overhauser effect spectroscopy |
| HMBC | - | heteronuclear multiple bond coherence |
| HSQC | - | heteronuclear multiple quantum coherence |
| GC – MS | - | gas chromatography – mass spectrometry |
| LRMS | - | low resolution mass spectroscopy |
| EIMS | - | electron impact mass spectroscopy |
| I.R. | - | infra – red |
| Mp | - | melting point |
| t.l.c | - | thin layer chromatography |
| PTLC | - | preparative thin layer chromatography |
| Lit. | - | literature |
| s | - | singlet |
| d | - | doublet |
| t | - | triplet |
| q | - | quartet |
| m | - | multiplet |
| dd | - | doublet of doublets |
| bs | - | broad singlet |
| Hz | - | Hertz |
| MHz | - | mega Hertz |
| ppm | - | parts per million |
| nm | - | nanometers |
| U.V. | - | ultraviolet |
| TMS | - | tetramethyl silane |
| <i>L</i> -Phe | - | <i>L</i> -phenylalanine |
| NADPH | - | nicotinamide adenine dinucleotide phosphate |
| ATP | - | adenosine triphosphate |
| ADP | - | adenosine diphosphate |
| Ad | - | adenosine |
| SAM | - | <i>S</i> -adenosylmethionine |
| PAL | - | phenylalanine ammonia lyase |
| IPP | - | isopentenyl pyrophosphate |
| DMAPP | - | dimethylallyl pyrophosphate |
| FPP | - | farnesyl pyrophosphate |
| MPO | - | myeloperoxidase |
| DPPH | - | α,α -diphenyl- β -picrylhydrazyl |

LIST OF SCHEMES

| | PAGE NO. |
|---|----------|
| CHAPTER 1 | |
| Scheme 1.1: The production of Ca and Mg bisulphite by reacting MgO and CaCO ₃ with SO ₂ | 2 |
| Scheme 1.2: Simplified flow diagram of the kraft process | 5 |
| Scheme 1.3: Simplified flow diagram of sulphite pulping | 7 |
| CHAPTER 2 | |
| Scheme 2.1: Shikimate pathway showing the formation of monolignols | 16 |
| Scheme 2.2: Radical pairing of resonance structures to form dimers | 17 |
| Scheme 2.3: Dirigent – mediated formation of (+)-pinoresinol | 19 |
| Scheme 2.4: Formation of lignosulphonates | 24 |
| Scheme 2.5: A typical condensation reaction | 25 |
| Scheme 2.6: Classification of terpenoids | 27 |
| Scheme 2.7: Formation of DMAPP and IPP from mevalonic acid | 29 |
| Scheme 2.8 The formation of squalene | 30 |
| Scheme 2.9: Cyclisation of squalene epoxide to form lanosterol and cycloartenol | 31 |
| Scheme 2.10: Mechanism showing the alkylation of C-24 | 32 |
| CHAPTER 3 | |
| Scheme 3.1: Fragmentation patterns of compound 3 | 54 |
| CHAPTER 4 | |
| Scheme 4.1: The chemical reactions occurring during the amine extraction of lignosulphonates | 91 |
| Scheme 4.2: Formation of diazomethane | 92 |
| CHAPTER 5 | |
| Scheme 5.1: Formation of ROS <i>via</i> the enzyme NADPH oxidase | 106 |
| Scheme 5.2: Mechanism of reaction of the DPPH radical | 108 |

LIST OF FIGURES

PAGE NO.

CHAPTER 1

- Figure 1.1: Chipping of wood logs 1
Figure 1.2: Batch cooking of wood chips in large digesters 2

CHAPTER 2

- Figure 2.1: Schematic illustration of the structure of a cell wall 12
Figure 2.2: The building units of lignin 14
Figure 2.3: Structural diversity in lignans and neolignans 14
Figure 2.4: The podophyllotoxin group of lignans 21
Figure 2.5: Structures of biologically active lignans 22
Figure 2.6: Lignans identified in humans 23
Figure 2.7: Structures of common mammalian and plant steroids 28

CHAPTER 3

- Figure 3.1: Structure of compound 1, *epi*-syringaresinol 42
Figure 3.2: NOESY correlations of compound 1 44
Figure 3.3: HMBC correlations (C→H) of compound 1 45
Figure 3.4: COSY correlations of compound 1 46
Figure 3.5: Structure of compound 2, *meso*-syringaresinol 48
Figure 3.6: HMBC correlations (C→H) of compound 2 50
Figure 3.7: NOESY correlations of compound 2 51
Figure 3.8: Structure of compound 3, *meso*-yangambin 53
Figure 3.9: HMBC correlations (C→H) of compound 3 56
Figure 3.10: Structure of compound 4, methoxyeugenol 58
Figure 3.11: HMBC correlations (C→H) of compound 4 60
Figure 3.12: NOESY correlations of compound 4 60
Figure 3.13: COSY correlations of compound 4 61
Figure 3.14: Structure of compound 5, β -oxysinapyl alcohol 63
Figure 3.15: HMBC correlations (C→H) of compound 5 65
Figure 3.16: COSY correlations of compound 5 65
Figure 3.17: Structure of compound 6, sinapyl aldehyde 67
Figure 3.18: COSY correlations of compound 6 68

| | |
|--|----|
| Figure 3.19: HMBC correlations (C→H) of compound 6 | 69 |
| Figure 3.20: NOESY correlations of compound 6 | 70 |
| Figure 3.21: Structure of compound 7, acetovanillone | 72 |
| Figure 3.22: NOESY and COSY correlations of compound 7 | 73 |
| Figure 3.23: HMBC correlations (C→H) of compound 7 | 74 |
| Figure 3.24: Structure of compound 8, vanillin | 76 |
| Figure 3.25: HMBC correlations (C→H) of compound 8 | 77 |
| Figure 3.26: COSY correlations of compound 8 | 77 |
| Figure 3.27: NOESY correlations of compound 8 | 78 |
| Figure 3.28: Structure of compound 9, syringaldehyde | 80 |
| Figure 3.29: HMBC correlations (C→H) of compound 9 | 81 |
| Figure 3.30: NOESY correlations of compound 9 | 82 |
| Figure 3.31: Structure of compound 10, β -sitosterol | 83 |

CHAPTER 5

| | |
|---|-----|
| Figure 5.1: Structure of <i>epi</i> -syringaresinol and cedpetine | 107 |
|---|-----|

CHAPTER 6

| | |
|---|-----|
| Figure 6.1: Structures of compounds isolated in this work | 112 |
|---|-----|

LIST OF TABLES

| | PAGE NO. |
|---|----------|
| CHAPTER 3 | |
| Table 3.1: NMR spectral data for compound 1 (400MHz, CDCl ₃) | 46 |
| Table 3.2: NMR spectral data for compound 2 (400MHz, CDCl ₃) | 52 |
| Table 3.3: NMR spectral data for compound 3 (400MHz, CDCl ₃) | 57 |
| Table 3.4: NMR spectral data for compound 4 (400MHz, CDCl ₃) | 62 |
| Table 3.5: NMR spectral data for compound 5 (400MHz, CDCl ₃) | 66 |
| Table 3.6: NMR spectral data for compound 6 (400MHz, CDCl ₃) | 71 |
| Table 3.7: NMR spectral data for compound 7 (400MHz, CDCl ₃) | 75 |
| Table 3.8: NMR spectral data for compound 8 (400MHz, CDCl ₃) | 79 |
| Table 3.9: NMR spectral data for compound 9 (400MHz, CDCl ₃) | 82 |
| | |
| CHAPTER 5 | |
| Table 5.1: IC ₅₀ (µg/ml) values of <i>epi</i> -syringaresinol and cedpetine | 107 |
| | |
| CHAPTER 6 | |
| Table 6.1: Estimated concentration of compounds isolated in this work contained in main effluent holding | 114 |
| | |
| APPENDIX B | |
| Table B1: Data for the conductometric titration to determine the sulphonic acid content of the calcium spent liquor effluent | 221 |

ABSTRACT

SAPPI SAICCOR is a pulp and paper mill situated in Umkomaas, 50 kms south of the port of Durban in South Africa. It was the first company to produce high grade dissolving pulp from the *Eucalyptus* tree and is currently the world's largest manufacturer of chemical cellulose.

SAICCOR is one of the few pulp and paper mills that produces its dissolving pulp by the acid sulphite process using both calcium and magnesium as bases in the form of calcium bisulphite and magnesium bisulphite. Four streams of effluent are produced during their process, namely, the calcium spent liquor, the magnesium pulp condensate and two streams from the bleaching stages.

An acid hydrolysis of the effluent streams yielded a range of organic compounds such as lignans and lignin – type precursors as well as a triterpenoid. Column chromatography and thin layer chromatography, using various ratios of hexane, dichloromethane, ethyl acetate and methanol, were carried out in isolating and purifying the compounds. The structures of these compounds were determined using NMR spectroscopic and mass spectrometric techniques.

TABLE OF CONTENTS

PAGE NO.

| | |
|------------------------------|------|
| <i>Preface</i> | iii |
| <i>Acknowledgements</i> | iv |
| <i>List of Abbreviations</i> | vi |
| <i>List of Schemes</i> | vii |
| <i>List of Figures</i> | viii |
| <i>List of Tables</i> | x |
| <i>Abstract</i> | xi |

CHAPTER 1 : INTRODUCTION

| | |
|---|----|
| 1.1 An Overview of the SAPPI SAICCOR Process | 1 |
| 1.2 Characterisation of Pulping Liquors | 4 |
| 1.2.1 Sulphate Chemical Pulping | 5 |
| 1.2.2 Sulphite Chemical Pulping | 6 |
| 1.2.3 Compounds Previously Identified in Chemical Pulping Liquors | 8 |
| 1.3 Objective of Project | 9 |
| 1.4 References | 10 |

CHAPTER 2 : TYPES OF COMPOUNDS ISOLATED

| | |
|---|----|
| 2.1 Lignins and Lignans | 12 |
| 2.1.1 Introduction | 12 |
| 2.1.2 Lignin and Lignan Biosynthesis | 15 |
| 2.1.3 Biological Activity of Lignans | 20 |
| 2.2 Lignosulphonates | 23 |
| 2.2.1 Introduction | 23 |
| 2.2.2 The Formation of Lignosulphonates During Acid Bisulphite Pulping | 23 |
| 2.2.3 The Uses of Lignosulphonates | 25 |
| 2.3 Triterpenoids | 26 |
| 2.3.1 Introduction | 26 |
| 2.3.2 The Biosynthesis of Triterpenoids | 28 |
| 2.3.3 The Uses of Plant Sterols | 33 |
| 2.4 References | 34 |

CHAPTER 3 : RESULTS AND DISCUSSION

| | |
|---|----|
| 3.1 The Extraction of Lignosulphonates | 37 |
| 3.2 Hydrolysis of the Calcium Spent Liquor Effluent | 41 |
| 3.2.1 Structural Elucidation of Compound 1: <i>epi</i> -syringaresinol | 42 |
| 3.2.2 Structural Elucidation of Compound 2: <i>meso</i> -syringaresinol | 48 |
| 3.2.3 Structural Elucidation of Compound 3: <i>meso</i> -yangambin | 53 |
| 3.2.4 Structural Elucidation of Compound 4: methoxyeugenol | 58 |
| 3.2.5 Structural Elucidation of Compound 5: β -oxysinapyl alcohol | 63 |
| 3.2.6 Structural Elucidation of Compound 6: sinapylaldehyde | 67 |
| 3.2.7 Structural Elucidation of Compound 7: acetovanillone | 72 |
| 3.2.9 Structural Elucidation of Compound 8: vanillin | 76 |
| 3.2.10 Structural Elucidation of Compound 9: syringaldehyde | 80 |
| 3.2.11 Structural Elucidation of Compound 10: β -sitosterol | 83 |
| 3.3 Hydrolysis of the Magnesium Condensate Effluent | 84 |
| 3.4 References | 85 |

CHAPTER 4 : EXPERIMENTAL

| | |
|---|----|
| 4.1 Foreword to Experimental | 87 |
| 4.1.1 Nuclear Magnetic Resonance (NMR) Spectroscopy | 87 |
| 4.1.2 Infrared (I.R.) Spectroscopy | 87 |
| 4.1.3 Ultraviolet Absorption (U.V.) Spectrometry/Spectroscopy | 87 |
| 4.1.4 Gas Chromatography – Mass Spectroscopy (GC – MS) | 88 |
| 4.1.5 General Chromatography | 88 |
| 4.1.6 Preparative Thin Layer Chromatography (PTLC) | 88 |
| 4.1.7 Melting Points (Mp) | 89 |
| 4.2 Analysis of the Calcium Spent Liquor Effluent Stream | 89 |
| 4.2.1 Sampling Procedure | 89 |
| 4.2.2 The Extraction of Lignosulphonates | 89 |
| 4.2.2.1 Extraction Method 1 | 89 |
| 4.2.2.2 Extraction Method 2 | 91 |
| 4.2.3 The Lassaigne Sodium Fusion Test | 92 |
| 4.2.4 Methylation of Crude Lignosulphonate – Sugar Mixture with Diazomethane | 92 |

| | |
|---|-----|
| 4.2.4.1 Preparation of Ethereal Diazomethane | 92 |
| 4.2.4.2 Methylation Procedure | 93 |
| 4.2.5 Physical Data of Precipitate from First Extraction | 93 |
| 4.2.6 Physical Data of Precipitate from Second Extraction | 94 |
| 4.2.7 Physical Data of Methylated Product | 94 |
| 4.2.8 Hydrolysis of the Calcium Spent Liquor Effluent | 95 |
| 4.3 Analysis of the Magnesium Condensate Effluent Stream | 95 |
| 4.3.1 Sampling Procedure | 95 |
| 4.3.2 Hydrolysis of the Magnesium Condensate Effluent | 95 |
| 4.4 Physical Data of Isolated Organic Compounds | 96 |
| 4.4.1 Physical Data for Compound 1 | 96 |
| 4.4.2 Physical Data for Compound 2 | 96 |
| 4.4.3 Physical Data for Compound 3 | 97 |
| 4.4.4 Physical Data for Compound 4 | 98 |
| 4.4.5 Physical Data for Compound 5 | 98 |
| 4.4.6 Physical Data for Compound 6 | 99 |
| 4.4.7 Physical Data for Compound 7 | 99 |
| 4.4.8 Physical Data for Compound 8 | 100 |
| 4.4.9 Physical Data for Compound 9 | 101 |
| 4.4.10 Physical Data for Compound 10 | 101 |
| 4.5 References | 103 |

CHAPTER 5 : BIOLOGICAL ACTIVITY OF COMPOUND 1

| | |
|------------------------------------|-----|
| 5.1 The Chemiluminescence Bioassay | 105 |
| 5.1.1 Introduction | 105 |
| 5.1.2 Experimental Procedure | 106 |
| 5.1.3 Results | 107 |
| 5.2 The DPPH Bioassay | 108 |
| 5.2.1 Introduction | 108 |
| 5.2.2 Experimental Procedure | 109 |
| 5.2.3 Results | 109 |
| 5.3 Discussion | 109 |
| 5.4 References | 110 |

CHAPTER 6 : CONCLUSION

| | |
|----------------|-----|
| 6.1 Discussion | 111 |
| 6.2 References | 115 |

APPENDIX A

| | |
|-------------------------------|-----|
| List of Spectra in Appendix A | 117 |
|-------------------------------|-----|

APPENDIX B

| | |
|----------------------------|-----|
| List of Data in Appendix B | 220 |
|----------------------------|-----|

CHAPTER 1 : INTRODUCTION

1.1 AN OVERVIEW OF THE SAPPI SAICCOR PROCESS

The SAPPI SAICCOR factory is situated in Umkomaas, 50 kms south of the port of Durban in South Africa. It was originally set up in 1952 by Courtaulds (UK), Snia Viscosa (Italy) and the Industrial Development Corporation (SA) to supply dissolving pulp for Courtaulds' viscose rayon fibre and cellophane film processes¹. By the time SAICCOR was acquired by the SAPPI group in September 1988, it had become one of the largest mills of its sort in the world. Today it is the world's single largest manufacturer of chemical cellulose with the capacity to produce approximately 600 000 tons of pulp per year, most of which is exported to Europe, America and Asia. It is also well renowned for being the first company to produce high grade dissolving pulp from the *Eucalyptus* tree¹.

SAPPI SAICCOR is one of the few pulp and paper mills that produces its dissolving pulp by the acid sulphite process, using both calcium (Ca) and magnesium (Mg) as bases. The first step is the chipping of approximately 5 300 tons per day of wood logs (Figure 1.1)¹. SAICCOR uses hardwood timber only, mainly *Eucalyptus grandis* and *Acacia mearnsii* in the ratio 90:10.

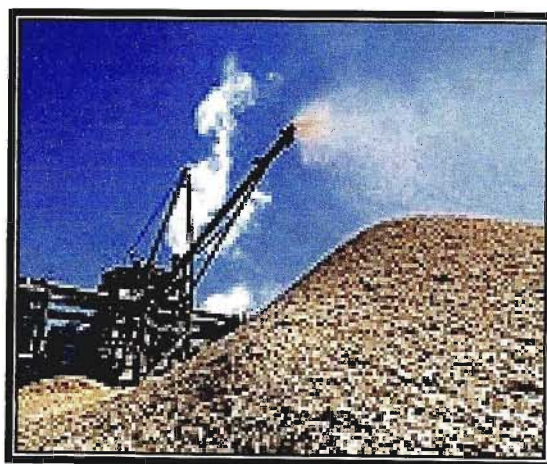


Figure 1.1: Chipping of wood logs¹

The wood chips are then transferred to large digesters for batch cooking (Figure 1.2).

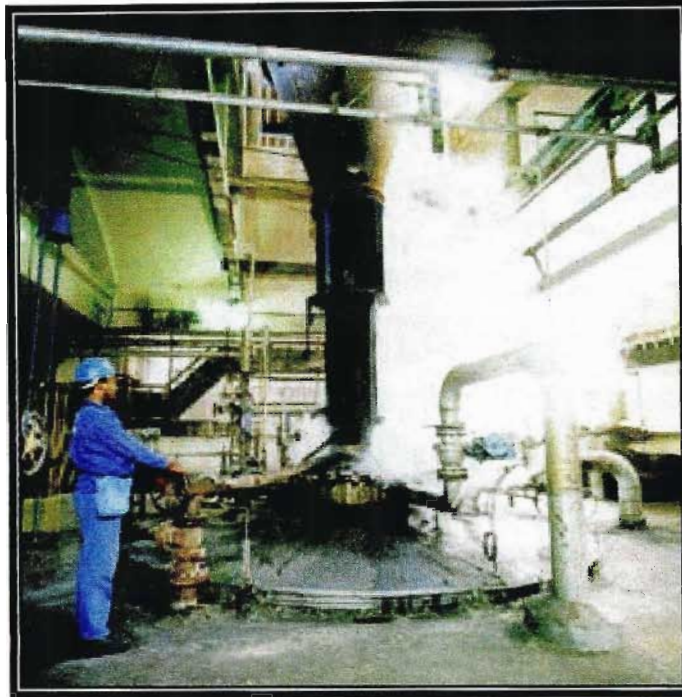
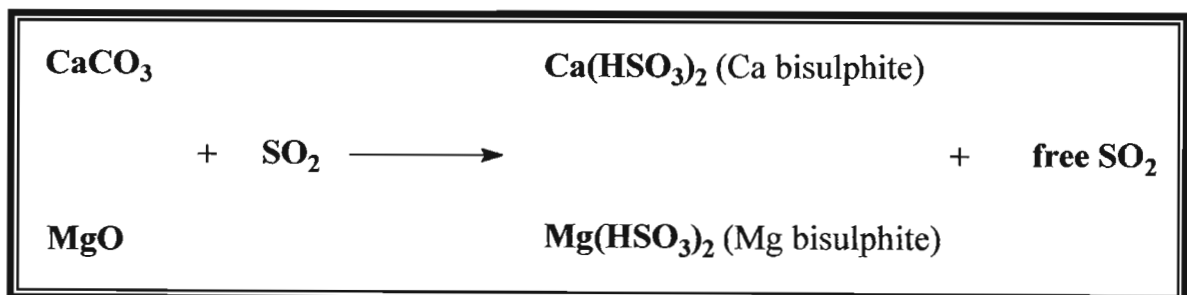


Figure 1.2: Batch cooking of wood chips in large digesters¹

Fifteen of these digesters use calcium bisulphite and eight use magnesium bisulphite. The calcium bisulphite and magnesium bisulphite are obtained on site by reacting magnesium oxide (MgO) and calcium carbonate (CaCO₃) with sulphur dioxide (SO₂) as shown in Scheme 1.1.



Scheme 1.1: The production of Ca and Mg bisulphite by reacting MgO and CaCO₃ with SO₂

The magnesium pulp section operates as a closed cycle where the thin liquor is evaporated to form a thick liquor, which is then burned to produce energy. The resulting ash is slurried and pretreated to form magnesium oxide cooking liquor, which is then fed back to the digesters for the next batch cooking. Thus there is almost complete recovery of the magnesium oxide base material. The only waste going to the effluent stream is the condensate formed during evaporation of the thin liquor.

The calcium – based section produces a large proportion of the total effluent in the form of spent liquor, which contains approximately 16 % of total dissolved solids². This calcium spent liquor is, unfortunately, not recyclable. However, approximately 50 % of the effluent from this stream is pumped to Lignotech, a subsidiary of SAICCOR, where the crude lignosulphonates are removed for commercial purposes and the remaining effluent goes to the main effluent drain³.

The wood chips are cooked in the digesters with liquor under high temperature (140°C) and pressure (10 bar). This process renders the lignin and hemicellulose in the wood soluble, which can then be washed out into the effluent streams.

The resultant raw pulp from both the calcium and magnesium sections is then washed and screened separately before being combined and passed through a five – stage bleaching process, which is an Elemental Chlorine Free (ECF) process. The introduction of ECF bleaching coupled with SAICCOR'S unique pulp washing system has resulted in a significant reduction of the pulp's average dirt count making it one of the key environmental improvements at SAICCOR¹.

The first bleaching stage, the O₂ stage, uses oxygen and sodium hydroxide (NaOH). It is responsible for the removal of about half of the lignin from the pulp as well as some hemicellulose and low molecular weight cellulose. The D₁ stage uses chlorine dioxide (ClO₂), which solubilises the remaining lignin for the next caustic extraction stage. The third stage, the E₀ stage, uses sodium hydroxide (NaOH) to extract and remove all the solubilised lignin. Detergent is also added to this stage to remove any unwanted resins present. The D₂ stage uses chlorine dioxide (ClO₂) to brighten the pulp and to break down any remaining lignin residues without affecting the cellulose. The final bleaching stage, the H – stage, uses sodium hypochlorite (NaOCl) to further brighten the pulp and to

chemically break down the cellulose to the correct molecular size for use by SAICCOR'S customers.

The final stage of the bleaching process is the only stage that uses clean fresh water for washing. The other stages use water that is recycled counter – current. At the O₂ and E_o stages, half of the washings are diluted with fresh water and the other half is removed to form the remaining two contributors of the final effluent.

After bleaching, the pulp is subjected to screening to remove any non – cellulose matter before being dried as a continuous sheet, which is cut and baled or reeled. SAICCOR produces their high quality dissolving pulp at a rate of approximately 1 600 tons per day¹. Their product is used in the manufacturing of a wide range of products such as viscose, cellophane, lyocell, ethers, sausage casings, speciality paper and much more.

The four main streams of effluent, i.e. the calcium spent liquor, the magnesium pulp condensate and the two streams from the bleaching stage, combine to form the main effluent before being pumped out to sea through a 7 km pipeline. Thus, the main effluent should contain a large proportion of lignins and lignosulphonates, as the main aim of the process is to produce a high – grade cellulose pulp free of lignin. Other components of the effluent would be hemicelluloses, resin acids, tannins and sugars.

1.2 CHARACTERISATION OF PULPING LIQUORS

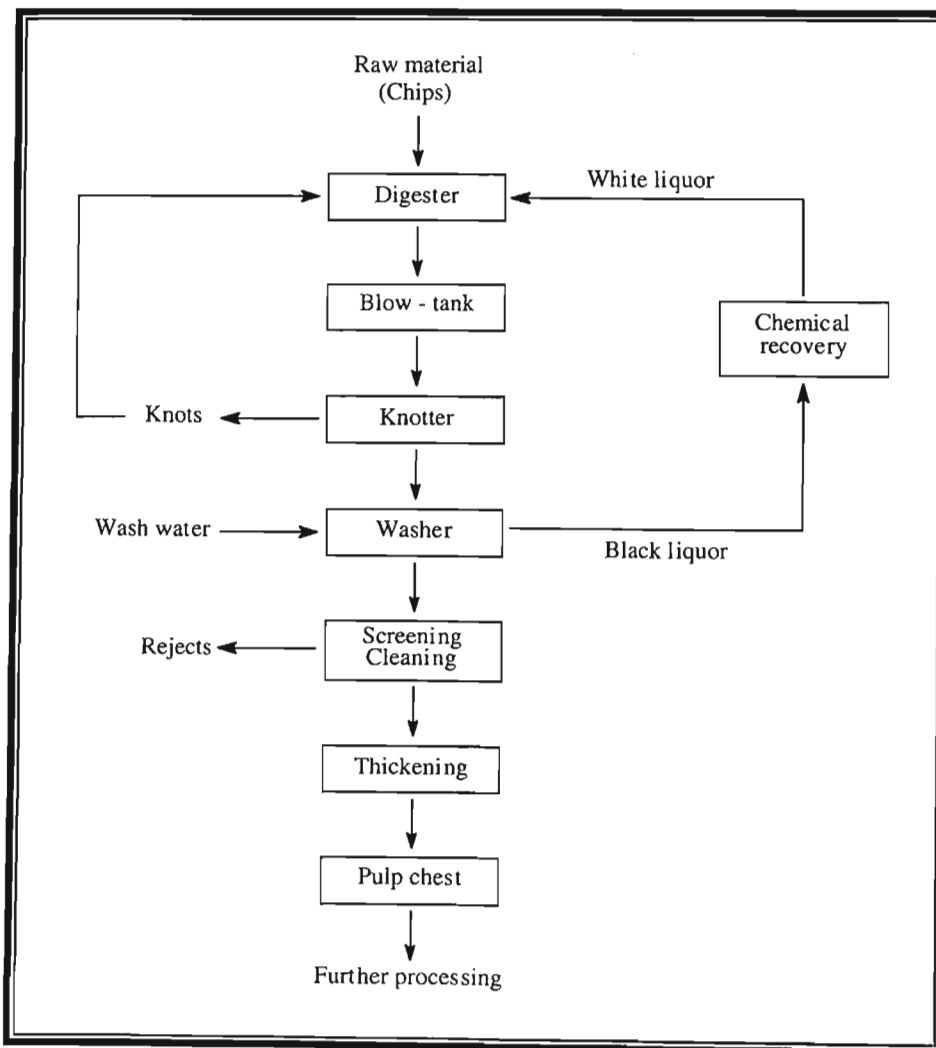
The characterisation of pulping liquors has been carried out since the early 1950s. Studies have shown that the spent liquor from chemical pulping contain varying amounts of organic compounds from all wood constituents. The nature and concentrations of these compounds depend largely on the type of wood material used for pulp production, the type of pulping method employed and the composition of the cooking liquors⁴.

There are two major chemical pulping processes, *viz.* sulphate pulping and sulphite pulping. These two processes are the most widely used today and a brief discussion on each process shall be given here.

1.2.1 Sulphate Chemical Pulping

This process is usually referred to as the kraft or alkaline process and is currently the most widely used chemical pulping method. The process was originally patented in 1884 by C.S. Dahl^{5,6}. “Kraft” is the German word for strength and is used to describe the pulps made by the sulphate process and the paper made from such pulps.

In this process, the wood chips are cooked in large digesters with fresh cooking liquor from the chemical recovery line at temperatures between 160 and 180°C and at pressures between 7 and 11 bar⁷. The principal cooking chemicals, which are contained in the white liquor, are sodium hydroxide (NaOH) and sodium sulphide (Na₂S) at a pH of approximately 14. A simplified flow diagram of the kraft process is shown in Scheme 1.2.



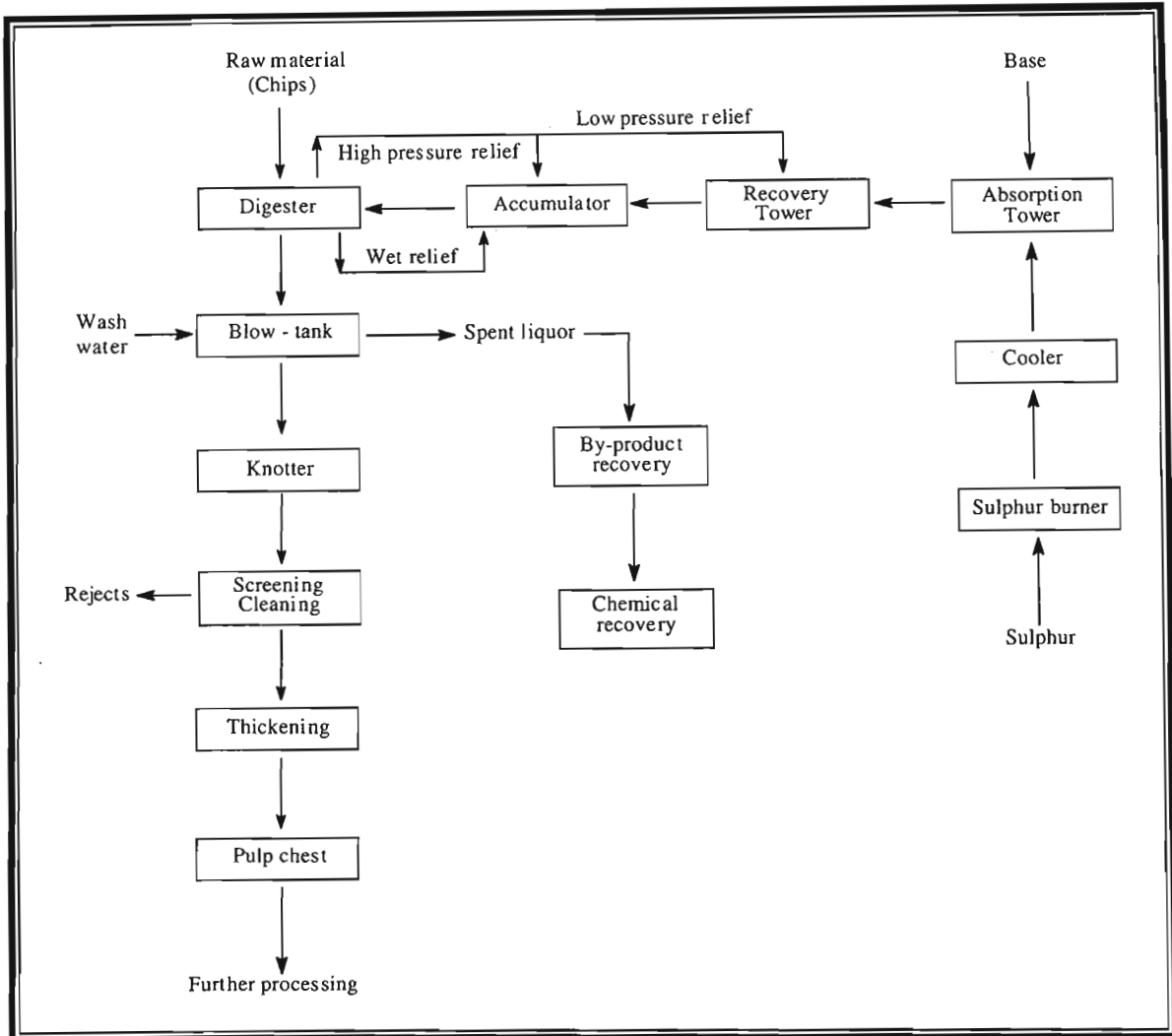
Scheme 1.2: Simplified flow diagram of the kraft process⁷

The kraft process removes almost all the lignin from the pulp and preserves the cellulose fibres, producing a pulp of high physical strength. The process can be performed on both hardwoods and softwoods of any species. There is also a well – established chemical recovery system for the recycling of the pulping chemicals. However, the main drawbacks of sulphate pulping are the odour problems, the dark colour of the unbleached pulp and lower yields than in sulphite pulping⁷.

1.2.2 Sulphite Chemical Pulping

Unlike the kraft process, the sulphite process is characterised by covering the whole pH range, therefore, a high flexibility in pulp yields and properties is possible⁸. The composition of sulphite pulping liquors varies with respect to the proportions of sulphur – containing species present, that is, sulphur dioxide (SO_2), hydrogen sulphite ions (HSO_3^-) and sulphite ions (SO_3^{2-}). These are dependent on the actual pH of the cooking liquor and the type of base added^{7,8}. The most commonly used bases in sulphite pulping are calcium, magnesium, sodium and ammonia.

There are five principle types of sulphite pulping processes, *viz.* acidic sulphite pulping, bisulphite pulping, multi-stage sulphite pulping, neutral sulphite pulping and alkaline sulphite pulping⁷. Scheme 1.3 outlines the general steps involved in sulphite pulping.



Scheme 1.3: Simplified flow diagram of sulphite pulping⁷

The wood chips are commonly pre-steamed before being filled into the digesters to improve the penetration of the cooking liquor. The cooking liquor is heated using a heat exchanger to the maximum cooking temperature, which varies between 125 and 180°C and a maximum pressure of up to 10 bar. In general, sulphite pulping uses sulphurous acid (H_2SO_3) and an alkali (for example NaOH) to produce pulps of lower physical strength than kraft pulp. However, its yield is higher at a given kappa number[†] and the unbleached pulp itself is bright and easy to bleach.

[†] Kappa number is an indication of the amount of residual lignin left in pulp after pulping and is generally used to determine the grade of pulp produced and its end uses. The reaction of potassium permanganate with residual lignin is used in the determination of the Kappa number.

One of the most promising advances in sulphite pulping is the alkaline sulphite process (AS) using sodium sulphite and sodium hydroxide in combination at pH levels up to 13. The process combines the advantages of kraft pulping (namely strong pulps and no limitation to wood species) with sulphite pulping characteristics such as high yields of bright and well bleachable pulps and fewer or no odour problems⁷.

1.2.3 Compounds Previously Identified in Chemical Pulping Liquors

Delignification during both sulphate and sulphite chemical pulping, using various different types of bases, produces a complex mixture of products ranging from simple phenolic compounds to large macromolecules. These compounds form the major components of the total dissolved solids present in spent liquor effluents.

Studies on the fractionation of black liquor obtained from a *Eucalyptus globulus* bleached kraft pulp mill showed the presence of many different types of compounds⁹. The ether – soluble fractions were found to contain aromatic acids and phenolic compounds⁹. The major components were identified as syringaldehyde, acetosyringone, syringol and syringaresinol⁹. Other compounds isolated from these fractions included vanillic acid, acetovanillone, 1,1'-disyringylethane, 2,6-dimethoxyhydroquinone, 4,4'-dihydroxy-3,3'-dimethoxystilbene and aspidinol⁹. A number of aliphatic carboxylic acids, such as lactic acid, 2-hydroxy acetic acid and oxalic acid, were also isolated from the liquid phase of the black liquor⁹. The water – soluble fractions contained predominantly carbohydrates with xylose and galactose as the major sugars⁹.

The importance of sulphite pulping has decreased during the recent decades, thus most of the information on the composition of sulphite spent liquors dates from the 1950s and 1960s⁴. Early studies on the spent liquor of sulphite pulped aspen wood showed the presence of a large number of low – molecular weight aromatic compounds. These compounds were identified as vanillin, syringaldehyde, syringol, 4-hydroxybenzoic acid, dihydroconiferyl alcohol, syringaresinol and α -conidendrin¹⁰⁻¹².

Recent studies have concentrated on the isolation and characterisation of lignosulphonates from spent bisulphite liquor. A large number of sulphonated lignin – derived monomers and dimers have been isolated and identified using high performance liquid

chromatography (HPLC)^{13,14}. Examples of such compounds include 1-syringyl-2-propene-1-sulphonic acid, methyl-3,4-dimethoxybenzenesulphonate, 3-guaiacylpropanal-3-sulphonic acid and 1,2-disulphonomethyl-1-(3',4'-dimethoxyphenyl)-propane^{13,14}.

1.3 OBJECTIVE OF PROJECT

A preliminary study undertaken by the Natural Products Research Group in the School of Pure and Applied Chemistry at the University of Natal, Durban, on SAPPI SAICCOR pulp mill's effluent concentrated on the characterisation of the compounds contained in the neutral organic extracts of all four effluent streams. A number of known organic compounds were isolated and characterised. These included a mixture of lignan isomers, *epi*-syringaresinol and *meso*-syringaresinol and lignin-type precursors such as 3-(4'-hydroxy-3',5'-dimethoxyphenyl)-prop-1-ene, 2,6-dimethoxy-1,4-benzoquinone, 3-(4'-hydroxy-3',5'-dimethoxyphenyl)-1-hydroxy-propane-2-one, syringaldehyde and vanillin^{15,16}. However, the bulk of the effluent, which was not extracted into the organic phase and remained in the aqueous phase, was not fully characterised. Thus, the aim of this project was to extract, separate and identify the remaining water – soluble compounds present.

SAPPI SAICCOR'S stated intention is to improve the quality of the mill effluent before it is disposed of into the sea. The results obtained from this study will be used to identify any commercially exploitable compounds contained in their effluent streams, which can be extracted and marketed, thereby reducing the impact of industrial waste effluent on the environment.

1.4 REFERENCES

1. *Sappi Saiccor*, brochure produced by SAPPI SAICCOR.
2. Moodley, B., 2001, *Characterisation of SAPPI SAICCOR Pulp Mill's Effluent*, MSc Dissertation, School of Pure and Applied Chemistry, University of Natal, Durban.
3. Personal communication with Mr John Thubron – Technical Process Manager at SAPPI SAICCOR.
4. Sjöström, E. and Alén, R., 1999, *Analytical Methods in Wood Chemistry Pulping and Papermaking*, Springer : Berlin, p193-220.
5. Grant, J., 1958, *Cellulose Pulp & Allied Products*, 3rd ed., Thomas Reed & Company limited : London, p30.
6. Smook, G.A., 1992, *Handbook for Pulp & Paper Technologists*, 2nd ed., Angus Wilde Publications Inc. : Vancouver, p38.
7. Fengel, D. and Wegener, G., 1983, *Wood : Chemistry, Ultrastructure and Reactions*, Walter de Gruyter & Co. : Berlin, p414-462.
8. Gullichsen, J. and Paulapuro, H., 2000, *Forest Products Chemistry*, Fapet Oy : Helsinki, p78-79.
9. Neto, C.P., Belino, E., Evtuguin, D. and Silvestre, A.J.D., 1999, Total Fractionation and Analysis of Organic Components of Industrial *Eucalyptus globulus* Kraft Black Liquor, *Appita*, **52**, 213-217.
10. Pearl, I.A., and Beyer, D.L., 1961, Studies on the Chemistry of Aspenwood. VII. Further Studies on Ether Extractives of Commercial Aspen Spent Sulfite Liquor, *Journal of Organic Chemistry*, **26**, 546-550.

11. Pearl, I.A., and Beyer, D.L., 1964, Studies on the Chemistry of Aspenwood. XVII. The Ether – Insoluble, Water – Soluble Components of Aspen Spent Sulfite Liquor, *Tappi*, **47**, 458-462.
12. Pearl, I.A., and Beyer, D.L., 1964, The Ether – Insoluble, Water – Soluble Components of Several Spent Sulfite Liquors, *Tappi*, **47**, 779-782.
13. Bialski, A.M., Luthe, C.E., Fong, J.L. and Lewis, N.G., 1986, Sulphite – Promoted Delignification of Wood : Identification of Paucidisperse Lignosulphonates, *Canadian Journal of Chemistry*, **64**, 1336-1343.
14. Luthe C.E., 1990, Isolation and Characterisation of Lignosulphonates from an Ultra High Yield Neutral Sulphite Pulping Effluent, *Holzforschung*, **44**, 107-112.
15. Moodley, B., Mulholland, D.A. and Marsh, J.J., 2003, The Characterisation of Organic Components in the Calcium and Magnesium Effluent Streams at Sappi Saiccor, *Water SA*, **29**, 237-240.
16. Moodley, B., Mulholland, D.A. and Marsh, J.J., 2003, The Characterisation of Organic Components in the O – and E – Stage Bleaching Effluent Streams at Sappi Saiccor, *Water SA*, **29**, 241-243.

CHAPTER 2 : TYPES OF COMPOUNDS ISOLATED

2.1 LIGNINS AND LIGNANS

2.1.1 Introduction

Trees are classified into two broad categories, namely softwoods (gymnosperms) and hardwoods (angiosperms). Softwoods are also commonly referred to as conifers since they produce naked seeds in cones, while hardwood trees produce covered seeds within flowers^{1a}. This is considered the major botanical basis for their classification.

The major difference between softwoods and hardwoods, with regard to the macroscopic structure of the wood, is the presence of vessels in hardwoods. Vessels are structures composed of cells created exclusively for the conduction of water. Softwoods lack vessels but have cells called tracheids, which perform a dual role of conduction and support. In general, hardwood fibres are shorter and thicker than softwood fibres².

Despite the fact that the macroscopic structures of softwoods and hardwoods are different, the structures of their cell walls are remarkably similar. Figure 2.1 shows a schematic representation of the various layers which make up a typical cell wall.

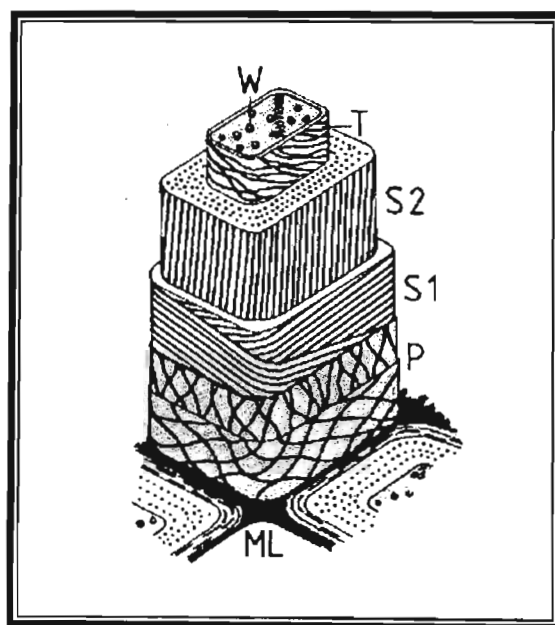


Figure 2.1: Schematic illustration of the structure of a cell wall^{3a}

Between each individual cell, there is a thin layer, the middle lamella (ML). It functions to bond the cells together and is composed almost entirely of lignin. The outermost layer is the primary wall (P), consisting of cellulose, hemicellulose, pectin and protein embedded between lignin^{4a}. The secondary wall is not homogenous and can be subdivided into three layers. The thin outer S₁ layer is rich in lignin and closely resembles the primary wall. The central S₂ layer is the thickest wall layer, forming the bulk of the fibre. It contains more cellulose and less lignin than the S₁ layer. The inner thin S₃ layer is also sometimes referred to as the tertiary wall and is rich in hemicellulose. In the centre of the fibre is a void called the lumen (W), which is sometimes covered with warts^{3a}.

Therefore, the three structural constituents of wood are cellulose, hemicelluloses and lignin. The effluent streams from SAPPi SAICCOR are known to contain a large proportion of lignin and thus the chemistry of lignin will be discussed further.

Next to cellulose, lignin is the most abundant and important organic substance in the plant world^{3b}. It is considered the major non – carbohydrate component of wood and accounts for between 15 % and 40 % of the total mass^{5a,6}. Lignin is an amorphous polymer with a chemical structure that distinctly differs from the other macromolecular constituents of wood. Lignin typically occurs in the vascular tissue between the walls of cells where it performs a multiple function that is essential to the life of the plant. It is specialised for the internal transport of water, nutrients and metabolites to other parts of the plant. Secondly, lignins impart rigidity to the cell walls thus providing mechanical strength for the plant by resisting the impact of compression and bending on the plant^{5a}. Finally, lignified tissues effectively resist attacks by microorganisms by impeding penetration of destructive enzymes into the cell wall^{5a}.

The primary precursors and building blocks of all lignins are phenylpropanoid (C₆-C₃) units, that is, *p*-hydroxycinnamyl alcohols, namely, coniferyl alcohol (**2-1**), sinapyl alcohol (**2-2**) and *p*-coumaryl alcohol (**2-3**) as shown in Figure 2.2.

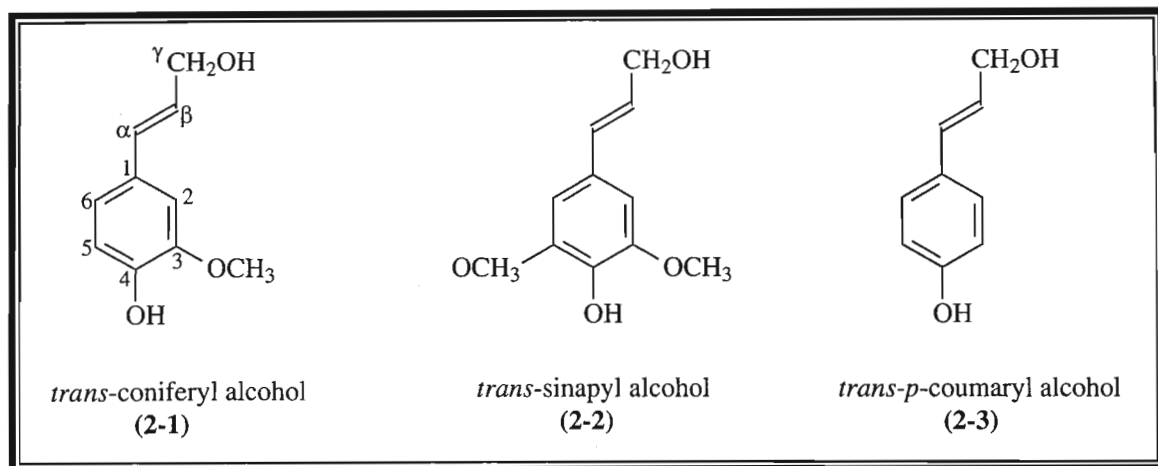


Figure 2.2: The building units of lignin^{1b}

Lignans are closely related to lignins. They usually occur as dimers of phenylpropanoid units linked by the central carbon atoms (C-8/C-8') of their propane side chains. Phenylpropane dimers which are linked through atomic centres other than the 8,8' carbons are termed neolignans^{7,8} (Figure 2.3).

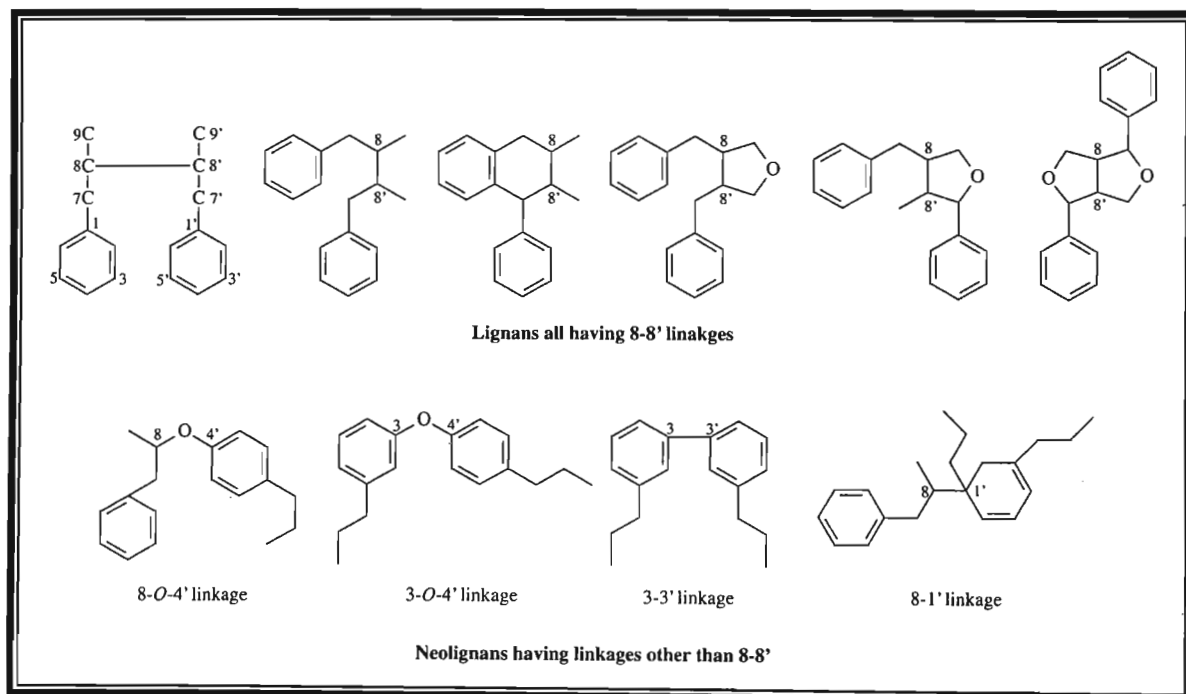


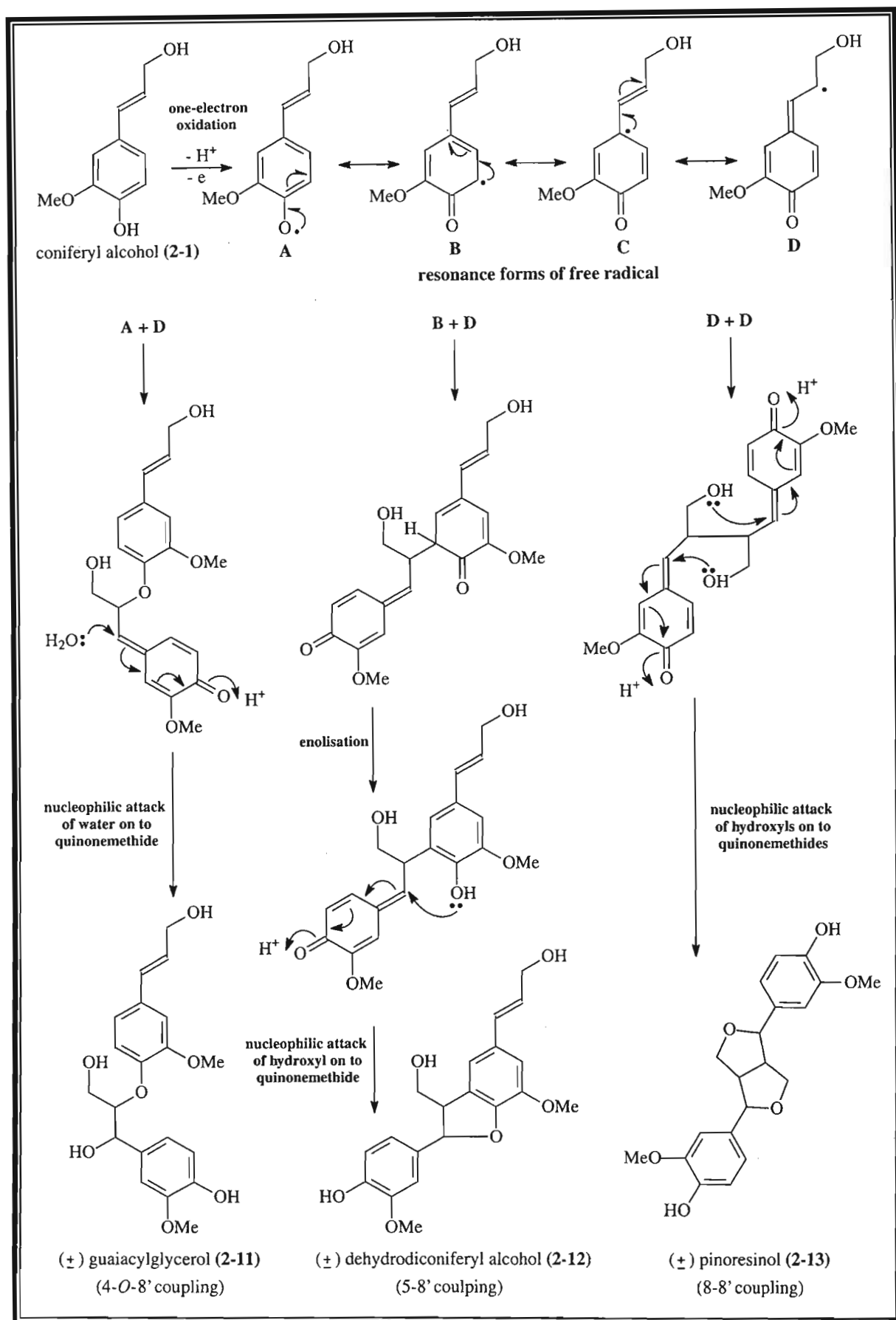
Figure 2.3: Structural diversity in lignans and neolignans⁸

Lignans can be found in all plant parts, including stems, roots, rhizomes, seeds, oils, flowers, leaves and bark⁹. They were originally thought to be low molecular weight lignin fragments, although unlike lignin they are optically active⁷. As previously described, lignins play a role of structural reinforcement in plant tissues whilst lignans are closely related to non – structural phenolic metabolites, that is, they play a defensive role in plants^{7,10}.

2.1.2 Lignin and Lignan Biosynthesis

The biosynthesis of lignins and lignans are very much similar to one another, although, it is becoming increasingly more evident that both these biosynthetic pathways are fully independent of each other⁹.

Lignins and lignans are derived from *L*-phenylalanine (**2-4**), a common precursor for a wide range of natural products. The first step is the elimination of ammonia from the side – chain of *L*-phenylalanine (**2-4**) to generate the appropriate *trans* – cinnamic acid (**2-5**)¹¹. This is achieved *via* the enzyme phenylalanine ammonia lyase (PAL). Other cinnamic acid derivatives (**2-6** to **2-10**) are produced by further hydroxylation and methylation reactions, sequentially building up the substitution pattern typical of the shikimate pathway metabolites, i.e. an *ortho* oxygenation pattern^{11a}. The *p*-hydroxycinnamyl alcohols, namely, coniferyl alcohol (**2-1**), sinapyl alcohol (**2-2**) and *p*-coumaryl alcohol (**2-3**), are formed by enzymatic reduction of the corresponding acids (Scheme 2.1).

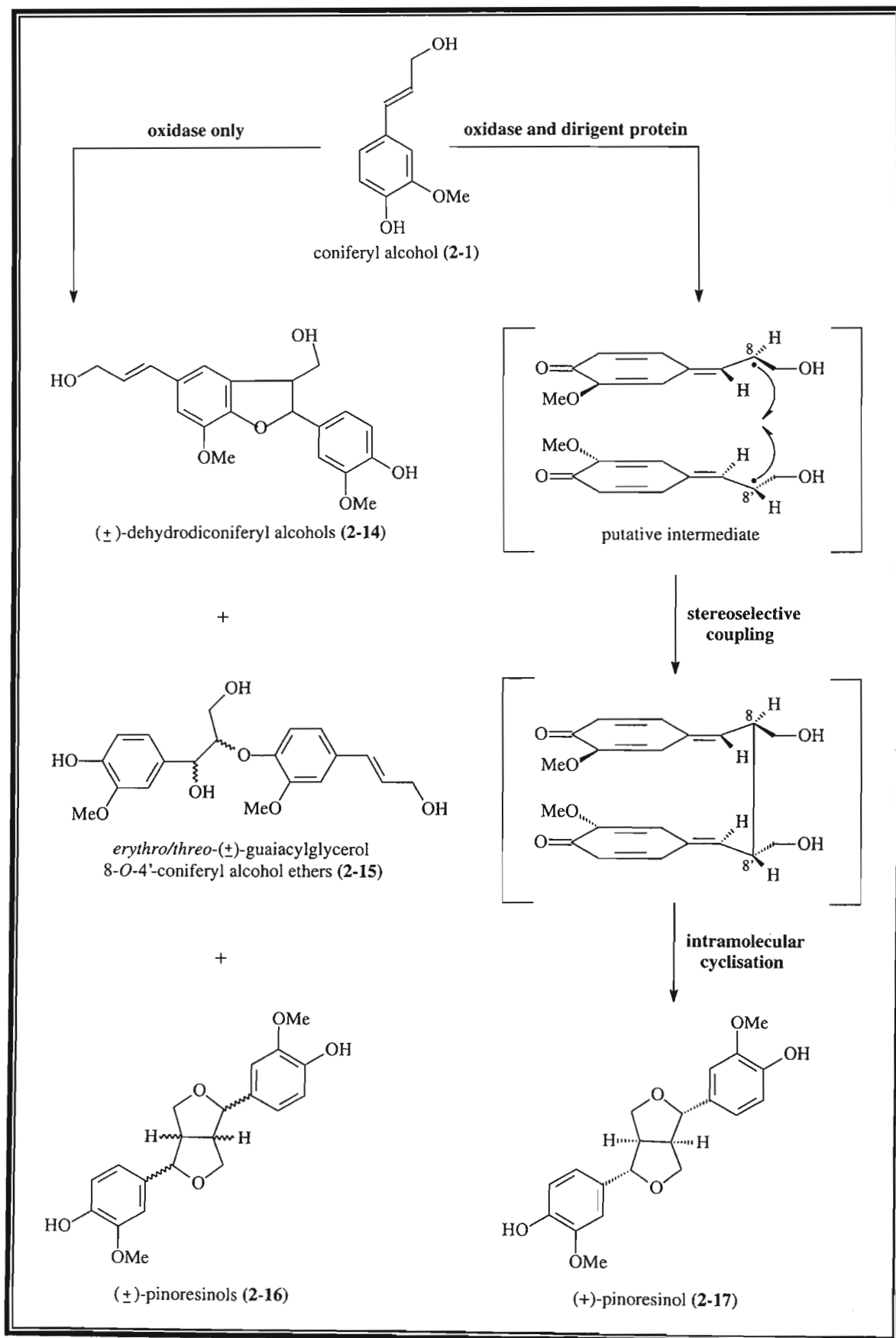
Scheme 2.2: Radical pairing of resonance structures to form dimers^{11a}

As mentioned earlier, lignins and lignans are products of distinct metabolic pathways and hence are catalysed by different enzymes. This results in lignans being normally enantiomerically pure because they arise from stereochemically – controlled coupling^{11a}. The enzymes controlling lignin biosynthesis, however, appear to generate products lacking optical activity.

The accepted view of lignin and lignan biosynthesis since the 1950s has been that these molecules were formed due to completely random coupling of two phenolic monomer radicals. The oxidative enzymes, such as peroxidases and laccases, were required only to generate the corresponding free radicals but nothing except chemical control was thought to dictate the coupling reactions and polymer structure^{12,13}. However, this theory could not explain the regio- and stereospecificity observed in lignin formation and the optically active lignans found in nature¹⁰.

The discovery of a new class of proteins in 1997 by Norman G. Lewis, Laurence B. Davin and Simo Sarkanen gave a new perspective on the controlled coupling of free radicals in lignin and lignan biosynthesis. They called these proteins “dirigent” proteins from the Latin “dirigere”, which means to guide or align. These proteins show no catalytic activity but apparently have sites that bind either the monomers or the monomer radicals in specific orientations that lead to selective coupling^{10,14}.

The dirigent protein was first isolated from *Forsythia intermedia*, a plant that both produces and further metabolises enantiomerically pure (+)-pinoresinol (**2-17**), a dimeric lignan formed from two achiral molecules of coniferyl alcohol (**2-1**). Studies from an *in vitro* system containing the dirigent protein, an oxidant and coniferyl alcohol monomers (**2-1**) produced (+)-pinoresinol (**2-17**) in almost 100 % optical purity. A similar system with only the oxidant and the monomers yielded racemic mixtures of random coupling products¹⁰. Kinetic studies suggested that the protein functioned in a very unique manner, whereby the oxidative enzymes first generate the free – radical intermediates, which are then presumed to be captured by the dirigent protein. These are then bound and orientated in such a manner that coupling can only provide the product (+)-pinoresinol (**2-17**)¹². Scheme 2.3 illustrates the proposed mechanism, whereby the dirigent protein prevents scrambling of phenolic radical couplings in the formation of (+)-pinoresinol (**2-17**).

Scheme 2.3: Dirigent – mediated formation of (+)-pinoresinol^{10,12}

The discovery of the involvement of dirigent proteins in the biosynthesis of optically active lignan dimers has led Lewis, Davin and Sarkanen to propose that the monomer – specific binding sites in these proteins must also account for the specificity observed during lignification. Firstly, the lignin precursors make their way to precise lignin initiation sites situated at the farthest end of the cell wall. Here, the dirigent proteins are thought to control monomer composition, the sequence of inter – unit linkages as well as the phenoxy radical coupling processes. Once a primary lignin chain has formed, template polymerisation occurs, which enables lignin to grow from the initiation sites back towards the plasma membrane^{10,12,13}. However, this new model has received widespread criticism and much more experimental evidence is needed to support this theory¹³.

2.1.3 The Biological Activity of Lignans

Lignans display a wide variety of biological activities. Various lignans are known to have anti – tumour, anti – mitotic and anti – viral activity and to specifically inhibit certain enzymes¹⁵. Toxicity to fungi, insects and vertebrates is also observed for some lignans¹⁵.

Podophyllotoxin (**2-18**) and related lignans, constituents of the medicinal resin extracted from the roots of the *Podophyllum* species and numerous other plants, have clinically useful cytotoxic and anti – cancer benefits^{11a,15}. The resin is effective in the treatment of *Condyloma acuminata* or venereal warts, a condition which can be sexually transmitted. Deoxypodophyllotoxin (**2-19**) from the fruit of *Juniperus communis* shows antiherpetic activity¹⁵. The podophyllotoxin group of lignans were found to be unsuitable for clinical use as anti – cancer agents due to their toxic side effects. However, the semi – synthetic derivatives etoposide (**2-20**) and teniposide (**2-21**) are excellent anti – tumour agents and have been employed for the treatment of testicular cancers^{11a,12}.

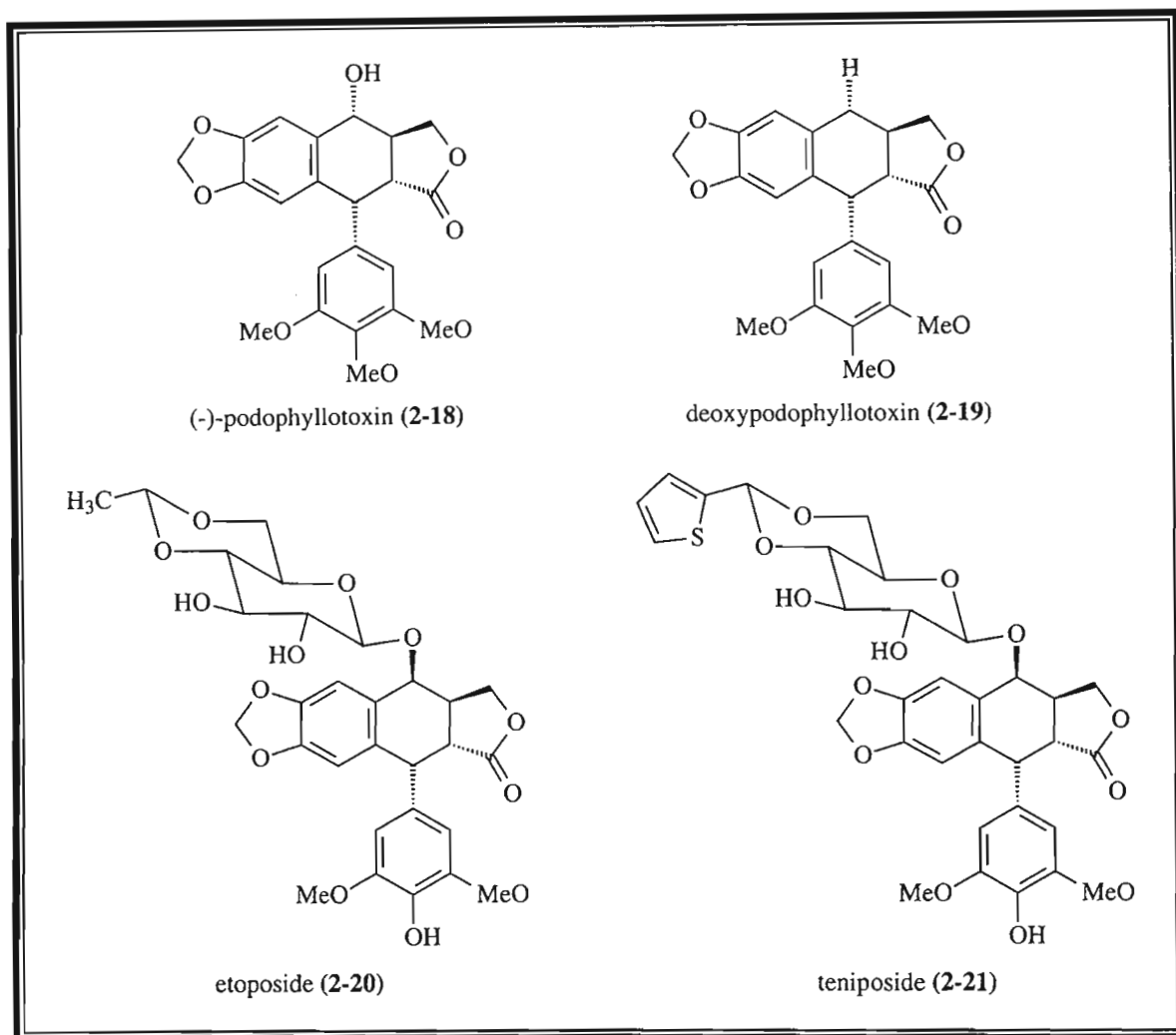


Figure 2.4: The podophyllotoxin group of lignans

(+)-Sesamin (2-22) and asarinin (2-23) are used in enhancing the toxicity of a wide variety of insecticides. These lignans display the same potency as commercially used synthetic insecticide synergists¹⁵. (+)-Sesamin (2-22) and (+)-sesamol (2-24), isolated from the sesame plant *Sesamum indicum* and nordihydroguaiaretic acid (2-25) from *Larrea tridentata* are used as anti – oxidants in seed oil¹². (-)-Secoisolariciresinol (2-26), secoisolariciresinol diglucoside (2-27) and (-)-matairesinol (2-28) are the “chemopreventative agents” of many edible plants which help protect against the onset of breast and prostate cancers¹². The schisandran lignan (+)-gomisin A (2-29), from *Schisandra chinensis*, is used in the treatment of liver disorders and kadsurenone (2-30) from *Piper futokadsura* is a platelet – activating factor¹².

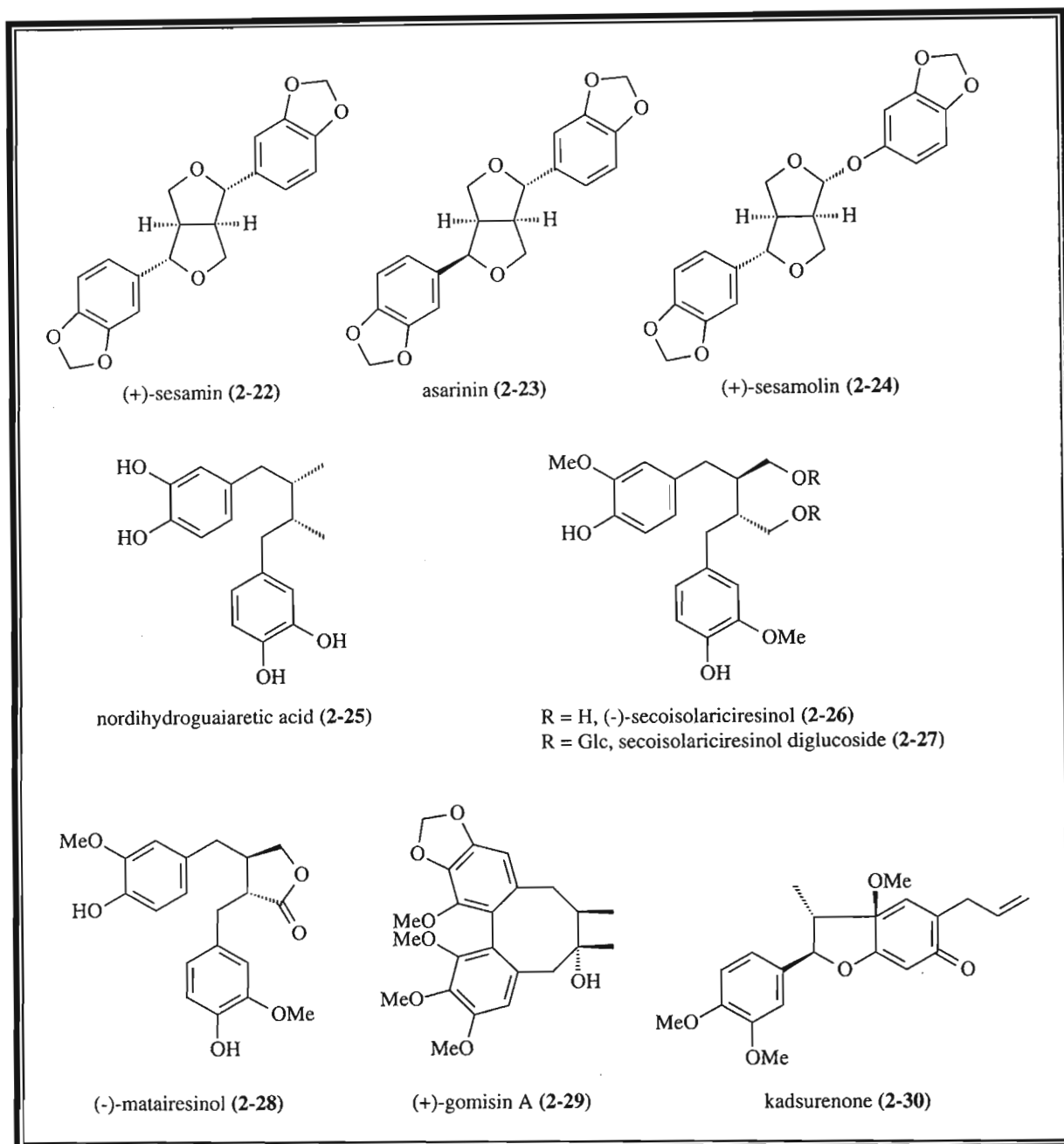


Figure 2.5: Structures of biologically active lignans

Lignans have also recently been identified in the urine and blood of humans and primates. The compounds (-)-enterolactone (2-31) and enterodiol (2-32) have been found as glucuronides in the urine of humans, baboons, vervet monkeys and rats¹⁵. The level of (-)-enterolactone (2-31) in human urine, plasma and bile is comparable to that of steroid metabolites¹⁵. There is a possibility that these lignans possess hormonal activity in humans or they may probably be metabolic products of the microflora of the gut¹⁵. The most interesting point to note is that both (-)-enterolactone (2-31) and enterodiol (2-32)

are hydroxylated only at the *meta* position, a substitution pattern that is not observed in plant products. However, more evidence is needed to clarify the role of these compounds in mammalian physiology.

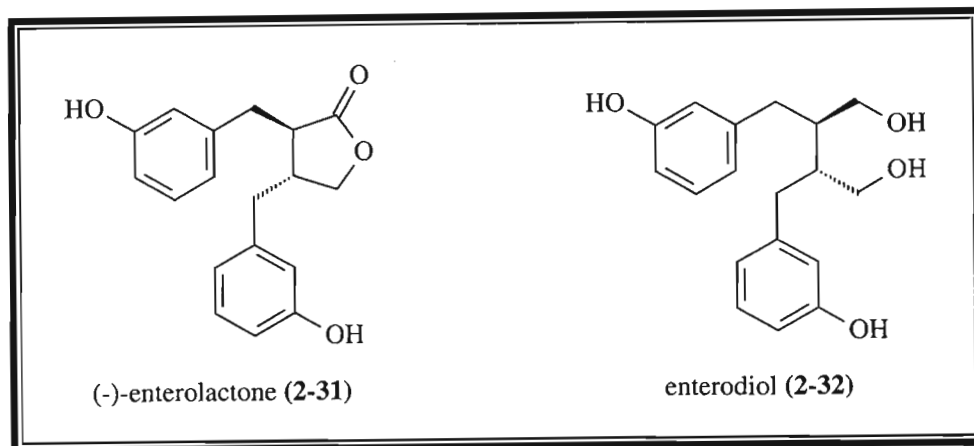


Figure 2.6: Lignans identified in humans

2.2 LIGNOSULPHONATES

2.2.1 Introduction

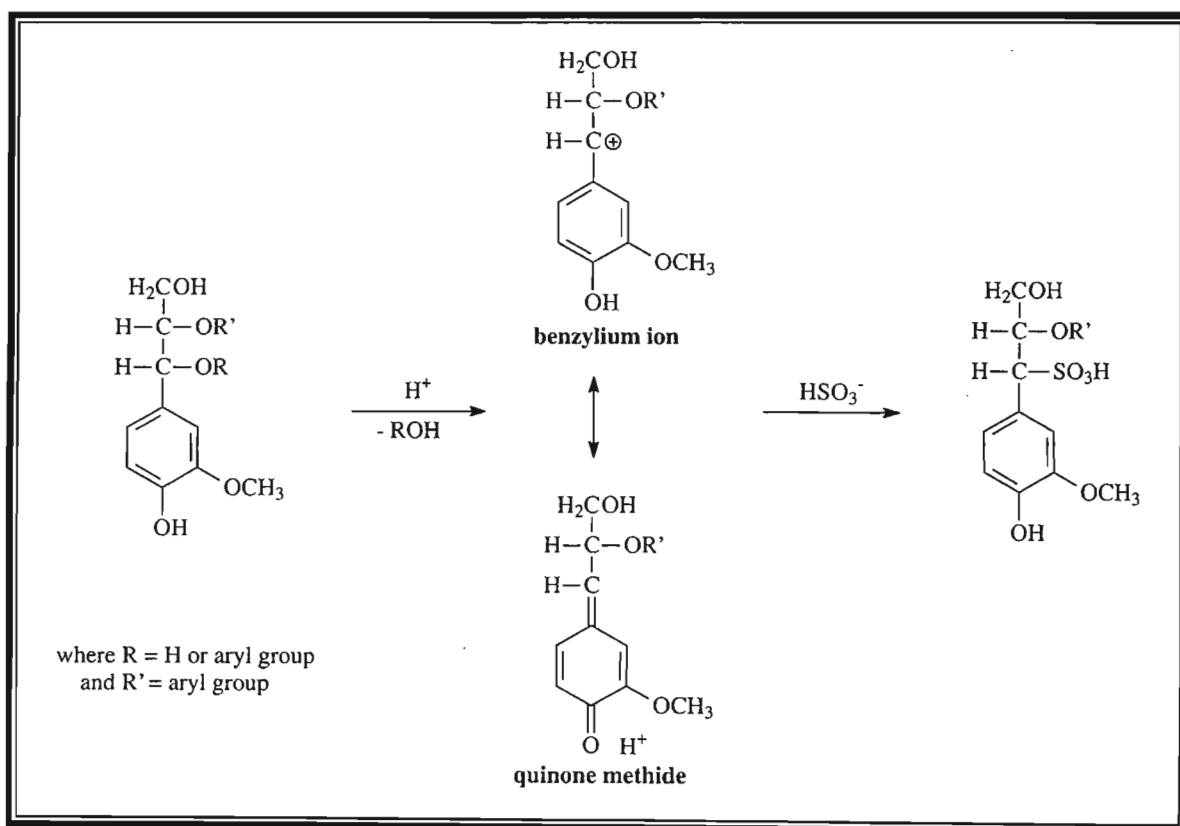
In its natural state, lignin is insoluble in water and is termed hydrophobic (non – wettable). When reacted with the chemicals present in acid bisulphite pulping liquor it is converted to lignosulphonates, which is now completely soluble in water and hydrophilic (wetable)¹⁶. Lignosulphonates are, therefore, defined as the soluble derivatives of lignin and it is in this form that lignin is commercially available¹⁷.

2.2.2 The Formation of Lignosulphonates During Acid Bisulphite Pulping

In acid bisulphite pulping, delignification is achieved through the combined effects of two major reactions, that is, sulphonation and hydrolysis. Sulphonation acts to soften the lignin and increase its hydrophilic properties whilst hydrolysis breaks lignin bonds so that new and smaller soluble lignin fragments are formed¹⁶.

The most reactive site for the formation of lignosulphonates is the alpha – carbon or benzylic position in the phenyl propane unit. The phenolic structures are transformed into

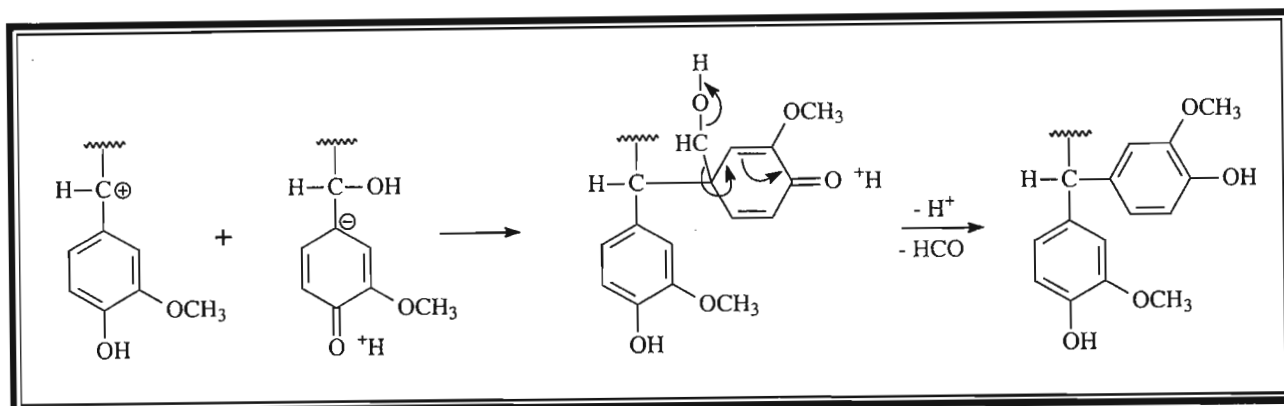
intermediary carbonium ions (benzylium ions) or quinone methide structures^{1c,16}. These structures are then sulphonated by attack of hydrated SO_2 or HSO_3^- present in the cooking liquor resulting in lignin that is soluble in the aqueous liquor^{1c}. The beta – carbon position of the propane side chain is less active and is usually involved in beta – phenolic ether linkages. However, this position can also be sulphonated after cleavage of the oxygen link in neutral and slightly alkaline conditions¹⁶. This type of sulphonation is generally accelerated by sulphonation at the adjacent alpha – carbon position¹⁶.



Scheme 2.4: Formation of liginosulphonates^{1c,4b}

Sulphonation can take place over the whole pH range but tends to decrease rapidly towards the strongly alkaline range. The introduction of sulphonic acid groups onto the phenyl propane structure causes the formerly neutral inactive compound to become a strong organic acid¹⁶. The sulphonated complex carries an equivalent amount of positive base ions with it (for example, Na^+ , Ca^{2+} , Mg^{2+}) in order to satisfy electroneutrality. When the water is removed from such a structure the positive base ion joins the negative macro ion to form a liginosulphonate salt¹⁶.

The desired sulphonation reactions compete with condensation reactions, especially at low pH values^{3c}. Condensation reactions result in the formation of carbon – carbon bonds between the benzylium ions at the alpha – carbon position and weakly nucleophilic positions of other phenylpropane units. This leads to an increased molecular weight of the lignosulphonates and a decrease in solubility of lignin in the aqueous liquor^{12a}.



Scheme 2.5: A typical condensation reaction^{3c}

2.2.3 The Uses of Lignosulphonates

Lignosulphonates have been used for many years in a wide variety of commercial applications which impact on many facets of our daily lives. The usefulness of lignosulphonate products comes from their adhesive (binding), dispersing, complexing and emulsifying properties.

One of its earliest applications, used since the 1900s, has been in the textile dyeing industry where they were used as a tanning agent, in combination with chrome tanning agents, for the tanning of leather. They also found their use as ore binders and as protective colloids for preventing scale formation in steam boiler and feed line systems^{3d}.

One of the largest applications for lignosulphonates is as an additive in the cement and concrete industries where they are used as dispersing agents to reduce the amount of water required to obtain the desired fluidity of the concrete mixtures. This results in concrete with increased density, higher compressive strength and better uniformity and durability^{3d,18,19}. Lignosulphonates can also be utilised as set retarding agents in applications where concrete needs to remain fluid over extended periods of time¹⁸. They

also serve as grinding aids for cements where their function is to reduce the agglomeration of the ground particles and to keep the surfaces of the grinding equipment clean and free^{5b}.

Lignosulphonates have also found their use in the oil and gas drilling industry. They act as thinners and dispersants in oil well – drilling muds where they are able to improve the flow properties of drilling fluids as well as being stable enough to facilitate drilling at high temperatures^{5b}. Their dispersive properties have also made them suitable for use as dispersants in ceramics, clays, pigments and insecticides^{3d}.

From the late 1920s until the present, lignosulphonates have been sprayed on roads to produce a hard durable surface and to control dust^{5b}. The dispersing and binding action of the lignosulphonates causes the natural clays of the soil to pack closer together forming an impermeable layer, keeping the road free of surface water^{5b,19}. In addition, lignosulphonates have also been used as binders in pellets for animal feed products, fertilisers and herbicides as well as in coal and charcoal briquettes^{5b,18,20}.

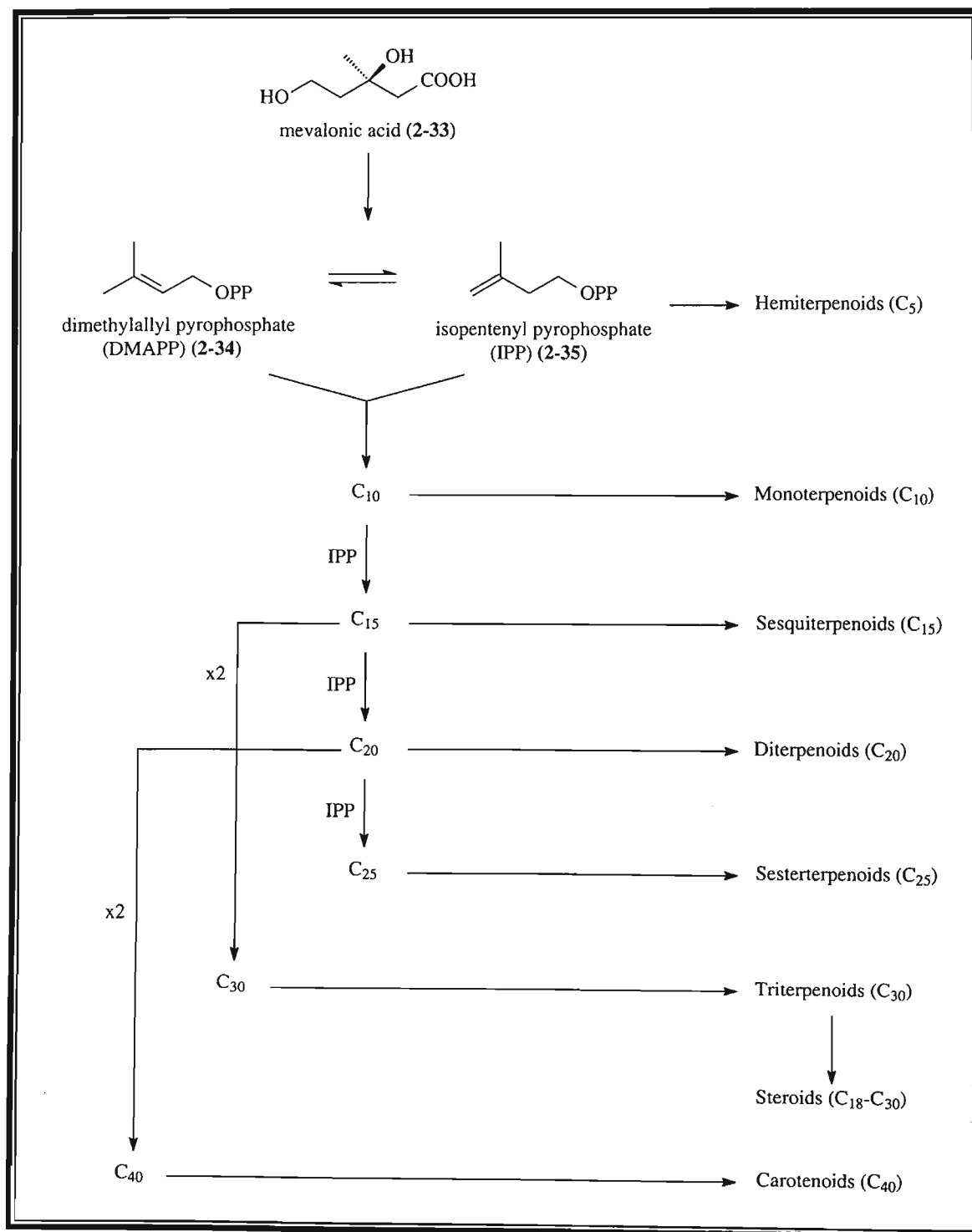
2.3 TRITERPENOIDS

2.3.1 Introduction

The terpenoids are amongst the most structurally diverse group of naturally – occurring compounds, which are widely distributed throughout the plant and animal kingdoms. They are composed of C₅ isoprene (2-methyl-1,3-butadiene) building units, which are derived from a biosynthetic pathway involving mevalonic acid (**2-33**) as the precursor.

The terpenoids can be subdivided into several classes according to the number of isoprene units linked in the carbon skeleton, *viz.* hemiterpenoids, C₅ (1 unit); monoterpenoids, C₁₀ (2 units); sesquiterpenoids, C₁₅ (3 units); diterpenoids, C₂₀ (4 units); sesterterpenoids, C₂₅ (5 units); triterpenoids, C₃₀ (6 units); and carotenoids, C₄₀ (8 units) as shown in Scheme 2.6. The isoprene units are linked according to the “isoprene rule” which means that they are joined together in a regular head – to – tail orientation. However, this rule is only strictly followed for up to five units. Many of the higher

terpenoids (C_{30} and C_{40}) display tail – to – tail linkages and some are modified further by cyclisation and/or rearrangement reactions.



Scheme 2.6: Classification of terpenoids^{11b}

Steroids are considered to be modified triterpenoids containing a tetracyclic ring structure. Both triterpenoids and steroids occur mainly as fatty acid esters and as glycosides but also in the free form. The major sterol found in mammals is cholesterol (C_{27}) (2-36), which acts as a precursor for other steroid structures such as sex hormones and corticosteroids. The main sterols found in plants are campesterol (2-37) and sitosterol (2-38), which are respectively 24-methyl and 24-ethyl analogues of cholesterol^{11c}. Stigmasterol (2-39) is another common plant sterol, containing unsaturation in the side chain, a feature never seen in mammalian sterols^{11c}.

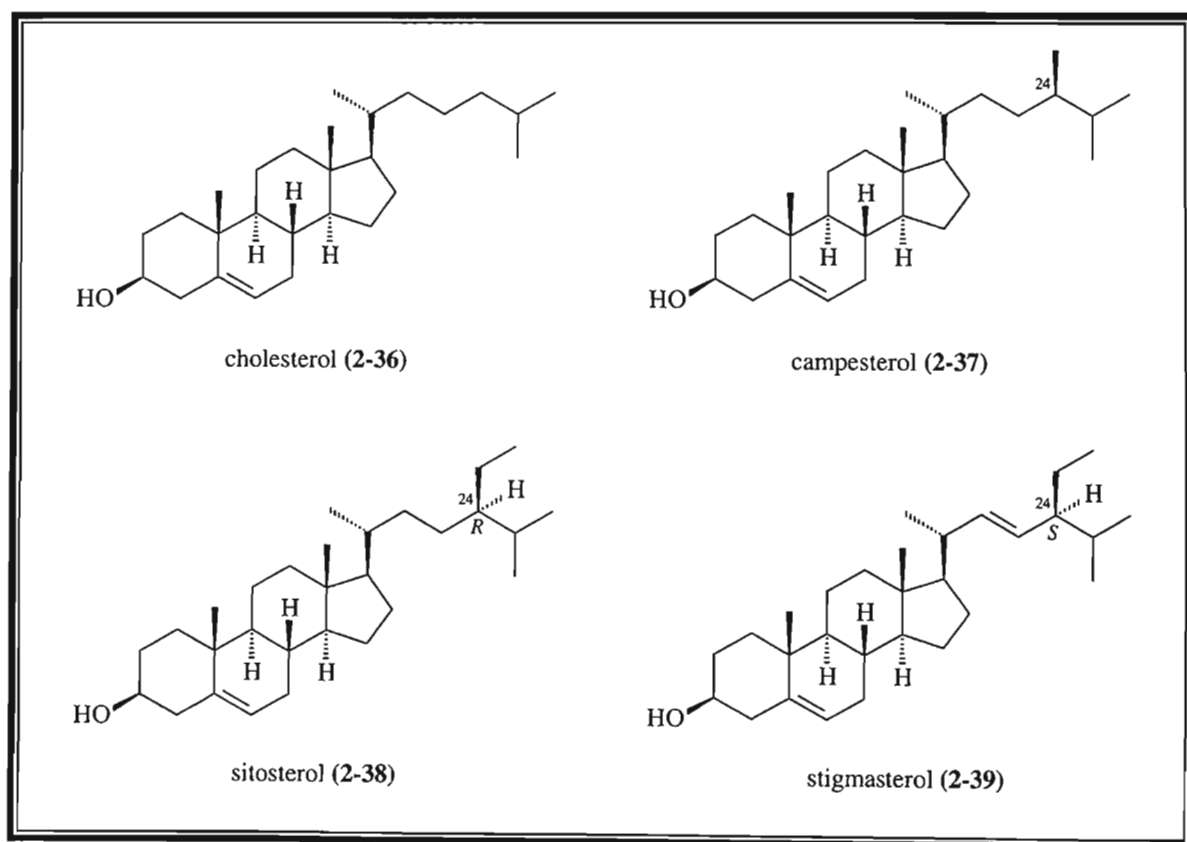
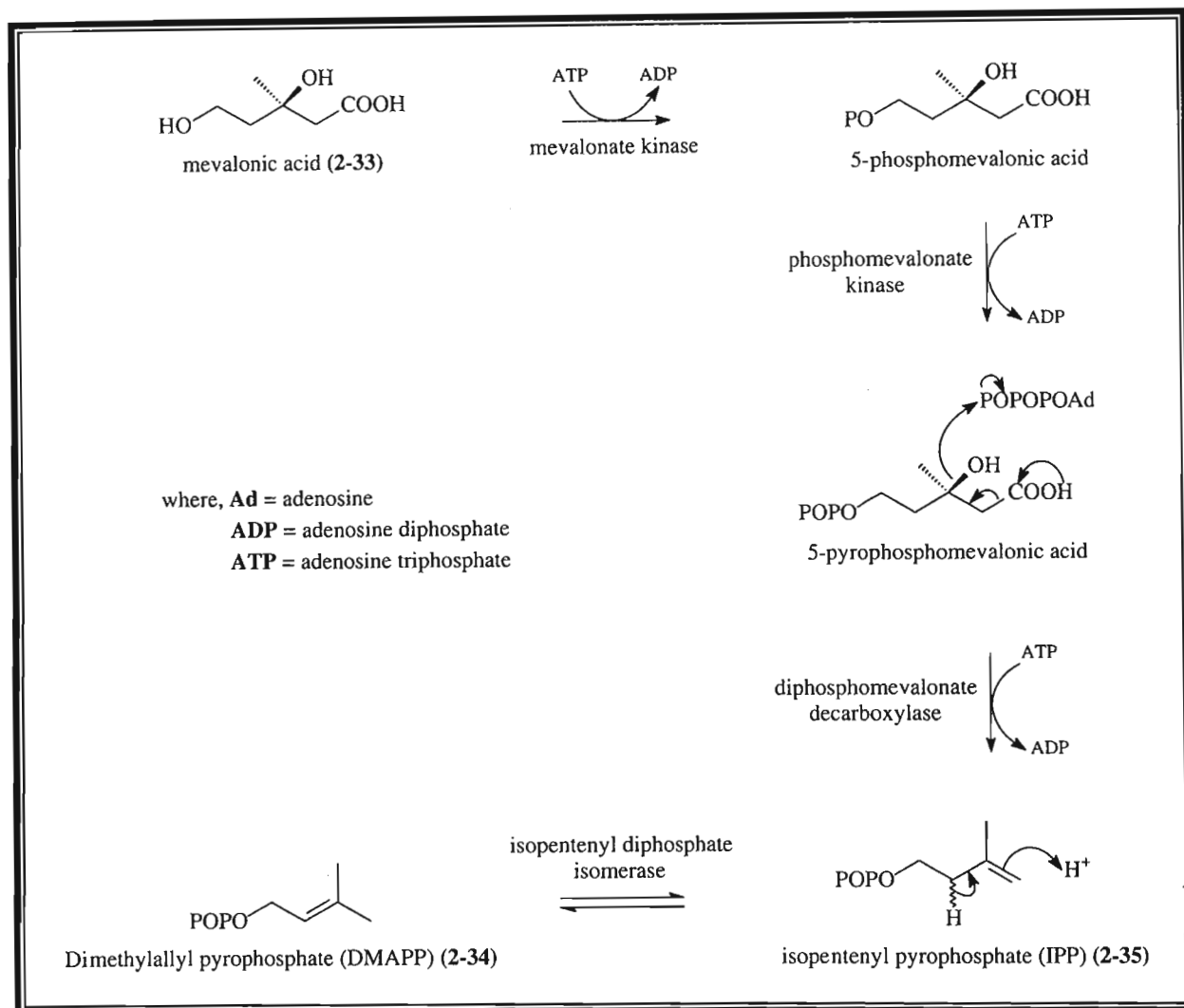


Figure 2.7: Structures of common mammalian and plant steroids

2.3.2 The Biosynthesis of Triterpenoids

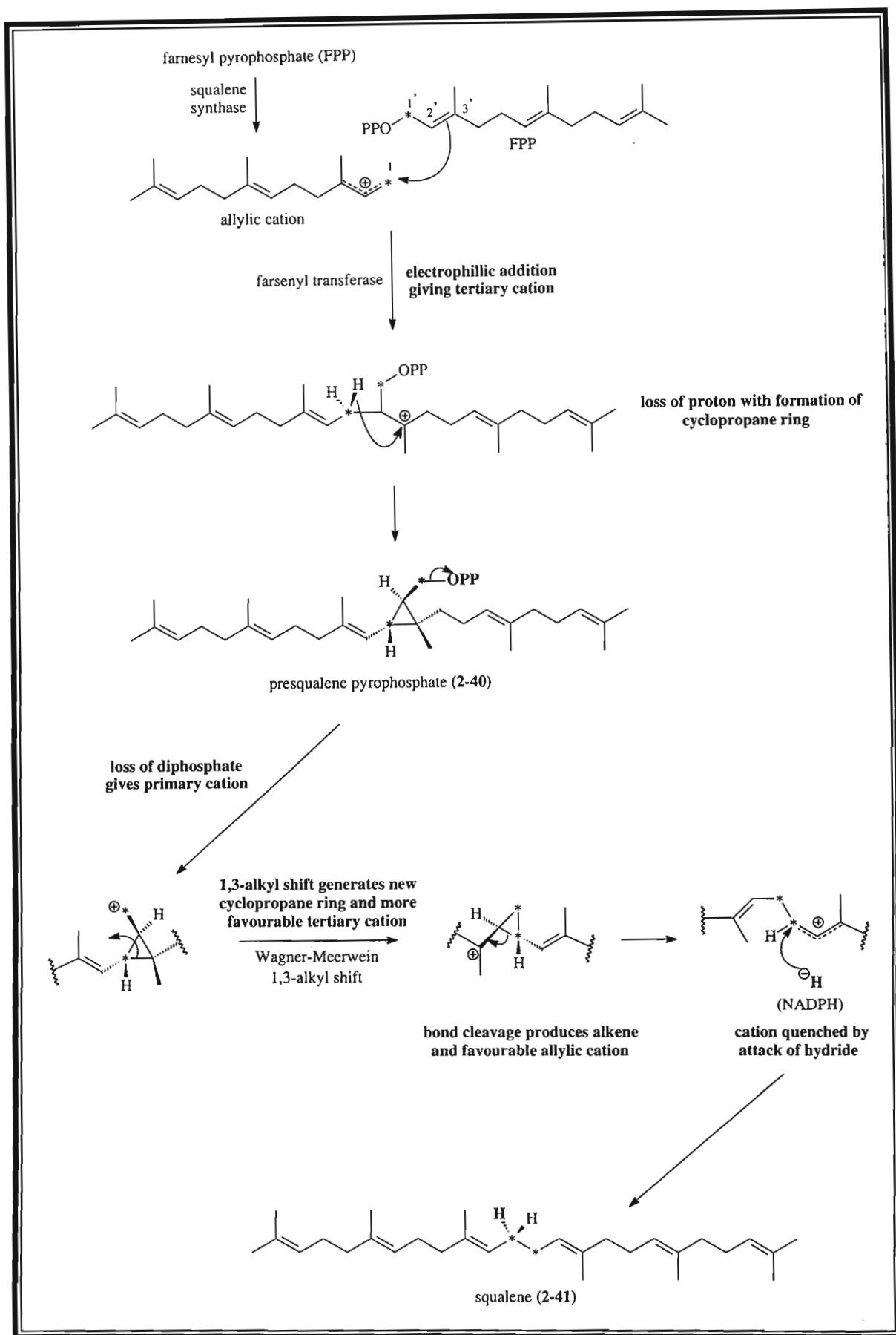
The compound isoprene itself, although naturally – occurring, is not involved in the biosynthesis of terpenoids. The biochemically active isoprene units are the diphosphate (pyrophosphate) esters, dimethylallyl pyrophosphate (DMAPP) (2-34) and isopentenyl pyrophosphate (IPP) (2-35)^{11b}. These compounds are derived from mevalonic acid (2-33),

which undergoes a series of enzyme – catalysed phosphorylation reactions as shown in Scheme 2.7.

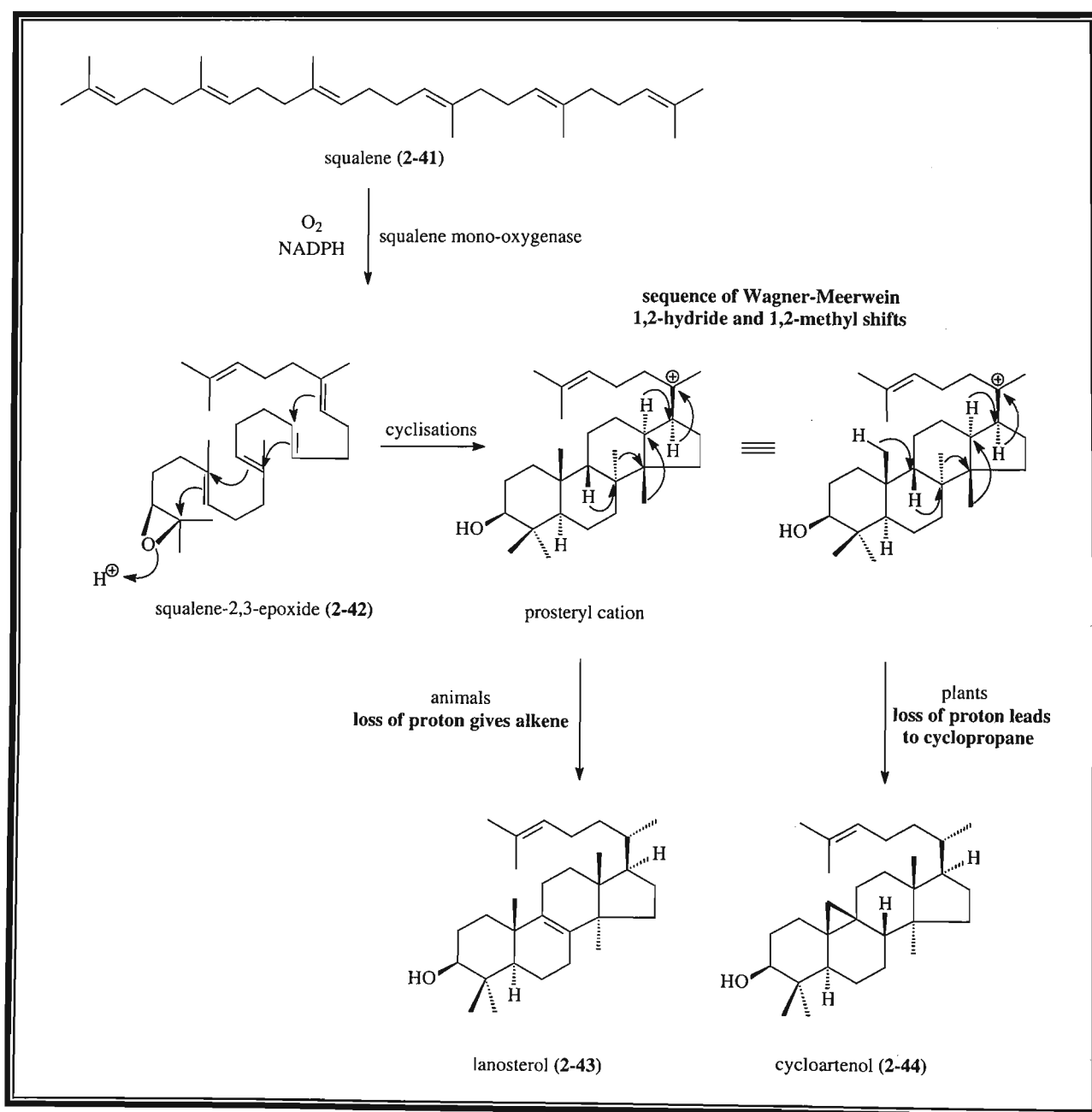


Scheme 2.7: Formation of DMAPP and IPP from mevalonic acid²¹

A series of enzyme – catalysed condensation reactions involving IPP (2-35) and DMAPP (2-34) leads successively to the formation of geranyl pyrophosphate (GPP), farnesyl pyrophosphate (FPP) and geranylgeranyl pyrophosphate (GGPP), which are the precursors for monoterpenoids (C_{10}), sesquiterpenoids (C_{15}) and diterpenoids (C_{20}) respectively. The NADPH – dependant enzyme farnesyl transferase joins two molecules of farnesyl pyrophosphate, tail – to – tail, to give presqualene pyrophosphate (2-40) (Scheme 2.8), which then undergoes diphosphate elimination and rearrangement to yield the hydrocarbon squalene (2-41). This reaction is catalysed by squalene synthase and is NADPH dependent^{11d}.

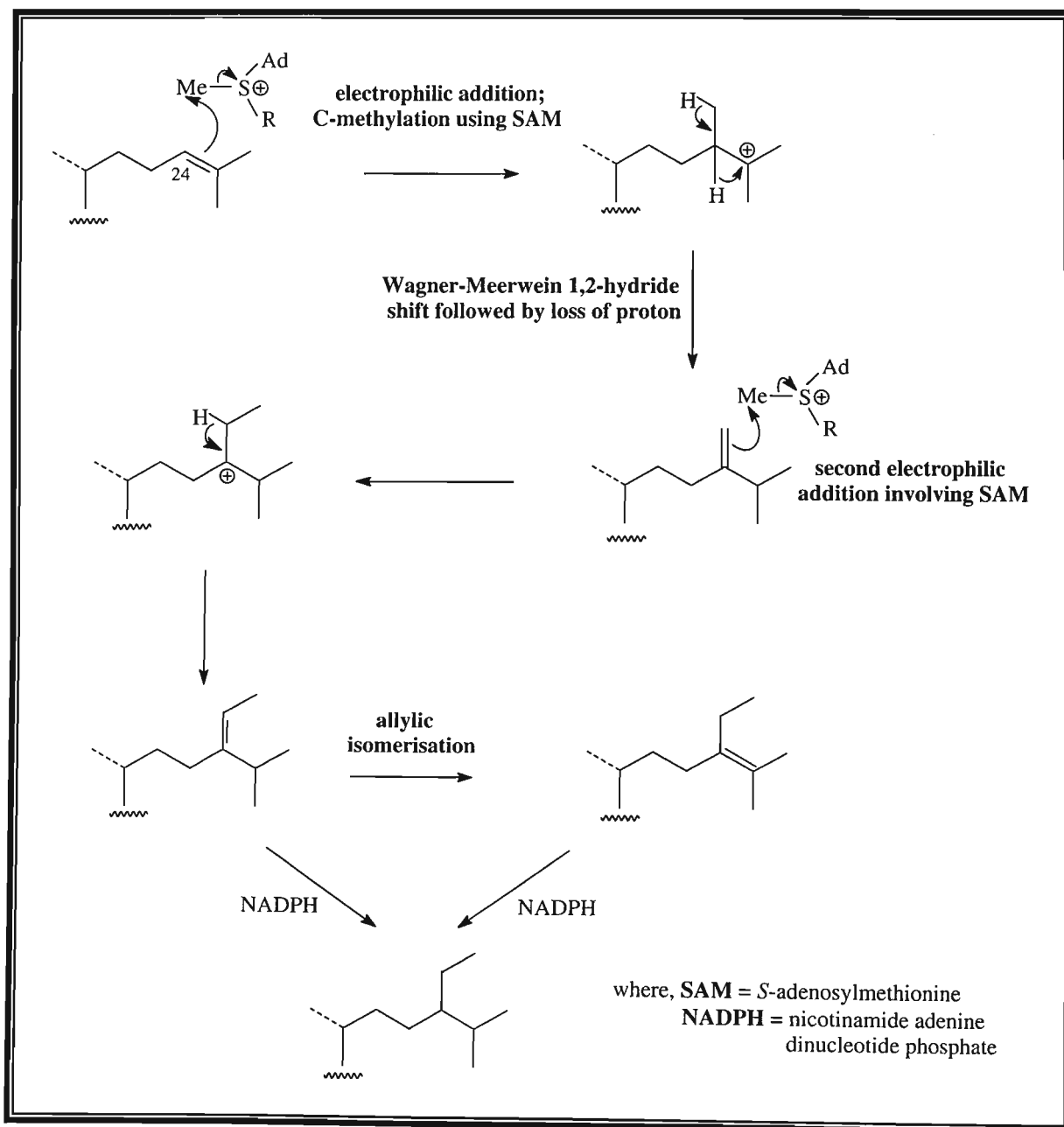
Scheme 2.8: The formation of squalene^{11d}

Squalene (**2-41**) was originally isolated from the liver oil of shark and is considered the precursor to the biosynthesis of triterpenoids and steroids. The enzymatic oxidation of squalene (**2-41**) forms the intermediate squalene-2,3-epoxide (**2-42**), which undergoes cyclisation to form compounds with C₃₀ skeleta. Depending on the conformation adopted by squalene-2,3-epoxide (**2-42**) prior to cyclisation, it can form either the animal triterpenoid, lanosterol (**2-43**) or the plant triterpenoid, cycloartenol (**2-44**)^{11d} (Scheme 2.9).



Scheme 2.9: Cyclisation of squalene epoxide to form lanosterol and cycloartenol^{11d}

As mentioned earlier, the main plant sterols contain an additional one – carbon (methyl) or two – carbon (ethyl) group on the side chain attached at C-24^{11c}. These extra carbon substituents originate from *S*-adenosylmethionine (SAM). The double bond on the side chain of cycloartenol (**2-44**) undergoes methylation *via* SAM to yield a carbocation, which undergoes a hydride shift and loss of a proton to generate the 24 - methylene side – chain. This is then reduced to the 24–methyl by allylic isomerisation and together with the simultaneous ring opening of the cyclopropane ring, forms the desired sterols (Scheme 2.10).



Scheme 2.10: Mechanism showing the alkylation of C-24^{11c}

2.3.3 The Uses of Plant Sterols

Studies have proven that diets rich in vegetables and fruits help prevent the development of various types of cancers, cardiovascular diseases, diabetes and other common ailments. One of the main substances responsible for these health promoting effects are the plant sterols, which are present as important metabolites in all higher plants, ferns and algae²².

The initial research into the biological importance of sterols began in the 1930's in Germany but it was only in the 1950's when D.W. Petersen from the University of California first discovered that phytosterols actually block the absorption of cholesterol in humans. Further studies have shown that the sterols, particularly β -sitosterol, stigmasterol and campesterol, combine with cholesterol contained in high – fat foods in the intestine of humans to form a crystalline matrix, which cannot be absorbed and is easily excreted by the body²³.

Plant sterols are also known to regulate the immune system by promoting the activity of cytotoxic cells, which are essential in the defence of viral and bacterial diseases, such as tuberculosis, in the body. In addition, these compounds have also been found to possess strong anti – inflammatory and anti – pyretic (fever – reducing) properties²⁴. Current research is based on investigating the benefits of plant sterols on other diseases such as benign prostatic hyperplasia, tumours in the colon, psoriasis, rheumatoid arthritis some cancers, coronary disease, and even HIV and AIDS²³.

2.4 REFERENCES

1. Gullichsen, J. and Paulapuro, H., 2000, *Forest Products Chemistry*, Fapet Oy : Helsinki, p12(a), 39(b), 81-83(c).
2. Smook, G.A., 1992, *Handbook for Pulp & Paper Technologists*, 2nd ed., Angus Wilde Publications Inc. : Vancouver, p17.
3. Fengel, D. and Wegener, G., 1983, *Wood : Chemistry, Ultrastructure and Reactions*, Walter de Gruyter & Co. : Berlin, p15(a), 132(b), 282-283(c), 546-548(d).
4. Sjöström, E., 1981, *Wood Chemistry – Fundamentals and Applications*, Academic Press : New York, p13-16(a), 112-114(b).
5. Sarkanen, K.V. and C.H. Ludwig, 1971, *Lignins – Occurrence, Formation, Structure and Reactions*, Wiley – Interscience : New York, p1(a), 846-859(b).
6. Higuchi, T., Kirk, T.K. and Chang, H-M., 1980, *Lignin Biodegradation : Microbiology, Chemistry and Potential Applications*, Vol. 1, CRC Press : Florida, p2.
7. Wallis, A.F.A., 1998, Structural Diversity in Lignans and Neolignans, In : *Lignin and Lignan Biosynthesis*, Lewis, N.G. and Sarkanen, S. (Eds), American Chemical Society Symposium Series 697, American Chemical Society : Washington, DC, p323-333.
8. Cheplogoi, P.K., 2001, *Extractives from the Meliaceae, Kirkiaceae and Rutaceae*, PhD Thesis, School of Pure and Applied Chemistry, University of Natal, Durban, South Africa, p96.
9. Lewis, N.G., Sarkanen, S. and Davin, L.B., 1998, Lignin and Lignan Biosynthesis : Distinctions and Reconciliations, In : *Lignin and Lignan Biosynthesis*, Lewis, N.G. and Sarkanen, S. (Eds), American Chemical Society Symposium Series 697, American Chemical Society : Washington, DC, p1-27.

10. Rouhi, A. M., 2000, Lignin and Lignan Biosynthesis, *Chemical and Engineering News*, **78**, 29-32.
11. Dewick, P.M., 2002, *Medicinal Natural Products : A Biosynthetic Approach*, 2nd ed., John Wiley & Sons Ltd : England, p130-137(a), 167-172(b), 252-254(c), 212-219(d).
12. Davin, L. B. and Lewis, N. G., 2000, Dirigent Proteins and Dirigent Sites Explain the Mystery of Specificity of Radical Precursor Coupling in Lignan and Lignin Biosynthesis, *Plant Physiology*, **123**, 453-461.
13. Rouhi, A. M., 2001, Only Facts Will End Lignin War, *Chemical and Engineering News*, **79**, 52-56.
14. Davin, L. B., Wang, H. B., Crowell, A. L., Bedgar, D. L., Martin, D. M., Sarkanen, S. and Lewis, N. G., 1997, Stereoselective Biomolecular Phenoxy Radical Coupling by an Auxiliary (Dirigent) Protein Without an Active Center, *Science*, **275**, 362-366.
15. MacRae, W. D. and Towers, G. H. N., 1984, Biological Activities of Lignans, *Phytochemistry*, **23**, 1207-1220.
16. Ingruber, O. V., Kocurek, M. J. and Wong, A., 1985, *Pulp and Paper Manufacture : Vol. 4 Sulphite Science and Technology*, Joint Textbook Committee of the Paper Industry : Montreal, p31-34.
17. <http://www.r-w-d.co.uk/Lignosulphonates.html>
18. <http://www.lignin.info.htm>
19. <http://www.fraserpapersparkfalls.com>
20. Lin, S.Y. and Lebo, S.E., Jr., 1995, *Lignin, Kirk – Othmer Encyclopedia of Chemical Technology*, 4th ed., Volume 14, p310.
21. <http://www.chem.qmw.ac.uk/iubmb/enzyme/reaction/terp/terp.html>

22. Pegel, K.H., 1997, The Importance of Sitosterol and Sitosterolin in Human and Animal Nutrition, *South African Journal of Science*, **93**, 263-268.
23. <http://www.naturleaf.com>
24. Gupta, M.B., Nath, R., Srivastava, N., Shanker, K., Kishore, K. and Bhargava, K.P., 1980, Anti – Inflammatory and Antipyretic Activities of β -sitosterol, *Planta Medica*, **39**, 157-163.

CHAPTER 3 : RESULTS AND DISCUSSION

During acid bisulphite pulping, delignification is achieved by reacting the wood chips with sulphurous acid, thus transforming the insoluble lignin into lignosulphonate, which is completely soluble in water and easily eliminated into the effluent streams. These effluent streams, therefore, contain a concentrated mixture of predominantly lignosulphonates and sugars. Lignosulphonates form a potentially valuable source of chemicals with various uses (Refer to Section 2.2.3 in Chapter 2), thus their extraction in pure form from SAPPI SAICCOR'S effluent could prove to be commercially advantageous to the company.

The two streams of effluent resulting from the batch cooking of wood chips, *viz.* the calcium spent liquor and the magnesium pulp condensate, make up the bulk of the total waste effluent pumped out to sea. Therefore, this project was focused on characterising the water – soluble compounds contained in these two effluent streams only.

3.1 THE EXTRACTION OF LIGNOSULPHONATES

An examination of early literature revealed that 2-naphthylamine was used as the precipitant in the analysis of lignosulphonates from sulphite pulp mill effluents¹. However, the Food and Drug Administration (FDA) USA and the UK Carcinogenic Substances Regulations declared this chemical a carcinogen^{1,2}. Later references mentioned the use of long – chain aliphatic amines dissolved in a suitable organic solvent to precipitate out lignosulphonates from sulphite effluents³⁻⁵. These amines are believed to act as “carriers” capable of reacting reversibly with the lignosulphonates to yield a product that is selectively soluble in the organic phase rather than the aqueous phase and can be simply precipitated from the spent liquor. Studies have shown that more polar organic solvents give a higher degree of extraction and also that primary amines are more efficient than secondary or tertiary amines³.

An extraction of lignosulphonates from the aqueous portion of the calcium spent liquor was initially attempted using the method described by Kontturi and Sundholm as well as Lin^{3,4}. The first step in this method involved complexing the solubilised lignosulphonates with a long – chain aliphatic amine to form a water – insoluble lignosulphonate acid –

amine complex. This complex was then extracted into an organic solvent to separate it from other non – lignin contaminants. The lignosulphonates were thereafter regenerated, in the form of a salt, into the aqueous phase by the addition of an alkali such as sodium hydroxide (NaOH). Details of the extraction procedure can be found in Section 4.2.2.1 of Chapter 4.

A brown – coloured precipitate with a mass of 0.81g (w/w % = 1.05 %) was obtained from the extraction of the aqueous portion of the calcium spent liquor effluent stream. The precipitate was found to be insoluble in dichloromethane (MeCl₂) and methanol (MeOH) but soluble in water. A solution of the sample dissolved in water was left to air evaporate producing white square – shaped crystals resembling sugar granules. The precipitate was subjected to an ignition test by heating a sample on a crucible lid. The sample melted easily forming a black residue. No smoke was given off but a characteristic odour of burnt sugar was produced. A Lassaigne sodium fusion test performed on the precipitate gave a positive result for the presence of sulphur (Refer to Section 4.2.3 of Chapter 4 for details of test).

The ¹H NMR spectrum (**Spectrum i**) of the precipitate was run in deuterated water (D₂O). After saturation of the solvent peak the spectrum showed peaks between δ 3.0 ppm and δ 5.5 ppm indicating the presence of sugar molecules. A few peaks could also be seen in the aromatic region of the spectrum (δ 6.5 ppm – δ 7.0 ppm). This suggested that the precipitate contained a mixture of aromatic compounds and sugar molecules with the proportion of sugars being much greater. The ¹³C NMR spectrum (**Spectrum ii**) showed peaks between δ 60 ppm and δ 100 ppm, which confirmed the presence of sugars in the sample. No separation was observed when a solution of the sample was run on a thin layer chromatography plate. A preparative thin layer chromatography plate separation (both normal and reverse phase) was also unsuccessful.

The infrared spectrum (**Spectrum iii**) displayed a strong distinct band at 3416 cm⁻¹, which was characteristic of hydroxyl (O-H) stretching. The bands between 2800 cm⁻¹ and 3000 cm⁻¹ were due to C-H stretching whilst the bands found at about 1600 cm⁻¹ – 1400 cm⁻¹ were characteristic of C=C stretching of an aromatic ring. The broad bands between 1140 cm⁻¹ and 1000 cm⁻¹ indicated the presence of sugar or polysaccharide moieties in

the sample⁶. The appearance of a shoulder peak at 1209 cm^{-1} confirmed the presence of sulphonic acid groups in the sample⁶.

An ultraviolet absorption spectrum (**Spectrum iv**) of the precipitate dissolved in water showed a high absorption maximum at approximately 210 nm and a smaller less pronounced absorption maximum at approximately 280 nm. These values compared favourably with the ultraviolet spectra shown in literature for pine, beech and spruce wood lignosulphonates⁶.

From the above results it could be concluded that the brown precipitate obtained from the extraction of the calcium spent liquor contained a mixture of predominantly sugars and small amounts of lignosulphonates.

An analogous extraction of lignosulphonates from the aqueous phase of the calcium spent liquor was attempted using the method described by Luthe and Lewis^{7,8}. This procedure involved successive complexation and extraction of the lignosulphonates with the amine dissolved in the organic solvent. The pH of the aqueous phase was adjusted prior to each complexation/extraction step. The resulting organic layers were combined and treated with an alkali (NaOH) to recover the lignosulphonates. Details of this extraction procedure can be found in Section 4.2.2.2 of Chapter 4.

A yellowish – brown crystalline material with a mass of 5.53 g (w/v % = 1.23 %) was obtained from this extraction method. The crystals were found to be soluble only in water. The Lassaigne sodium fusion test carried out on a sample of the crystals gave a positive result for the presence of sulphur. The infrared spectrum (**Spectrum v**) showed a band at 1207 cm^{-1} , which confirmed the presence of sulphonic acid groups in the sample.

The ^1H NMR spectrum (**Spectrum vi**) showed peaks between δ 3.0 ppm and δ 5.0 ppm, corresponding to sugar molecules and fewer peaks in the aromatic region between δ 6.5 ppm and δ 7.0 ppm. Once again, this suggested that the sample contained a mixture of sugars with a low concentration of aromatics present. The ^{13}C NMR spectrum (**Spectrum vii**) displayed peaks between δ 60.0 ppm and δ 104.0 ppm indicating the presence of sugars in the sample.

Poor separation was obtained on thin layer chromatography plates and preparative thin layer chromatography plates.

The crystalline material produced from the second liginosulphonate extraction procedure also contained a mixture of liginosulphonates with sugars. The isolation of pure liginosulphonates has been known to be difficult due to the hydrophilic nature of these compounds. All structural analysis and manipulations have to be performed in aqueous media. Luthe and Lewis, therefore, developed a method to derivatise liginosulphonates thus rendering them organic soluble.

An attempt was made to try and derivatise the yellowish – brown crystalline material containing the mixture of liginosulphonates and sugars. The method described by Luthe and Lewis involved first converting the liginosulphonate salt into its free acid form and then treating it with freshly prepared ethereal diazomethane to form the corresponding sulphonic acid methyl esters^{7,8}. Details on the preparation of diazomethane as well as the actual methylation procedure can be found in Section 4.2.4 of Chapter 4.

A dark brown precipitate of mass 205 mg was obtained after evaporation of the ether. The precipitate was now found to be partially soluble in water but completely soluble in methanol. The ¹H NMR spectrum (**Spectrum viii**), run in deuterated methanol (CD₃OD), appeared different from the original spectrum. It showed proton resonances between δ 3.0 ppm – δ 5.0 ppm, weak resonances between δ 6.2 ppm – δ 7.0 ppm and a doublet at δ 2.7 ppm. However, the spectrum did not show any methyl ester resonances, which usually appear as strong peaks in the region of δ 4.0 ppm. The ¹³C NMR spectrum (**Spectrum ix**) showed peaks at δ 154 ppm and at δ 108 ppm. Three strong peaks were seen at δ 80 ppm and a few peaks were observed below δ 60 ppm. It was initially thought that the sugar molecules were methylated instead of the sulphonic acid groups but methylation with diazomethane has been known not to work on sugars⁹.

Luthe and Lewis reported no difficulties when using ethereal diazomethane as a derivitising agent^{7,8}. Their compounds contained electron – withdrawing substituents, such as carbonyl groups or sulphonic acid groups, at the benzylic position, which facilitated methylation of the phenolic hydroxyl groups. However, previous researchers have reported that derivitisation using diazomethane was unsuccessful¹⁰.

The aqueous phase of the calcium spent liquor was then subjected to an acid hydrolysis using concentrated hydrochloric acid in an attempt to hydrolyse the sugars (Refer to Section 4.2.8 of Chapter 4 for details of hydrolysis procedure). However, this resulted in the de – polymerisation of the lignin molecule releasing more lignin monomers and dimers into the organic phase. These organic compounds were extracted into chloroform and characterised. Column chromatography and thin layer chromatography using varying ratios of solvents were carried out in isolating and purifying these compounds. The structures of these compounds were determined using NMR and infrared spectroscopy and gas chromatography – mass spectrometry (GC – MS), which will be discussed in this chapter.

3.2 HYDROLYSIS OF THE CALCIUM SPENT LIQUOR EFFLUENT

Hydrolysis of the aqueous phase of the calcium spent liquor effluent stream yielded a number of organic compounds such as two isomers of syringaresinol, *meso*-yangambin, sinapyl aldehyde, methoxyeugenol, β -oxysinapyl alcohol, acetovanillone, syringaldehyde, vanillin and a common plant triterpenoid, β -sitosterol.

3.2.1 Structural Elucidation of Compound 1: *epi*-syringaresinol

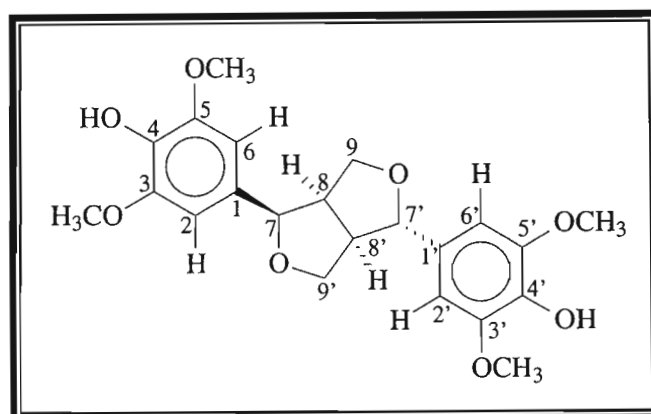


Figure 3.1: Structure of compound 1, *epi*-syringaresinol

The mass spectrum of compound 1 (**Spectrum 1.1**) showed a molecular ion $[M^+]$ peak at m/z 418, which corresponded to a molecular formula of $C_{22}H_{26}O_8$ (calculated molar mass = 418.442). The number of carbon atoms corresponded to twice that of a lignin monomer and therefore suggested that compound 1 had a dimeric structure, indicating the presence of a lignan. The peak at m/z 210 corresponded to the splitting of the dimer to form a monomer. The peak at m/z 182 suggested the loss of an ethylene group from the propyne side chain resulting in the formation of syringaldehyde and the loss of a further hydrogen atom from this species lead to the formation of the base peak at m/z 181¹¹.

The infrared spectrum of compound 1 (**Spectrum 1.2**) showed a broad band at 3425 cm^{-1} indicating the presence of a hydroxy group substituent. The bands at 2943 cm^{-1} and 2850 cm^{-1} were typical of C-H stretching whilst the bands at 1612 cm^{-1} and 1524 cm^{-1} corresponded to C=C stretching of an aromatic ring. The other strong peak at 1113 cm^{-1} was due to C-O stretching and the bands between 1350 cm^{-1} and 1300 cm^{-1} were typical of syringyl ring breathing¹².

The ^1H NMR spectrum (**Spectrum 1.4**) showed a single strong peak at δ 6.57 ppm, integrating to two protons, which was characteristic of two equivalent aromatic ring proton resonances (H-2 and H-6). The other strong singlet at δ 3.87 ppm was due to the methoxy group protons. The two singlets at δ 5.53 ppm and δ 5.51 ppm integrating to one proton each corresponded to the protons of the hydroxy groups on each aromatic ring. The doublets at δ 4.82 ppm (1H, d, $J = 5.31\text{ Hz}$) and δ 4.39 ppm (1H, d, $J = 7.14\text{ Hz}$)

corresponded to oxygenated methine group protons. These protons have shifted downfield due to the deshielding effect of the attached electronegative oxygen atoms of the two dihydrofuran rings and the benzylic effect of the aromatic rings and may be attributed to H-7 and H-7' respectively. The proton resonances at δ 2.88 ppm (1H, m) and δ 3.30 ppm (2H, m) corresponded to H-8' and H-8 respectively. The doublet at δ 4.12 ppm (1H, d, $J = 9.71$ Hz) was due to one of the oxygenated methylene protons at C-9' that had shifted downfield. Two methylene proton resonances due to one of the protons at C-9 and one at C-9' occurred at δ 3.84 ppm (2H, m), superimposed and hidden beneath the methoxy group proton resonance. The fourth methylene proton signal was located at δ 3.30 ppm, superimposed with the H-8 signal.

The ^{13}C NMR spectrum (**Spectrum 1.5**) showed two methine carbon resonances at δ 50.0 ppm and δ 54.5 ppm corresponding to C-8 and C-8' respectively, two oxygenated methylene group carbons at δ 69.6 ppm and δ 70.9 ppm corresponding to C-9 and C-9' respectively and two oxygenated methine group carbons at δ 82.1 ppm and δ 87.8 ppm corresponding to C-7 and C-7' respectively. Once again, the oxygenated carbon resonances were deshielded and hence occurred further downfield. The two strong sharp peaks at δ 102.2 ppm and δ 102.7 ppm were due to the protonated carbons of the aromatic rings. The strong peak at δ 56.3 ppm was characteristic of methoxy group carbon resonances. The carbon resonances between δ 129 ppm and δ 147 ppm were due to the fully substituted carbons of the aromatic rings and were assigned using the HMBC NMR spectrum.

The integration in the ^1H NMR spectrum suggested that both aromatic rings were symmetrical, however, the doubling of the non – aromatic peaks in the ^{13}C NMR spectrum indicated that the molecule as a whole was not symmetrical.

The relative stereochemistry of the molecule was determined from the NOESY NMR spectrum (**Spectrum 1.8**). Correlations were seen from the aromatic protons to the methoxy group protons and the benzylic protons at positions 7 and 7' as well as the protons of the methine groups at positions 8 and 8'. Weak NOESY correlations to the protons of the methylene groups at positions 9 and 9' were also observed. The methine proton at C-7 was assigned the relative stereochemistry of α and it showed NOESY correlations to one of the methylene protons at C-9' and one at C-9 as well as the methine

proton at position 8. This suggested that one of the protons at C-9' and one at C-9 as well as the proton at C-8 were all on the same side of the molecule as H-7 α and could therefore be placed at the α position in the molecule. A coupling constant of 5.31 Hz for the H-7 doublet also suggested a *cis* configuration between the protons at C-7 and C-8. The methine proton at C-7' did not show any correlation to any of the protons placed in the α position which implied that it must be in the β position. NOESY correlations from H-7' to the second methylene protons at H-9 β and H-9' β suggested that these three protons were on the same side of the molecule, which confirmed that H-7' is in the β position. The H-8' proton did not correlate to H-7' β and was therefore assigned the α position. Weak correlations in the NOESY NMR spectrum from the C-8' proton to H-9' α and H-9 α confirmed that it was in the α position. Table 3.1 and Figure 3.2 show the relevant NOESY correlations. From the above analysis the stereochemistry of the fused tetrahydrofuran rings can be assigned as 7R, 7'S, 8R and 8'R.

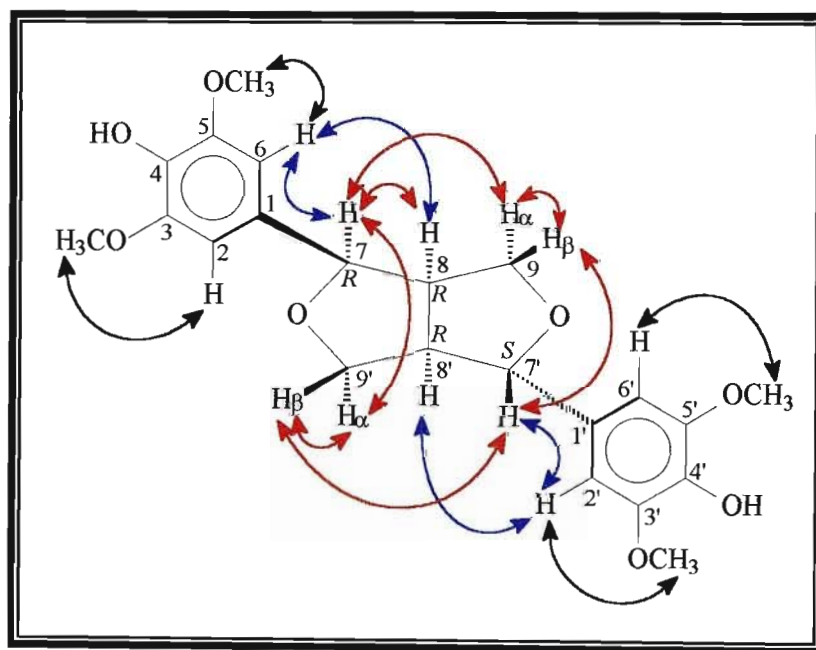


Figure 3.2: NOESY correlations of compound 1

The HMBC NMR spectrum (**Spectrum 1.7**) was used to confirm the above assignments and to assign the remaining fully substituted carbon resonances in the aromatic rings. The carbon peak at δ 147.0 ppm showed strong 3J correlations to the methoxy group protons as well as to the protons of the hydroxy groups. 2J correlations to the aromatic proton resonances were also observed. Therefore, that carbon peak was assigned to the equivalent carbon atoms with the attached methoxy groups on both aromatic rings (C-3,

C-5 and C-3', C-5'). Coupling (3J) was also seen from the carbon peaks at δ 133.6 ppm and δ 134.3 ppm to the corresponding adjacent aromatic protons and was assigned to C-4 and C-4' respectively. The peaks at δ 129.4 ppm and δ 132.1 ppm were assigned to C-1 and C-1' respectively because they showed HMBC correlations to the adjacent aromatic protons and to the adjacent methine protons. Figure 3.3 shows the relevant HMBC correlations within the aromatic rings (black arrows), within the tetrahydrofuran rings (blue arrows) and between the aromatic rings and the tetrahydrofuran rings (red arrows).

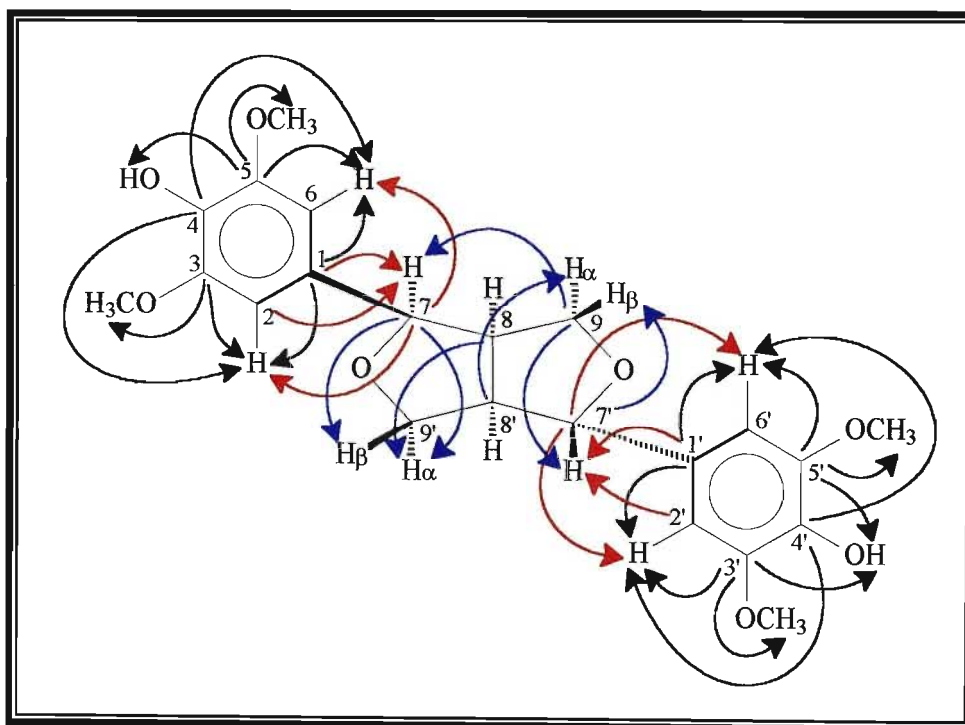


Figure 3.3: HMBC correlations (C→H) of compound 1

The COSY NMR spectrum (**Spectrum 1.9**) further supported the above structure. A strong correlation from the methine proton at position 8 to the protons of both the oxygenated methine (H-7) and methylene groups (2H-9) were observed. This confirmed that the methine group at position 8 was between the methine and methylene groups at positions 7 and 9 respectively. A COSY correlation was also seen between the two non-equivalent methylene protons at C-9. The COSY NMR spectrum also showed coupling between the aromatic protons and the protons of the methoxy groups, which confirmed that the aromatic protons were adjacent to the methoxy groups on the aromatic ring (Figure 3.4).

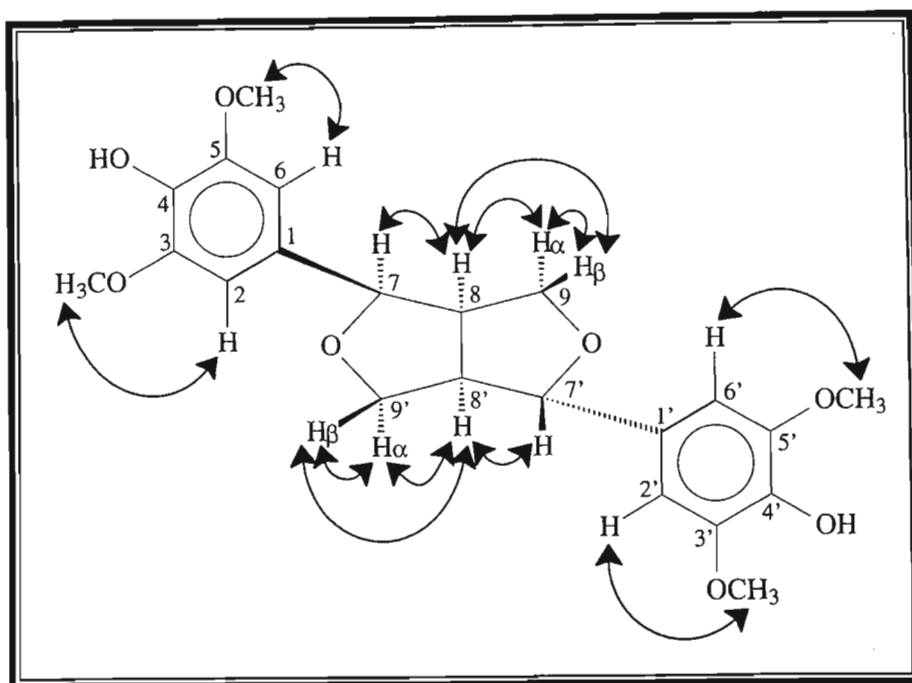


Figure 3.4: COSY correlations of compound 1

Table 3.1: NMR spectral data for compound 1 (400MHz, CDCl₃)

| Position | ¹ H (ppm) | ¹³ C (ppm) | HMBC (C→H) | NOESY | COSY |
|----------------|-------------------------|-----------------------|---|--|--------------------------|
| 1 | | 129.4 | H-7 (² J), H-2/6 (² J) | | |
| 2 | 6.57 s | 102.2 | H-7, H-6 | OCH ₃ , H-7, H-9 _{α/β} , H-8 | H-7, OCH ₃ |
| 3 | | 146.9 | OCH ₃ , OH, H-2/6 (² J) | | |
| 4 | | 133.6 | OH (² J), H-2/6 | | |
| 5 | | 146.9 | OCH ₃ , OH, H-2/6 (² J) | | |
| 6 | 6.57 s | 102.2 | H-7, H-2 | OCH ₃ , H-7, H-9 _{α/β} , H-8 | H-7, OCH ₃ |
| 7 | 4.82 d (J = 5.31 Hz) | 82.1 | H-8', H-8 (² J), H-9, H-9', H-2/6 | H-2/6, H-9 _α , H-9' _α , H-8 | H-8, H-2/6 |
| 8 | 3.30 m | 50.0 | H-9', H-9 (² J), H-7 (² J) | H-2/6, H-7, H-9 _α , H-9' _α , H-8' | H-9 _{α/β} , H-7 |
| 9 _α | 3.84 m | 69.6 | H-8 (² J), H-7 | H-7, H-9 _β , H-8, H-8', H-2/6 | H-9 _β , H-8 |
| 9 _β | 3.30 m | 69.6 | H-8 (² J), H-7 | H-2/6, H-7', H-9 _α | H-9 _α , H-8 |

| | | | | | |
|------------------|-------------------------|-------|--|-----------------------------------|------------------------|
| 1' | | 132.1 | H-8', H-7' (² J), H-2'/6' (² J) | | |
| 2' | 6.57 s | 102.7 | H-7', H-6' | H-7', H-8', H-9'α/β | H-7', OCH ₃ |
| 3' | | 147.1 | OCH ₃ , OH, H-2'/6' (² J) | | |
| 4' | | 134.3 | OH (² J), H-2'/6' | | |
| 5' | | 147.1 | OCH ₃ , OH, H-2'/6' (² J) | | |
| 6' | 6.57 s | 102.7 | H-7', H-2' | H-7', H-8', H-9'α/β | H-7', OCH ₃ |
| 7' | 4.39 d (J = 7.14 Hz) | 87.9 | H-8' (² J), H-9, H-9', H-2'/6' | H-2'/6', H-9'β, H-9β | H-8', H-2'/6' |
| 8' | 2.88 m | 54.5 | H-9, H-9' (² J), H-7' (² J) | H-2'/6', H-9'α, H-9α, H-8 | H-9'α/β, H-7' |
| 9'α | 3.84 m | 70.9 | H-8, H-7' | H-7, H-9'β, H-8, H-8', H-2'/6' | H-9'β, H-8' |
| 9'β | 4.13 d (J = 9.71 Hz) | 70.9 | H-8, H-7' | H-7', H-9'α, H-2'/6' | H-9'α, H-8' |
| OCH ₃ | 3.87 s | 56.3 | | H-2/6, H-2'/6', OH | H-2/6, H-2'/6' |
| OH | 5.52 s | | | OCH ₃ | |

Note: All HMBC correlations are ³J correlations unless otherwise stated.

Compound 1 was isolated as a white crystalline solid and was identified as the lignan known as (+)-*epi*-syringaresinol, which had been previously isolated from *Liriodendron tulipifera* and is a degradation product of birch lignin¹³. The ¹H and ¹³C NMR data compared favourably to the values obtained from literature¹³. It was the major component of the hydrolysed aqueous phase of the calcium spent liquor effluent stream with an approximate concentration of 0.014 g/L.

3.2.2 Structural Elucidation of Compound 2: *meso*-syringaresinol

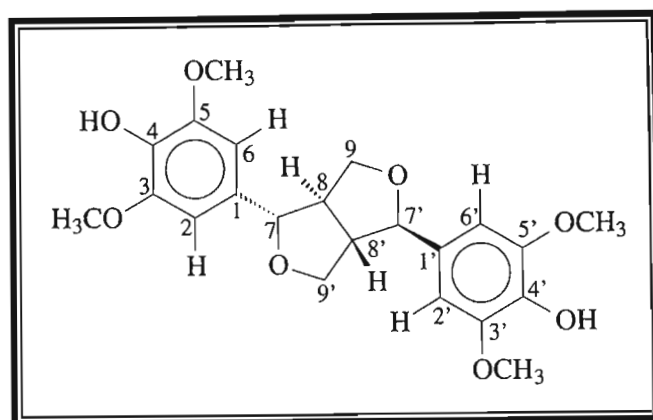


Figure 3.5: Structure of compound 2, *meso*-syringaresinol

Compound 2 was isolated as a mixture with compound 1 (*epi*-syringaresinol). It was identified as a stereoisomer of compound 1 in that it had the same molecular structure and formula but the stereochemistry at the chiral centres of the two tetrahydrofuran rings were different. Attempts to separate the mixture using column and thin layer chromatography were unsuccessful[†]. However, the structure of compound 2 was fully elucidated by subtracting the peaks of the known compound, *epi*-syringaresinol, and also by comparing the NMR data to that found in literature.

The mass spectrum of compound 2 (**Spectrum 2.1**) showed a molecular ion [M⁺] peak at m/z 418, which was the same as *epi*-syringaresinol and thus confirmed that it was a structural isomer of compound 1. The fragmentation pattern was the same as in compound 1 with the splitting of the dimer to form the lignin monomer (m/z 210), the loss of an ethylene group from the propyne side chain to give syringaldehyde (m/z 182) and the further loss of a hydrogen atom to give the base peak at m/z 181¹¹.

The infrared spectrum of compound 2 (**Spectrum 2.2**) displayed an intense broad band at 3420 cm⁻¹ indicating the presence of a hydroxyl substituent in the molecule. This was confirmed by the appearance of a sharp peak at 1116 cm⁻¹, which was due to C-O stretching. The peaks at 2936 cm⁻¹ and 2850 cm⁻¹ were typical of aliphatic C-H stretching vibrations and the sharp peaks in the region 1650 – 1450 cm⁻¹ corresponded to C=C

[†] The mixture appeared as one spot on a thin layer chromatography plate irrespective of the solvent system used to develop the plate. Separation of the two isomers would probably require the use of an HPLC equipped with a chiral column, which was unavailable.

stretching of an aromatic ring. The medium absorption band at 1327 cm^{-1} was indicative of syringyl breathing¹².

The ^1H and ^{13}C NMR spectra of compound 2 (with *epi*-syringaresinol impurity peaks subtracted) showed fewer peaks than those seen for compound 1, which indicated that this compound was probably symmetrical. Therefore, the assignment of the peaks, based on NMR data, of only one half of the molecule will be discussed in detail.

The ^1H NMR spectrum (**Spectrum 2.4**) showed a strong peak at δ 6.56 ppm (singlet), integrating to two protons, which was due to the two equivalent aromatic proton resonances (H-2 and H-6). The singlet at δ 3.87 ppm (6H, $2 \times \text{OCH}_3$) was characteristic of two equivalent methoxy group proton resonances and the peak at δ 5.52 ppm was due to the proton of the hydroxy group attached to C-4 in the structure. The above peaks confirmed that the aromatic ring was symmetrical and the same as in compound 1. The doublet at δ 4.70 ppm ($J = 4.40\text{ Hz}$) integrated to one proton only and was ascribed to the methine proton at C-7. The peaks at δ 4.25 ppm and δ 3.87 ppm (hidden beneath and superimposed with the methoxy group signal) were due to the two non – equivalent protons of the methylene group at position 9. The H-7 and 2H-9 proton resonances were shifted downfield due to the deshielding effect of the electronegative oxygen atom attached to both groups. The remaining multiplet at δ 3.07 ppm was attributed to the methine group proton at C-8.

The ^{13}C NMR spectrum (**Spectrum 2.5**) showed a methine carbon resonance at δ 54.3 ppm due to the proton at position 8. The oxygenated methine and methylene group carbon resonances of position 7 and 9 occurred at δ 86.0 ppm and δ 71.7 ppm respectively. Once again, these two peaks appeared further downfield because of the attached electronegative oxygen atom. The intense peaks at δ 56.3 ppm and δ 102.6 ppm are typical of methoxy group carbon and protonated aromatic carbon resonances respectively. The remaining fully substituted carbons of the aromatic ring are shown between δ 132 ppm and δ 147 ppm and were assigned based on HMBC correlations. The intensity of the carbon resonances for compound 2 was twice that of compound 1, which suggested that the ratio of compound 2 to compound 1 in the mixture was 2:1.

In the HMBC NMR spectrum of compound 2 (**Spectrum 2.8**) the carbon peak at δ 117.1 ppm showed strong 3J correlations to the methoxy protons and the protons of the aromatic ring and was, therefore, assigned to C-3 and C-5 where the methoxy groups are attached. The carbon resonance at δ 134.3 ppm displayed 3J correlations to the aromatic protons only and was ascribed to the carbon at position 4. The carbon peak at δ 132.1 ppm showed weak 2J correlations to H-7 and the aromatic protons and was assigned to C-1. Figure 3.6 shows the relevant HMBC correlations observed for compound 2 with strong 3J correlations shown in red.

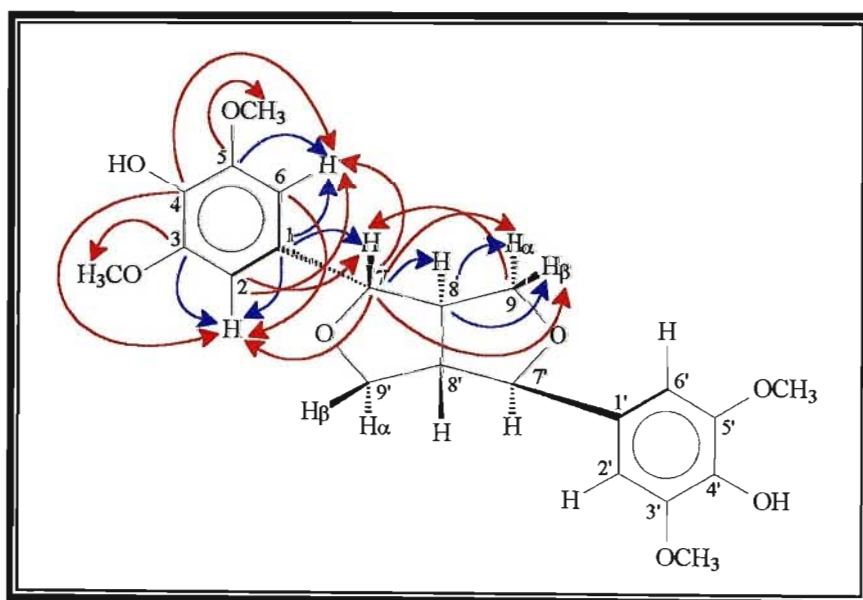


Figure 3.6: HMBC correlations (C→H) of compound 2

The HSQC NMR spectra (**Spectra 2.6 and 2.7**) showed a correlation from the C-9 carbon peak at δ 71.7 ppm to the proton resonance hidden beneath the methoxy proton signal and to the multiplet at δ 4.25 ppm. The spectra also confirmed that the peaks at δ 4.70 ppm and δ 3.07 ppm corresponded to the carbon peaks at δ 86.1 ppm and δ 54.4 ppm respectively. The peak at δ 6.55 ppm, due to the two aromatic proton resonance, corresponded to the same single carbon peak at δ 102.6 ppm and the carbon resonance at δ 56.3 ppm corresponded to the methoxy group protons.

The relative stereochemistry of this half of the structure was verified using the NOESY correlations (**Spectrum 2.9**). The H-7 proton showed a strong correlation to one of the methylene group protons at δ 3.87 ppm (H-9 β) and was, therefore, given the relative stereochemistry of β . H-7 also showed a weak correlation to the proton at position 8

which suggested that these two protons were *trans* to each other. Thus H-8 was assigned to the α position (opposite of H-7). The assignment of H-8 α was confirmed by a strong NOESY correlation between H-8 and the other methylene proton at δ 4.25 ppm (H-9 α). The two non-equivalent methylene protons, H-9 α and H-9 β , showed strong correlations to each other. NOESY correlations were also observed between the aromatic protons, H-2 and H-6, and H-7, H-8 and the methoxy group protons.

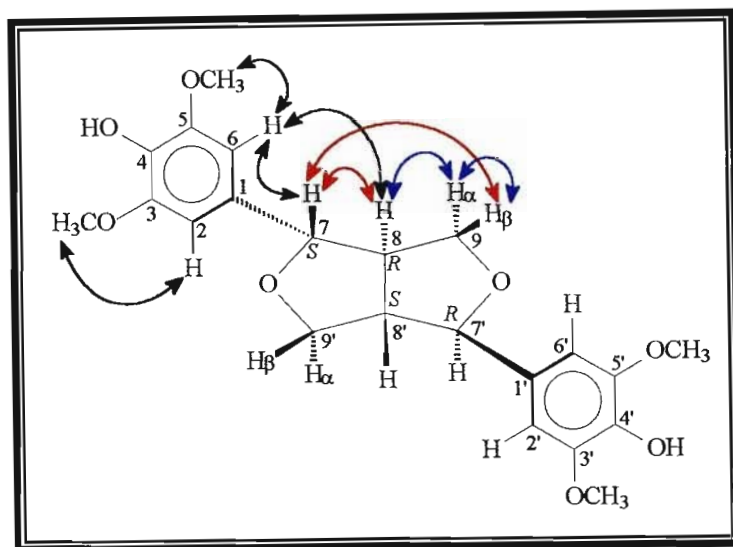


Figure 3.7: NOESY correlations of compound 2

With H-7 in the β position and H-8 in the α position, the stereochemistry at C-7 was assigned as *S* and at C-8 as *R*. Since the molecule had already been established as being symmetrical, the stereochemistry at C-7' was, therefore, assigned as *R* and at C-8' as *S* as shown in Figure 3.7 above.

The COSY NMR spectrum (**Spectrum 2.10 and 2.11**) showed a correlation from the aromatic protons to the protons of the methoxy groups. This confirmed that the aromatic protons were adjacent to the methoxy groups in the aromatic ring. The methine proton at C-8 showed strong correlations to H-7 and 2H-9, which confirmed that the methine group at position 8 was between the oxygenated methine and methylene groups at positions 7 and 9 respectively. A COSY correlation was also seen between the two non-equivalent methylene protons at C-9. Table 3.2 lists the COSY correlations observed for compound 2.

Table 3.2: NMR spectral data for compound 2 (400MHz, CDCl₃)

| Position | ¹ H (ppm) | ¹³ C (ppm) | HMBC (C→H) | NOESY | COSY |
|------------------|-------------------------|-----------------------|--|---|-------------------------|
| 1 | | 132.1 | H-7 (² J), H-2/6 (² J) | | |
| 2 | 6.56 s | 102.6 | H-7 (³ J), H-6 (³ J) | H-7, H-9 α , OCH ₃ , H-8 | OCH ₃ , H-7 |
| 3 | | 147.1 | OCH ₃ (³ J), H-2 (² J) | | |
| 4 | | 134.3 | H-2/6 (³ J) | | |
| 5 | | 147.1 | OCH ₃ (³ J), H-6 (² J) | | |
| 6 | 6.56 s | 102.6 | H-7 (³ J), H-2 (³ J) | H-7, H-9 α , OCH ₃ , H-8 | OCH ₃ , H-7 |
| 7 | 4.70 d (J = 4.40 Hz) | 86.0 | H-9 α/β (³ J), H-2/6 (³ J) | H-2/6, H-9 β , H-8 | H-2/6, H-8 |
| 8 | 3.07 m | 54.3 | H-9 α/β (² J), H-7 (² J) | H-2/6, H-7, H-9 α | H-7, H-9 α/β |
| 9 α | 4.25 m | 71.7 | H-7 (³ J) | H-2/6, H-9 β , H-8 | H-9 β , H-8 |
| 9 β | 3.87 m | 71.7 | H-7 (³ J) | H-7, H-9 α | H-9 α , H-8 |
| OCH ₃ | 3.87 s | 56.3 | | H-2/6 | H-2/6 |
| OH | 5.52 bs | | | | |

Compound 2 was identified as the stereoisomer of compound 1 known as *meso*-syringaresinol. It is the second major compound isolated from the hydrolysed aqueous phase of the calcium spent liquor effluent stream. The mixture of the two isomers had a combined approximate concentration of 0.142 g/L. Taking into consideration that the ratio of compound 2 to compound 1 in the mixture was 2:1, the approximate concentration of compound 2 was, therefore, estimated to be 0.095 g/L.

3.2.3 Structural Elucidation of Compound 3: *meso*-yangambin

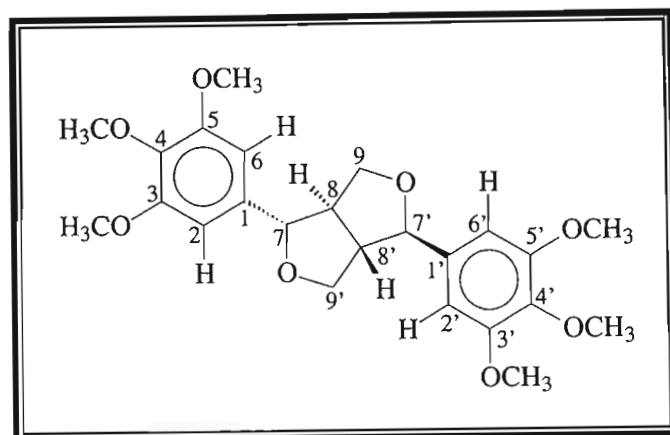
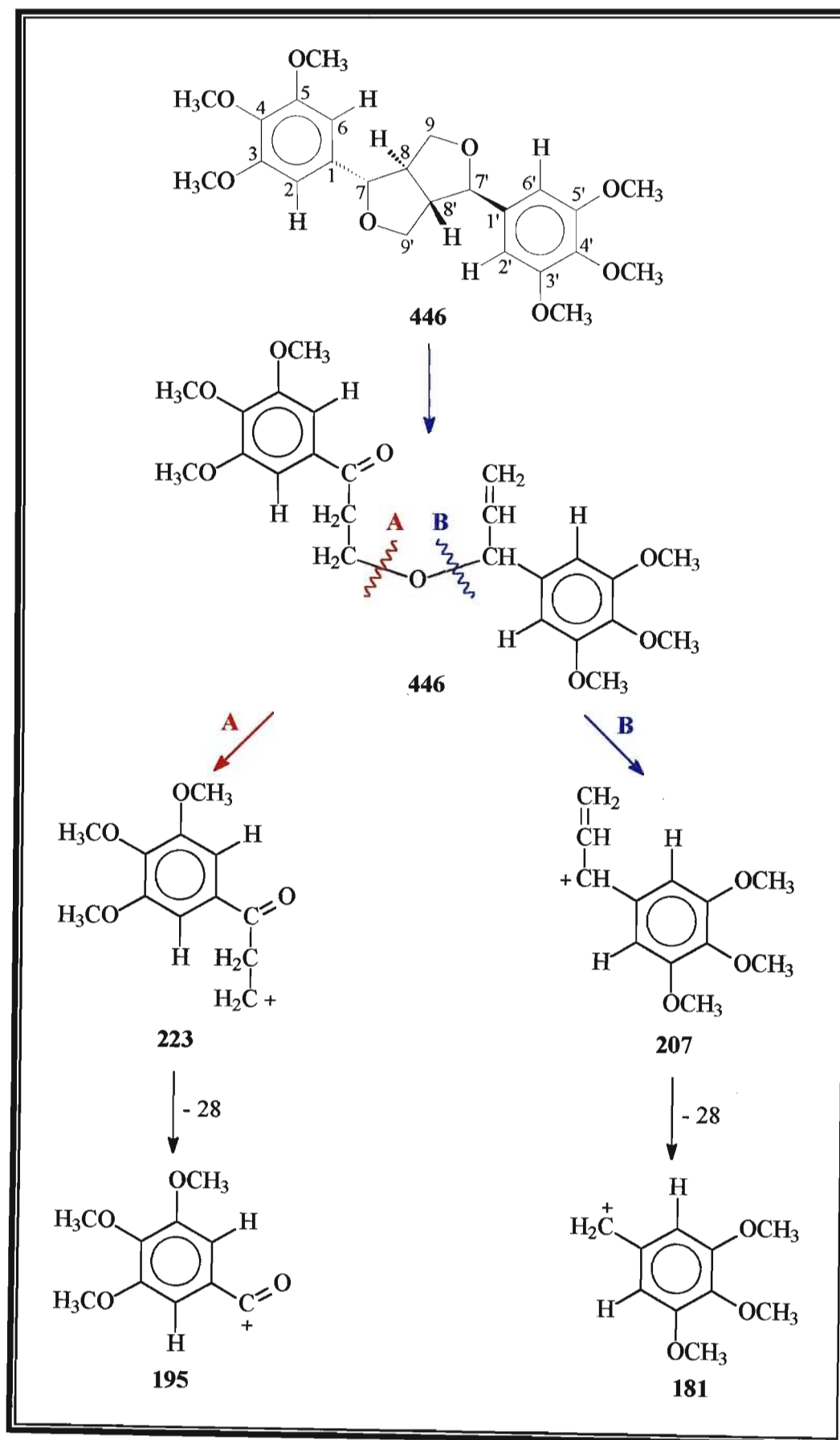


Figure 3.8: Structure of compound 3, *meso*-yangambin

The ^1H and ^{13}C NMR spectra of compound 3 were similar to that of compound 2, *meso*-syringaresinol. Only half of the expected proton and carbon resonances were seen, which suggested that compound 3 must also have a symmetrical structure.

The infrared spectrum (**Spectrum 3.2**) revealed a broad band at 3429 cm^{-1} , which is usually due to the presence of a hydroxy group substituent. However, this band is very much weaker compared to that seen in the infrared spectrum of compound 2 (**Spectrum 2.2**), which suggested that the hydroxyl substituent was possibly absent in this compound or could have been due to water present in the sample. The strong bands at 2926 cm^{-1} and 2849 cm^{-1} are typical of C-H stretching and the bands between 1500 cm^{-1} and 1600 cm^{-1} are due to C=C stretching of an aromatic ring. The strong peak at 1131 cm^{-1} corresponds to C-O stretching.

The mass spectrum of compound 3 (**Spectrum 3.1**) showed a molecular ion $[\text{M}^+]$ peak at m/z 446, corresponding to a molecular formula of $\text{C}_{24}\text{H}_{30}\text{O}_8$. The peaks in the spectrum indicated two fragmentation patterns for this compound as described by Pelter¹⁴. Firstly, the peak at m/z 223 corresponded to the fragmentation of the lignan dimer to form the monomer as shown by path A in Scheme 3.1. A further loss of an ethylene group from the propyne side chain results in a peak at m/z 195. If path B is followed then the splitting of the dimer is unequal giving rise to the peak at m/z 207. The base peak at m/z 181, once again, suggested fragmentation of an ethylene group from the side chain.

Scheme 3.1: Fragmentation patterns of compound 3^{11,14}

The ^1H NMR spectrum (**Spectrum 3.4**) showed peaks at δ 6.55 ppm (4H, s, H-2/2' and H-6/6'), δ 4.73 ppm (2H, d, H-7/7'), δ 4.29 ppm (2H, m, H-9 α /9' α), δ 3.92 ppm (2H, m, H-9 β /9' β), δ 3.08 (2H, m, H-8/8') and δ 3.86 ppm (12H, s, 4 x OCH₃). These chemical shifts were similar to the chemical shifts of the corresponding protons of *meso*-syringaresinol, which suggested that these protons were in the same positions in the structure as in compound 2. An additional singlet at δ 3.82 ppm integrating to six protons indicated the presence of an extra methoxy group in the molecule. The absence of the hydroxy group proton resonance at approximately δ 5.50 ppm suggested that it was replaced by the extra methoxy group at carbon position 4 and 4' in compound 3.

The ^{13}C NMR spectrum of compound 3 (**Spectrum 3.5**) was compared to that of *meso*-syringaresinol. It showed an extra peak at δ 60.8 ppm, which confirmed the presence of an extra methoxy group in the structure. Also, the intensity of the extra methoxy carbon resonance was half that of the four equivalent methoxy carbon resonances at δ 56.2 ppm. The ^{13}C NMR data for compound 3 is shown in Table 3.3.

The HSQC NMR spectrum (**Spectrum 3.6**) further supported the structure of compound 3 by showing that the methoxy protons at δ 3.82 ppm corresponded to the carbon signal at δ 60.8 ppm and the carbon peak at δ 56.2 ppm corresponded to the four equivalent methoxy group protons at δ 3.86 ppm.

In the HMBC NMR spectrum (**Spectrum 3.7**), the carbon peak at δ 137.4 ppm showed strong 3J correlations to the methoxy protons at δ 3.82 ppm and to the aromatic protons (H-2/2' and H-6/6') and was, therefore, assigned to C-4/4' where the extra methoxy group is attached. The carbon peak at δ 153.4 ppm showed strong 3J correlations to the methoxy group protons at δ 3.86 ppm as well as to the aromatic protons and was ascribed to C-3/3' and C-5/5'. The other fully substituted carbon signal at δ 136.7 ppm was assigned to C-1/1' because it showed weak 2J correlations to the aromatic protons. The protonated aromatic carbon resonance δ 102.8 ppm showed strong HMBC correlations to the H-7/7' proton and to the aromatic protons. The relative HMBC correlations of the tetrahydrofuran rings were similar to that of compound 2 and is shown in Figure 3.9 and listed in Table 3.3.

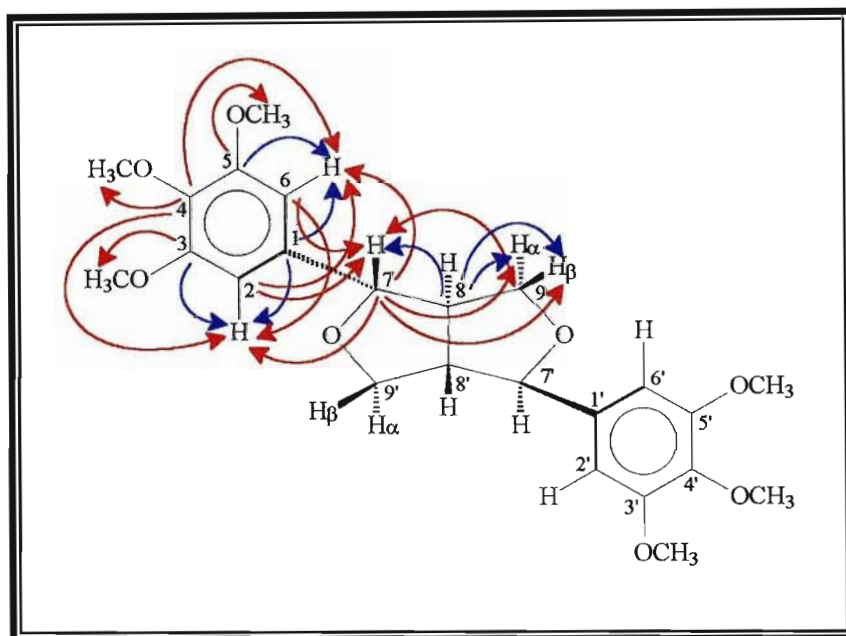


Figure 3.9: HMBC correlations (C→H) of compound 3

The relative stereochemistry of one half of the structure was confirmed using the NOESY NMR spectrum (**Spectrum 3.8**). A strong correlation was seen between H-7 and one of the methylene group protons (H-9 β), therefore, H-7 was placed in the β position. A weak correlation was also seen between H-7 and the proton at C-8, which indicated that they are *trans* to each other thus H-8 was placed in the α position. The other methylene proton H-9 α showed a strong NOESY correlation to H-8 which confirmed that it was in the α position. Therefore, the relative stereochemistry at C-7 could be assigned as *S* and at C-8 as *R* as in compound 2. Since the molecule is symmetrical the relative stereochemistry at C-7' was thus assigned as *R* (opposite to C-7) and at C-8' as *S* (opposite to C-8).

Table 3.3: NMR spectral data for compound 3 (400MHz, CDCl₃)

| Position | ¹ H (ppm) | ¹³ C (ppm) | HMBC (C→H) | NOESY | COSY |
|----------------------|-------------------------|-----------------------|--|---|--------------------------|
| 1 | | 136.7 | H-2/6 (² J) | | |
| 2 | 6.55 s | 102.8 | H-7 (³ J), H-6 (³ J) | H-7, H-9 _α , 3,5-OCH ₃ , H-8 | 3-OCH ₃ , H-7 |
| 3 | | 153.4 | 3-OCH ₃ (³ J), H-2 (² J) | | |
| 4 | | 137.4 | 4-OCH ₃ (³ J), H-2/6 (³ J) | | |
| 5 | | 153.4 | 5-OCH ₃ (³ J), H-6 (² J) | | |
| 6 | 6.55 s | 102.8 | H-7 (³ J), H-2 (³ J) | H-7, H-9 _α , 3,5-OCH ₃ , H-8 | 5-OCH ₃ , H-7 |
| 7 | 4.73 d (J = 4.40 Hz) | 85.9 | H-9 _{α/β} (³ J), H-2/6 (³ J) | H-2/6, H-9 _β , H-8 | H-2/6, H-8 |
| 8 | 3.08 m | 54.3 | H-9 _{α/β} (² J), H-7 (² J) | H-2/6, H-7, H-9 _α | H-7, H-9 _{α/β} |
| 9 _α | 4.29 m | 72.0 | H-7 (³ J) | H-2/6, H-9 _β , H-8 | H-9 _β , H-8 |
| 9 _β | 3.92 m | 72.0 | H-7 (³ J) | H-7, H-9 _α | H-9 _α , H-8 |
| 3,5-OCH ₃ | 3.86 s | 56.2 | | H-2/6, 4-OCH ₃ | H-2/6 |
| 4-OCH ₃ | 3.82 s | 60.8 | | 3,5-OCH ₃ | |

Compound 3 was identified as the dimethyl ether of *meso*-syringaresinol and was hence named *meso*-yangambin. The optical rotation was measured to be zero, which confirmed that this was a *meso* compound. *Meso*-yangambin was not listed in the dictionary of natural products, although, the (+)-form and *epi*-yangambin has been identified. Its approximate concentration in the hydrolysed aqueous phase of the calcium spent liquor effluent was 6.000×10^{-4} g/L.

3.2.4 Structural Elucidation of Compound 4: 3-(4'-hydroxy-3',5'-dimethoxyphenyl)-prop-1-ene (commonly known as methoxyeugenol)

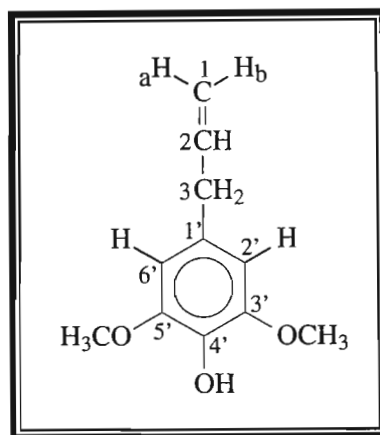


Figure 3.10: Structure of compound 4, methoxyeugenol

Low – resolution mass spectrometric analysis of compound 4 (**Spectrum 4.1**) showed a molecular ion $[M^+]$ peak at m/z 194, corresponding to a molecular formula of $C_{11}H_{14}O_3$. Fragmentation between C-2 and C-3 resulted in the loss of 27 mass units and gave a peak at m/z 167, which corresponded to the hydroxy, dimethoxytropylium ion.

The infrared spectrum (**Spectrum 4.2**) displayed a broad band at 3511 cm^{-1} indicating the presence of a hydroxy (OH) group substituent in the molecule. This was confirmed by a sharp band at 1116 cm^{-1} corresponding to C-O stretching. The bands between 1625 cm^{-1} and 1590 cm^{-1} were due to C=C stretching of an aromatic ring with the corresponding C-H stretching vibrations occurring between 3080 cm^{-1} and 3010 cm^{-1} . The strong bands at 2941 cm^{-1} and 2841 cm^{-1} were characteristic of C-H stretching of methine (CH) and methylene (CH_2) groups. The weak absorption at 1644 cm^{-1} is characteristic of vinyl group ($-\text{CH}=\text{CH}_2$) stretching.

The ^1H NMR spectrum (**Spectrum 4.4**) showed a resonance at δ 5.93 ppm (1H, m), which corresponded to the methine proton attached to the double bond carbon atom at position 2. The proton resonances at δ 5.09 ppm (1H, dd, $J_{1a,1b} = 1.74\text{ Hz}$, $J_{1a,2} = 3.39\text{ Hz}$) and δ 5.05 ppm (1H, dd, $J_{1a,1b} = 1.65\text{ Hz}$, $J_{1b,2} = 3.29\text{ Hz}$) corresponded to the two non – equivalent methylene group protons, H-1a and H-1b respectively. The doublet at δ 3.30 ppm (2H, d, $J = 6.78\text{ Hz}$) indicated the presence of an additional methylene group, which

suggested a $\text{CH}_2\text{-CH=CH}_2$ partial structure. The ^1H NMR spectrum also showed a strong singlet peak at δ 3.85 ppm integrating to six protons, which is typical of protons of two equivalent methoxy groups. The other strong singlet at δ 6.39 ppm, integrating to two protons, indicated two equivalent aromatic protons in the structure. The integration of the above peaks suggested a compound with a symmetrically substituted aromatic ring. The remaining peak at δ 5.38 ppm in the ^1H NMR spectrum was due to the hydroxy group proton signal.

The ^{13}C NMR spectrum (**Spectrum 4.6**) showed a strong peak at δ 56.2 ppm, which was characteristic of a methoxy group carbon resonance. The protonated aromatic carbon resonance occurred as an intense peak at δ 105.1 ppm. The peak at δ 40.3 ppm corresponded to a methylene group carbon resonance and was assigned to C-3. The remaining carbon signals between δ 115 ppm and δ 147 ppm were due to fully substituted carbons of the aromatic ring and the carbons attached to the double bond in the side chain and were assigned based on HMBC correlations.

In the HMBC NMR spectrum (**Spectrum 4.8**) a strong 3J correlation was seen between the carbon at δ 146.9 ppm and the protons of the methoxy groups as well as the proton of the hydroxy group and was therefore assigned to the equivalent carbons C-3' and C-5'. A weak 2J correlation was also observed from that carbon resonance to the aromatic proton resonance. The carbon resonance at δ 137.6 ppm showed a strong correlation to the methylene protons at C-3 and a weaker correlation to the methylene protons at C-1 and was thus assigned to C-2. The carbon signal at δ 132.9 ppm showed strong 3J coupling with the aromatic protons and weaker 2J coupling with the hydroxy group proton and could therefore be assigned to C-4'. Correlations from the carbon at δ 131.0 ppm to the protons at C-3 and to the aromatic protons allowed assignment of that carbon to C-1'. The carbon resonance at δ 115.7 ppm showed strong HMBC correlations to the methylene protons at C-3 only and was therefore ascribed to C-1. The protonated aromatic carbons (C-2' and C-6') at δ 105.1 ppm showed 3J correlations to the methylene protons at C-3. The C-3 peak showed correlations to the protons at C-1, C-2 and the aromatic protons (H-2' and H-6'). Figure 3.11 shows the relevant HMBC correlations with strong 3J correlations in red.

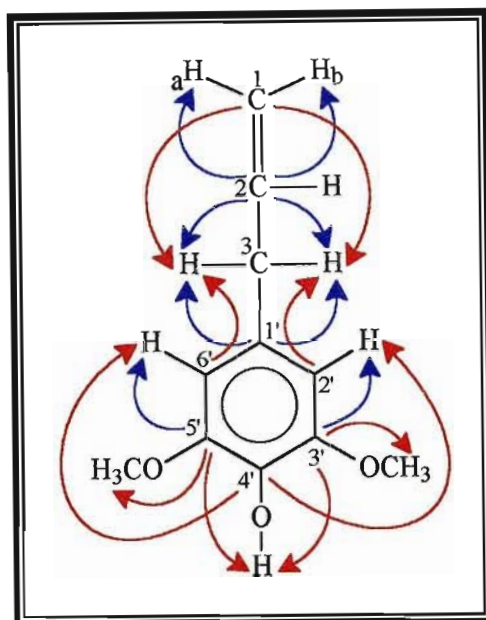


Figure 3.11: HMBC (C→H) correlations of compound 4

The NOESY NMR spectrum (**Spectrum 4.9**) was used to confirm the structure of compound 4. NOESY correlations were observed between the aromatic protons and the protons of the methoxy groups as well as the methylene group protons at C-3. The H-2 proton showed coupling to both the methylene group protons while the 2H-1 protons showed correlations to the methine proton at C-2 and the methylene protons at C-3.

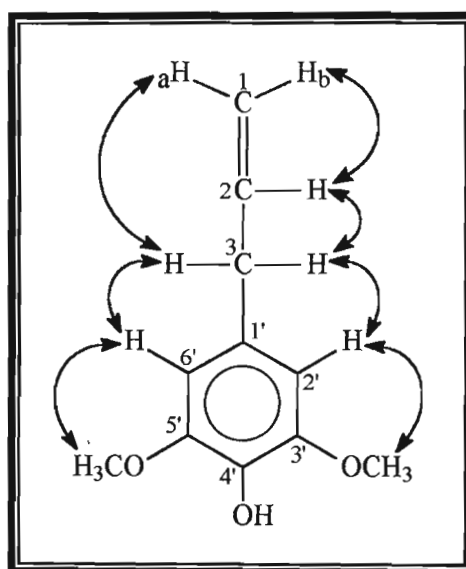


Figure 3.12: NOESY correlations of compound 4

The COSY NMR spectrum (**Spectrum 4.10**) was used to confirm the positioning of the methine and methylene groups in the side chain. COSY correlations were seen from the methine proton at C-2 to both the methylene group proton resonances at C-1 and C-3. Correlations were also observed between the two non – equivalent methylene protons at C-1. The 2H-3 protons and the methoxy proton resonances both showed correlations to the two aromatic proton resonances.

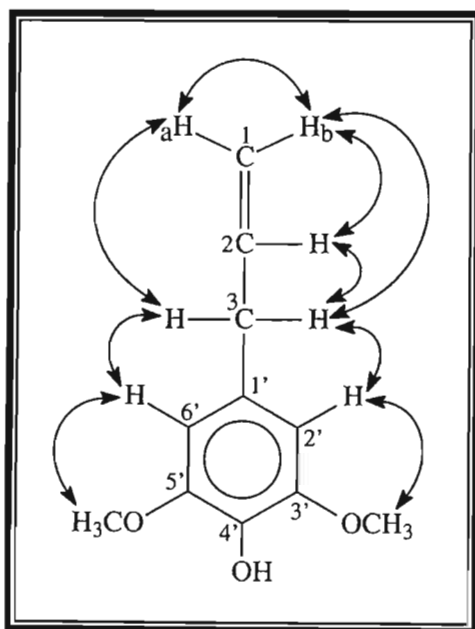


Figure 3.13: COSY correlations of compound 4

Table 3.4: NMR spectral data for compound 4 (400MHz, CDCl₃)

| Position | ¹ H (ppm) | ¹³ C (ppm) | HMBC (C→H) | NOESY | COSY |
|------------------|-------------------------|-----------------------|---|-------------------------|-------------------------|
| 1' | | 131.0 | H-3 (² J), H-2'/6' (² J) | | |
| 2' | 6.39 s | 105.1 | H-3 (³ J), H-6' (³ J) | OCH ₃ , H-3 | OCH ₃ , H-3 |
| 3' | | 146.9 | OCH ₃ (³ J), OH (³ J), H-2' (² J) | | |
| 4' | | 132.9 | OH (² J), H-2'/6' (³ J) | | |
| 5' | | 146.9 | OCH ₃ (³ J), OH (³ J), H-6' (² J) | | |
| 6' | 6.39 s | 105.1 | H-3 (³ J), H-2' (³ J) | OCH ₃ , H-3 | OCH ₃ , H-3 |
| 1a | 5.09 d (J = 1.65 Hz) | 115.7 | H-3 (³ J) | H-2, H-3 | H-3, H-2, H-1b |
| 1b | 5.05 m | 115.7 | H-3 (³ J) | H-2, H-3 | H-3, H-2, H-1a |
| 2 | 5.93 m | 137.6 | H-3 (² J), H-1a/b (² J) | H-1a/b, H-3 | H-3, H-1a/b |
| 3 | 3.30 d (J = 6.78 Hz) | 40.3 | H-1a/b (³ J), H-2 (² J), H-2'/6' (³ J) | H-2'/6', H-1a/b, H-2 | H-2'/6', H-2, H-1a/b |
| OCH ₃ | 3.85 s | 56.2 | | H-2'/6' | H-2'/6' |
| OH | 5.38 bs | | | | |

Compound 4 was identified as 3-(4'-hydroxy-3',5'-dimethoxyphenyl)-prop-1-ene or more commonly known as methoxyeugenol. It has been previously isolated from the sassafras root and from nutmeg and is a common compound found in wood products¹⁵. Its concentration in the calcium spent liquor effluent is approximately 1.440×10^{-3} g/L.

3.2.5 Structural Elucidation of Compound 5: 3-(4'-hydroxy-3',5'-dimethoxyphenyl)-1-hydroxy-propan-2-one (commonly known as β -oxysinapyl alcohol)

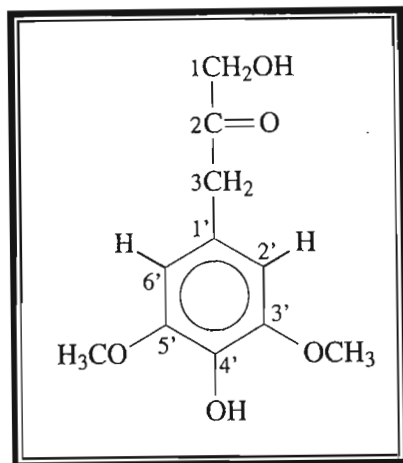


Figure 3.14: Structure of compound 5, β -oxysinapyl alcohol

The mass spectrum of compound 5 (**Spectrum 5.1**) showed a molecular ion [M^+] peak at m/z 226. This corresponded to a molecular formula of $C_{11}H_{14}O_5$. The base peak at m/z 167 ($M^+ - 59$) was due to a loss of the carbonyl group and the hydroxy methylene substituent. This resulted from α – cleavage between positions 3 and 2 to yield the corresponding substituted tropylium ion.

The infrared spectrum (**Spectrum 5.2**) showed a broad band at 3426 cm^{-1} , which indicated the presence of hydroxy group substituents. The corresponding C-O stretching vibration was observed as an intense peak at 1119 cm^{-1} . The strong absorptions between 2800 cm^{-1} and 3000 cm^{-1} were due to C-H stretching of the methylene groups. The characteristic carbonyl group frequency of the ketone group occurred at 1726 cm^{-1} in the spectrum. The peaks at 1614 cm^{-1} and 1518 cm^{-1} were typical of C=C stretching of an aromatic ring.

The resonances at δ 3.62 ppm (2H, s) and δ 4.28 ppm (2H, s) in the proton NMR spectrum of compound 5 (**Spectrum 5.4**) indicated the presence of two deshielded methylene groups in the structure. The HSQC NMR spectrum (**Spectrum 5.6**) was used to assign these two peaks. Two methylene group carbon resonances at δ 45.9 ppm and δ 67.4 ppm were observed in the spectrum. The methylene group carbon resonance at δ 67.4 ppm correlated to the methylene group protons at δ 4.28 ppm and was assigned to

C-1. Both the proton and carbon resonances of the methylene group at position 1 were located further downfield due to the deshielding effect of the attached hydroxyl group. The carbon resonance at δ 45.9 ppm correlated to the methylene group protons at δ 3.62 ppm and was, therefore, attributed to C-3.

The ^1H NMR spectrum also showed a strong singlet at δ 6.40 ppm integrating to two protons, which was characteristic of two equivalent aromatic ring protons. The strong singlet peak at δ 3.86 ppm (6H, s) was typical of two equivalent methoxy group protons and the low intensity peak at approximately δ 5.45 ppm was due to the phenolic proton. The integration of the aromatic group substituents confirmed the symmetrical nature of the ring.

The ^{13}C NMR spectrum (**Spectrum 5.5**) confirmed the presence of a carbonyl group in the molecule with a peak at δ 207.6 ppm corresponding to C-2. The spectrum also displayed the strong characteristic peak of a methoxy group carbon resonance at δ 56.3 ppm and the protonated aromatic carbon resonances, C-2' and C-6', were found at δ 105.9 ppm. The three remaining peaks in the spectrum were due to the fully substituted carbons of the aromatic ring and were assigned based on HMBC correlations.

The carbonyl peak at δ 207.5 ppm showed HMBC correlations (**Spectrum 5.7**) to the protons of both methylene groups, which confirmed its position at C-2 between the two methylene groups. The carbon peak at δ 147.3 ppm showed strong (3J) HMBC correlations to the protons of the methoxy groups as well as 2J correlations to the aromatic protons (H-2' and H-6') and was therefore assigned to the equivalent carbons C-3' and C-5'. The carbon resonance at δ 134.2 ppm showed 3J correlations to the aromatic protons at δ_{H} 6.41 ppm only and was ascribed to C-4'. The remaining unassigned carbon peak was thus attributed to carbon position 1' in the molecule and it showed HMBC correlations (2J) to the aromatic protons as well as the protons of the methylene group at position 3. The protonated aromatic carbon resonances showed 3J correlations to the methylene protons at C-3 only. The methylene carbon peak at C-1 showed 3J correlations to the protons of the other methylene group (2H-3) only. Figure 3.15 shows the relevant HMBC correlations with strong 3J correlations shown in red.

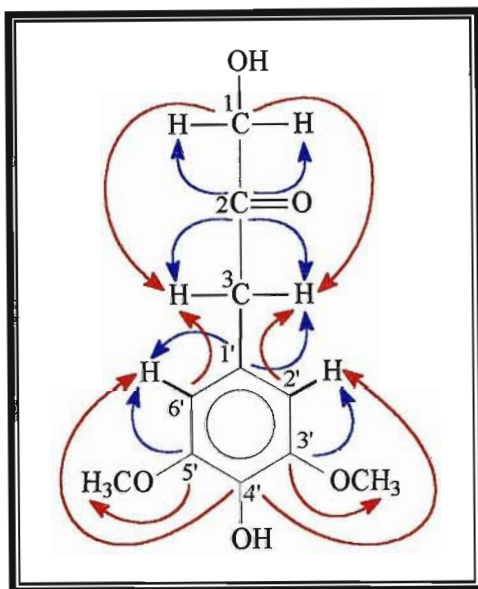


Figure 3.15: HMBC (C→H) correlations of compound 5

The COSY NMR spectrum (**Spectrum 5.9**) showed correlations from the aromatic protons, H-2' and H-6', to the protons of the methylene group at C-3 and to the protons of the methoxy groups. Weak COSY correlations were also seen between the protons of the two methylene groups.

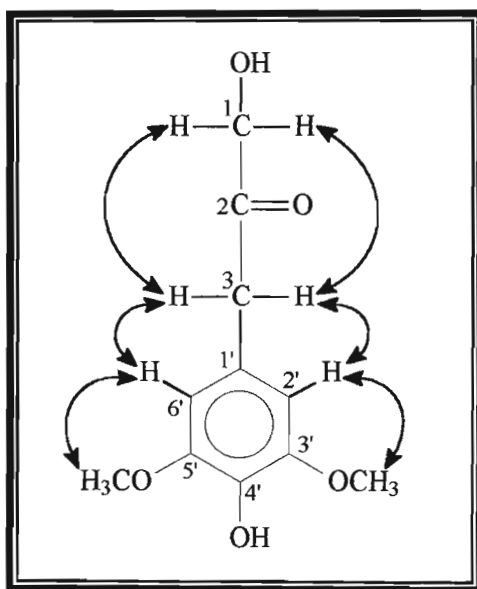


Figure 3.16: COSY correlations of compound 5

The NOESY NMR spectrum (**Spectrum 5.8**) further supported the structure of compound 5.

Table 3.5: NMR spectral data for compound 5 (400MHz, CDCl₃)

| Position | ¹ H (ppm) | ¹³ C (ppm) | HMBC (C→H) | NOESY | COSY |
|------------------|----------------------|-----------------------|--|-----------------------|-----------------------|
| 1' | | 123.6 | H-3 (² J), H-2'/6' (² J) | | |
| 2' | 6.40 s | 105.9 | H-3 (³ J) | H-3, OCH ₃ | H-3, OCH ₃ |
| 3' | | 147.3 | OCH ₃ (³ J), H-2' (² J) | | |
| 4' | | 134.2 | H-2'/6' (³ J) | | |
| 5' | | 147.3 | OCH ₃ (³ J), H-6' (² J) | | |
| 6' | 6.40 s | 105.9 | H-3 (³ J) | H-3, OCH ₃ | H-3, OCH ₃ |
| 1 | 4.28 s | 67.4 | H-3 (³ J) | H-3 | H-3 |
| 2 | | 207.5 | H-3 (² J), H-1 (² J) | | |
| 3 | 3.62 s | 45.9 | H-2'/6' (³ J) | H-1, H-2'/6' | H-2'/6', H-1 |
| OCH ₃ | 3.86 s | 56.3 | | H-2'/6' | H-2'/6' |
| OH | 5.45 bs | | | | |

Compound 5 was identified as 3-(4'-hydroxy-3',5'-dimethoxyphenyl)-1-hydroxy-propan-2-one or more commonly known as β-oxysinapyl alcohol. It was previously isolated as one of the most abundant constituents of the acidolysis of birch lignin¹⁶. It had an approximate concentration of 1.164×10^{-3} g/L in the hydrolysed aqueous phase of the calcium spent liquor effluent.

3.2.6 Structural Elucidation of Compound 6: 3-(4'-hydroxy-3',5'-dimethoxyphenyl)-prop-2-en-al (or more commonly known as sinapyl aldehyde)

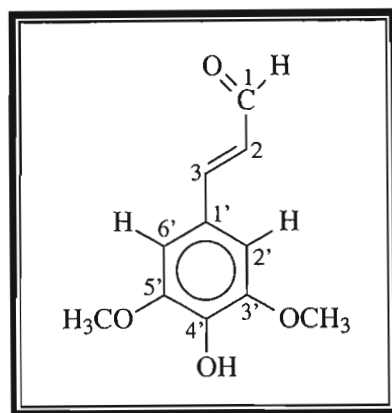


Figure 3.17: Structure of compound 6, sinapyl aldehyde

The mass spectrum of compound 6 (**spectrum 6.1**) showed a molecular ion $[M^+]$ peak at m/z 208, correct for a molecular formula of $C_{11}H_{12}O_4$. The peak at m/z 207 $[M - H]^+$ is characteristic of an aldehyde group. Fragmentation between C-2 and C-1 resulted in a peak at m/z 180, which was due to the loss of the aldehyde substituent. The peak at m/z 165 is due to the loss of an additional 15 mass units $[M - CHO - CH_3]^+$, which is probably due to fragmentation of one of the methoxy group substituents.

The infrared spectrum of compound 6 (**Spectrum 6.2**) showed a characteristic broad band at 3403 cm^{-1} , which was due to a hydroxy group substituent. The sharp band at 1670 cm^{-1} was due to the presence of an α,β -unsaturated carbonyl group while the bands at 2844 cm^{-1} and 2941 cm^{-1} , corresponding to C-H stretching, strongly suggested that the compound possessed an aldehyde group. The strong sharp peak at 1122 cm^{-1} was typical of C-O stretching and the peaks between 1650 cm^{-1} and 1450 cm^{-1} were characteristic of C=C stretching of an aromatic ring. The intense peak at 1339 cm^{-1} corresponded to syringyl ring breathing¹².

The ^1H NMR spectrum (**Spectrum 6.4**) showed a single sharp peak at δ 6.79 ppm, integrating to two protons, indicating two equivalent aromatic proton resonances (H-2 and H-6). The other strong peak at δ 3.92 ppm, integrating to six protons, was characteristic of protons of two equivalent methoxy groups. The broad low intensity peak at δ 5.85 ppm (1H) was due to a phenolic group proton resonance. The doublet at δ 9.63

ppm (1H, d, $J=7.69$ Hz), the double doublet at δ 6.59 ppm (1H, dd, $J_{2,3} = 15.75$ Hz, $J_{1,2} = 7.87$ Hz) and the doublet at δ 7.36 ppm (1H, d, $J = 15.75$ Hz) indicated the presence of a *trans* CH=CH-CHO group. The coupling constant of approximately 16 Hz confirmed that H-7 and H-8 are *trans* to each other. From Figure 3.17 it could be seen that both H-1 of the aldehyde substituent and H-3 were split into doublets as a result of H-2, while H-2, in turn, was split by H-3 into a doublet and further by H-1 resulting in a double doublet. The coupling of these three protons in the side chain was confirmed by the COSY NMR spectrum.

In the COSY NMR spectrum of compound 6 (**Spectrum 6.9**) a strong correlation was seen from the double doublet of H-2 to the doublet protons of both H-3 and H-1. This confirmed that the methine group at position 8 was between the methine and aldehyde groups at positions 3 and 1 respectively. A COSY correlation was also seen between the aromatic protons and the protons of the methoxy groups, which confirmed that the aromatic protons were adjacent to the methoxy groups on the aromatic ring.

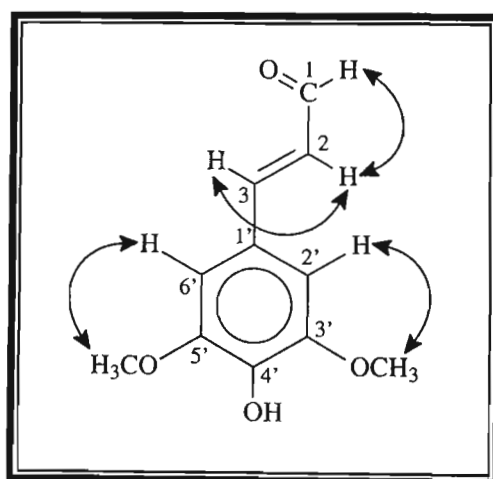


Figure 3.18: COSY correlations of compound 6

The HSQC NMR spectrum (**Spectrum 6.6**) showed that the proton of the aldehyde group corresponded to the carbon resonance at δ 193.5 ppm, the aromatic protons (H-2' and H-6') corresponded to the carbon resonance at δ 105.5 ppm and the methoxy group protons correlated with the carbon resonance at δ 56.4 ppm. The double doublet at δ 6.59 ppm (H-8) corresponded to the carbon resonance at δ 126.7 ppm and the doublet at δ 7.36 ppm (H-7) corresponded to the peak at δ 153.2 ppm in the ^{13}C NMR spectrum. The

remaining carbon resonances were due to fully substituted carbons of the aromatic ring and these were assigned based on HMBC correlations.

In the HMBC NMR spectrum (**Spectrum 6.7**) there was a strong correlation between the carbon at δ 147.3 ppm and the protons of the two methoxy groups, therefore, that peak could be assigned to C-3' and C-5. The spectrum also showed a weaker 2J correlation with the aromatic ring protons (H-2' and H-6'). The aldehyde group carbon at δ 193.5 ppm showed a strong 3J correlation to the methine proton at δ 7.36 ppm (H-3). The carbon resonance at δ 126.7 ppm showed a weaker 2J correlation to the peak at δ 9.63 ppm only. This confirmed the assignment of that peak to C-2 in the ^{13}C NMR spectrum. The carbon resonances at δ 138.0 ppm and δ 153.2 ppm each showed strong correlations to the aromatic protons only and could therefore be assigned to C-4' and C-3 or *vice versa*. However, as discussed earlier, the carbon resonance at δ 153.2 ppm corresponded to C-3. Thus the resonance at δ 138.0 ppm was assigned to C-4'. The carbon resonance at δ 125.5 ppm showed a strong 3J correlation to the double doublet of H-2 and a weak 2J correlation to the aromatic proton resonance and was, therefore, assigned to the carbon at position 1' in the structure. Figure 3.19 shows the relevant HMBC correlations with strong 3J correlations shown in red.

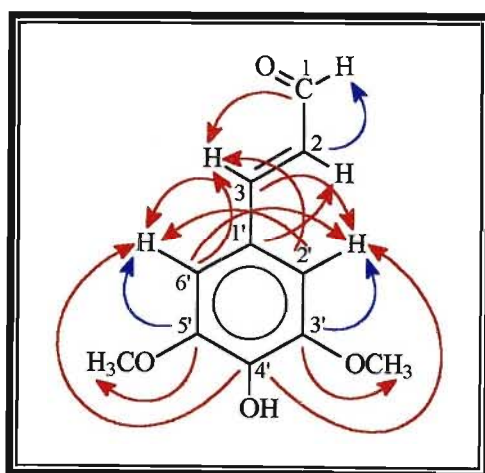


Figure 3.19: HMBC correlations (C→H) of compound 6

The NOESY NMR spectrum (**Spectrum 6.8**) showed strong correlations between the aromatic protons and the protons of the methoxy group. NOESY correlations were also observed between the aromatic protons and the protons at positions 3 and 2. The H-1 proton showed NOESY correlations to the protons at position 2 and position 3.

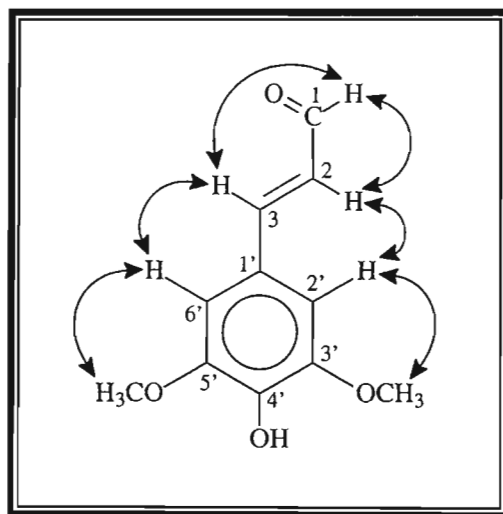


Figure 3.20: NOESY correlations of compound 6

Table 3.6: NMR spectral data for compound 6 (400MHz, CDCl₃)

| Position | ¹ H (ppm) | ¹³ C (ppm) | HMBC (C→H) | NOESY | COSY |
|------------------|--|-----------------------|--|--------------------------------|------------------|
| 1' | | 125.5 | H-2 (³ J), H-2'/6' (² J) | | |
| 2' | 6.79 s | 105.5 | H-3 (³ J), H-6' (³ J) | OCH ₃ , H-3, H-2 | OCH ₃ |
| 3' | | 147.3 | OCH ₃ (³ J), H-2' (² J) | | |
| 4' | | 138.0 | H-2'/6' (³ J) | | |
| 5' | | 147.3 | OCH ₃ (³ J), H-6' (² J) | | |
| 6' | 6.79 s | 105.5 | H-3 (³ J), H-2' (³ J) | OCH ₃ , H-3, H-2 | OCH ₃ |
| 3 | 7.36 d (J = 15.75 Hz) | 153.2 | H-2'/6' (³ J) | H-2'/6', H-1 | H-2 |
| 2 | 6.59 dd (J _{2,3} = 15.75 Hz, J _{1,2} = 7.87 Hz) | 126.7 | H-1 (² J) | H-2'/6', H-1 | H-3, H-1 |
| 1 | 9.63 d (J = 7.69 Hz) | 193.5 | H-3 (³ J) | H-2, H-3 | H-3, H-2 |
| OCH ₃ | 3.92 s | 56.4 | | H-2'/6' | H-2'/6' |
| OH | 5.85 bs | | | | |

Compound 6 was hence identified as *trans*-3-(4'-hydroxy-3',5'-dimethoxyphenyl)-prop-2-en-al or *trans*-3,5-dimethoxy-4-hydroxycinnamaldehyde, the common name of which is sinapyl aldehyde. This compound is recognized as a characteristic component of hardwood extractives¹⁷. Its approximate concentration was 7.440×10^{-4} g/L in the calcium spent liquor stream.

3.2.7 Structural Elucidation of Compound 7: acetovanillone

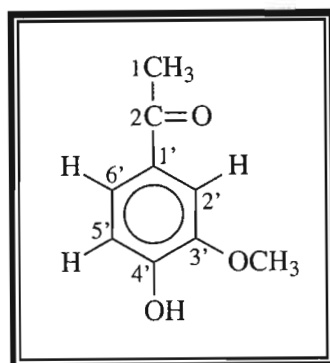


Figure 3.21: Structure of compound 7, acetovanillone

The mass spectrum of compound 7 (**Spectrum 7.1**) showed a molecular ion $[M^+]$ peak at m/z 166, which was consistent with a molecular formula of $C_9H_{10}O_3$ and a double bond equivalence of 5 was deduced. The peak at m/z 151 corresponded to the loss of the methyl group from the side chain.

In the infrared spectrum (**Spectrum 7.2**) a strong absorption at 1666 cm^{-1} indicated the presence of a carbonyl group in the compound. The broad band at 3404 cm^{-1} was typical of O-H stretching and the strong peak at 1307 cm^{-1} , due to C-O stretching confirmed the occurrence of a hydroxy group. The two bands at 2948 cm^{-1} and 2850 cm^{-1} were characteristic of aliphatic C-H stretching. Strong sharp bands between $1650 - 1450\text{ cm}^{-1}$ indicated that the compound was of an aromatic nature while the band at 1154 cm^{-1} suggested that the aromatic ring was 1,3,4-trisubstituted.

The ^1H NMR spectrum (**Spectrum 7.4**) showed a single strong peak at δ 3.94 ppm, integrating to three protons, which was characteristic of the protons of a methoxy group. The single strong peak at δ 2.48 ppm corresponded to an uncoupled methyl group that is shifted downfield due to the attached electronegative carbonyl group. The broad low intensity peak at approximately δ 6.25 ppm was typical of a hydroxyl group proton resonance. The resonances in the region δ 6.90 ppm to δ 7.60 ppm were due to the protons on the aromatic ring (**Spectrum 7.5**). The resonance at δ 6.95 (1H, d, $J = 8.24\text{ Hz}$) was due to H-5' and was *ortho* coupled to H-6'. The resonance at δ 7.58 ppm (1H, dd, $J_{5',6'} = 8.24\text{ Hz}$, $J_{2',6'} = 1.83\text{ Hz}$) was attributed to H-6' as it was observed to be *ortho* coupled to H-5' resulting in a doublet followed by further splitting into a double

doublet as a result of *meta* coupling to H-2'. The H-2' proton signal was observed at δ 7.55 ppm (1H, d, $J = 1.83$ Hz). While at this point it was known that the aromatic ring was 1,3,4-trisubstituted, the position of the methoxy and hydroxy groups was uncertain. The NOESY and COSY NMR spectra were used to assign the positions of these two groups on the aromatic ring.

From the NOESY and COSY NMR spectra (**Spectra 7.9 and 7.10**) a strong correlation was observed between the H-2' proton signal and the protons of the methoxy group only. Therefore, the methoxy group must be attached to the C-3' position on the aromatic ring and the hydroxy group was thus placed at position 4'. Strong correlations were also observed between H-5' and H-6' protons in both the spectra.

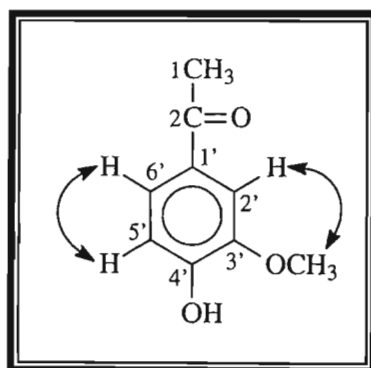


Figure 3.22: NOESY and COSY correlations of compound 7

The ^{13}C NMR spectrum (**Spectrum 7.6**) showed the presence of two carbonyl peaks at δ 190.2 ppm and 201.8 ppm. However, the peak at δ 190.2 ppm was attributed to the carbonyl carbon at position 2 as it showed HMBC correlations to the methyl group and to the aromatic protons (H-2'/6') (**Spectrum 7.8**). This was confirmed by comparing the ^{13}C NMR spectra of compound 7 with that of the library spectrum¹⁸. The ^{13}C NMR spectrum also showed an intense peak at δ 56.1 ppm, which is typical of a methoxy carbon resonance and the quartet at δ 26.6 ppm, which was ascribed to the methyl group carbon at position 2. Here again, the carbon signal was shifted downfield due to the attached carbonyl group. The three carbon signals at δ 111.1 ppm, δ 114.3 ppm and δ 126.9 ppm were due to the protonated carbon atoms of the aromatic ring and were assigned using the HSQC NMR spectrum. The remaining peaks in the ^{13}C NMR spectrum were due to fully substituted carbon atoms and were assigned based on HMBC correlations.

The HSQC NMR spectrum (**Spectrum 7.7**) showed that the proton resonances at δ 6.95 ppm (H-5'), δ 7.55 ppm (H-2') and δ 7.58 ppm (H-6') correlated to the carbon signals at δ 114.3 ppm (C-5'), δ 111.1 ppm (C-2') and δ 126.9 ppm (C-6') respectively. The HSQC NMR spectrum also showed that the carbon peak at δ 56.1 ppm corresponded to the methoxy group protons and the oxygenated methyl carbon at δ 26.6 ppm correlated to the methyl group protons at δ 2.48 ppm.

The HMBC NMR spectrum showed strong 3J correlations from the carbon peak at δ 146.9 ppm to the methoxy group protons and to H-5' and was, therefore assigned to C-3' where the methoxy group is attached. A weak 2J correlation was also observed to the proton at position 2'. The carbon resonance at δ 152.0 ppm showed strong 3J correlations to the aromatic protons H-2' and H-6' as well as weak 2J correlations to the H-5' aromatic proton and was thus ascribed to C-4'. The peak at δ 124.4 ppm showed strong 3J correlations to the H-5' proton and weaker 2J correlations to the H-2' and H-6' proton resonances and was, therefore, attributed to the carbon at position 1'. The C-2' carbon resonance showed strong 3J correlations to the H-6' proton whilst the C-6' carbon resonance showed strong HMBC correlations to the H-2' proton. The carbonyl carbon of the ketone group at C-2 showed correlations to the methyl protons of C-1 and to the aromatic protons H-2' and H-6'. Figure 3.23 shows the relevant HMBC correlations of compound 7 with strong 3J correlations shown in red.

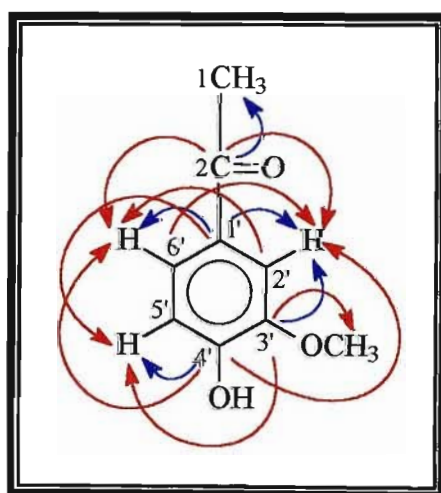


Figure 3.23: HMBC (C→H) correlations of compound 7

Table 3.7: NMR spectral data for compound 7 (400MHz, CDCl₃)

| Position | ¹ H (ppm) | ¹³ C (ppm) | HMBC (C→H) | NOESY | COSY |
|------------------|---|-----------------------|---|------------------|------------------|
| 1' | | 124.4 | H-5' (³ J), H-2'/6' (² J) | | |
| 2' | 7.55 d (J = 1.83 Hz) | 111.1 | H-6' (³ J) | OCH ₃ | OCH ₃ |
| 3' | | 146.9 | OCH ₃ (³ J), H-2' (² J), H-5' (³ J) | | |
| 4' | | 152.0 | H-2'/6' (³ J), H-5' (² J) | | |
| 5' | 6.95 d (J = 8.24 Hz) | 114.3 | | H-6' | H-6' |
| 6' | 7.58 dd (J _{2',6'} = 1.83 Hz, J _{5',6'} = 8.24 Hz) | 126.9 | H-2' (³ J) | H-5' | H-5' |
| 1 | 2.48 s | 26.6 | | | |
| 2 | | 190.2 | H-1 (² J), H-2'/6' (³ J) | | |
| OCH ₃ | 3.94 s | 56.1 | | H-2' | H-2' |
| OH | 6.25 bs | | | | |

Compound 7 was identified as 4'-hydroxy-3'-methoxyacetophenone or more commonly called acetovanillone. It is the methyl ketone of vanillin and has been previously isolated from cacti and also from the roots of *Picrorhiza kurroo*¹⁵. Its concentration in the hydrolysed aqueous phase of the calcium spent liquor effluent is 3.840 x 10⁻⁴ g/L.

3.2.8 Structural Elucidation of Compound 8: Vanillin

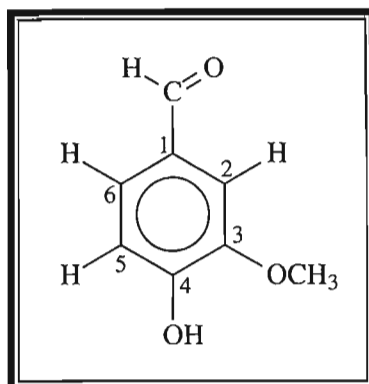


Figure 3.24: Structure of compound 8, vanillin

The mass spectrum of compound 8 (**Spectrum 8.1**) showed a molecular ion $[M^+]$ peak at m/z 152, which corresponded to a molecular formula of $C_8H_8O_3$. The fragmentation pattern observed in the spectrum was consistent with an aldehyde. Characteristic peaks occurred at m/z 151 $[M - H]^+$, m/z 123 $[M - CHO]^+$ and m/z 109 $[M - CHO - CH_3]^+$.

The infrared spectrum (**Spectrum 8.2**) displayed a broad band at 3356 cm^{-1} characteristic of O-H stretching. The sharp band at 1674 cm^{-1} was due to the presence of a carbonyl group while the two bands between 2700 cm^{-1} and 2860 cm^{-1} strongly suggested that the compound possessed an aldehyde group. The strong sharp peaks between 1650 cm^{-1} and 1450 cm^{-1} were due to C=C stretching of an aromatic ring and the corresponding C-H stretching bands occurred at 2924 cm^{-1} . The peaks between 1300 cm^{-1} and 1150 cm^{-1} are typical of C-O stretching vibrations.

The ^1H NMR spectrum (**Spectrum 8.4**) showed a peak at δ 3.95 ppm, integrating to three protons, which is characteristic of a methoxy group proton resonance. A peak at δ 9.81 ppm, integrating to a single proton only, was due to the proton of the aldehyde substituent. The broad low intensity peak at approximately δ 6.20 ppm was attributed to a phenolic group proton. The doublet at δ 7.03 ppm (1H, d, $J = 8.61\text{ Hz}$) was due to the H-5 proton resonance and it showed *ortho* coupling to H-6. The proton resonance at δ 7.42 ppm (1H, dd, $J_{5,6} = 8.24\text{ Hz}$, $J_{2,6} = 1.65\text{ Hz}$) was ascribed to H-6 because it was observed to be *ortho* coupled to H-5 resulting in a doublet followed by further splitting into a doublet of doublets as a result of *meta* coupling to H-2. The H-2 signal at δ 7.40 (1H, d, $J = 1.83\text{ Hz}$) was superimposed with the H-6 signal (**Spectrum 8.5**).

In the carbon spectrum (**Spectrum 8.6**), the resonance at δ 190.9 ppm was due to the carbonyl carbon of the aldehyde group and the strong peak at δ 56.1 ppm corresponded to the methoxy group carbon resonance. The peaks between δ 108.0 ppm and δ 128.0 ppm were due to protonated aromatic carbon resonances while the peaks between δ 129.0 ppm and δ 152.0 ppm were due to the fully substituted carbon atoms of the aromatic ring.

The HSQC NMR spectrum of compound 8 (**Spectrum 8.7**) showed that the carbon signals at δ 114.4 ppm, δ 127.6 ppm and δ 108.7 ppm corresponded to C-2, C-5 and C-6 respectively.

In the HMBC NMR spectrum (**Spectrum 8.8**) the carbon resonance at δ 147.1 ppm showed strong 3J correlations to the methoxy proton resonance as well as to H-5 and weak 2J correlations to H-2. This carbon was, therefore, assigned to C-3 where the methoxy group is attached. Strong 3J correlations were observed between the peak at δ 151.7 ppm and H-2/6. This carbon resonance also showed weak 2J correlations to H-5 and was thus ascribed to C-4. The peak at δ 129.9 ppm showed strong HMBC correlations to H-5 and weak correlations to H-2/6 as well as to the aldehyde proton resonance and was, therefore, assigned to C-1. The spectrum also showed strong 3J correlations from the carbonyl carbon to the aromatic proton resonances, H-2 and H-6 as well as a weak 2J correlation from the carbon at position 5 to H-6 only. The C-2 and C-6 carbon signals showed strong correlations to H-2 and H-6 as well as to the aldehyde proton resonance. The relevant HMBC correlations can be seen in Figure 3.25 below and in Table 3.9.

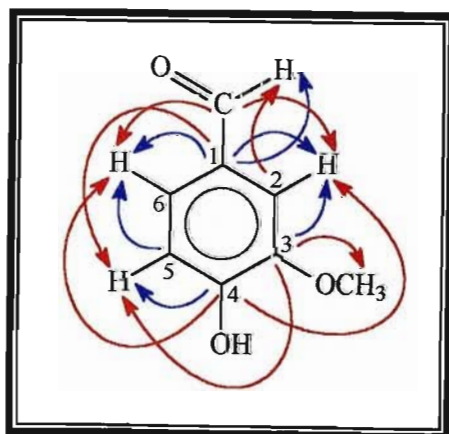


Figure 3.25: HMBC (C→H) correlations of compound 8

The COSY NMR spectrum (**Spectrum 8.9 and 8.10**) was used to confirm the positioning of the aldehyde group, methoxy group and the aromatic protons. COSY correlations were seen between H-5 and H-6, which proved that these two protons were adjacent to each other on the aromatic ring. Correlations were also seen between H-2 and the methoxy group protons only. This confirmed that the methoxy group was adjacent to the H-2 proton and therefore the hydroxy group had to be placed at position 4.

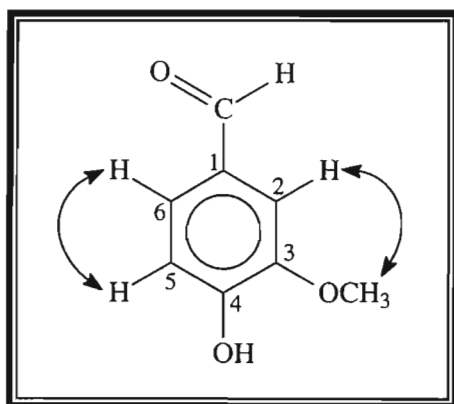


Figure 3.26: COSY correlations of compound 8

The NOESY NMR spectrum (**Spectrum 8.8**) further supported the structure of compound 8. NOESY correlations were seen between the aldehyde proton and the aromatic protons, H-2 and H-6. The spectrum also showed NOESY correlations between the methoxy group protons and the H-2 proton only. The H-5 proton correlated only to the H-6 proton.

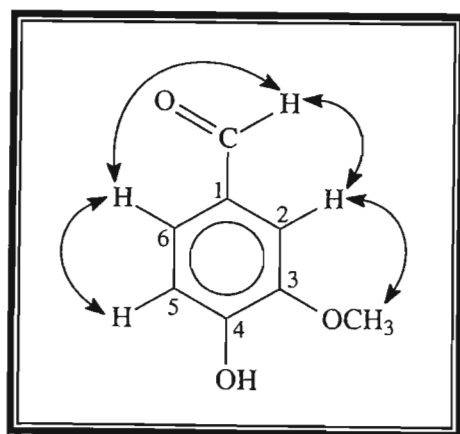


Figure 3.27: NOESY correlations of compound 8

Table 3.8: NMR spectral data for compound 8 (400MHz, CDCl₃)

| Position | ¹ H (ppm) | ¹³ C (ppm) | HMBC (C→H) | NOESY | COSY |
|------------------|---|-----------------------|---|------------------------|------------------|
| 1 | | 129.9 | H-5 (³ J), H-2/6 (² J), CHO (² J) | | |
| 2 | 7.40 d (J=1.83 Hz) | 108.7 | H-6 (³ J), CHO (³ J) | OCH ₃ , CHO | OCH ₃ |
| 3 | | 147.1 | OCH ₃ (³ J), H-2 (² J), H-5 (³ J) | | |
| 4 | | 151.7 | H-2/6 (³ J), H-5 (² J) | | |
| 5 | 7.03 d (J = 8.61 Hz) | 114.4 | H-6 (² J) | H-6 | H-6 |
| 6 | 7.42 dd (J _{2,6} = 1.65 Hz, J _{5,6} = 8.24 Hz) | 127.6 | H-2 (³ J), CHO (³ J) | H-5 | H-5 |
| CHO | 9.81 s | 190.9 | H-2/6 (³ J) | H-2/6 | |
| OCH ₃ | 3.95 s | 56.1 | | H-2 | H-2 |
| OH | 6.20 bs | | | | |

Compound 8 was isolated as a white crystalline solid with a characteristic sweet odour. It was identified as vanillin, which is a common degradation product of sulphite effluents and its approximate concentration was calculated to be 1.800×10^{-3} g/L in the calcium spent liquor effluent.

3.2.9 Structural Elucidation of Compound 9: syringaldehyde

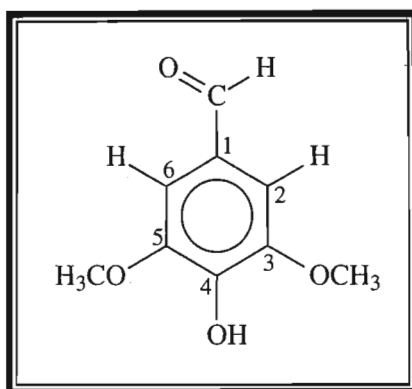


Figure 3.28: Structure of compound 9, syringaldehyde

Compound 9 had an expected molar mass of 182.19 g/mol. This was confirmed by the molecular ion peak at m/z 182 in the mass spectrum (**Spectrum 9.1**). The distinct peak at $[M - 1]^+$ corresponds to the loss of a proton, which is characteristic of an aldehyde group. The peak at m/z 165 indicated a further loss of 17 mass units, which corresponded to the loss of a hydroxyl group.

The infrared spectrum (**Spectrum 9.2**) showed a broad band at 3283 cm^{-1} characteristic of O-H stretching of a hydroxyl group substituent. The two weak absorptions at 2944 cm^{-1} and 2840 cm^{-1} were due to C-H stretching of the aldehyde group while the sharp peak at 1678 cm^{-1} is characteristic of carbonyl group stretching, which could be ascribed to the aldehyde constituent. The peaks between 1650 cm^{-1} and 1450 cm^{-1} were due to C=C stretching of an aromatic ring and the peak at 1110 cm^{-1} is typical of C-O stretching. The distinct sharp peak at 1334 cm^{-1} was attributed to syringyl ring breathing¹².

The ^1H NMR spectrum of this compound (**Spectrum 9.4**) is very simple showing four singlet peaks only. The singlet at δ 9.78 ppm (1H) could be ascribed to the proton of the aldehyde group and the intense singlet at δ 3.94 ppm (6H) is characteristic of the protons of a methoxy group. The singlet at δ 7.12 ppm (2H) was due to the two equivalent aromatic protons, H-2 and H-6. The broad low intensity peak at approximately δ 6.15 ppm (1H) is typical of the proton resonance of a hydroxy group substituent. The integration of the peaks were 1:2:1:6, which suggested that the molecule was symmetrical.

The ^{13}C NMR spectrum of compound 9 (**Spectrum 9.5**) showed a peak at δ 190.8 ppm, which corresponded to the carbonyl group carbon of the aldehyde substituent. The peaks at δ 56.4 ppm and δ 106.6 ppm could be attributed to the carbons of the methoxy groups and the aromatic methine groups respectively. These two peaks are due to two carbon atoms each thus confirming that the compound was symmetrical. The HSQC NMR spectrum (**Spectrum 9.6**) confirmed the assignment of the above peaks. The peaks between δ 128 ppm and δ 148 ppm are due to the fully substituted carbons of the aromatic ring and were assigned based on HMBC correlations.

The HMBC NMR spectrum (**Spectrum 9.7**) showed correlations from the carbon resonance at δ 147.3 ppm to the protons of the methoxy group, the hydroxy proton resonance and the aromatic proton resonances. Therefore, that resonance was assigned to the equivalent carbons C-3 and C-5 where the methoxy groups are attached. The carbon signal at δ 140.8 ppm showed strong 3J correlations to the aromatic protons and weak 2J correlations to the phenolic proton and was ascribed to C-4. The carbon peak at δ 128.3 ppm correlated to the protons of the aromatic ring and the aldehyde proton and was assigned to carbon position 1. The carbon of the aldehyde group showed strong 3J correlations to the aromatic protons only and the protonated carbon resonances (C-2 and C-6) showed strong 3J correlations to the aromatic protons as well as to the proton of the aldehyde group.

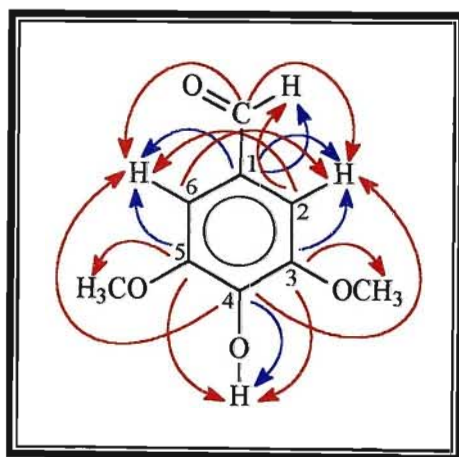


Figure 3.29: HMBC correlations (C→H) of compound 9

The NOESY NMR spectrum of compound 9 (**Spectrum 9.8**) was used to show the correlation between hydrogen atoms through space. Correlations were observed between the aldehyde proton and the protons of the aromatic ring (H-2 and H-6), as well as between the aromatic ring protons and the methoxy group protons. This confirmed the positioning of the methoxy groups at carbons 3 and 5 and the two aromatic methine groups at positions 2 and 6.

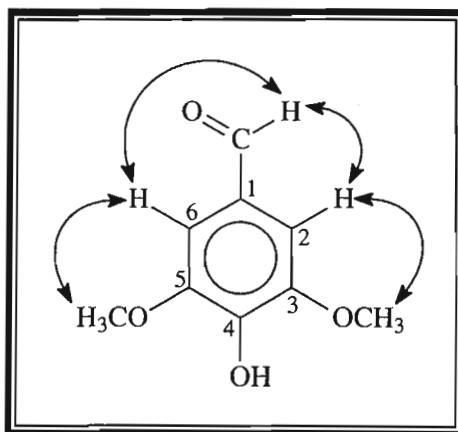


Figure 3.30: NOESY correlations of compound 9

Table 3.9: NMR spectral data for compound 9 (400MHz, CDCl₃)

| Position | ¹ H (ppm) | ¹³ C (ppm) | HMBC (C→H) | NOESY |
|------------------|----------------------|-----------------------|---|------------------------|
| 1 | | 128.3 | CHO (² J), H-2/6 (² J) | |
| 2 | 7.12 s | 106.6 | H-6 (³ J), CHO (³ J) | OCH ₃ , CHO |
| 3 | | 147.3 | OCH ₃ (³ J), H-2 (² J), OH (³ J) | |
| 4 | | 140.8 | H-2/6 (³ J), OH (² J) | |
| 5 | | 147.3 | OCH ₃ (³ J), H-6 (² J), OH (³ J) | |
| 6 | 7.12 s | 106.6 | H-2 (³ J), CHO (³ J) | OCH ₃ , CHO |
| CHO | 9.78 s | 190.8 | H-2/6 (³ J) | H-2/6 |
| OCH ₃ | 3.94 s | 56.4 | | H-2/6 |
| OH | 6.15 bs | | | |

Compound 9 was identified as 4-hydroxy-3,5-dimethoxybenzaldehyde or commonly known as syringaldehyde. It is a regular component of sulphite effluents and its concentration in the calcium spent liquor was approximated at 2.160×10^{-3} g/L.

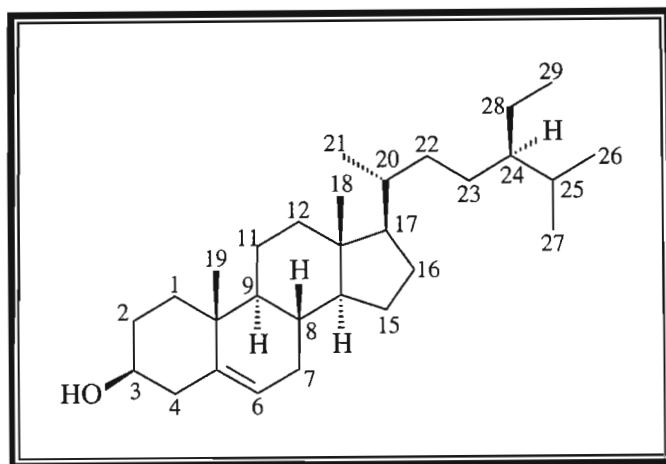
3.2.10 Structural Elucidation of compound 10: β -sitosterol

Figure 3.31: Structure of compound 10, β -sitosterol

Compound 10 was isolated as a white crystalline solid and was immediately identified as a common widely occurring phytosterol. It has been known to be the dominating steroid in both softwood and hardwood pulps and has previously been reported in bleaching effluents¹⁹.

An infrared spectrum (**Spectrum 10.1**) showed absorption peaks at 3437 cm^{-1} (O-H stretching), 2936 cm^{-1} and 2865 cm^{-1} (aliphatic C-H stretching), 1466 cm^{-1} (C-H deformation), 1377 cm^{-1} (CH_3 symmetrical deformations) and 1047 cm^{-1} (C-O stretching).

The ^1H NMR spectrum (**Spectrum 10.2**) indicated the presence of six methyl groups between δ 0.60 ppm and δ 1.0 ppm. The spectrum also showed a multiplet in the double bond region at δ 5.32 ppm and was assigned to the methine proton at position 6. The other multiplet at δ 3.50 ppm was ascribed to the H-3 α methine proton, which had shifted downfield due to the attached electronegative hydroxyl group.

The ^{13}C NMR spectrum (**Spectrum 10.3**) showed a methine carbon resonance at δ 72.0 ppm that has shifted downfield because of the electronegative oxygen atom. This peak was, therefore, assigned to the carbon at position 3. The carbon resonances at δ 141.0 ppm and δ 121.9 ppm are located in the double bond region of the spectrum and were

assigned to the fully substituted carbon at C-5 and the methine carbon at C-6 respectively.

A direct comparison of the ^1H and ^{13}C NMR spectra of compound 11 with that of library spectra identified this compound as β -sitosterol²⁰. It had an approximate concentration of 4.400×10^{-4} g/L in the hydrolysed portion of the calcium spent liquor effluent stream.

3.3 HYDROLYSIS OF THE MAGNESIUM CONDENSATE EFFLUENT

The aqueous phase of the magnesium pulp condensate effluent stream was also subjected to an acid hydrolysis. (Refer to section 4.3.2 of chapter 4 for details of hydrolysis procedure). The following compounds were identified in the organic extract of the hydrolysed magnesium condensate :- two isomers of syringaresinol (~ 0.043 g/L), β -oxysinapyl alcohol ($\sim 8.880 \times 10^{-4}$ g/L), acetovanillone ($\sim 4.200 \times 10^{-4}$ g/L), syringaldehyde ($\sim 1.472 \times 10^{-3}$ g/L) and vanillin ($\sim 1.052 \times 10^{-3}$ g/L). All these compounds have been previously isolated from the hydrolysed calcium spent liquor effluent stream and their detailed structural elucidations can be read in Section 3.2 of this chapter.

3.4 REFERENCES

1. Lussi, M. and Neytzell-de Wilde, F.G., 1987, Quantitative Analysis of Lignosulphonate Using Benzethonium Chloride – Preliminary Investigations, *Water SA*, **13**, 225-228.
2. Searle, C.E., 1986, Chemical Carcinogens and Cancer Prevention, *Chemistry in Britain*, **22**, 211-220.
3. Kontturi, A.-K. and Sundholm, G., 1986, The Extraction and Fractionation of Lignosulphonates with Long Chain Aliphatic Amines, *Acta Chemica Scandinavica*, **A40**, 121-125.
4. Lin, S. Y., 1992, Commercial Spent Pulping Liquors, In: Lin, S.Y. and Dence, C. W. (Eds), *Methods in Lignin Chemistry*, Springer – Verlag : Berlin, p75-80.
5. Eisenbraun, E.W., 1963, The Separation and Fractionation of Lignosulfonic Acids from Spent Sulfite Liquor with Tri-n-Hexylamine in Organic Solvents, *Tappi*, **46**, 104-107.
6. Fengel, D. and Wegener, G., 1983, *Wood : Chemistry, Ultrastructure and Reactions*, Walter de Gruyter & Co. : Berlin, p157-164.
7. Luthe, C.E. and Lewis, N.G., 1986, Identification and Characterisation of Paucidisperse Lignosulphonates, *Holzforschung*, **40**, 153-157.
8. Luthe, C.E., 1990, Isolation and Characterisation of Lignosulphonates from an Ultra High Yield Neutral Sulphite Pulping Effluent, *Holzforschung*, **44**, 107-112.
9. Personal communication with Prof. B.C. Rogers – lecturer at the University of Durban – Westville.
10. King, E.G., Brauns, F. and Hibbert H., 1935, Lignin Sulphonic Acid – A Preliminary Investigation on its Isolation and Structure, *Canadian Journal of Research*, **13(B)**, 88-102.

11. Duffield, A.M., 1967, Mass Spectrometric Fragmentation of Some Lignans, *Journal of Heterocyclic Chemistry*, **4**, 16-22.
12. Sarkanen, K.V. and Ludwig, C.H., 1971, *Lignins : Occurrence, Formation, Structure and Reactions*, John Wiley and Sons : New York, p267-293.
13. Briggs, L.H., Cambie, R.C. and Crouch, R.A.F., 1968, Lirioresinol-C Dimethyl Ether, a Diaxially Substituted 3,7-Dioxabicyclo[3,3,0]octane Lignan from *Macropiper excelsum* (Forst.f.) Miq., *Journal of Chemical Society (C)*, 3042-3045.
14. Pelter, A., 1967, The Mass Spectra of Oxygen Heterocycles. Part IV. The Mass Spectra of some Complex Lignans, *Journal of Chemical Society (C)*, 1376-1380.
15. Dictionary of Natural Products (DNP) on CD – ROM, **version 11.2**, 1982 – 2003, Chapman and Hall Electronic Publishing Division : London.
16. Lundquist, K., 1973, Acid Degradation of Lignin. VIII. Low Molecular Weight Phenols from Acidolysis of Birch Lignin, *Acta Chemica Scandinavica*, **27**, 2597-2606.
17. Black, R.A., Rosen, A.A. and Adams, S.L., 1953, The Chromatographic Separation of Hardwood Extractive Components Giving Colour Reactions with Phloroglucinol, *Journal of the American Chemical Society*, **75**, 5344-5346.
18. *Aldrich Library of ¹³C and ¹H FT NMR Spectra*, 1993, (2), 329A.
19. Gullichsen, J. and Paulapuro, H., 2000, *Forest Products Chemistry*, Fapet Oy : Helsinki, p35-39.
20. *Aldrich Library of ¹³C and ¹H FT NMR Spectra*, 1993, (3), 569A.

CHAPTER 4 : EXPERIMENTAL

4.1 FOREWORD TO EXPERIMENTAL

4.1.1 Nuclear Magnetic Resonance (NMR) Spectroscopy

All ^1H , ^{13}C and two – dimensional NMR spectra were recorded at room temperature on a 300 MHz Varian Gemini spectrophotometer or a 400 MHz Varian UNITY – INOVA spectrophotometer. The solvents used were deuterated chloroform (CDCl_3), deuterated methanol (CD_3OD) or deuterated water (D_2O). The chemical shift values were all recorded in ppm relative to TMS (tetramethylsilane). The spectra were referenced according to the central line of the CDCl_3 signal at $\delta_{\text{H}} = 7.24$ ppm and $\delta_{\text{C}} = 77.2$ ppm, the CD_3OD signal at $\delta_{\text{H}} = 3.34$ ppm and $\delta_{\text{C}} = 49.0$ ppm and for the D_2O signal at $\delta_{\text{H}} = 4.61$ ppm.

4.1.2 Infrared (I.R.) Spectroscopy

All infrared spectra were recorded using a Nicolet Impact 400D Fourier – Transform Infrared (FT – IR) spectrometer, which was calibrated against an air background. The compounds were dissolved in dichloromethane and added dropwise onto the surface of a NaCl window. The solvent was allowed to air evaporate, leaving a thin film of sample on the disc for analysis. The precipitates obtained from the lignosulphonate extraction procedures were analysed using KBr discs. All data were acquired using the OMNIC software.

4.1.3 Ultraviolet Absorption (U.V.) Spectrometry/Spectroscopy

The ultra – violet absorption spectra were obtained on a Varian Cary 1E double beam ultraviolet – visible spectrophotometer, serial number 95071136. The U.V. spectra of the lignosulphonate mixtures were run in deionised water using matched glass cuvettes. The instrument was zeroed against deionised water. The U.V. spectra of the isolated organic compounds were run in dichloromethane using matched quartz cuvettes and the instrument was zeroed against dichloromethane.

4.1.4 Gas Chromatography – Mass Spectroscopy (GC-MS)

All samples were injected manually, using a 1 μ l syringe, onto a HP5 – MS column in the GC – MS with a 1 : 50 split ratio. The starting temperature was 50°C and the sample was held at this temperature for two minutes. The temperature was then ramped at 20°C per minute until a temperature of 300°C was reached. Thereafter, the sample was held for a further fifteen minutes at this maximum temperature. A solvent delay of two minutes was set. Low – resolution mass spectrometry was carried out on an Agilent 5973 mass spectrometer connected to a 6890 GC.

4.1.5 General Chromatography

The organic compounds were isolated using gravity column chromatography thin layer chromatography. Different sized columns were used ranging from 1 – 5 cm in diameter depending on the amount of sample available and the purification stage. Final purifications were generally carried out on an open 0.75 cm diameter Pasteur pipette column. The columns were packed with Merck Art. 9385 silica gel as the stationary phase and separations were carried out under gravity. The mobile phase for both column and thin layer chromatography consisted of varying ratios of hexane, dichloromethane, ethyl acetate and methanol. Thin layer chromatography was carried out on 0.2 mm silica gel, aluminium – backed plates (Merck Art. 5554). The plates were first viewed under U.V. light (336 nm and 254 nm). The plates were then developed using anisaldehyde : concentrated H₂SO₄ : methanol (1:2:97) spray reagent and then heated.

4.1.6 Preparative Thin Layer Chromatography (PTLC)

Some compounds, which were visible under U.V. light, were purified using this technique. The aluminium – backed t.l.c plates were lined with the extract sample 15 mm from the bottom edge. The plates were lined by dipping a capillary tube into the extract sample dissolved in a minimum volume of dichloromethane and allowing it to run onto the silica gel by touching the tip of the tube to the plate. The plates were dried and then developed in a chromatography tank. Compounds of interest were marked as bands under the U.V. light. The marked bands were then cut into small pieces, dissolved in 50 %

methanol in dichloromethane, filtered through cotton wool to remove the silica gel and thereafter the solvent was evaporated.

4.1.7 Melting Points (Mp)

The melting points of all the organic compounds isolated were determined using a Kofler micro – hot stage melting point apparatus and are uncorrected.

4.1.8 Optical Rotation

Optical Rotations were measured using a Perkin Elmer Model 341 Polarimeter, serial number 8995. A quartz Microcell with a tube length of 100 mm and a volume of 1.0 ml was used. The samples were recorded at 20.0°C in chloroform.

4.2 ANALYSIS OF THE CALCIUM SPENT LIQUOR EFFLUENT STREAM

4.2.1 Sampling Procedure

The calcium spent liquor effluent was sampled after the washing and screening stages as the waste spent liquor goes to the effluent drain but before it is pumped to Lignotech. The sample was collected in plastic containers from a sampling spigot of a storage tank. The high pressures necessary for a continuous flow through the pipelines ensured the homogeneity of the effluent sample. The collected sample had a temperature between 85 and 100°C and a pH between 1 and 2 (universal indicator paper).

4.2.2 The Extraction of Lignosulphonates

4.2.2.1 Extraction Method 1^{1,2}

A 500 ml sample of the cooled calcium spent liquor was extracted with 3 x 500 ml portions of chloroform to remove any organic components. Thereafter, the number of sulphonic acid groups in the aqueous phase was determined by a conductometric titration³. This was carried out using a Microprocessor Conductivity meter LF 320 at room temperature with a standard conductivity cell TetraCon® 325 electrode having a

cell constant of 1.000 cm^{-1} . The instrument was first calibrated with the 0.01 M KCl standard provided, which had a conductivity of 1.408 mS/cm at a cell constant of 1.000 cm^{-1} . The conductivity of deionised water was determined as 0.00 mS/cm at a cell constant of 1.000 cm^{-1} .

The conductivity titration was carried out on the aqueous phase of the calcium spent liquor sample of mass 50.05 g . The sample was titrated with a 0.1 M solution of NaOH (prepared by dissolving 2.0 g of NaOH in 500 ml of deionised water) in 0.5 ml increments. The results obtained (Table B1, Appendix B) were plotted on a graph (Graph B1, Appendix B) and the sulphonic acid content was calculated to be $4.995 \times 10^{-5} \text{ mol/g}$. The relevant calculations are shown in Appendix B. This value was used to determine the mass of sample needed such that the concentration of sulphonic acid groups in the sample is equivalent to the concentration of amine to be used.

Step 1:

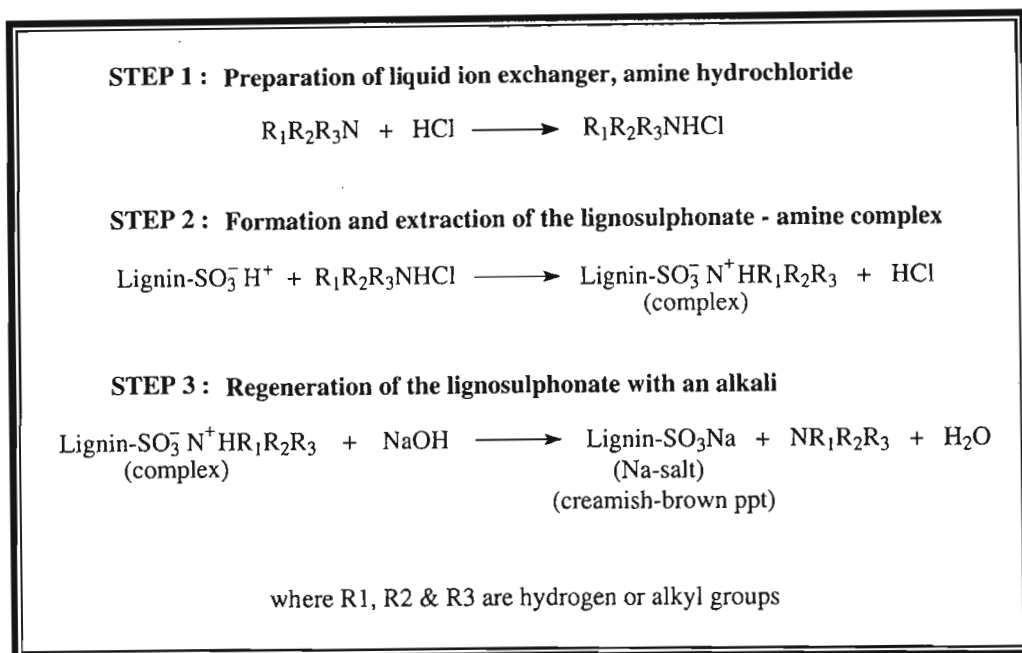
A liquid ion exchanger was prepared by mixing 1 M HCl (150 ml) with a solution of dodecylamine in butanol for 10 minutes in a separating funnel.

Step 2:

The top organic layer (mass = 100.37 g) was removed and added to the aqueous phase of the calcium spent liquor (mass = 77.36 g). The mixture was stirred continuously for 30 minutes at a temperature of $49 - 54^\circ\text{C}$. Thereafter, the two phases were allowed to separate for 2 hours in a separating funnel. The temperature was maintained at $50 - 60^\circ\text{C}$ to facilitate phase separation. The top organic layer was removed and used in step 3.

Step 3:

The organic layer was adjusted to pH 9 using a 1 M NaOH solution and universal indicator paper. The mixture was again allowed to separate for 24 hours at a temperature of $50 - 60^\circ\text{C}$. The bottom aqueous layer was extracted with $3 \times 100 \text{ ml}$ portions of butanol to remove as much of the amine as possible. Thereafter, the aqueous layer was evaporated on a BUCHI Rotavapor and a creamish – brown precipitate (mass = 0.81 g) was collected.



Scheme 4.1: The chemical reactions occurring during the amine extraction of lignosulphonates^{1,2}

4.2.2.2 Extraction Method 2^{4,5}

A 450 ml sample of the aqueous phase of the calcium spent liquor was filtered, neutralised with a saturated NaHCO₃ solution and then concentrated to 200 ml using a BUCHI Rotavapor. The sample was then extracted with 4 x 200 ml portions of diethyl ether followed by 5 x 300 ml portions of butanol. The pH of the aqueous layer was adjusted to 2 with Amberlite 120 (H⁺) resin. Thereafter, the aqueous layer was mixed with dicyclohexylamine (10 ml) and dichloromethane : butanol (5:1, 200 ml) for 5 minutes and separated. The aqueous layer was readjusted to pH 2 with 18 N H₂SO₄ and an analogous extraction sequence was performed three more times. The resulting organic layers were combined and the pH was adjusted to 11 using a 1 M NaOH solution and allowed to separate. Finally, the bottom aqueous layer was washed with 4 x 100 ml portions of diethyl ether, neutralised with Amberlite 120 (H⁺) resin and freeze – dried to give a yellowish – brown crystalline material of mass 5.53 g.

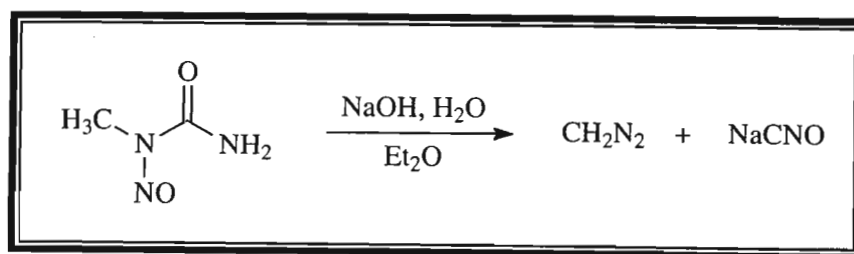
4.2.3 The Lassaigne Sodium Fusion Test⁶

A small portion of the sample to be analysed (~ 50 mg) was placed at the bottom of a short hard – glass fusion tube and a small piece of metallic sodium was positioned halfway down the tube. The mixture was heated carefully over a Bunsen flame until the product was fully roasted. The red – hot glass tube was then immediately plunged into a larger wide – mouthed test – tube containing about 10 ml of deionised water, maintained at a 45° angle at all times. A vigorous reaction occurred causing the smaller fusion tube to fracture and the excess sodium oxide to react with the water. The contents of the larger test – tube was boiled gently for 1 minute and then filtered. The clear sodium fusion solution (SFS) obtained was tested for the presence of sulphur. This was done by dissolving a few crystals of sodium nitroprusside, $\text{Na}_2[\text{Fe}(\text{CN})_5\text{NO}]\cdot 2\text{H}_2\text{O}$, in water (~5 ml) and adding it to the filtrate (SFS). The filtrate turned a bright purple colour indicating the presence of sulphur in the sample. A control sample of aniline sulphate was used to compare the purple colour.

4.2.4 Methylation of Crude Lignosulphonate – Sugar Mixture with Diazomethane

4.2.4.1 Preparation of Ethereal Diazomethane⁷

Diethyl ether (100 ml) was added to a 10 % NaOH solution (100 ml) and the mixture was cooled to 5°C. Finely powdered nitrosomethylurea (500 mg) was added in small portions to this cooled mixture with continuous stirring and cooling. The resulting deep yellow ether layer (top layer) contained the dissolved diazomethane and was decanted and used directly in the methylation procedure.



Scheme 4.2: Formation of Diazomethane⁷

4.2.4.2 Methylation Procedure^{4,5}

To a suspension of the lignosulphonate – sugar mixture (250 mg) in MeOH (10 ml) was added Amberlite 120 (H⁺) resin (7 g). The solution was stirred at room temperature until the mixture was completely soluble in the MeOH (approximately 10 minutes). The resin was filtered off and the filtrate was cooled in ice. The freshly prepared solution of ethereal diazomethane was added in portions to the cooled filtrate until gas evolution ceased. After evaporation of the solvent, a dark brown precipitate of mass 205 mg was obtained.

N.B. The methylation procedure was first attempted on a known compound, *p*-hydroxybenzoic acid, to confirm that the procedure gives successful results and to ensure that the nitrosomethylurea used had not decomposed.

4.2.5 Physical Data of Precipitate from First Extraction

Mass : 0.81 g

Physical Appearance : creamish – brown precipitate

Solubility : water

I.R. Data : ν_{\max}^{KBr} cm⁻¹ : 3416 (O-H stretching), 2938, 2848 (C-H stretching), 1584, 1415 (aromatic C=C stretching), 1209 (sulphonic acid groups), 1131, 1052 (sugar or polysaccharide moieties)

U.V. Data : $\lambda_{\max}^{\text{water}}$ nm (log ϵ) : 205 (3.25), 272 (3.37)

¹H NMR Spectral Data : δ_{H} (ppm) (D₂O, 400 MHz, solvent suppression)
3.0 – 5.5 (sugar molecules), 6.5 – 7.0 (aromatics)

¹³C NMR Spectral Data : δ_{C} (ppm) (D₂O, 300 MHz)
60 – 104 (sugar molecules)

4.2.6 Physical Data of Precipitate from Second Extraction

Mass : 5.53 g

Physical Appearance : yellowish – brown crystalline material

Solubility : water

I.R. Data : $\nu_{\text{max}}^{\text{KBr}}$ cm^{-1} : 3415 (O-H stretching), 2950, 2860 (C-H stretching), 1593, 1425 (aromatic C=C stretching), 1207 (sulphonic acid groups), 1117, 1051 (sugar or polysaccharide moieties)

^1H NMR Spectral Data : δ_{H} (ppm) (D_2O , 400 MHz, solvent suppression)
3.0 – 5.0 (sugar molecules), 6.5 – 7.0 (aromatics)

^{13}C NMR Spectral Data : δ_{C} (ppm) (D_2O , 300 MHz)
60 – 104 (sugar molecules)

4.2.7 Physical Data of Methylated Product

Mass : 205 mg

Physical Appearance : dark brown precipitate

Solubility : partially soluble in water, completely soluble in methanol

^1H NMR Spectral Data : δ_{H} (ppm) (D_2O , 400 MHz, solvent suppression)
1.9 (s), 2.7 (d), 3.0 – 5.0 (sugar molecules), 6.2 – 7.0 (aromatics)

^{13}C NMR Spectral Data : δ_{C} (ppm) (D_2O , 300 MHz)
154.1, 107.8, 79.7, 79.3, 78.9, 61.1, 56.6, 56.5, 56.4, 48.1, 48.0, 39.5, 30.8, 30.5, 27.1

4.2.8 Hydrolysis of the Calcium Spent Liquor Effluent

25 Litres of calcium spent liquor was extracted with chloroform to remove any organic components. The large volume was extracted in batches of 5 litres using 3 x 1.5 litre portions of chloroform for each batch. The organic portions were evaporated using a BUCHI Rotavapor to recover the chloroform. The aqueous portions were acidified with concentrated HCl to a pH of below 1 (universal indicator paper) and boiled on a hotplate for approximately 4 hours. The cooled solution was re-extracted with the recycled chloroform as described above and the organic portions were, once again, evaporated using the BUCHI Rotavapor.

4.3 ANALYSIS OF THE MAGNESIUM CONDENSATE EFFLUENT STREAM

4.3.1 Sampling Procedure

The magnesium effluent is burned to produce energy and the resulting ash is slurried and pre – treated to recover the MgO. During the burning process, some of the gases condense to form a colourless magnesium condensate, which goes to the effluent drain. Some of this colourless condensate is also used as wash water during the washing and screening stages, which gives it a reddish – brown colour. A sample of the magnesium condensate, which had been used for washing, was collected in plastic containers from a sampling spigot. The collected sample had a temperature between 85 and 100°C and a pH between 2 and 3 (universal indicator paper).

4.3.2 Hydrolysis of the Magnesium Condensate Effluent

25 litres of the reddish – brown magnesium condensate was extracted with chloroform to remove any organic components. The large volume was extracted in the same manner as described for the calcium spent liquor effluent. The aqueous portions were acidified with concentrated HCl to a pH of below 1 (universal indicator paper) and boiled on a hotplate for approximately 4 hours. The cooled solution was re-extracted with the recycled chloroform and the organic portions were evaporated using the BUCHI Rotavapor.

4.4 PHYSICAL DATA OF ISOLATED ORGANIC COMPOUNDS

Mass of organic extract (Ca spent liquor) = 19.878 g

Mass of organic extract (Mg condensate) = 10.556 g

4.4.1 Physical Data for Compound 1

Name : *epi*-syringaresinol

Physical Appearance : white crystalline solid

Yield : 350 mg (Ca spent liquor), 1.08 g (Mg condensate – mixture of two isomers)

Melting Point : 190 – 195°C (Lit. = 210 – 211°C)⁸

Optical Rotation : $[\alpha]_{\text{D}}^{20} = +143.4^{\circ}$ ($c = 0.638$) (Lit. = $+127^{\circ}$)^{8,9}

Mass Spectral Data : LRMS : $[M^+]$ at m/z 418, $\text{C}_{22}\text{H}_{26}\text{O}_8$ requires 418.442 g/mol

EIMS : m/z : 418, 235, 210, 181, 167, 161, 140, 123, 95, 77, 55, 38

I.R. Data : $\nu_{\text{max}}^{\text{NaCl}} \text{ cm}^{-1}$: 3425 (O-H stretching), 2943, 2850 (aliphatic C-H stretching),
1612, 1524 (C=C stretching of an aromatic ring), 1350 – 1300
(syringyl ring breathing), 1113 (C-O stretching)

U.V. Data : $\lambda_{\text{max}}^{\text{CH}_2\text{Cl}_2} \text{ nm}$ ($\log \epsilon$) : 239 (3.27), 271 (3.33)

The ^1H and ^{13}C NMR spectral data are listed in Table 3.1 in Chapter 3.

4.4.2 Physical Data for Compound 2

Name : *meso*-syringaresinol

Physical Appearance : brown amorphous substance

Yield : 3.55 g (Ca spent liquor – mixture of two isomers), 1.08 mg (Mg condensate – mixture of two isomers)

Optical Rotation* : Lit. : $[\alpha]_{\text{D}}^{25} = 0^{\circ 10}$

* The optical rotation of compound 2, *meso*-syringaresinol, was not determined as it was isolated as a mixture with compound 1, *epi*-syringaresinol.

Mass Spectral Data : LRMS : $[M^+]$ at m/z 418, $C_{22}H_{26}O_8$ requires 418.442 g/mol

EIMS : m/z : 418, 235, 210, 181, 167, 161, 140, 123, 95, 77, 55, 36

I.R. Data : ν_{\max}^{NaCl} cm^{-1} : 3420 (O-H stretching), 2936, 2850 (aliphatic C-H stretching),
1618, 1516 (C=C stretching of an aromatic ring), 1327
(syringyl ring breathing), 1116 (C-O stretching)

U.V. Data : $\lambda_{\max}^{\text{CH}_2\text{Cl}_2}$ nm ($\log \epsilon$) : 235 (3.28), 276 (3.35)

The ^1H and ^{13}C NMR spectral data are listed in Table 3.2 in Chapter 3.

4.4.3 Physical Data for Compound 3

Name : *meso*-yangambin

Physical Appearance : pale yellow amorphous substance

Yield : 15 mg (Ca spent liquor)

Optical Rotation : $[\alpha]_{\text{D}}^{20} = 0^\circ$ ($c = 0.266$)

Mass Spectral Data : LRMS : $[M^+]$ at m/z 446, $C_{24}H_{30}O_8$ requires 446.496 g/mol

EIMS : m/z : 446, 281, 235, 224, 207, 195, 181, 125, 93, 73, 55, 38

I.R. Data : ν_{\max}^{NaCl} cm^{-1} : 3429 (O-H stretching), 2926, 2849 (aliphatic C-H stretching),
1594, 1512 (C=C stretching of an aromatic ring), 1131 (C-O
stretching)

U.V. Data : $\lambda_{\max}^{\text{CH}_2\text{Cl}_2}$ nm ($\log \epsilon$) : 233 (3.25), 275 (3.32)

The ^1H and ^{13}C NMR spectral data are listed in Table 3.3 in Chapter 3.

4.4.4 Physical Data for Compound 4

Name : methoxyeugenol

Physical Appearance : yellowish – brown amorphous substance with characteristic odour

Yield : 36.3 mg (Ca spent liquor)

Mass Spectral Data : LRMS : $[M^+]$ at m/z 194, $C_{11}H_{14}O_3$ requires 194.230 g/mol

EIMS : m/z : 194, 179, 167, 147, 131, 119, 91, 77, 65, 53, 39

I.R. Data : $\nu_{\max}^{NaCl} \text{ cm}^{-1}$: 3511 (O-H stretching), 3079, 3000 (aromatic C-H stretching), 2941, 2841 (aliphatic C-H stretching), 1644 (vinyl group stretching), 1618, 1518 (C=C stretching of an aromatic ring), 1328 (syringyl ring breathing), 1116 (C-O stretching)

U.V. Data : $\lambda_{\max}^{CH_2Cl_2} \text{ nm}$ (log ϵ) : 237 (3.53), 273 (3.59)

The 1H and ^{13}C NMR spectral data are listed in Table 3.4 in Chapter 3.

4.4.5 Physical Data for Compound 5

Name : β -oxysinapyl alcohol

Physical Appearance : brown amorphous substance

Yield : 29.1 mg (Ca spent liquor), 22.2 mg (Mg condensate)

Melting Point* : Lit. = 106.5 – 107.5°C¹¹

Mass Spectral Data : LRMS : $[M^+]$ at m/z 226, $C_{11}H_{14}O_5$ requires 226.228 g/mol

EIMS : m/z : 226, 167, 151, 123, 106, 78, 66, 53, 39

* The melting point of compound 5, β -oxysinapyl alcohol, was not determined as it was isolated as a gum.

I.R. Data : ν_{\max}^{NaCl} cm^{-1} : 3426 (O-H stretching), 2936, 2846 (aliphatic C-H stretching), 1726 (C=O stretching), 1614, 1518 (C=C stretching of an aromatic ring), 1338 (syringyl ring breathing), 1220, 1119 (C-O stretching)

U.V. Data : $\lambda_{\max}^{\text{CH}_2\text{Cl}_2}$ nm (log ϵ) : 238 (3.45), 289 (3.54)

The ^1H and ^{13}C NMR spectral data are listed in Table 3.5 in Chapter 3.

4.4.6 Physical Data for Compound 6

Name : sinapyl aldehyde

Physical Appearance : brown amorphous substance

Yield : 18.6 mg (Ca spent liquor)

Melting Point* : Lit. = 108.5 – 109.5°C⁸

Mass Spectral Data : LRMS : $[\text{M}^+]$ at m/z 208, $\text{C}_{11}\text{H}_{12}\text{O}_4$ requires 208.213 g/mol

EIMS : m/z : 208, 207, 180, 165, 137, 119, 91, 65, 52, 39

I.R. Data : ν_{\max}^{NaCl} cm^{-1} : 3403 (O-H stretching), 2941, 2844 (C-H stretching of aldehyde group), 1670 (C=O stretching), 1516, 1459 (C=C stretching of an aromatic ring), 1339 (syringyl ring breathing), 1219, 1122 (C-O stretching)

U.V. Data : $\lambda_{\max}^{\text{CH}_2\text{Cl}_2}$ nm (log ϵ) : 241 (3.54), 335 (3.69)

The ^1H and ^{13}C NMR spectral data are listed in Table 3.6 in Chapter 3.

* The melting point of compound 6, sinapyl aldehyde, was not determined as it was isolated as a gum.

4.4.7 Physical Data for Compound 7

Name : acetovanillone

Physical Appearance : yellow amorphous substance

Yield : 9.6 mg (Ca spent liquor), 10.5 mg (Mg condensate)

Melting Point* : Lit. = 115°C⁸

Mass Spectral Data : LRMS : [M⁺] at m/z 166, C₉H₁₀O₃ requires 166.176 g/mol

EIMS : m/z : 166, 151, 137, 119, 95, 77, 65, 51

I.R. Data : ν_{\max}^{NaCl} cm⁻¹ : 3404 (O-H stretching), 2948, 2850 (aliphatic C-H stretching), 1666 (C=O stretching), 1595, 1519 (C=C stretching of an aromatic ring), 1307 (C-O stretching), 1154 (1,3,4-trisubstituted aromatic ring)

U.V. Data : $\lambda_{\max}^{\text{CH}_2\text{Cl}_2}$ nm (log ϵ) : 233 (3.55), 315 (3.68)

The ¹H and ¹³C NMR spectral data are listed in Table 3.7 in Chapter 3.

4.4.8 Physical Data for Compound 8

Name : vanillin

Physical Appearance : white crystalline solid with characteristic sweet odour

Yield : 45.0 mg (Ca spent liquor), 26.3 mg (Mg condensate)

Melting Point : 79 – 82°C (Lit. = 81 – 82°C)⁸

Mass Spectral Data : LRMS : [M⁺] at m/z 152, C₈H₈O₃ requires 152.149 g/mol

EIMS : m/z : 152, 151, 123, 109, 81, 53, 39

* The melting point of compound 7, acetovanillone, was not determined as it was isolated as a gum.

I.R. Data : ν_{\max}^{NaCl} cm^{-1} : 3356 (O-H stretching), 2924 (aromatic C-H stretching), 2852, 2737 (C-H stretching of aldehyde group), 1674 (C=O stretching), 1597, 1510 (C=C stretching of an aromatic ring), 1350-1300 (syringyl ring breathing), 1300-1150 (C-O stretching)

U.V. Data : $\lambda_{\max}^{\text{CH}_2\text{Cl}_2}$ nm (log ϵ) : 233 (3.38), 274 (3.45), 303 (3.49)

The ^1H and ^{13}C NMR spectral data are listed in Table 3.8 in Chapter 3.

4.4.9 Physical Data for Compound 9

Name : syringaldehyde

Physical Appearance : yellow crystalline solid

Yield : 54.4 mg (Ca spent liquor), 36.8 mg (Mg condensate)

Melting Point : 108 – 111°C (Lit. = 113 – 114°C)⁸

Mass Spectral Data : LRMS : [M^+] at m/z 182, $\text{C}_9\text{H}_{10}\text{O}_4$ requires 182.175 g/mol

EIMS : m/z : 182, 181, 167, 165, 139, 111, 96, 79, 65, 51, 39

I.R. Data : ν_{\max}^{NaCl} cm^{-1} : 3283 (O-H stretching), 2944, 2840 (C-H stretching of aldehyde group), 1678 (C=O stretching), 1650-1450 (C=C stretching of an aromatic ring), 1334 (syringyl ring breathing), 1251, 1110 (C-O stretching)

U.V. Data : $\lambda_{\max}^{\text{CH}_2\text{Cl}_2}$ nm (log ϵ) : 235 (3.34), 296 (3.44)

The ^1H and ^{13}C NMR spectral data are listed in Table 3.9 in Chapter 3.

4.4.10 Physical Data for Compound 10

Name : β -sitosterol

Physical Appearance : white crystalline solid

Yield : 11.0 mg

Melting Point : 132 – 136°C (Lit. = 136 – 138°C)¹²

Optical Rotation : $[\alpha]_D^{20} = -32.28^\circ$ (c = 0.220) (Lit. = -35°)⁸

I.R. Data : ν_{\max}^{NaCl} cm^{-1} : 3437 (O-H stretching), 2936, 2865 (aliphatic C-H stretching),
1466 (C-H deformations), 1377 (CH₃ symmetrical deformations), 1047 (C-O stretching)

¹H NMR Spectral Data : δ_{H} (ppm) (CDCl₃, 300 MHz)
5.32 (1H, d, $J = 4.52$ Hz, H-6), 3.50 (1H, m, H-3), 0.98 (3H, s, H-19), 0.89 (3H, d, $J = 6.42$ Hz, H-21), 0.82 (3H, t, $J = 7.21$ Hz, H-29), 0.80 (3H, d, $J = 7.54$ Hz, H-26), 0.79 (3H, d, $J = 7.13$ Hz, H-27), 0.65 (3H, s, H-18)

¹³C NMR Spectral Data : δ_{C} (ppm) (CDCl₃, 300MHz)
140.8 (C-5), 121.7 (C-6), 71.8 (C-3), 56.8 (C-14), 56.0 (C-17), 50.1 (C-9), 45.8 (C-24), 42.7 (C-4), 42.3 (C-13), 39.8 (C-12), 37.2 (C-1), 36.5 (C-10), 36.1 (C-20), 33.9 (C-22), 31.9 (C-8), 31.7 (C-2), 29.7 (C-7), 29.1 (C-25), 28.3 (C-16), 26.0 (C-23), 24.3 (C-15), 23.1 (C-28), 21.1 (C-11), 19.8 (C-26), 19.4 (C-19), 19.0 (C-27), 18.8 (C-21), 12.0 (C-29), 11.9 (C-18)

4.5 REFERENCES

1. Kontturi, A.-K. and Sundholm, G., 1986, The Extraction and Fractionation of Lignosulphonates with Long Chain Aliphatic Amines, *Acta Chemica Scandinavica*, **A40**, 121-125.
2. Lin, S. Y., 1992, Commercial Spent Pulping Liquors, In : Lin, S.Y. and Dence, C. W. (Eds), *Methods in Lignin Chemistry*, Springer – Verlag : Berlin, p75-80.
3. Beatson, R.P., 1992, Determination of Sulfonate Groups and Total Sulfur, In : Lin, S.Y. and Dence, C. W. (Eds), *Methods in Lignin Chemistry*, Springer – Verlag : Berlin, p474-477.
4. Luthe, C.E. and Lewis, N.G., 1986, Identification and Characterisation of Paucidisperse Lignosulphonates, *Holzforschung*, **40**, 153-157.
5. Luthe, C.E., 1990, Isolation and Characterisation of Lignosulphonates from an Ultra High Yield Neutral Sulphite Pulping Effluent, *Holzforschung*, **44**, 107-112.
6. Mann, F. G. and Saunders, B. C., 1973, *Practical Organic Chemistry : New Impression*, 4th ed., Longman Group Limited, England, p321-326
7. Arndt, F., 1943, Note 3 In : *Organic Syntheses*, Collective Volume **2**, John Wiley and Sons Inc. : New York, p165-167.
8. Dictionary of Natural Products (DNP) on CD – ROM, **version 11.2**, 1982 – 2003, Chapman and Hall Electronic Publishing Division : London.
9. Briggs, L.H., Cambie, R.C. and Crouch, R.A.F., 1968, Lirioresinol-C Dimethyl Ether, a Diaxially Substituted 3,7-Dioxabicyclo[3,3,0]octane Lignan from *Macropiper excelsum* (Forst.f.) Miq., *Journal of Chemical Society (C)*, 3042-3045.
10. Moodley, B., 2001, *Characterisation of SAPPI SAICCOR Pulp Mill's Effluent*, MSc Dissertation, School of Pure and Applied Chemistry, University of Natal, Durban.

11. Lundquist, K., 1973, Acid Degradation of Lignin. VIII. Low Molecular Weight Phenols from Acidolysis of Birch Lignin, *Acta Chemica Scandinavica*, **27**, 2597-2606.

12. Lee, C-K. and Chang, M-H., 2000, The Chemical Constituents from the Heartwood of *Eucalyptus citriodora*, *Journal of the Chinese Chemical Society*, **47**, 555-560.

CHAPTER 5 : BIOLOGICAL ACTIVITY OF COMPOUND 1

The range of biological activities of lignans is broad. Refer to section 2.1.3 in chapter 2 for a description of some known biologically active lignans. The lignan, *epi-syringaresinol*, isolated from this work, was tested for its anti – inflammatory and anti – oxidant activities using the chemiluminescence and DPPH (α,α -diphenyl- β -picrylhydrazyl) bioassays respectively^{†‡}.

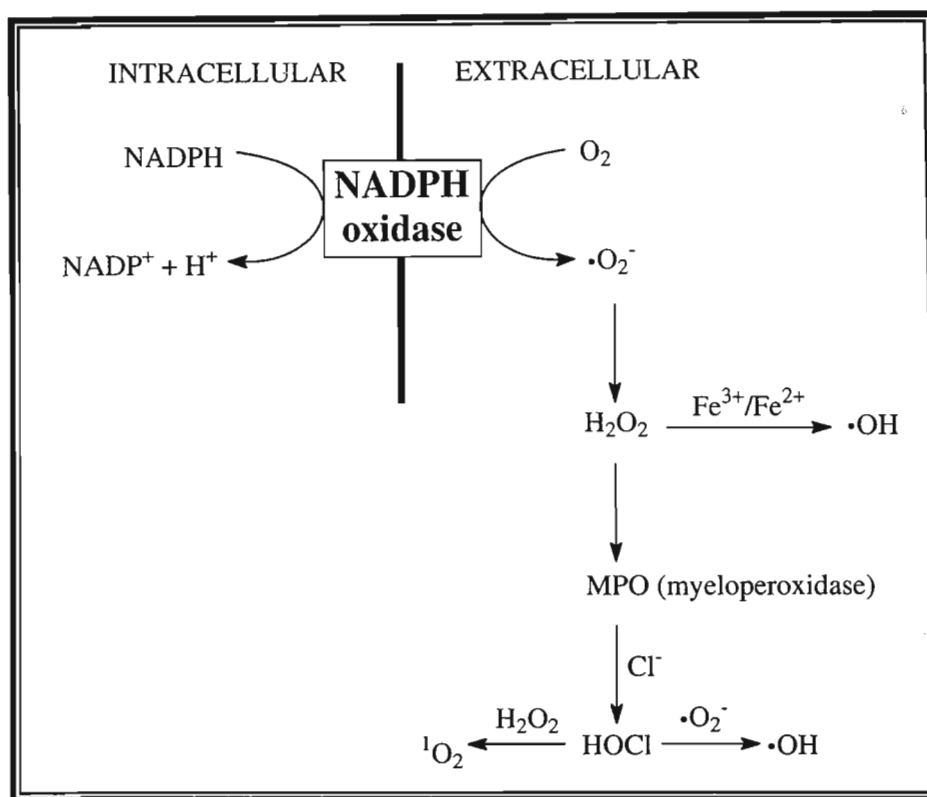
5.1 THE CHEMILUMINESCENCE BIOASSAY

5.1.1 Introduction

The inflammatory response caused by an infection stimulates special phagocytic cells known as polymorphonuclear leukocytes (PMNs)¹. These cells are essential to the host's defence mechanism against invading micro – organisms or other pathogens². They react by migrating to the site of inflammation where they ingest the foreign invader. The subsequent release of toxic reactive oxygen species (ROS) and proteolytic enzymes within the PMNs results in the inactivation of the ingested material^{2,3}. These ROS are generated *via* the “respiratory burst”. This process involves the intake of large amounts of molecular oxygen, which is reduced to the superoxide anion ($\cdot\text{O}_2^-$) by the activity of the enzyme NADPH oxidase^{1,2,4}. Superoxide anion is then converted into other ROS such as hydrogen peroxide (H_2O_2), hydroxyl radicals ($\cdot\text{OH}$) and hypochlorous acid (HOCl)². Scheme 5.1 illustrates the formation of ROS *via* NADPH oxidase.

[†] Both the chemiluminescence bioassay and DPPH bioassay were carried out by a fellow colleague, Miss Dashnie Naidoo, at the University of Utrecht, Netherlands, under the supervision of Dr. A.J.J. van den Berg.

[‡] From the three lignans isolated in this study, only *epi-syringaresinol* was isolated in its pure form at the time the bioassay screenings were undertaken.



Scheme 5.1: Formation of ROS via the enzyme NADPH oxidase⁴

Although the formation of ROS by PMNs is a physiological immune response by the host to kill invading micro – organisms, these toxic oxygen radicals can cause excessive tissue damage during chronic inflammation, for example during rheumatoid arthritis^{2,3}. The chemiluminescence bioassay tests the anti – inflammatory response of a compound by measuring the degree to which the compound inhibits the formation of ROS. In this study luminol – enhanced chemiluminescence was used to detect ROS production. During the reaction of luminol with the ROS, light is produced, which is measured with a photomultiplier tube as the so – called chemiluminescence⁵.

5.1.2 Experimental Procedure

PMNs were isolated from venous blood of five healthy volunteers. The cells were diluted to 1×10^7 PMNs per ml in HBSS (Hank's Buffered Salt Solution). The test sample was serially diluted to final volumes of 50 μl in a transparent flat – bottomed 96 – well microtitre plate. To each well, 50 μl of the PMN suspension, 50 μl of luminol and 50 μl of serum – treated zymosan (STZ) were added. STZ was added to activate the PMNs.

The controls consisted of cells with luminol and buffer. The chemiluminescence of each well was monitored every 2 minutes for 0.5 seconds during a 30 minute period using a Titertek Luminoskan luminometer. Maximum peak levels were used to calculate the inhibitory activity of the test sample in comparison with the control.

5.1.3 Results

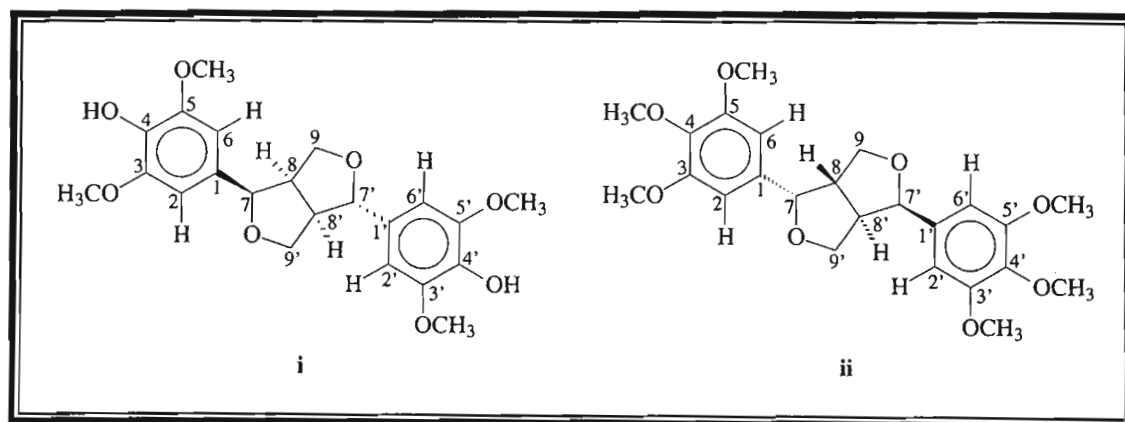


Figure 5.1: Structure of *epi*-syringaresinol (i) and cedpetine (ii)

The anti – inflammatory activity of compound 1, *epi*-syringaresinol, was tested against the PMNs of all five donors. The IC_{50} value recorded for each donor was the concentration in the test system giving 50 % inhibition. The values recorded were compared to those of the lignan, cedpetine[†], which has a similar structure to *epi*-syringaresinol (Figure 5.1). Table 5.1 lists the relative IC_{50} values obtained for both lignans from each donor.

Table 5.1 IC_{50} ($\mu\text{g/ml}$) values of *epi*-syringaresinol and cedpetine

| | <i>epi</i> -syringaresinol | cedpetine |
|----------------|--------------------------------|--------------------------------|
| | IC_{50} ($\mu\text{g/ml}$) | IC_{50} ($\mu\text{g/ml}$) |
| FIRST DONOR | 6.00 | >200 |
| SECOND DONOR | 4.43 | >200 |
| THIRD DONOR | 2.09 | >200 |
| FOURTH DONOR | 8.06 | - |
| FIFTH DONOR | 0.94 | - |
| AVERAGE | 4.30 | - |

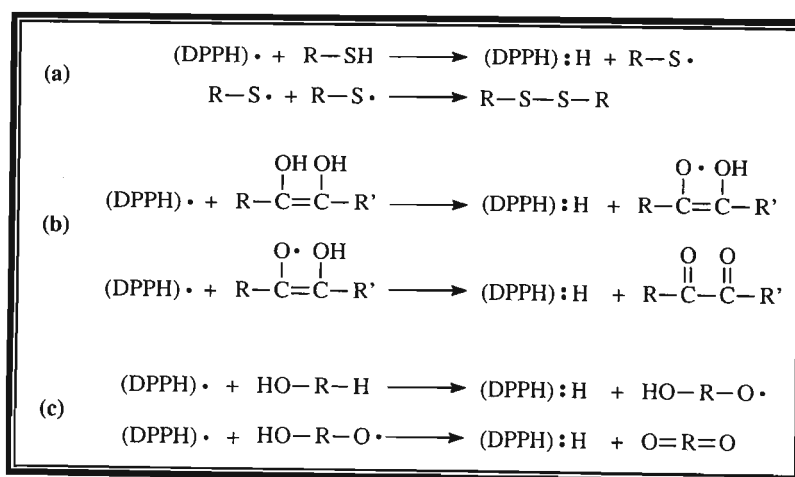
[†] Cedpetine was not isolated at the time the screenings were undertaken. However, this lignan was identified as one of the novel lignans isolated from *Cedrelopsis grevei* by Dashnie Naidoo during her MSc research study⁶.

From the above results it can be concluded that *epi*-syringaresinol is highly reactive and regarded as anti – inflammatory since it inhibits chemiluminescence at a low concentration. Cedpetine differs in structure to *epi*-syringaresinol by the stereochemistry of the two dihydrofuran rings and by the presence of methoxy groups instead of hydroxy groups at the C-4 and C-4' positions. However, cedpetine was observed to be inactive in the chemiluminescence. These results suggested that lignans with attached hydroxy groups at the 4/4' position show greater inhibition of ROS than lignans with attached methoxy groups at the same position and that the stereochemistry of the substituents in the two dihydrofuran rings could also affect the biological activity of the lignan.

5.2 THE DPPH BIOASSAY

5.2.1 Introduction

Compounds with anti – oxidant properties are useful in industry, especially the food industry. Anti – oxidants are capable of interacting with oxidative free radicals in the body thus preventing the accumulation of excessive free radicals in humans and other organisms. The anti – oxidant activity of a compound can be determined by the use of stable free radicals. In this study, the DPPH (α,α -diphenyl- β -picrylhydrazyl) radical was used to estimate the free radical scavenging activity of compound 1, *epi*-syringaresinol. DPPH has previously been reported as a “convenient and simple test to evaluate scavenging activity of natural products”⁷. Scheme 5.2 illustrates the mechanism of the reactions between the DPPH radical and various different oxidisable groups.



Scheme 5.2: Mechanism of reaction of the DPPH radical⁸

5.2.2 Experimental Procedure

Fresh DPPH stock solution was prepared by dissolving 8 mg of DPPH in 40 ml of 75 % ethanol to give a concentration of 0.2 mg/ml. The test sample was serially diluted to final volumes of 100 μ l in a transparent flat – bottomed 96 – well microtitre plate. Thereafter, 100 μ l of 75 % ethanol was added to wells A3 – G3, A6 – G6, A9 – G9 and A12 – G12; and 100 μ l of DPPH stock solution was added to the remaining wells from A to G. The controls were prepared as follows:- wells H1 – H4 were filled with 200 μ l of 75 % ethanol; wells H5 – H8 were filled with 150 μ l of 75 % ethanol and 50 μ l of DPPH stock solution; wells H9 – H12 were filled with 100 μ l of 75 % ethanol and 100 μ l of DPPH stock solution. The plate was covered and incubated for 15 minutes at room temperature before the absorption was read at a wavelength of 550 nm using an Elisareader. The IC₅₀ values were determined in comparison to the controls.

5.2.3 Results

An IC₅₀ value of 34 μ g/ml was recorded for compound 1, *epi*-syringaresinol. This value suggests that *epi*-syringaresinol is active at low concentrations, quenching the free radicals produced by DPPH and can be considered as an anti – oxidant.

5.3 DISCUSSION

Epi-syringaresinol showed strong anti – inflammatory activity in the chemiluminescence bioassay. However, the results obtained were insufficient in determining the exact mode of action of compound 1. Inhibition of chemiluminescence by a compound could be attributable to many factors :- the compound may be toxic and will, therefore, destroy the PMNs before the ROS are produced; the compound may inhibit the NADPH oxidase enzyme responsible for radical production; or the compound could be capable of scavenging off already formed ROS in the cell.

Epi-syringaresinol was found to be non – toxic and showed strong anti – oxidant activity in the DPPH bioassay. Therefore, based on the above results, it can be concluded that *epi*-syringaresinol is a non – toxic radical scavenger (anti – oxidant). However, further testing on compound 1 is necessary to determine its use, if any, in the food and drug industry.

5.4 REFERENCES

1. Stites, D.P., Stobo, J.D. and Wells, J.V. (Eds), 1987, Phagocytic Cells : Chemotaxis and Effector Functions of Macrophages and Granulocytes, In : *Basic and Clinical Immunology*, 6th ed., Prentice – Hall International Inc. : London, UK, p96-113.
2. DeLeo, F.R. and Quinn, M.T., 1996, Assembly of the Phagocyte NADPH Oxidase : Molecular Interaction of Oxidase Proteins, *Journal of Leukocyte Biology*, **60**, 677-691.
3. Halkes, S.B.A., 1998, *Filipendula ulmaria : A Study on the Immunomodulatory Activity of Extracts and Constituents*, PhD Thesis, University of Utrecht, Netherlands, p25-26.
4. Hampton, M.B., Kettle, A.J. and Winterbourn, C.C., 1998, Inside the Neutrophil Phagosome : Oxidants, Myeloperoxidase, and Bacterial Killing, *Blood : The Journal of the American Society of Hematology*, **92**, 3007-3017.
5. DeChatelet, L.R., Long, G.D., Shirley, P.S., Bass, D.A., Thomas, M.J., Henderson, F.W. and Cohen, M.S., 1982, Mechanism of the Luminol – Dependent Chemiluminescence of Human Neutrophils, *The Journal of Immunology*, **129**, 1589-1593.
6. Naidoo, D., 2001, *Extractives from the Meliaceae and Ptaeroxylaceae*, MSc dissertation, School of Pure and Applied Chemistry, University of Natal, Durban, South Africa.
7. Fourneau, C., Laurens, A., Hocquemiller, R. and Cavé, A., 1996, Radical Scavenging Evaluation of Green Tea Extracts, *Phytotherapy Research*, **10**, 529-530.
8. Blois, M.S., 1958, Antioxidant Determinations by the Use of a Stable Free Radical, *Nature*, **181**, 1199-1200.

CHAPTER 6 : CONCLUSION

6.1 DISCUSSION

SAPPI SAICCOR uses the acid sulphite process to produce its dissolving pulp. This type of pulping process converts insoluble lignin into soluble lignosulphonates, which is eliminated into the effluent streams. Therefore, the aqueous portions of the two effluent streams, namely, the calcium spent liquor and the magnesium condensate were analysed for lignosulphonates. However, the extraction and isolation of pure lignosulphonates proved to be very difficult, mainly due to the hydrophilic nature of these compounds. The two extraction procedures employed both yielded a mixture of lignosulphonates with a large proportion of sugars.

An attempt was then made to try and derivatise the crude lignosulphonate product, thus rendering it organic soluble. However, the methylation procedure using diazomethane was also unsuccessful. The results of the NMR and infrared spectroscopic data did not show the formation of methyl esters.

An acid hydrolysis of the aqueous phase using concentrated hydrochloric acid resulted in the degradation of the lignin molecules mainly by cleavage of the ether linkages to give considerable amounts of low molecular weight lignin monomers and dimers. These organic components were extracted into chloroform and characterised using various chromatographic and spectroscopic techniques.

The acid hydrolysis of the calcium spent liquor effluent stream yielded the lignans *epi*-syringaresinol (~ 0.014 g/L) and *meso*-syringaresinol (~ 0.095 g/L) as the major constituents as well as *meso*-yangambin ($\sim 6.000 \times 10^{-4}$ g/L). Lignin precursors such as methoxyeugenol ($\sim 1.440 \times 10^{-3}$ g/L), β -oxysinapyl alcohol ($\sim 1.164 \times 10^{-3}$ g/L), sinapyl aldehyde ($\sim 7.440 \times 10^{-4}$ g/L), acetovanillone ($\sim 3.840 \times 10^{-4}$ g/L), vanillin ($\sim 1.800 \times 10^{-3}$ g/L) and syringaldehyde ($\sim 2.160 \times 10^{-3}$ g/L) were also identified along with the common plant triterpenoid, β -sitosterol ($\sim 4.400 \times 10^{-4}$ g/L). Most of these compounds have been identified as degradation products of lignin and have been reported as common by-products in pulping effluents.

Hydrolysis of the aqueous phase of the magnesium condensate effluent stream also produced lignans and lignin precursors. The major constituents were the two isomers of the lignan, syringaresinol (~ 0.043 g/L). The lignin isomers identified in this stream were also isolated from the calcium spent liquor effluent stream. These included β -oxysinapyl alcohol ($\sim 8.880 \times 10^{-4}$ g/L), acetovanillone ($\sim 4.200 \times 10^{-4}$ g/L), syringaldehyde ($\sim 1.472 \times 10^{-3}$ g/L) and vanillin ($\sim 1.052 \times 10^{-3}$ g/L).

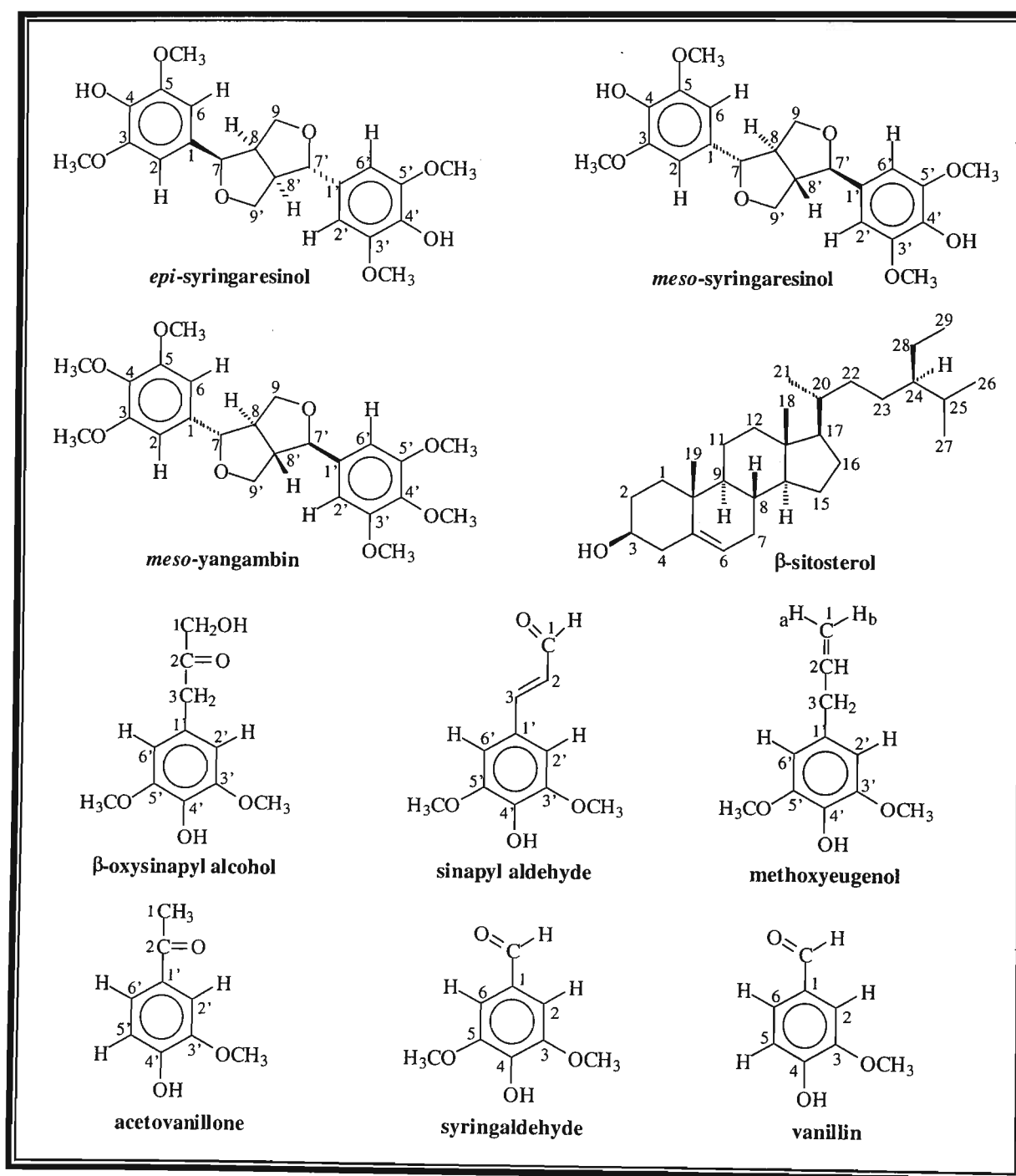


Figure 6.1: Structures of compounds isolated in this work

Syringaresinol has been reported to have cardio – protective, anti – viral, anti – bacterial and anti – cancer properties while its glucosides have been shown to possess sedative properties which aid 7-epimer isomer of syringaresinol, *epi*-syringaresinol, was tested in this work and it was found to be non – toxic and showed strong anti – inflammatory activity in the chemiluminescence bioassay and strong anti – oxidant activity in the DPPH bioassay.

Vanillin is considered to be a safe artificial flavouring and has also found widespread use in the cosmetic industry as an ingredient in perfumes. The anti – U.V. properties of vanillin is currently being investigated for use in plastics and suncreams³. Other biological uses of vanillin include inhibition of lipid peroxidation, treatment of dermatitis and as an antioxidant². However, in terms of hazard and toxicity, vanillin has been reported to have a LD₅₀ of 1580 mg/kg in rats and has reproductive effects².

Syringaldehyde has also been reported as hazardous with a LD₅₀ of 1000 mg/kg².

β-sitosterol alone and in combination with similar plant sterols, reduces blood levels of cholesterol by blocking the absorption of cholesterol in the body. It has also been effective in reducing the symptoms of benign prostatic hyperplasia⁴.

Using the average plant effluent flow rates of the two streams, the quantity of the organic compounds being passed to the main effluent holding was estimated (Table 6.1)^{5,6}.

Table 6.1: Estimated concentration of compounds isolated in this work contained in main effluent holding

| Compounds Isolated | Ca – spent liquor Flow rate ~ 75 m ³ /hour ⁸ | Mg condensate Flow rate ~ 183 m ³ /hour ⁹ |
|-----------------------------|---|--|
| <i>epi</i> -syringaresinol | ~ 1.050 kg/hour | ~ 7.869 kg/hour |
| <i>meso</i> -syringaresinol | ~ 7.125 kg/hour | ~ 7.869 kg/hour |
| <i>meso</i> -yangambin | ~ 0.045 kg/hour | - |
| methoxyeugenol | ~ 0.108 kg/hour | - |
| β -oxysinapyl alcohol | ~ 0.087 kg/hour | ~ 0.163 kg/hour |
| sinapyl aldehyde | ~ 0.056 kg/hour | - |
| acetovanillone | ~ 0.029 kg/hour | ~ 0.077 kg/hour |
| vanillin | ~ 0.135 kg/hour | ~ 0.193 kg/hour |
| syringaldehyde | ~ 0.162 kg/hour | ~ 0.269 kg/hour |
| β -sitosterol | ~ 0.033 kg/hour | - |

The aim of this project was to characterise the water – soluble compounds contained in SAPPI SAICCOR'S effluent streams with the intention of extracting any commercially exploitable compounds in order to improve the quality of the mill effluent before it is disposed of into the sea. The aqueous portion of SAICCOR'S effluent contains predominantly lignosulphonates and sugars. The isolation and characterisation of pure lignosulphonates was unsuccessful in this project and would require the use of other equipment and techniques such as ultrafiltration, ion exchange chromatography and HPLC, which was unavailable. However, a number of commercially useful compounds have been identified from the hydrolysed aqueous phase of the calcium spent liquor and the magnesium condensate. Future investigations should focus on possible extraction procedures to recover these viable components from the effluent streams.

6.2 REFERENCES

1. <http://www.healing-arts.org/children/ADHD/herbal.htm>
2. Dictionary of Natural Products (DNP) on CD – ROM, version 11.2, 1982 – 2003, Chapman and Hall Electronic Publishing Division : London.
3. <http://www.conveniencefood.us.rhodia.com/brochures/epv/page19.asp>
4. Berges, R.R., Windeler J. and Trampisch, H.J., 1995, Randomised, Placebo-Controlled, Double-Blind Clinical Trial of Beta – sitosterol in Patients with Benign Prostatic Hyperplasia, *Lancet*, **345**, 1529-1532.
5. Moodley, B., 2001, *Characterisation of SAPPI SAICCOR Pulp Mill's Effluent*, MSc Dissertation, School of Pure and Applied Chemistry, University of Natal, Durban.
6. Personal communication with Mr John Thubron – Technical Process Manager at SAPPI SAICCOR.

APPENDIX A

LIST OF SPECTRA IN APPENDIX A

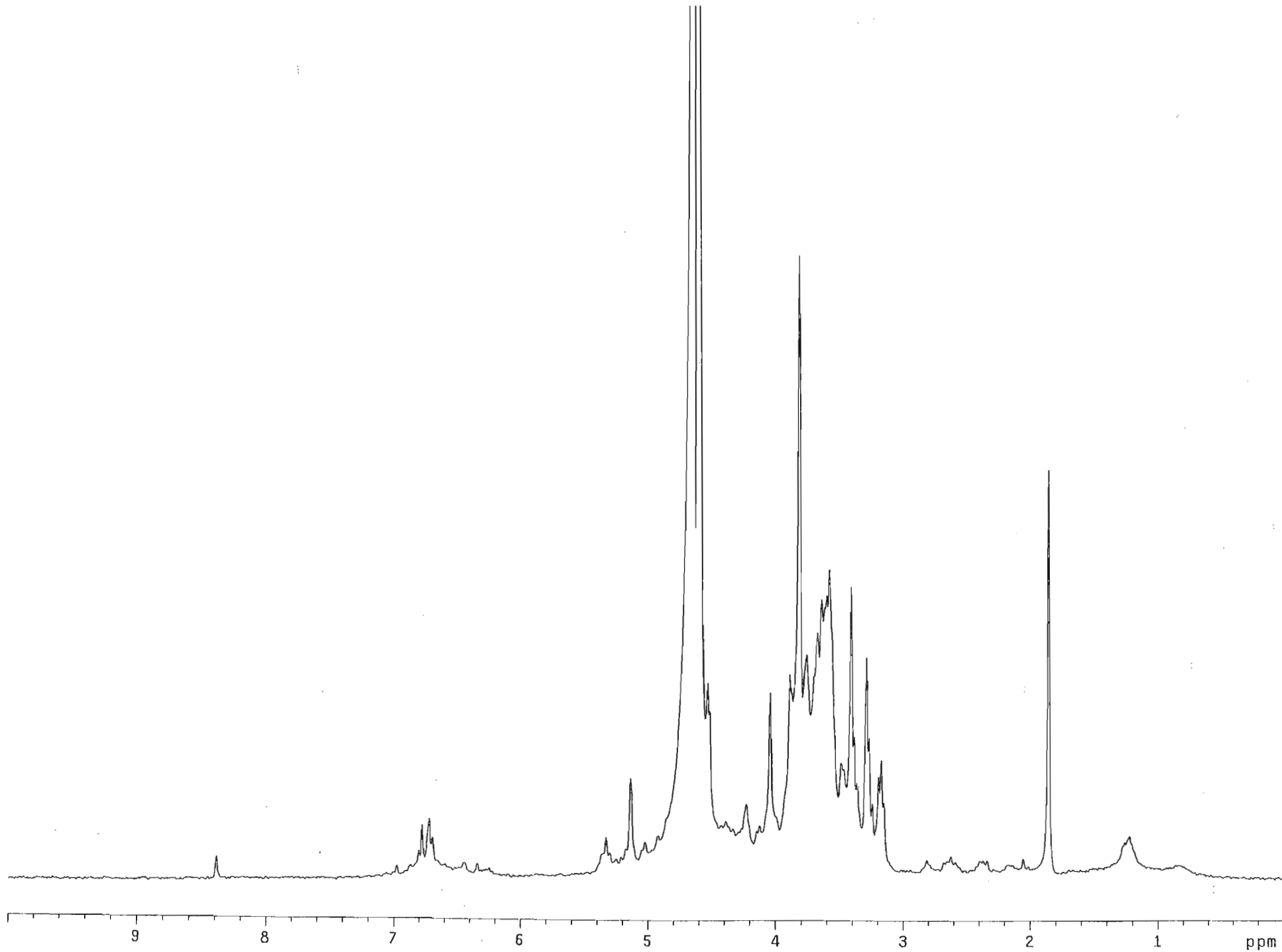
| | PAGE NO. |
|--|----------|
| Spectrum i : ^1H NMR spectrum of crude lignosulphonate precipitate (extraction method 1) (400MHz, D_2O) | 122 |
| Spectrum ii : ^{13}C NMR spectrum of crude lignosulphonate precipitate (extraction method 1) (300MHz, D_2O) | 123 |
| Spectrum iii : Infrared spectrum of crude lignosulphonate precipitate (extraction method 1) | 124 |
| Spectrum iv : UV spectrum of crude lignosulphonate precipitate (extraction method 1) in D_2O | 125 |
| Spectrum v : Infrared spectrum of crude lignosulphonate precipitate (extraction method 2) | 126 |
| Spectrum vi : ^1H NMR spectrum of crude lignosulphonate precipitate (extraction method 2) (400MHz, D_2O) | 127 |
| Spectrum vii : ^{13}C NMR spectrum of crude lignosulphonate precipitate (extraction method) (300MHz, D_2O) | 128 |
| Spectrum viii : ^1H NMR spectrum of crude methylated lignosulphonate precipitate (400 MHz, D_2O) | 129 |
| Spectrum ix : ^{13}C NMR spectrum of crude methylated lignosulphonate precipitate (300 MHz, D_2O) | 130 |
| | |
| Spectrum 1.1 : Mass spectrum of compound 1, <i>epi</i> -syringaresinol | 131 |
| Spectrum 1.2 : Infrared spectrum of compound 1, <i>epi</i> -syringaresinol | 132 |
| Spectrum 1.3 : UV spectrum of compound 1, <i>epi</i> -syringaresinol in CH_2Cl_2 | 133 |
| Spectrum 1.4 : ^1H NMR spectrum of compound 1, <i>epi</i> -syringaresinol (400MHz, CDCl_3) | 134 |
| Spectrum 1.5 : ^{13}C NMR spectrum of compound 1, <i>epi</i> -syringaresinol (400MHz, CDCl_3) | 135 |
| Spectrum 1.6 : HSQC NMR spectrum of compound 1, <i>epi</i> -syringaresinol (400MHz, CDCl_3) | 136 |
| Spectrum 1.7 : HMBC NMR spectrum of compound 1, <i>epi</i> -syringaresinol (400MHz, CDCl_3) | 137 |
| Spectrum 1.8 : NOESY NMR spectrum of compound 1, <i>epi</i> -syringaresinol (400MHz, CDCl_3) | 138 |

| | |
|---|-----|
| Spectrum 1.9 : COSY NMR spectrum of compound 1, <i>epi</i> -syringaresinol (400MHz, CDCl ₃) | 139 |
| Spectrum 2.1 : Mass spectrum of compound 2, <i>meso</i> -syringaresinol | 140 |
| Spectrum 2.2 : Infrared spectrum of compound 2, <i>meso</i> -syringaresinol | 141 |
| Spectrum 2.3 : UV spectrum of compound 2, <i>meso</i> -syringaresinol in CH ₂ Cl ₂ | 142 |
| Spectrum 2.4 : ¹ H NMR spectrum of compound 2, <i>meso</i> -syringaresinol (400 MHz, CDCl ₃) | 143 |
| Spectrum 2.5 : ¹³ C NMR spectrum of compound 2, <i>meso</i> -syringaresinol (400 MHz, CDCl ₃) | 144 |
| Spectrum 2.6 : HSQC NMR spectrum of compound 2, <i>meso</i> -syringaresinol (400 MHz, CDCl ₃) | 145 |
| Spectrum 2.7 : Expanded HSQC NMR spectrum of compound 2, <i>meso</i> -syringaresinol (400 MHz, CDCl ₃) | 146 |
| Spectrum 2.8 : HMBC NMR spectrum of compound 2, <i>meso</i> -syringaresinol (400 MHz, CDCl ₃) | 147 |
| Spectrum 2.9 : NOESY NMR spectrum of compound 2, <i>meso</i> -syringaresinol (400 MHz, CDCl ₃) | 148 |
| Spectrum 2.10: COSY NMR spectrum of compound 2, <i>meso</i> -syringaresinol (400 MHz, CDCl ₃) | 149 |
| Spectrum 2.11: Expanded COSY NMR spectrum of compound 2, <i>meso</i> -syringaresinol (400 MHz, CDCl ₃) | 150 |
| Spectrum 3.1 : Mass spectrum of compound 3, <i>meso</i> -yangambin | 151 |
| Spectrum 3.2 : Infrared spectrum of compound 3, <i>meso</i> -yangambin | 152 |
| Spectrum 3.3 : UV spectrum of compound 3, <i>meso</i> -yangambin in CH ₂ Cl ₂ | 153 |
| Spectrum 3.4 : ¹ H NMR spectrum of compound 3, <i>meso</i> -yangambin (400MHz, CDCl ₃) | 154 |
| Spectrum 3.5 : ¹³ C NMR spectrum of compound 3, <i>meso</i> -yangambin (400MHz, CDCl ₃) | 155 |
| Spectrum 3.6 : HSQC NMR spectrum of compound 3, <i>meso</i> -yangambin (400MHz, CDCl ₃) | 156 |
| Spectrum 3.7 : HMBC NMR spectrum of compound 3, <i>meso</i> -yangambin (400MHz, CDCl ₃) | 157 |

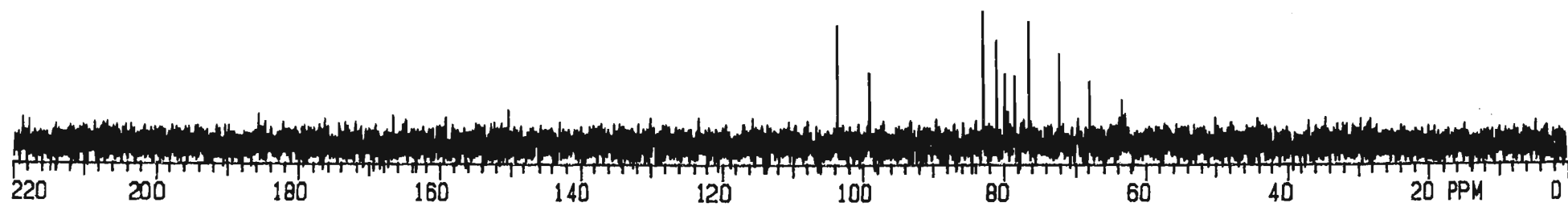
| | |
|--|-----|
| Spectrum 3.8 : NOESY NMR spectrum of compound 3, <i>meso</i> -yangambin (400MHz, CDCl ₃) | 158 |
| Spectrum 3.9 : COSY NMR spectrum of compound 3, <i>meso</i> -yangambin (400MHz, CDCl ₃) | 159 |
| Spectrum 4.1 : Mass spectrum of compound 4, methoxyeugenol | 160 |
| Spectrum 4.2 : Infrared spectrum of compound 4, methoxyeugenol | 161 |
| Spectrum 4.3 : UV spectrum of compound 4, methoxyeugenol in CH ₂ Cl ₂ | 162 |
| Spectrum 4.4 : ¹ H NMR spectrum of compound 4, methoxyeugenol (400 MHz, CDCl ₃) | 163 |
| Spectrum 4.5 : ¹³ C NMR spectrum of compound 4, methoxyeugenol (400 MHz, CDCl ₃) | 164 |
| Spectrum 4.6 : HSQC NMR spectrum of compound 4, methoxyeugenol (400 MHz, CDCl ₃) | 165 |
| Spectrum 4.7 : HMBC NMR spectrum of compound 4, methoxyeugenol (400 MHz, CDCl ₃) | 166 |
| Spectrum 4.8 : NOESY NMR spectrum of compound 4, methoxyeugenol (400 MHz, CDCl ₃) | 167 |
| Spectrum 4.9 : COSY NMR spectrum of compound 4, methoxyeugenol (400 MHz, CDCl ₃) | 168 |
| Spectrum 5.1 : Mass spectrum of compound 5, β-oxysinapyl alcohol | 169 |
| Spectrum 5.2 : Infrared spectrum of compound 5, β-oxysinapyl alcohol | 170 |
| Spectrum 5.3 : UV spectrum of compound 5, β-oxysinapyl alcohol in CH ₂ Cl ₂ | 171 |
| Spectrum 5.4 : ¹ H NMR spectrum of compound 5, β-oxysinapyl alcohol (400 MHz, CDCl ₃) | 172 |
| Spectrum 5.5 : ¹³ C NMR spectrum of compound 5, β-oxysinapyl alcohol (400 MHz, CDCl ₃) | 173 |
| Spectrum 5.6 : HSQC NMR spectrum of compound 5, β-oxysinapyl alcohol (400 MHz, CDCl ₃) | 174 |
| Spectrum 5.7 : HMBC NMR spectrum of compound 5, β-oxysinapyl alcohol (400 MHz, CDCl ₃) | 175 |
| Spectrum 5.8 : NOESY NMR spectrum of compound 5, β-oxysinapyl alcohol (400 MHz, CDCl ₃) | 176 |

| | |
|--|-----|
| Spectrum 5.9 : COSY NMR spectrum of compound 5, β -oxysinapyl alcohol (400 MHz, CDCl ₃) | 177 |
| Spectrum 6.1 : Mass spectrum of compound 6, sinapyl aldehyde | 178 |
| Spectrum 6.2 : Infrared spectrum of compound 6, sinapyl aldehyde | 179 |
| Spectrum 6.3 : UV spectrum of compound 6, sinapyl aldehyde in CH ₂ Cl ₂ | 180 |
| Spectrum 6.4 : ¹ H NMR spectrum of compound 6, sinapyl aldehyde (400 MHz, CDCl ₃) | 181 |
| Spectrum 6.5 : ¹³ C NMR spectrum of compound 6, sinapyl aldehyde (400 MHz, CDCl ₃) | 182 |
| Spectrum 6.6 : HSQC NMR spectrum of compound 6, sinapyl aldehyde (400 MHz, CDCl ₃) | 183 |
| Spectrum 6.7 : HMBC NMR spectrum of compound 6, sinapyl aldehyde (400 MHz, CDCl ₃) | 184 |
| Spectrum 6.8 : NOESY NMR spectrum of compound 6, sinapyl aldehyde (400 MHz, CDCl ₃) | 185 |
| Spectrum 6.9 : COSY NMR spectrum of compound 6, sinapyl aldehyde (400 MHz, CDCl ₃) | 186 |
| Spectrum 7.1 : Mass spectrum of compound 7, acetovanillone | 187 |
| Spectrum 7.2 : Infrared spectrum of compound 7, acetovanillone | 188 |
| Spectrum 7.3 : UV spectrum of compound 7, acetovanillone in CH ₂ Cl ₂ | 189 |
| Spectrum 7.4 : ¹ H NMR spectrum of compound 7, acetovanillone (400 MHz, CDCl ₃) | 190 |
| Spectrum 7.5 : Expanded ¹ H NMR spectrum of compound 7, acetovanillone (400 MHz, CDCl ₃) | 191 |
| Spectrum 7.6 : ¹³ C NMR spectrum of compound 7, acetovanillone (400 MHz, CDCl ₃) | 192 |
| Spectrum 7.7 : HSQC NMR spectrum of compound 7, acetovanillone (400 MHz, CDCl ₃) | 193 |
| Spectrum 7.8 : HMBC NMR spectrum of compound 7, acetovanillone (400 MHz, CDCl ₃) | 194 |
| Spectrum 7.9 : NOESY NMR spectrum of compound 7, acetovanillone (400 MHz, CDCl ₃) | 195 |

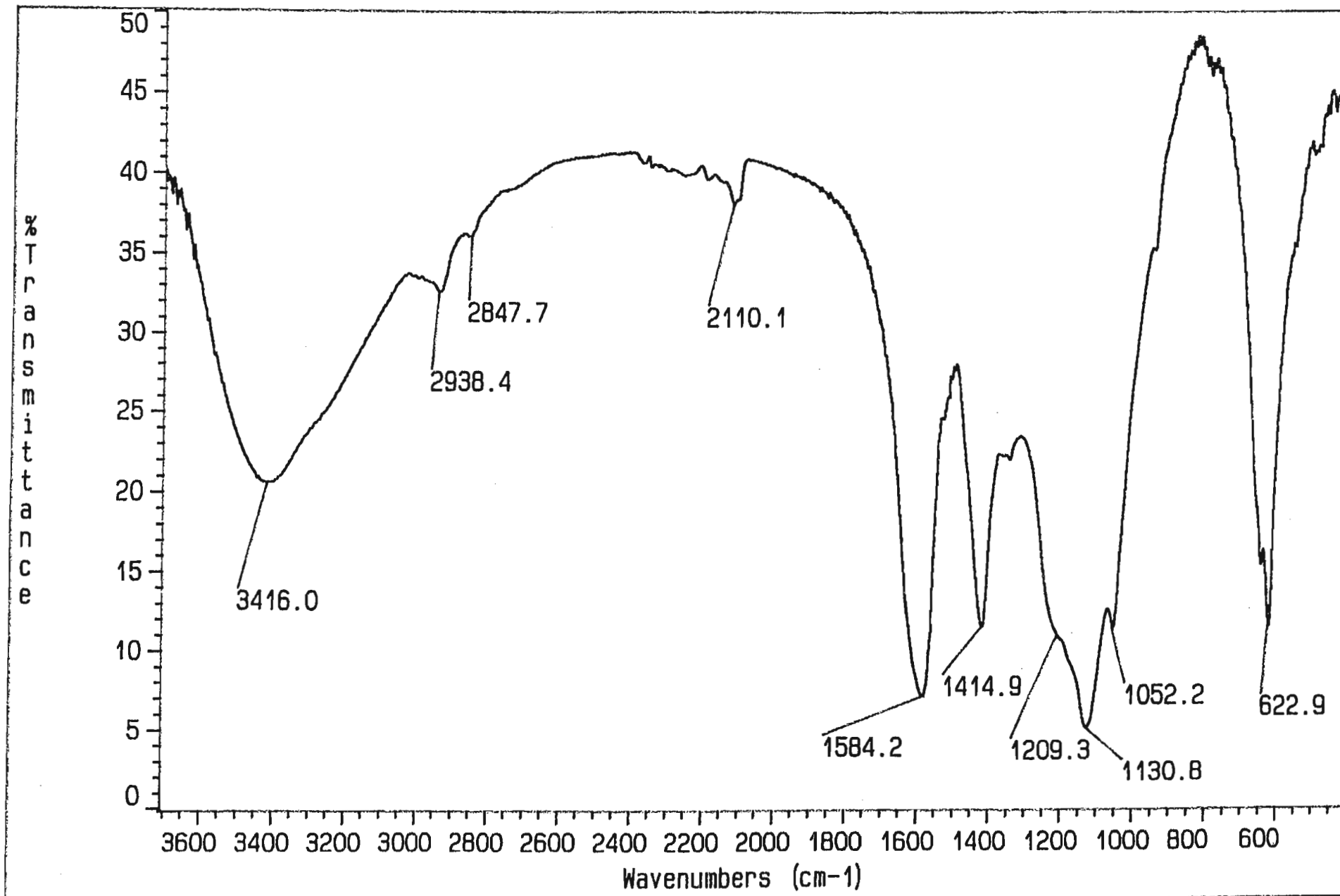
| | |
|--|-----|
| Spectrum 7.10 : COSY NMR spectrum of compound 7, acetovanillone (400 MHz, CDCl ₃) | 196 |
| Spectrum 8.1 : Mass spectrum of compound 8, vanillin | 197 |
| Spectrum 8.2 : Infrared spectrum of compound 8, vanillin | 198 |
| Spectrum 8.3 : UV spectrum of compound 8, vanillin in CH ₂ Cl ₂ | 199 |
| Spectrum 8.4 : ¹ H NMR spectrum of compound 8, vanillin (400 MHz, CDCl ₃) | 200 |
| Spectrum 8.5 : Expanded ¹ H NMR spectrum of compound 8, vanillin (400 MHz, CDCl ₃) | 201 |
| Spectrum 8.6 : ¹³ C NMR spectrum of compound 8, vanillin (400 MHz, CDCl ₃) | 202 |
| Spectrum 8.7 : HSQC NMR spectrum of compound 8, vanillin (400 MHz, CDCl ₃) | 203 |
| Spectrum 8.8 : HMBC NMR spectrum of compound 8, vanillin (400 MHz, CDCl ₃) | 204 |
| Spectrum 8.9 : NOESY NMR spectrum of compound 8, vanillin (400 MHz, CDCl ₃) | 205 |
| Spectrum 8.10 : COSY NMR spectrum of compound 8, vanillin (400 MHz, CDCl ₃) | 206 |
| Spectrum 8.11 : Expanded COSY NMR spectrum of compound 8, vanillin (400 MHz, CDCl ₃) | 207 |
| Spectrum 9.1 : Mass spectrum of compound 9, syringaldehyde | 208 |
| Spectrum 9.2 : Infrared spectrum of compound 9, syringaldehyde | 209 |
| Spectrum 9.3 : UV spectrum of compound 9, syringaldehyde in CH ₂ Cl ₂ | 210 |
| Spectrum 9.4 : ¹ H NMR spectrum of compound 9, syringaldehyde (400 MHz, CDCl ₃) | 211 |
| Spectrum 9.5 : ¹³ C NMR spectrum of compound 9, syringaldehyde (400 MHz, CDCl ₃) | 212 |
| Spectrum 9.6 : HSQC NMR spectrum of compound 9, syringaldehyde (400 MHz, CDCl ₃) | 213 |
| Spectrum 9.7 : HMBC NMR spectrum of compound 9, syringaldehyde (400 MHz, CDCl ₃) | 214 |
| Spectrum 9.8 : NOESY NMR spectrum of compound 9, syringaldehyde (400 MHz, CDCl ₃) | 215 |
| Spectrum 10.1 : Infrared spectrum of compound 10, β-sitosterol | 216 |
| Spectrum 10.2 : ¹ H NMR spectrum of compound 10, β-sitosterol (300 MHz, CDCl ₃) | 217 |
| Spectrum 10.3 : ¹³ C NMR spectrum of compound 10, β-sitosterol (300 MHz, CDCl ₃) | 218 |



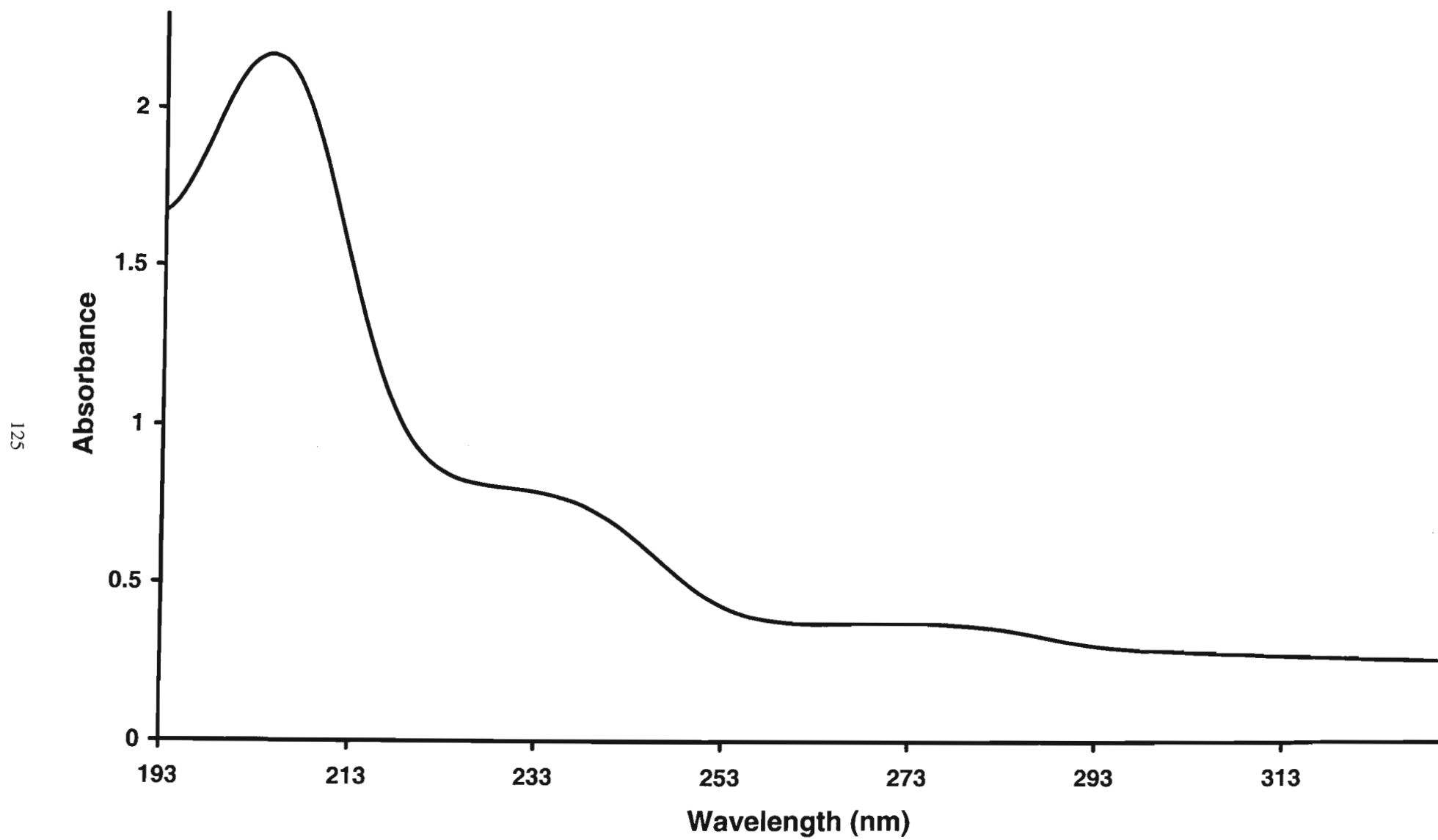
Spectrum i : ^1H NMR Spectrum of Crude Lignosulphonate Precipitate (Extraction Method 1)



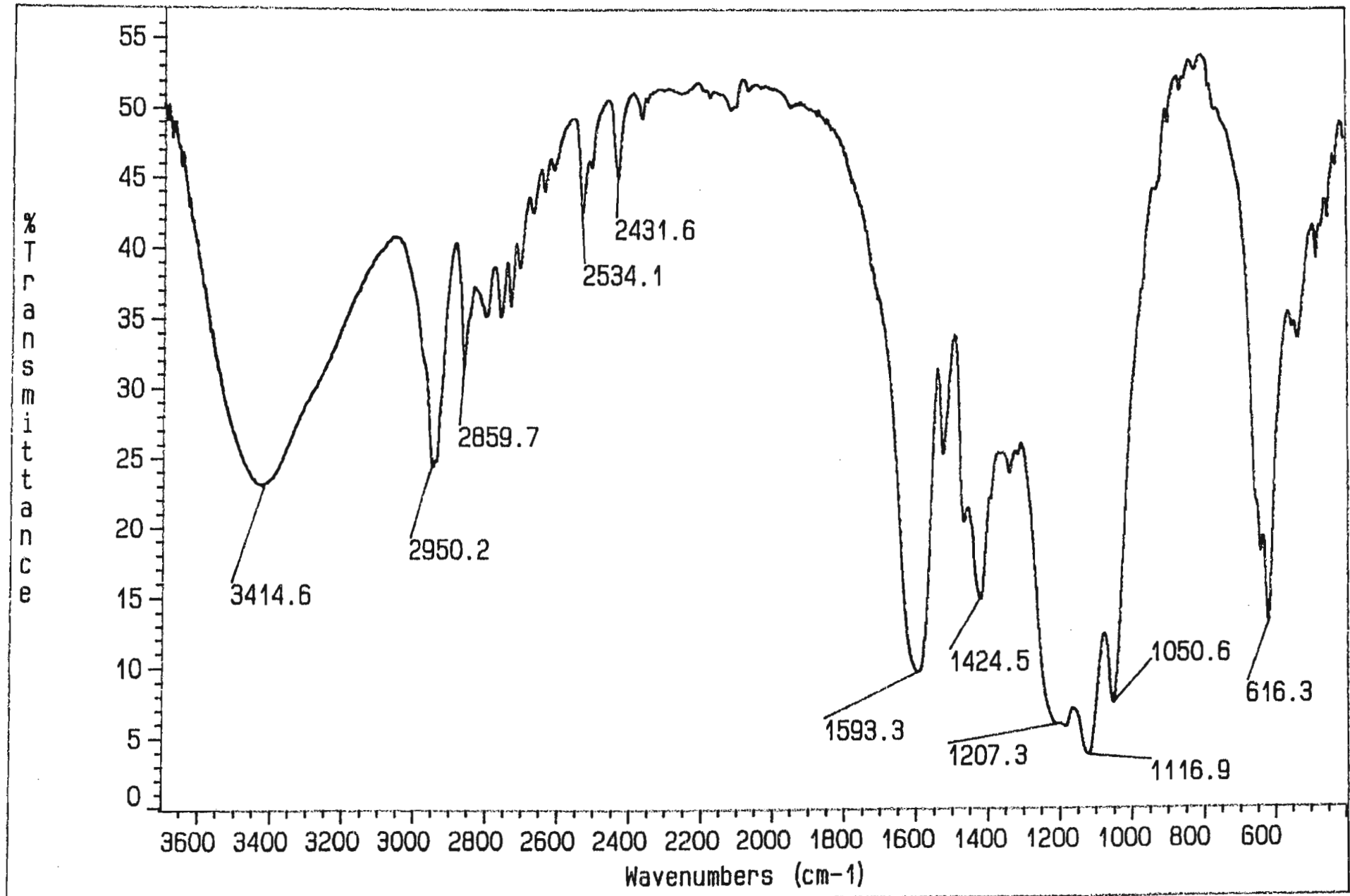
Spectrum ii : ^{13}C NMR Spectrum of Crude Lignosulphonate Precipitate (Extraction Method 1)



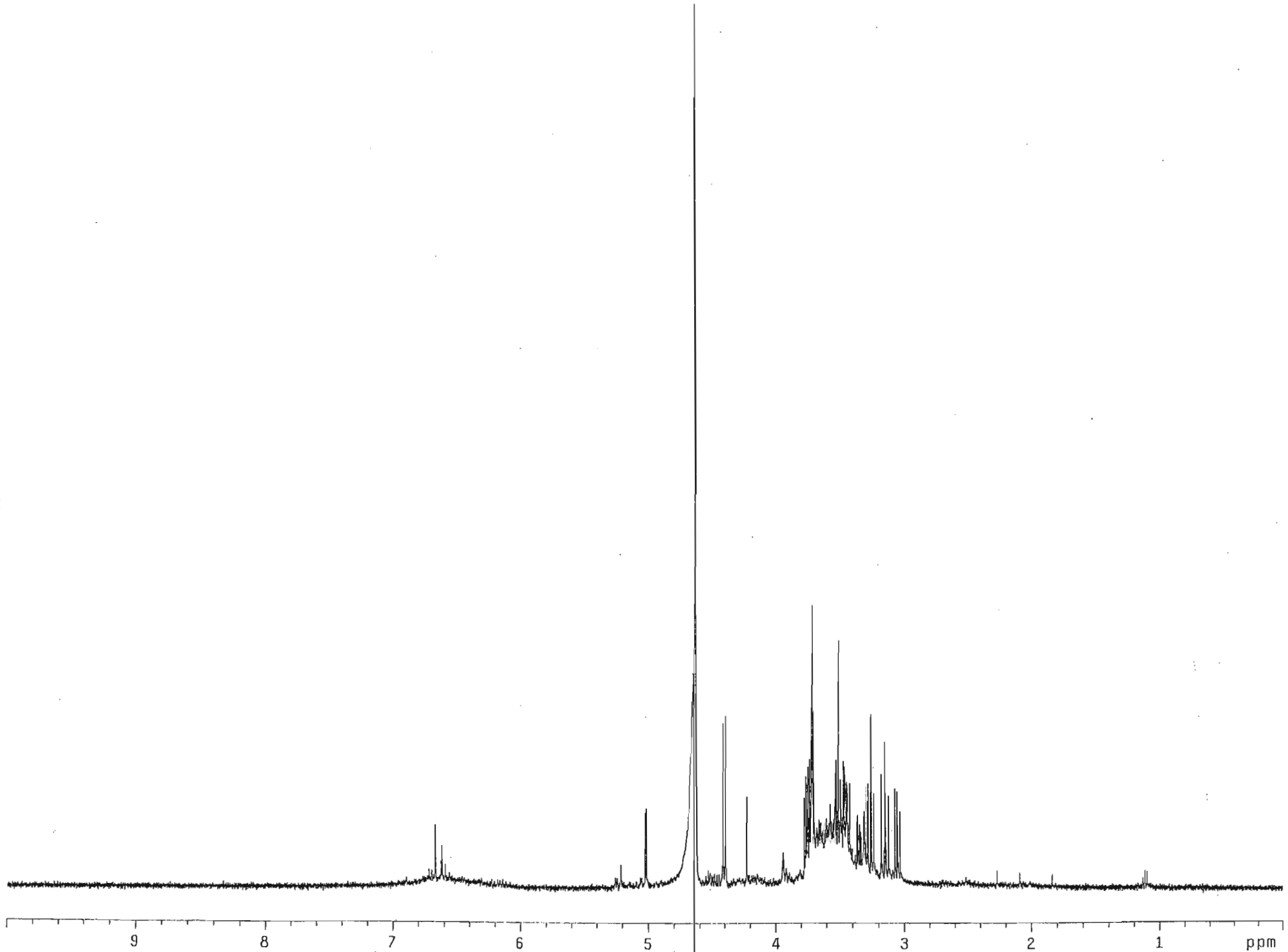
Spectrum iii : Infrared Spectrum of Crude Lignosulphonate Precipitate (Extraction Method 1)



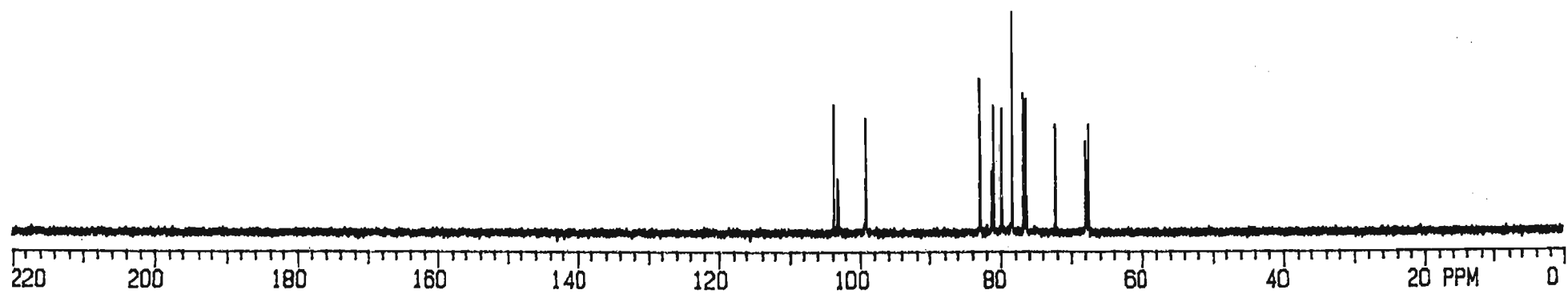
Spectrum iv : UV Spectrum of Crude Lignosulphonate Precipitate (Extraction Method 1)



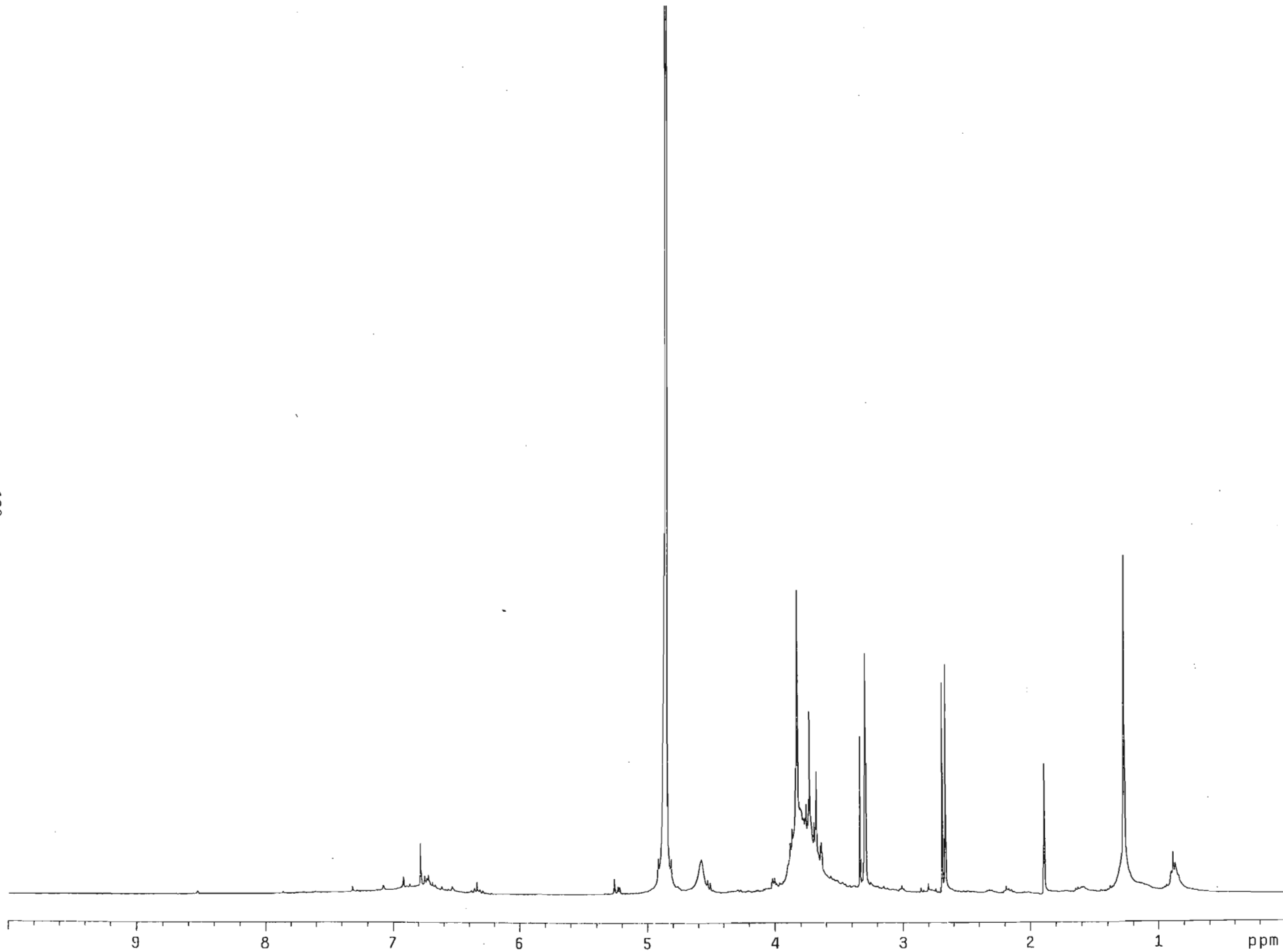
Spectrum v : Infrared Spectrum of Crude Lignosulphonate Precipitate (Extraction Method 2)



Spectrum vi : ^1H NMR Spectrum of Crude Lignosulphonate Precipitate (Extraction Method 2)

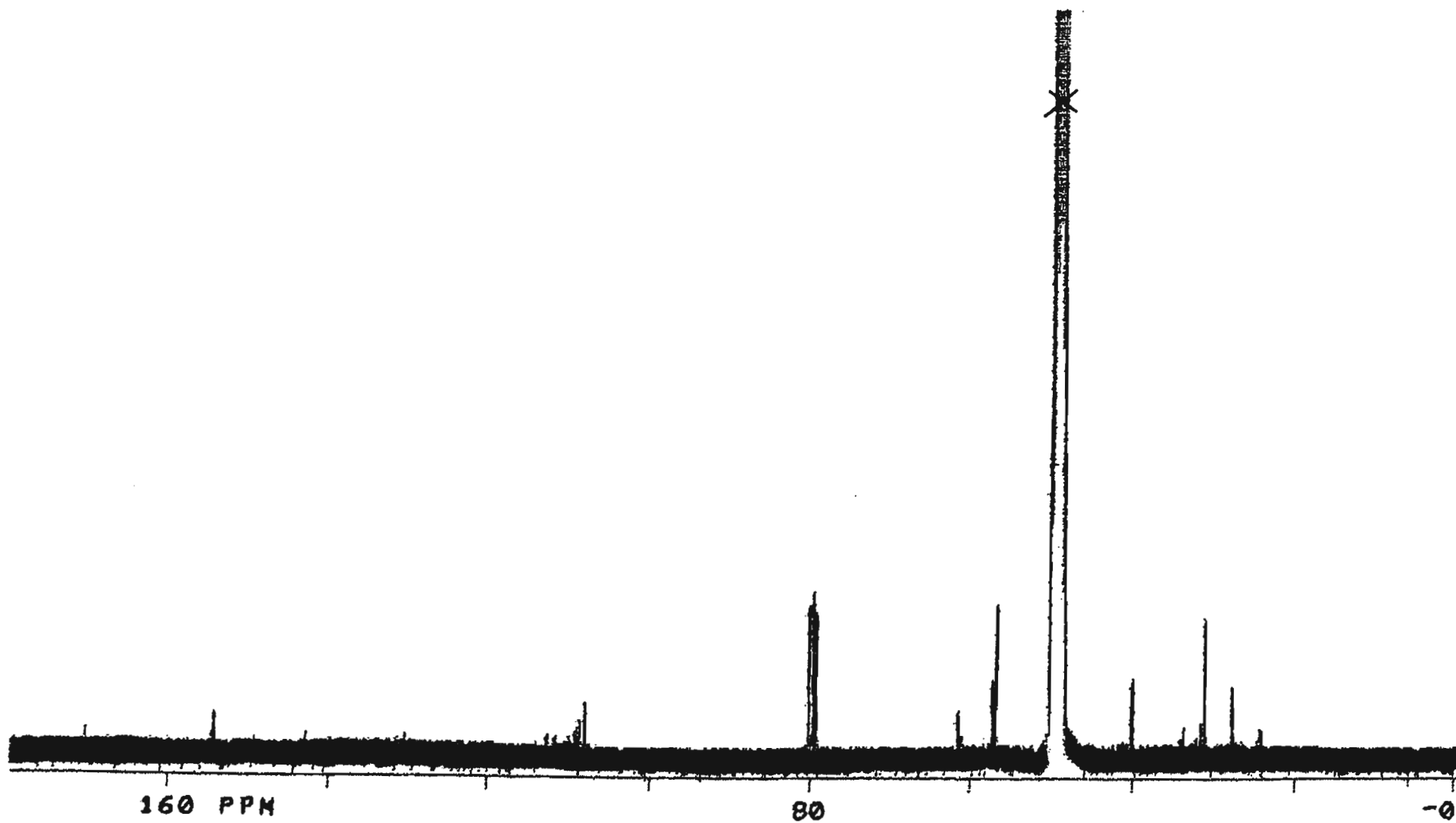


Spectrum vii : ^{13}C NMR Spectrum of Crude Lignosulphonate Precipitate (Extraction Method 2)

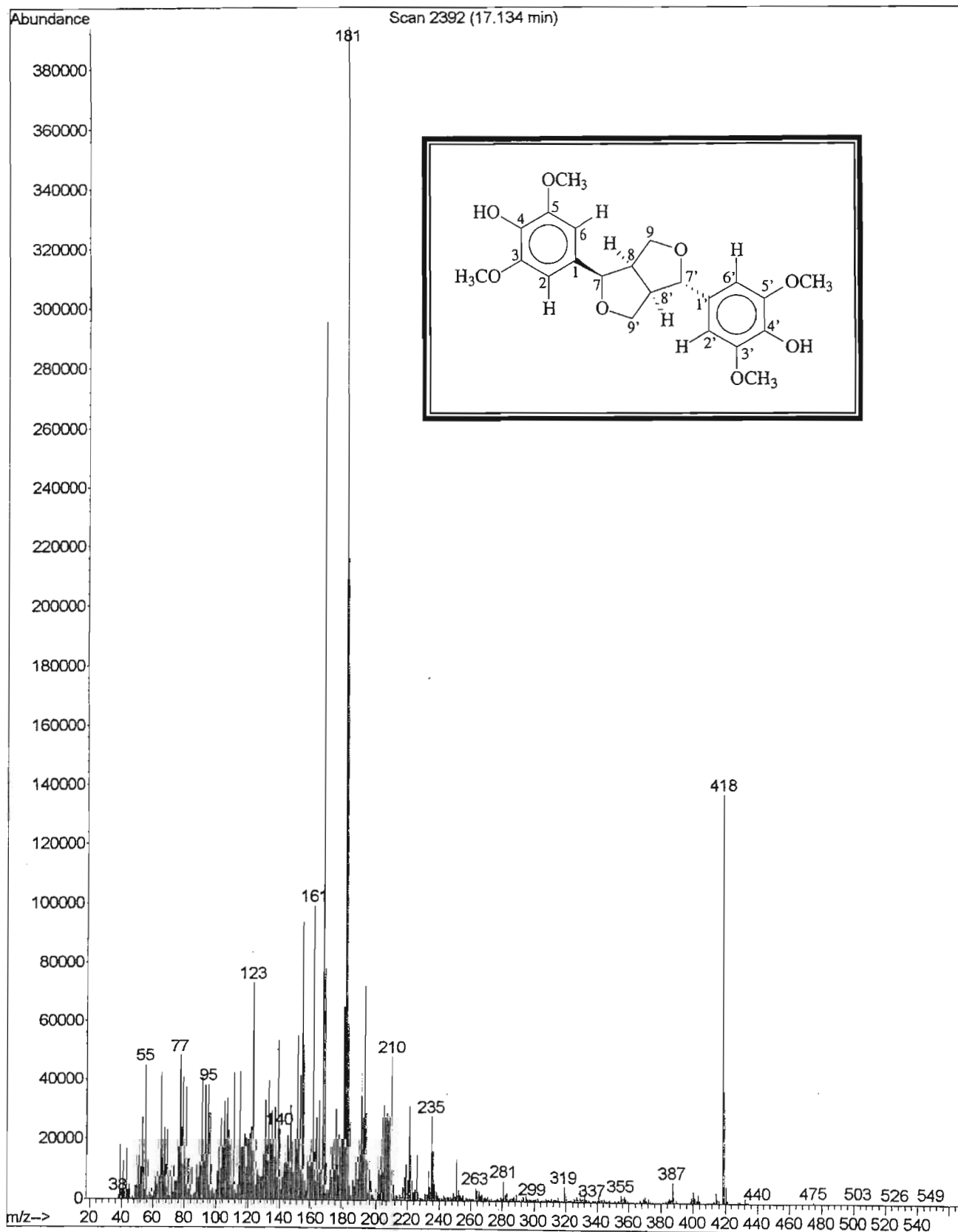


Spectrum viii : ^1H NMR Spectrum of Crude Methylated Lignosulphonate Precipitate

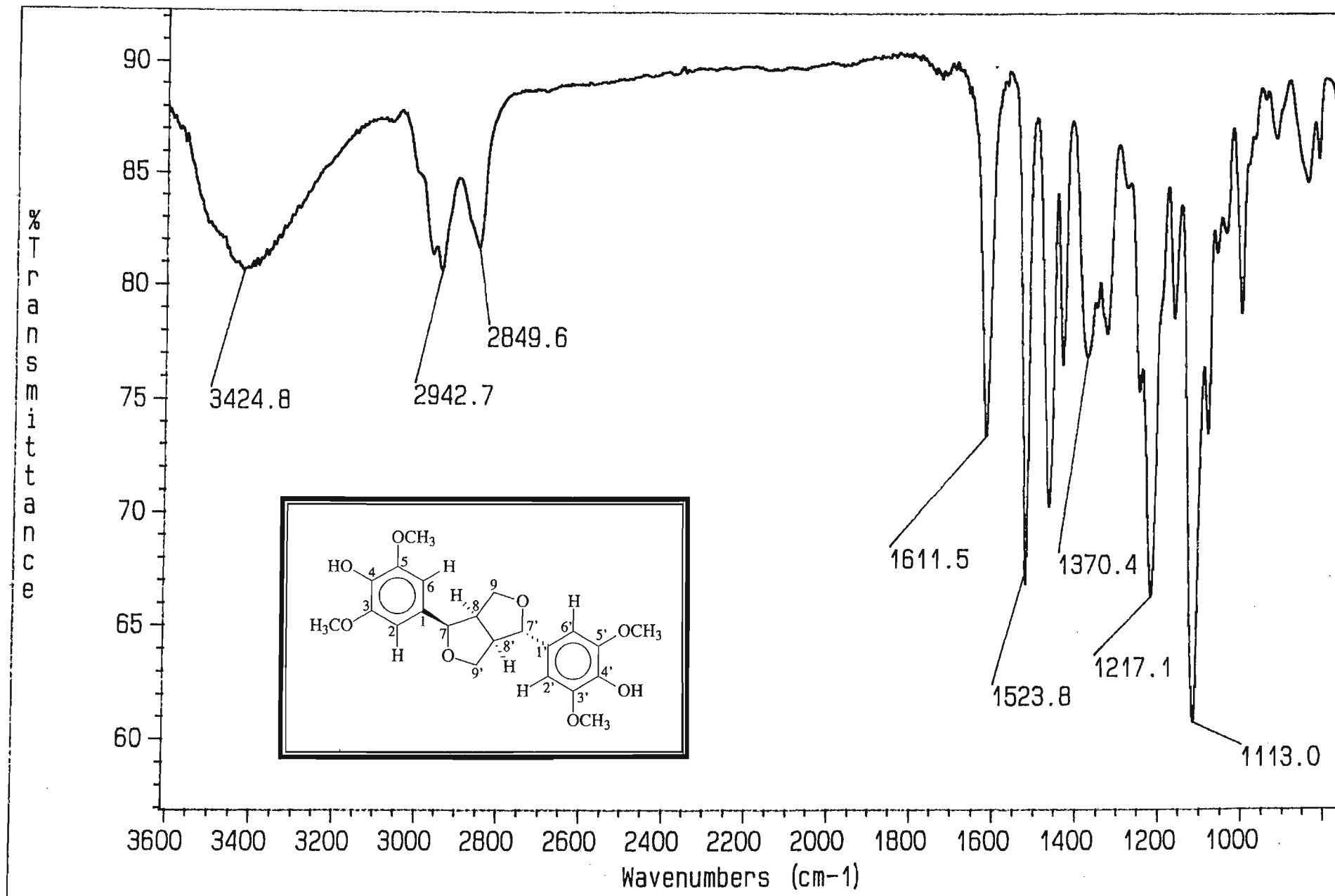
130



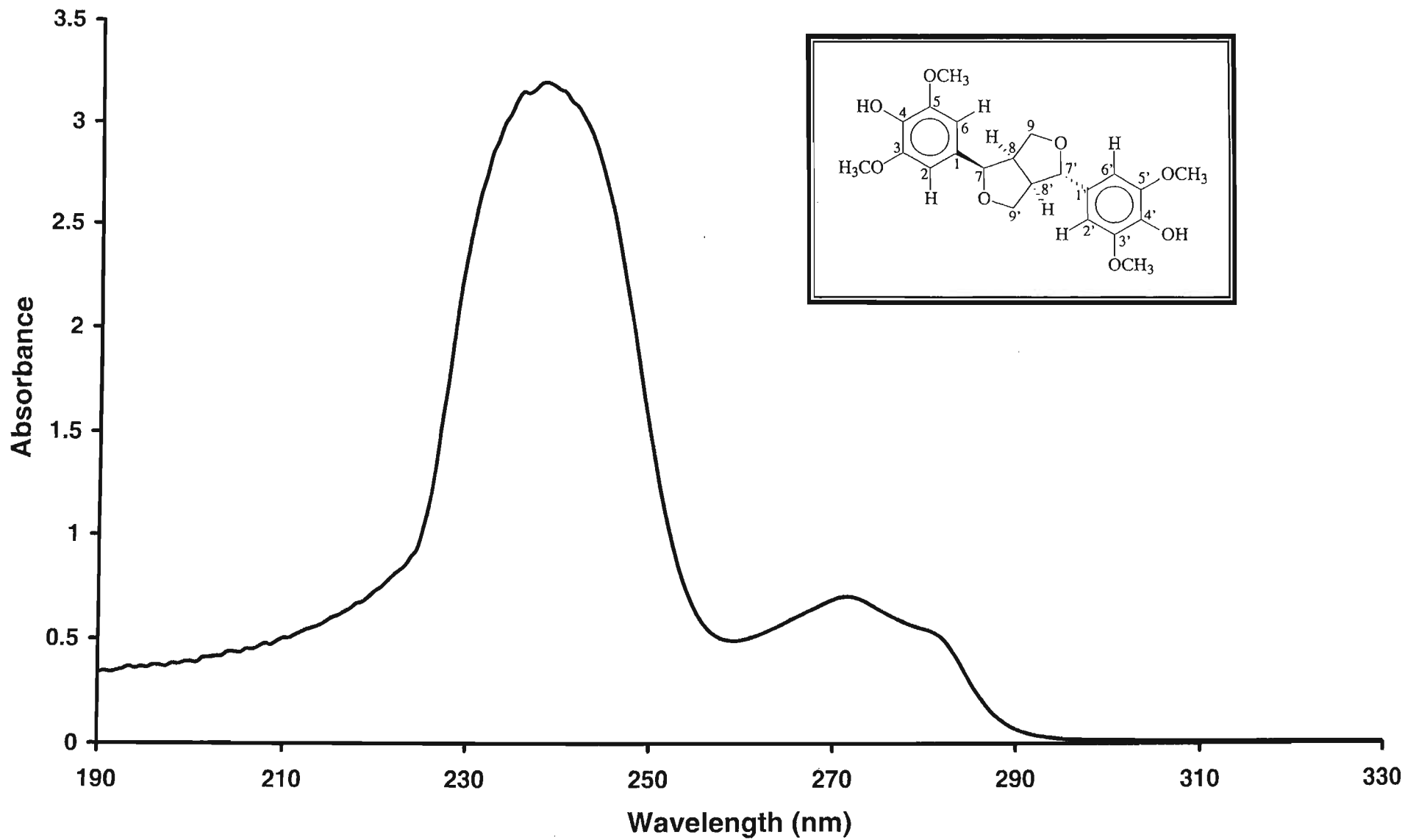
Spectrum ix : ^{13}C NMR Spectrum of Crude Methylated Lignosulphonate Precipitate



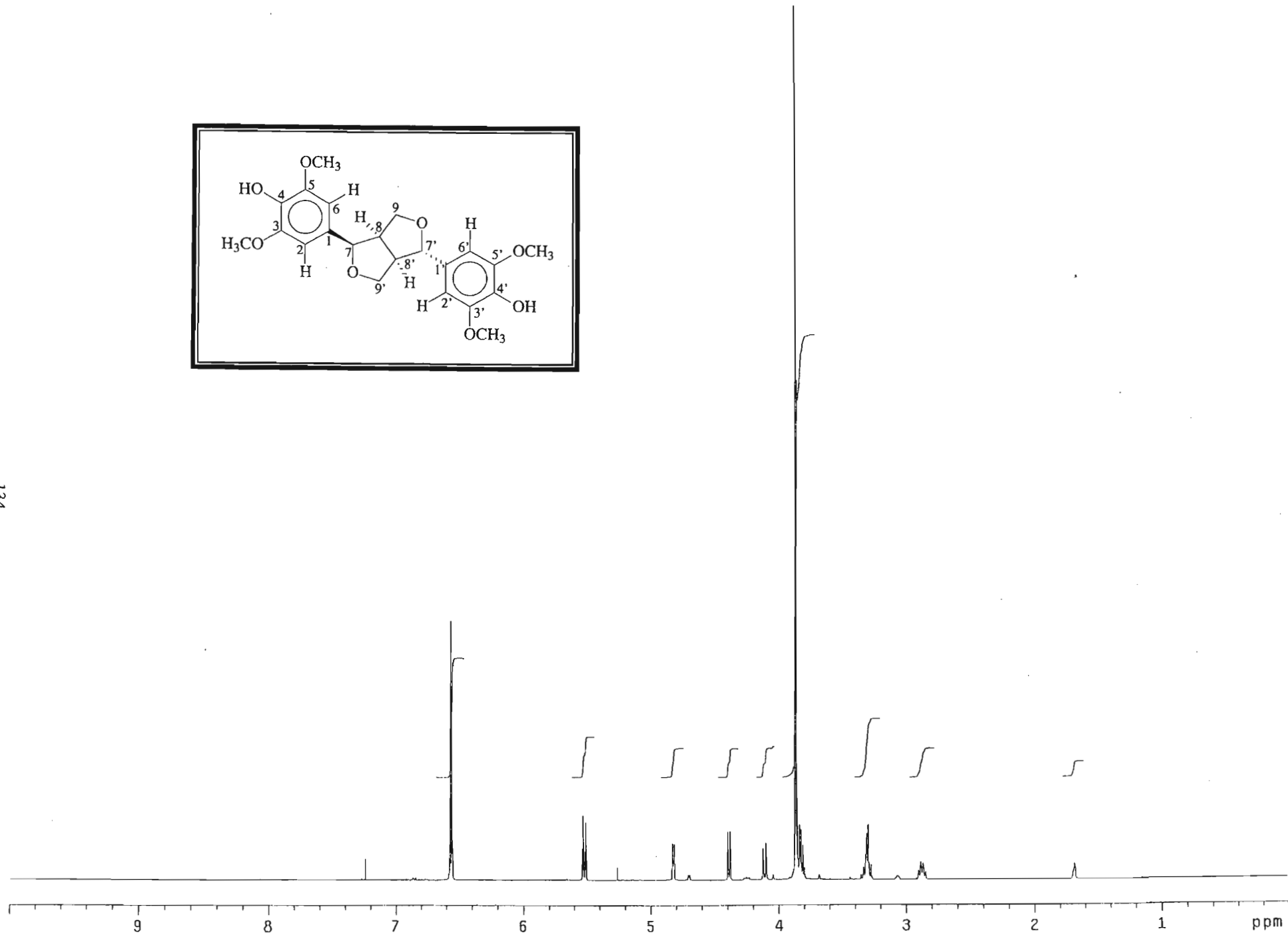
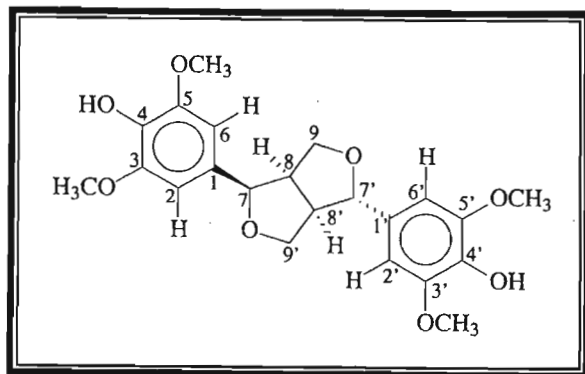
Spectrum 1.1 : Mass Spectrum of Compound 1, *epi*-syringaresinol



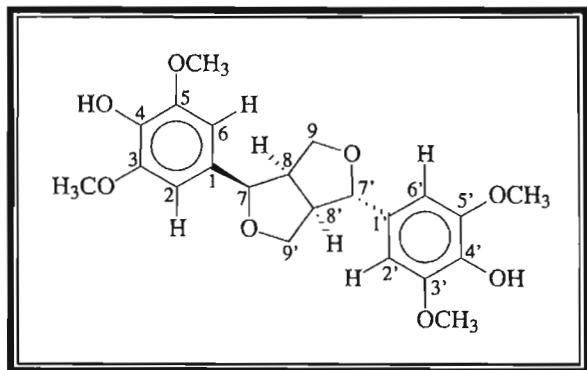
Spectrum 1.2 : Infrared Spectrum of Compound 1, *epi*-syringaresinol



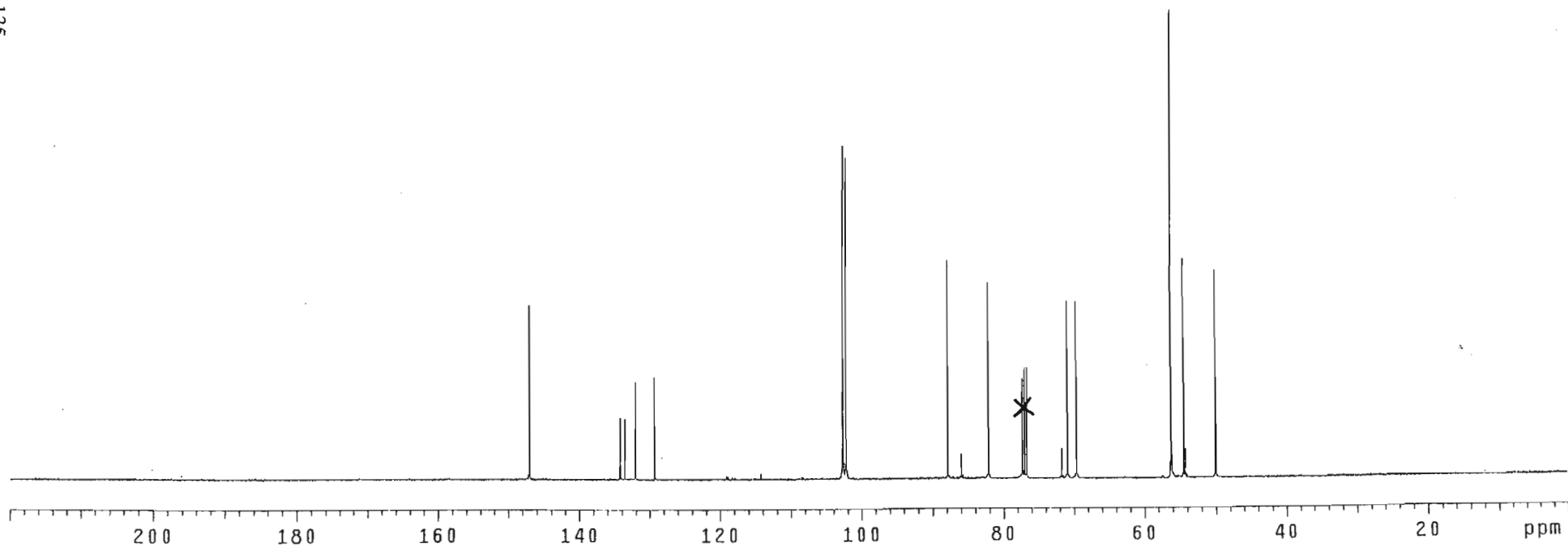
Spectrum 1.3 : UV Spectrum of Compound 1, *epi*-syringaresinol



Spectrum 1.4 : ¹H NMR Spectrum of Compound 1, *epi*-syringaresinol



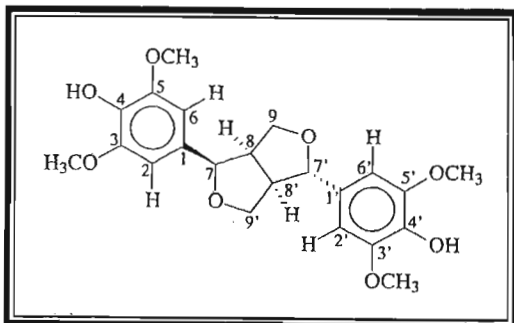
135



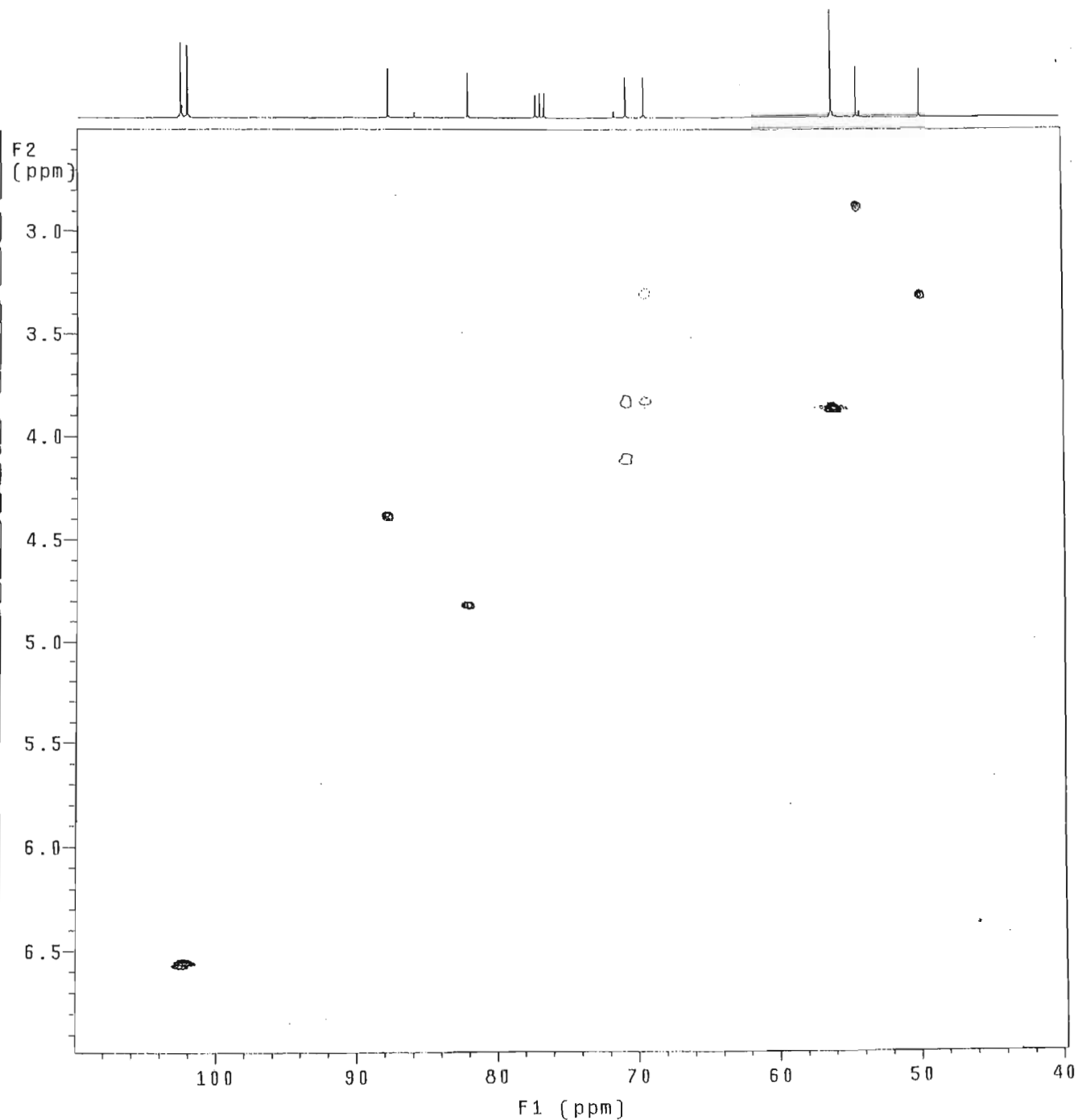
Spectrum 1.5 : ^{13}C NMR Spectrum of Compound 1, *epi*-syringaresinol

Gradient HSQC expt.
with mult. editing
probe=5mmASW

Pulse Sequence: ghsqc_da



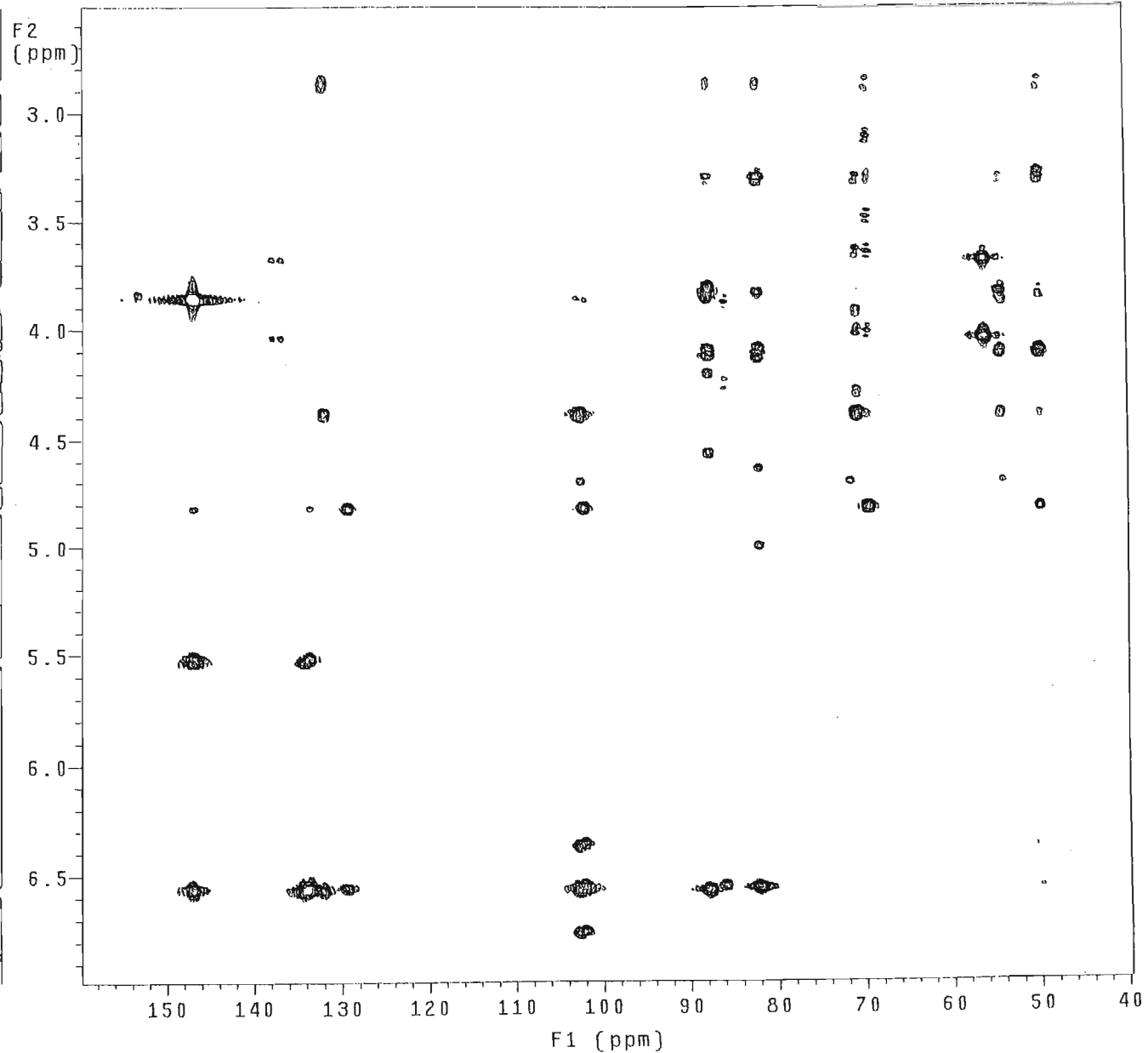
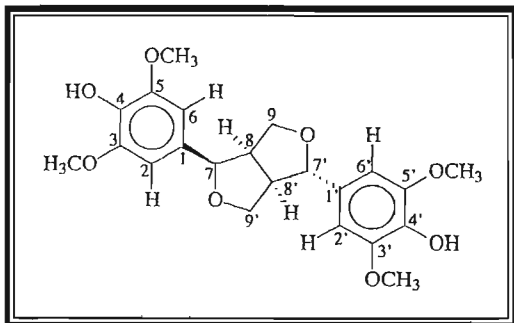
136



Spectrum 1.6 : HSQC NMR Spectrum of Compound 1, *epi*-syringaresinol

Gradient HMBC expt.
probe=5mmASW

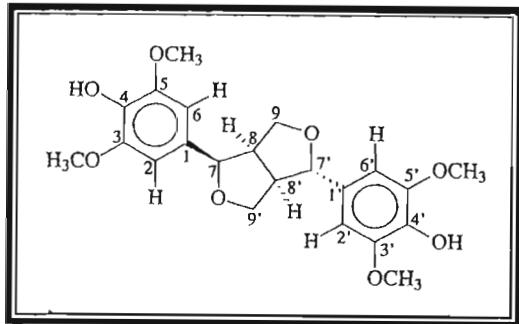
Pulse Sequence: ghmqc_da



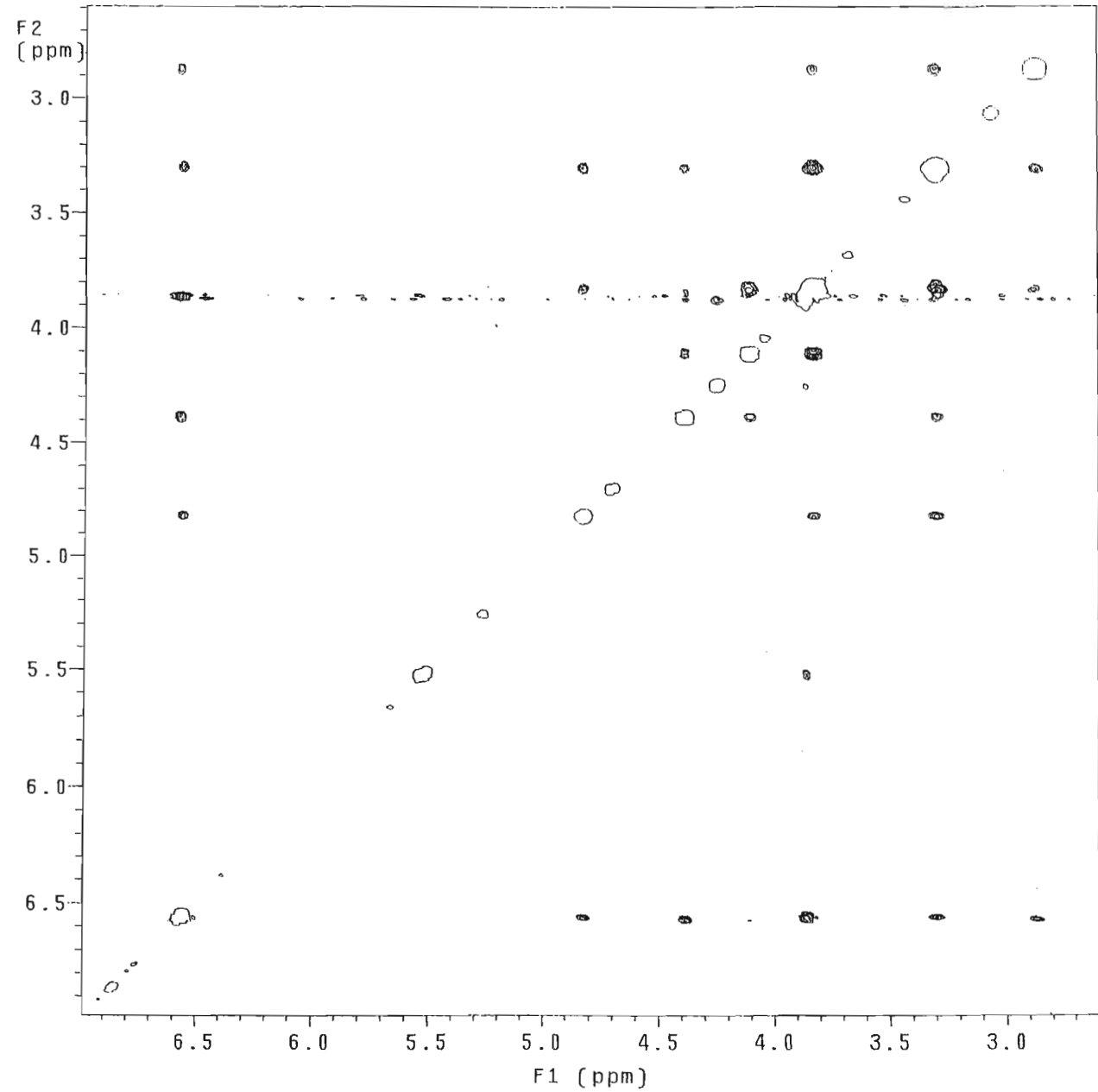
Spectrum 1.7 : HMBC NMR Spectrum of Compound 1, *epi-syringaresinol*

mix=1sec
probe=5mmASW

Pulse Sequence: noesy_da



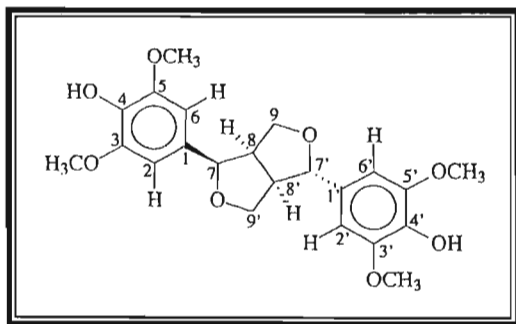
138



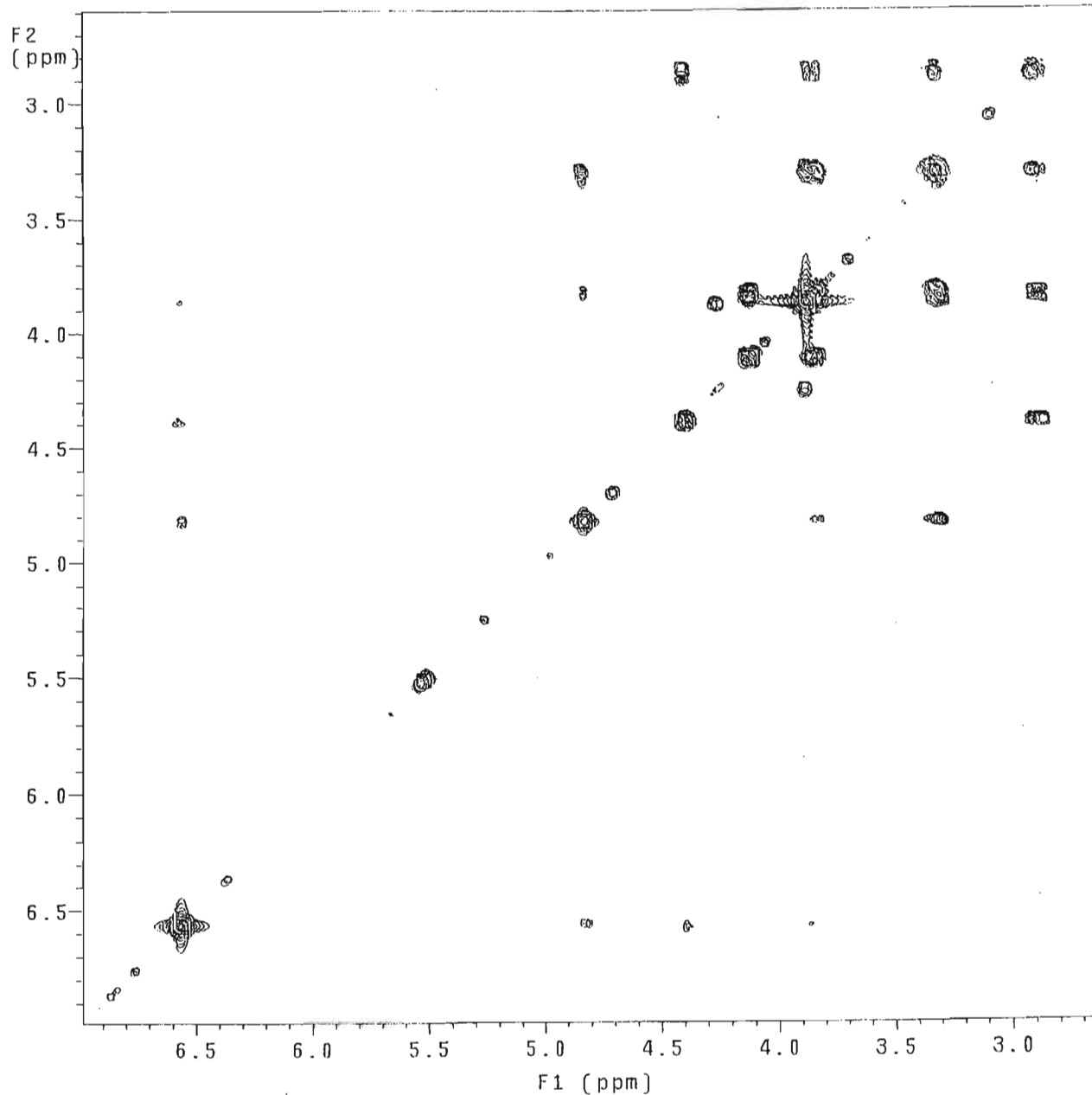
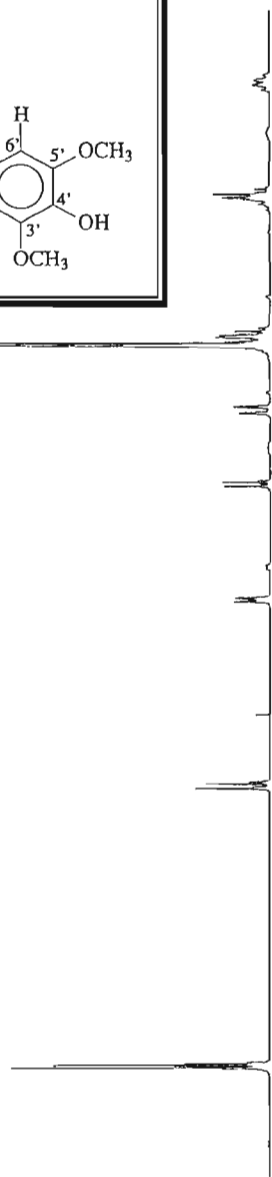
Spectrum 1.8 : NOESY NMR Spectrum of Compound 1, *epi*-syringaresinol

in cosy-90
probe=5mmASW

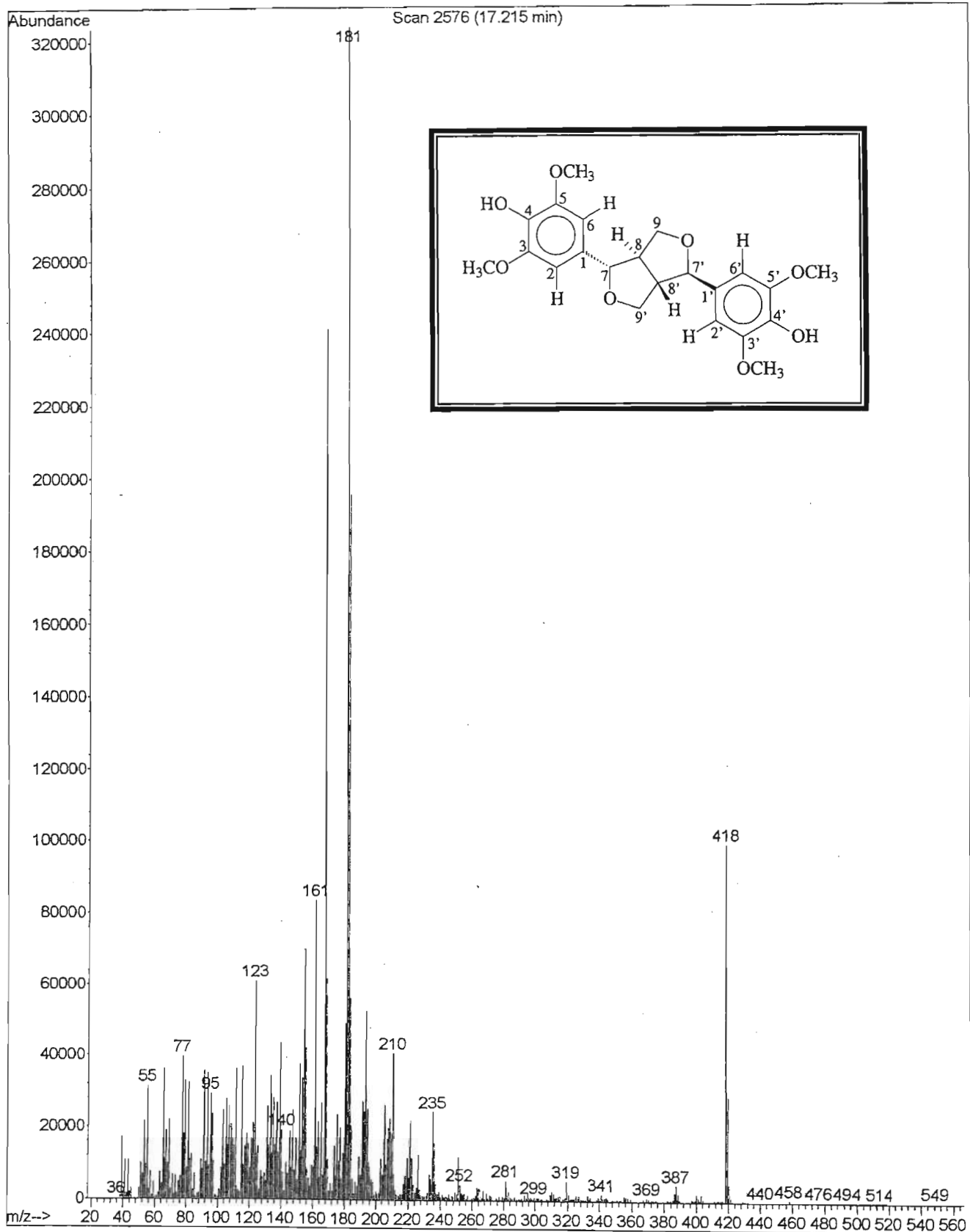
Pulse Sequence: relayh



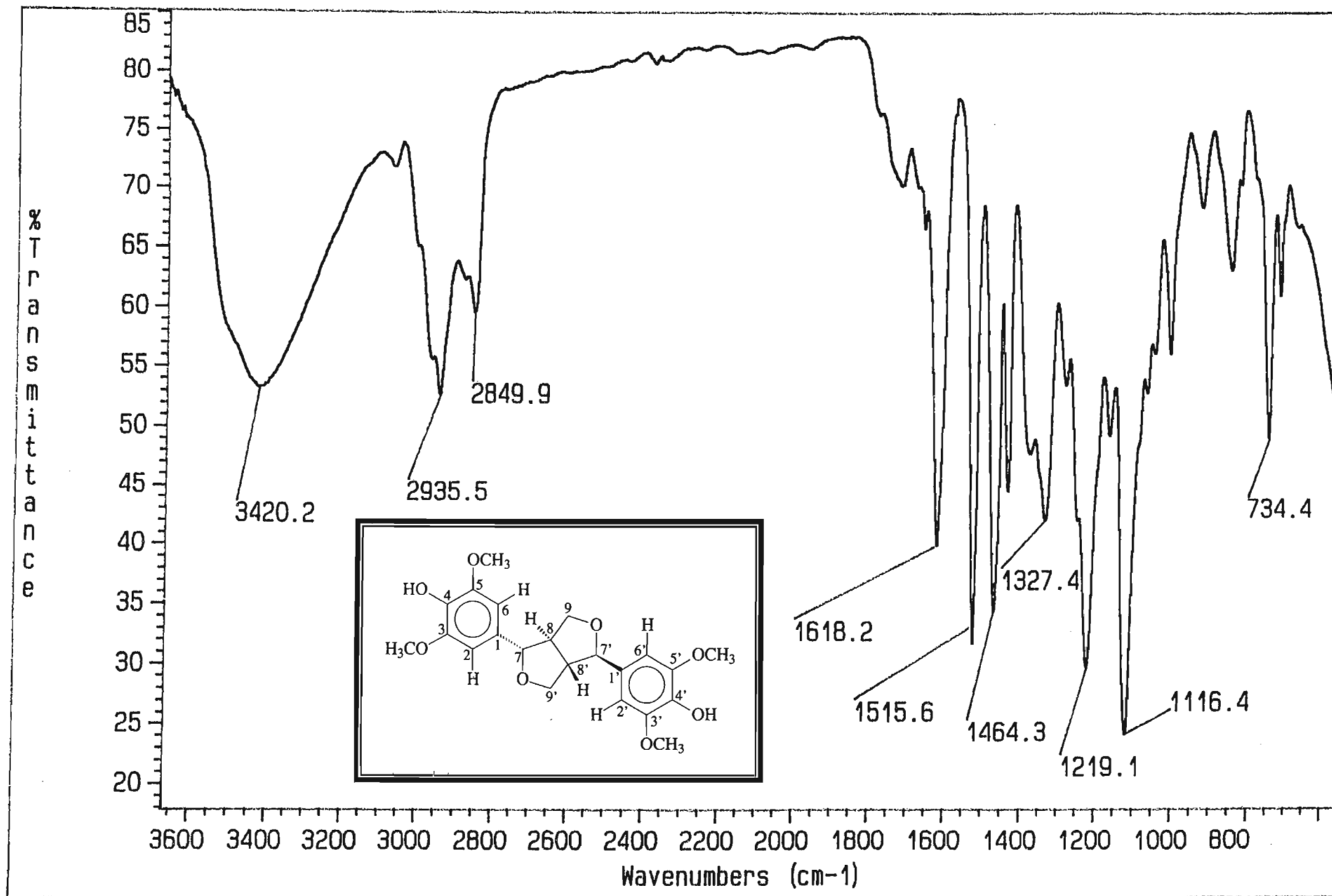
139



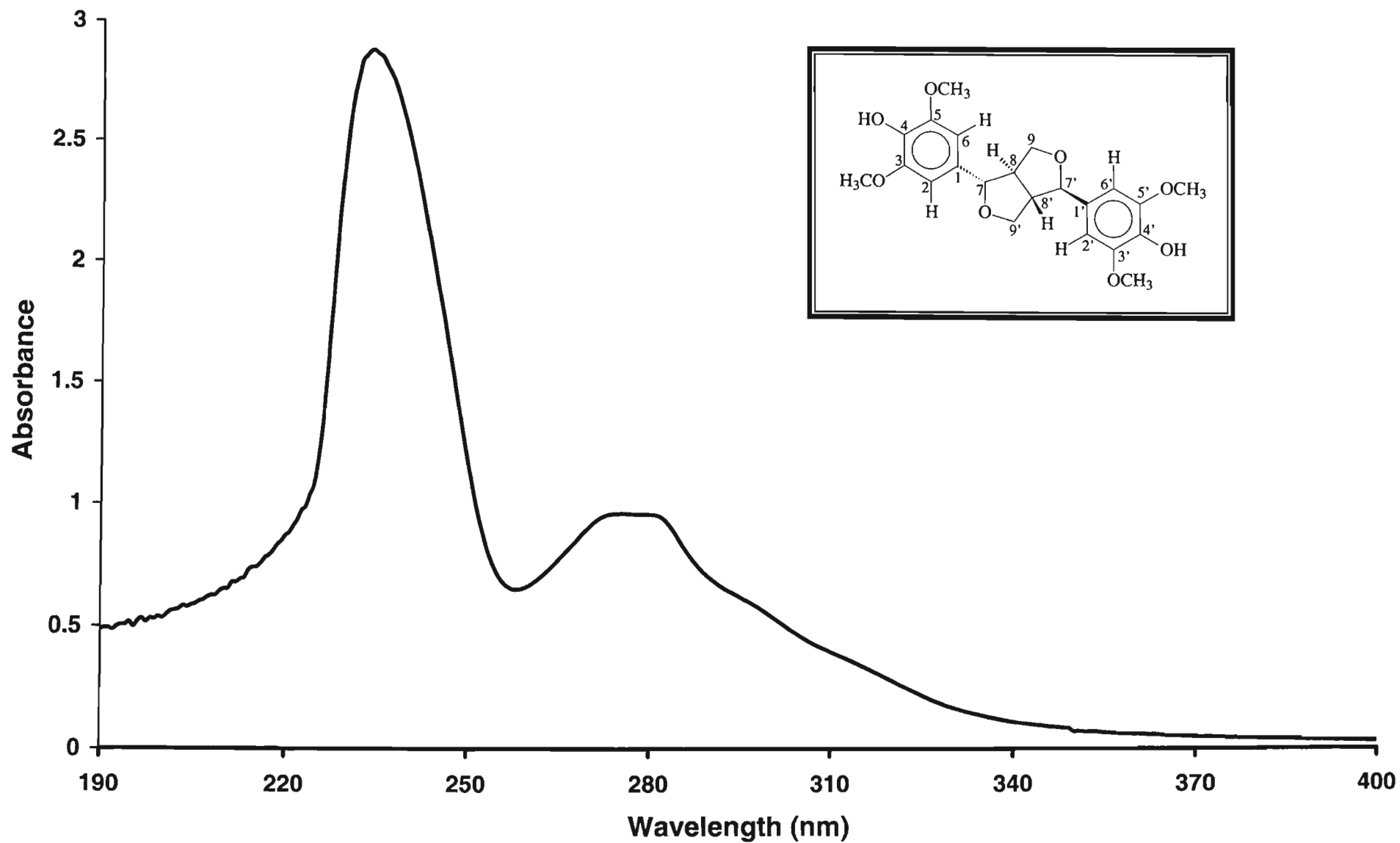
Spectrum 1.9 : COSY NMR Spectrum of Compound 1, *epi*-syringaresinol

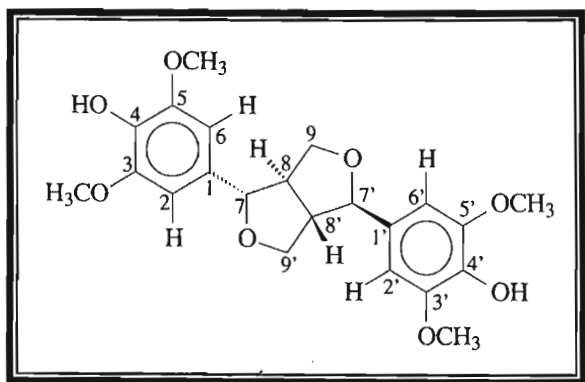




Spectrum 2.1 : Mass Spectrum of Compound 2, *meso*-syringaresinol

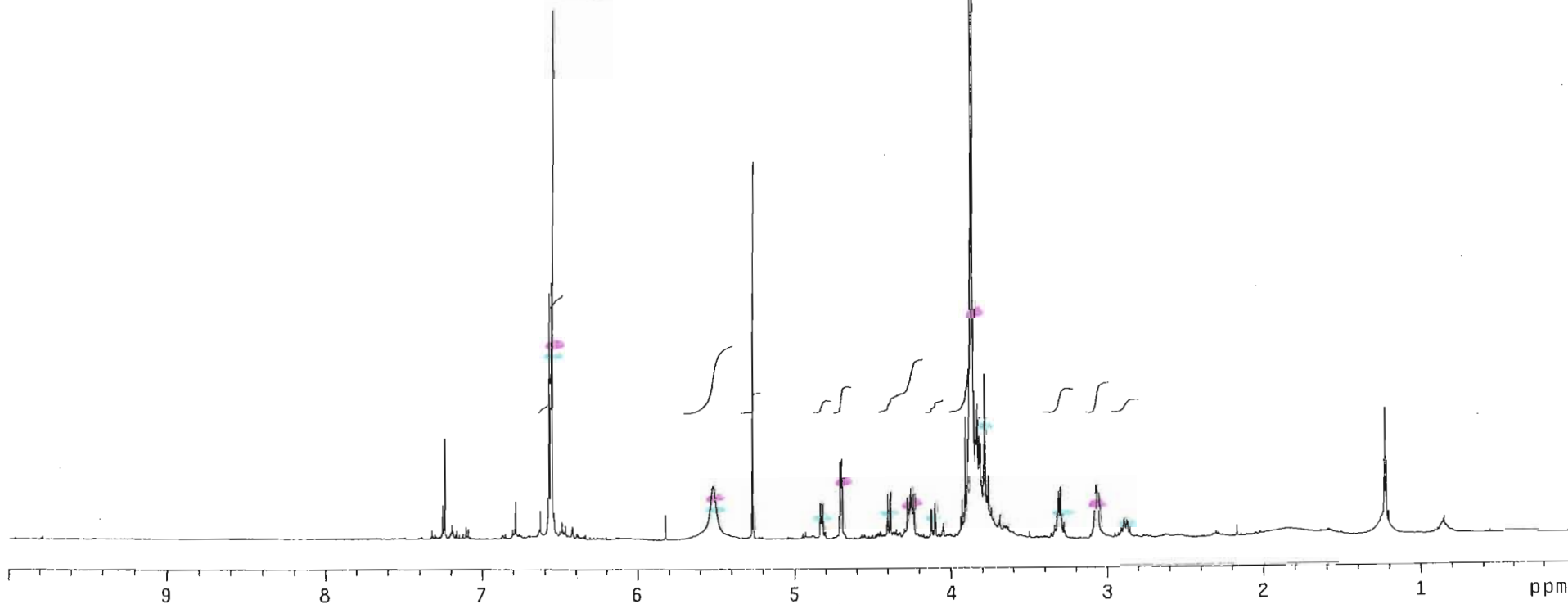


Spectrum 2.2 : Infrared Spectrum of Compound 2, *meso*-syringaresinol

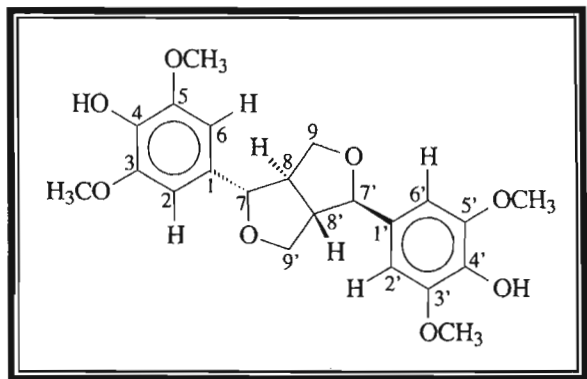
Spectrum 2.3 : UV Spectrum of Compound 2, *meso*-syringaresinol





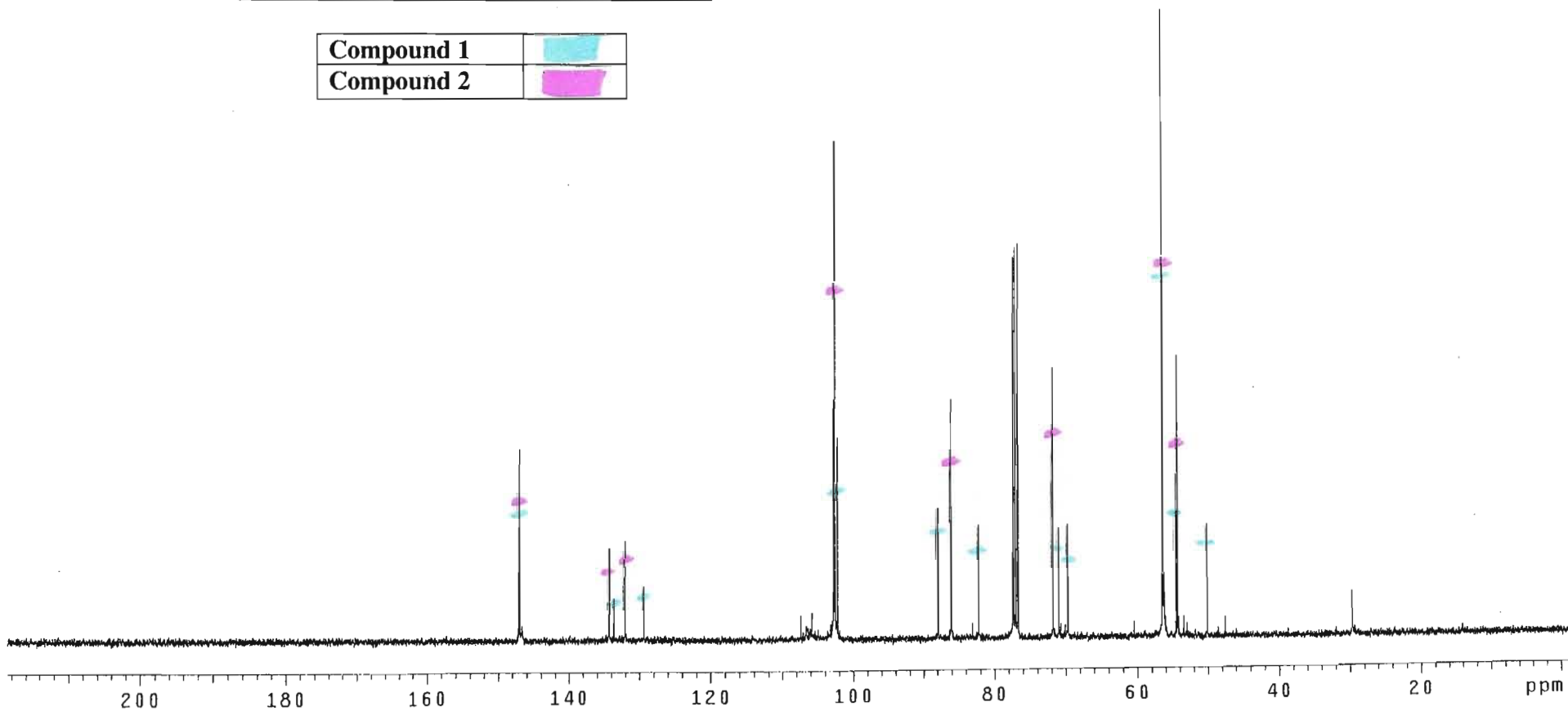
| | |
|------------|---|
| Compound 1 |  |
| Compound 2 |  |



Spectrum 2.4 : ^1H NMR Spectrum of Compound 2, *meso*-syringaresinol



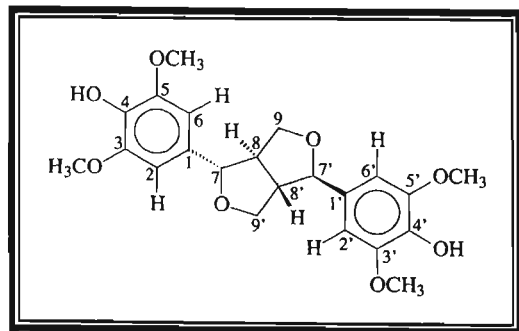
| | |
|------------|---|
| Compound 1 |  |
| Compound 2 |  |



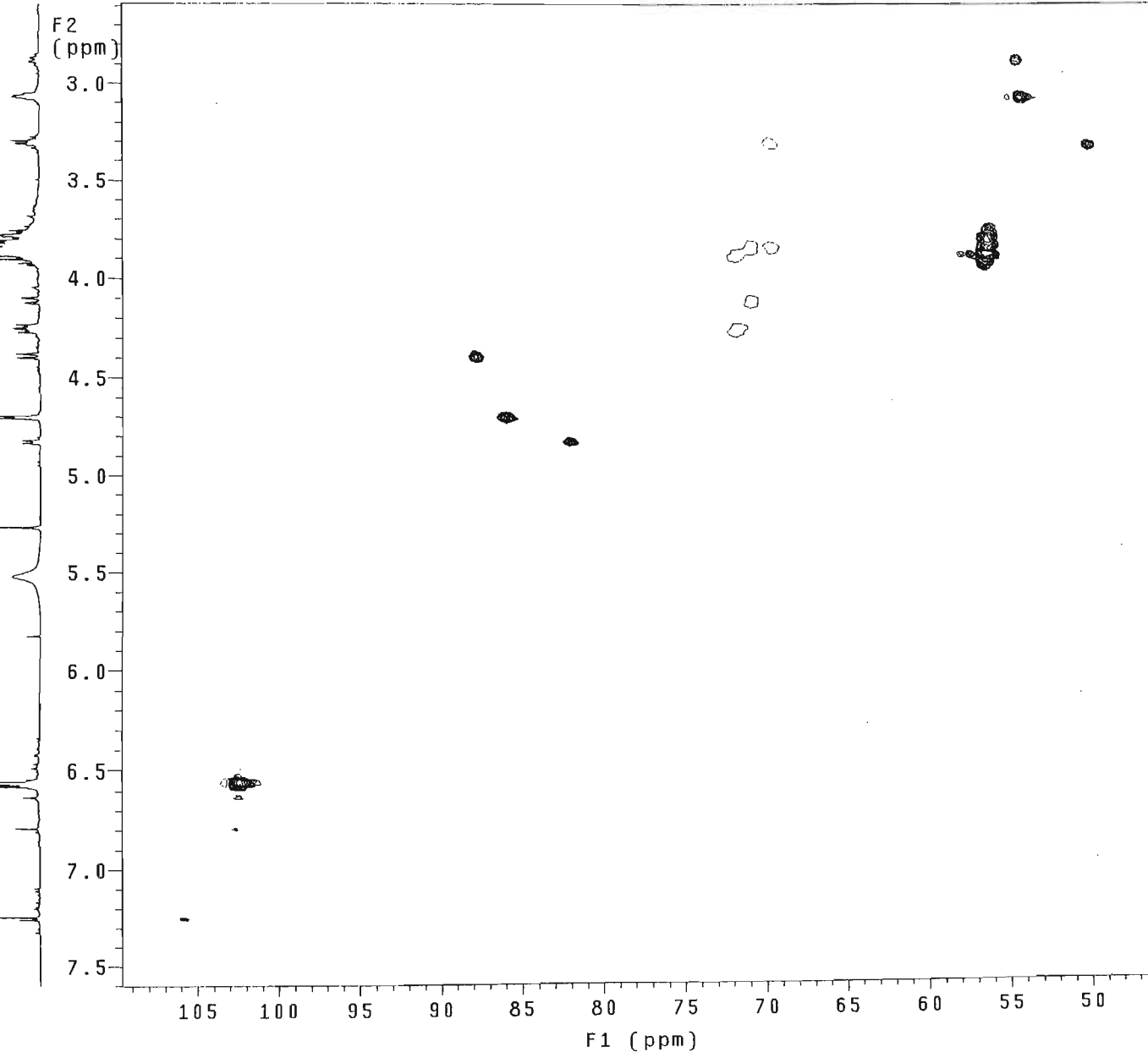
Spectrum 2.5 : ^{13}C NMR Spectrum of Compound 2, *meso*-syringaresinol

with mult.editing
probe=5mmASW

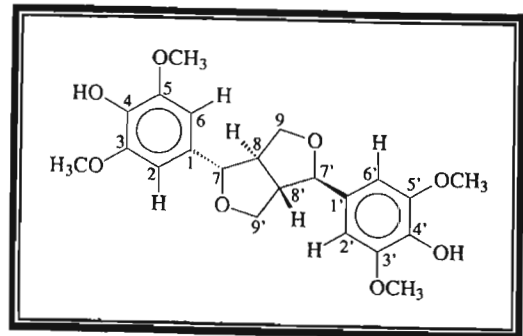
Pulse Sequence: ghsqc_da



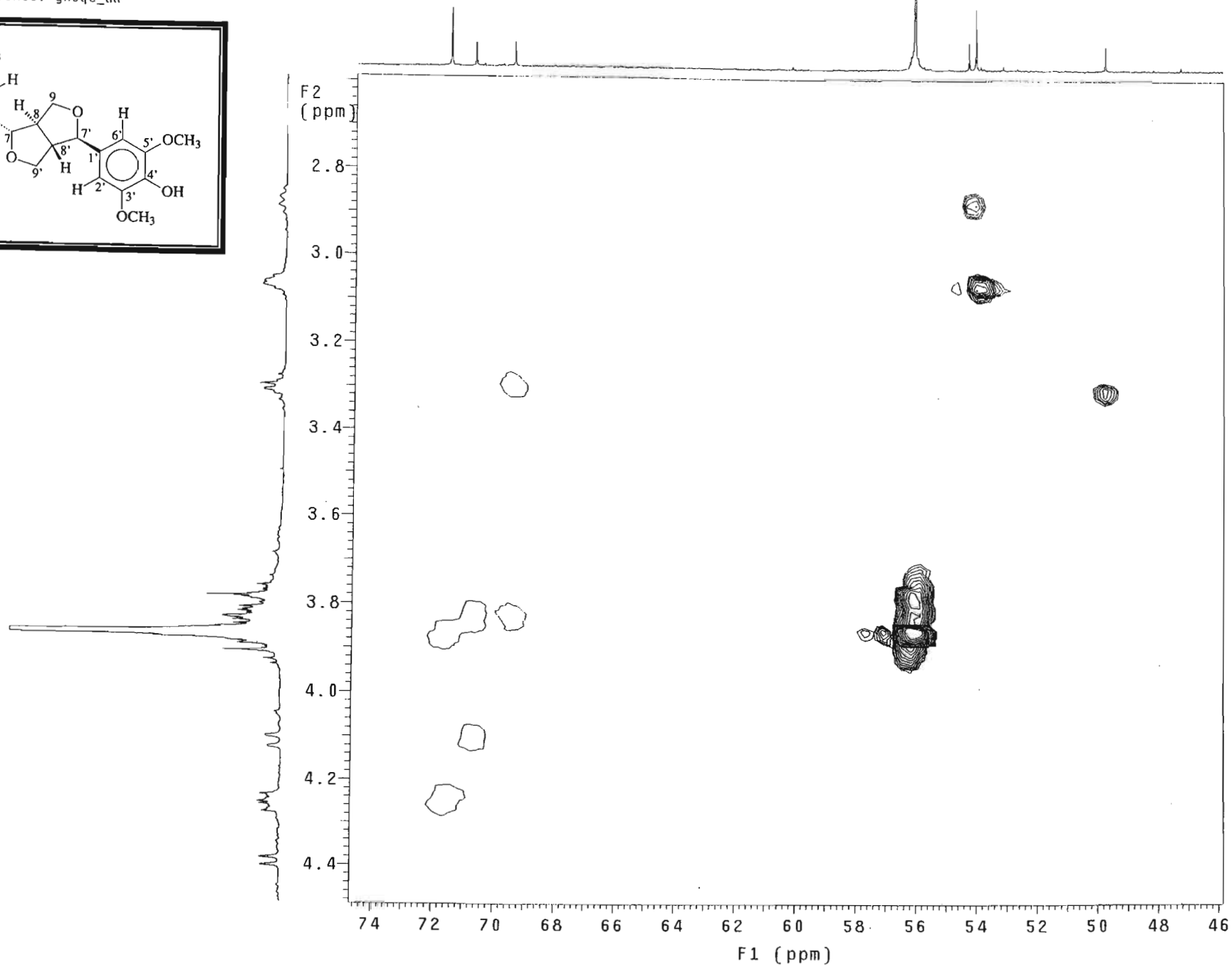
145



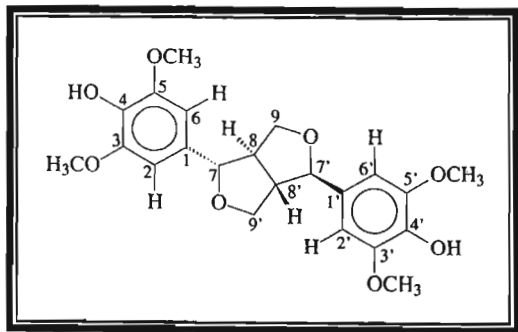
Spectrum 2.6 : HSQC NMR Spectrum of Compound 2, *meso*-syringaresinol



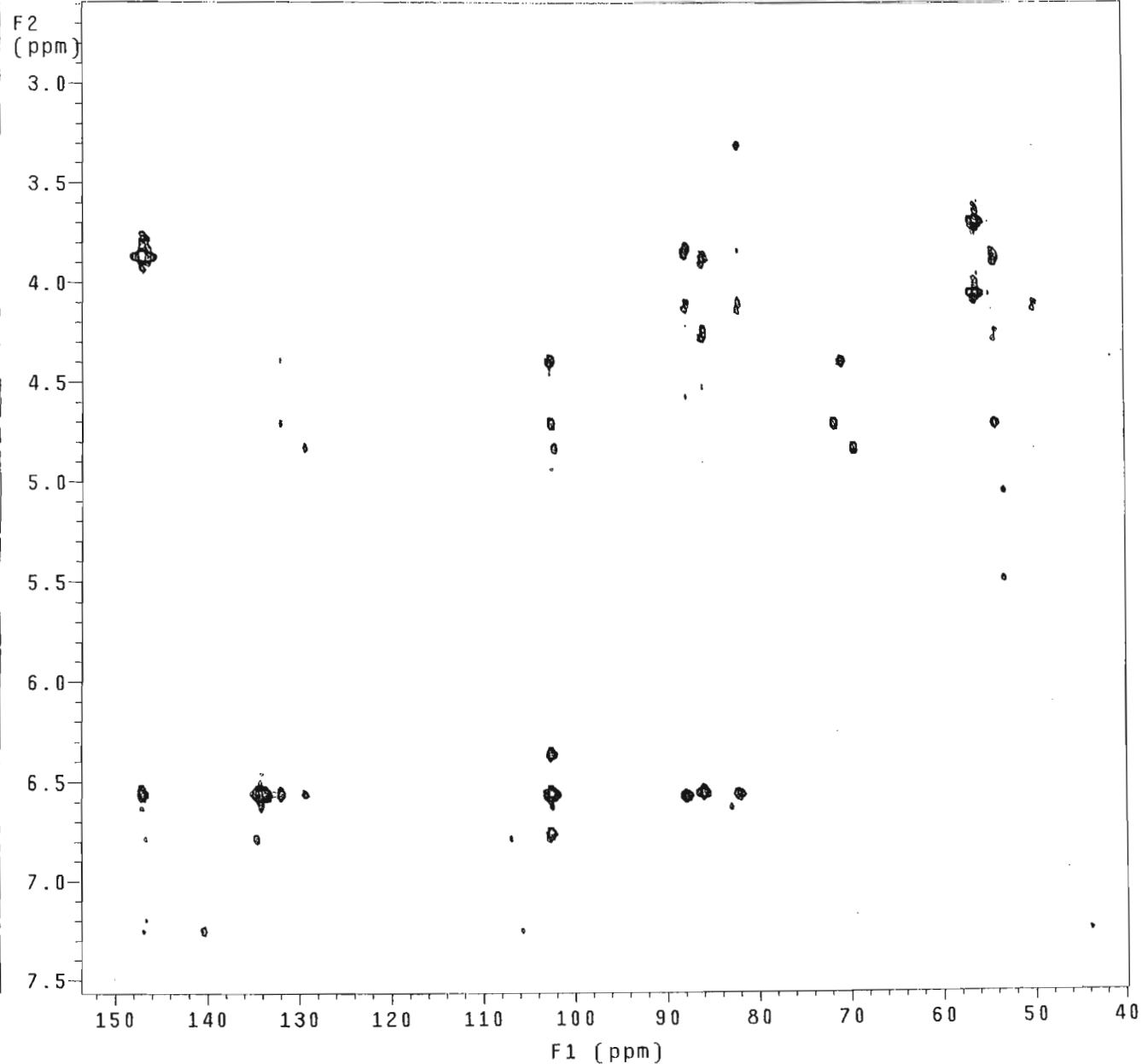
146



Spectrum 2.7 : Expanded HSQC NMR Spectrum of Compound 2, *meso*-syringaresinol

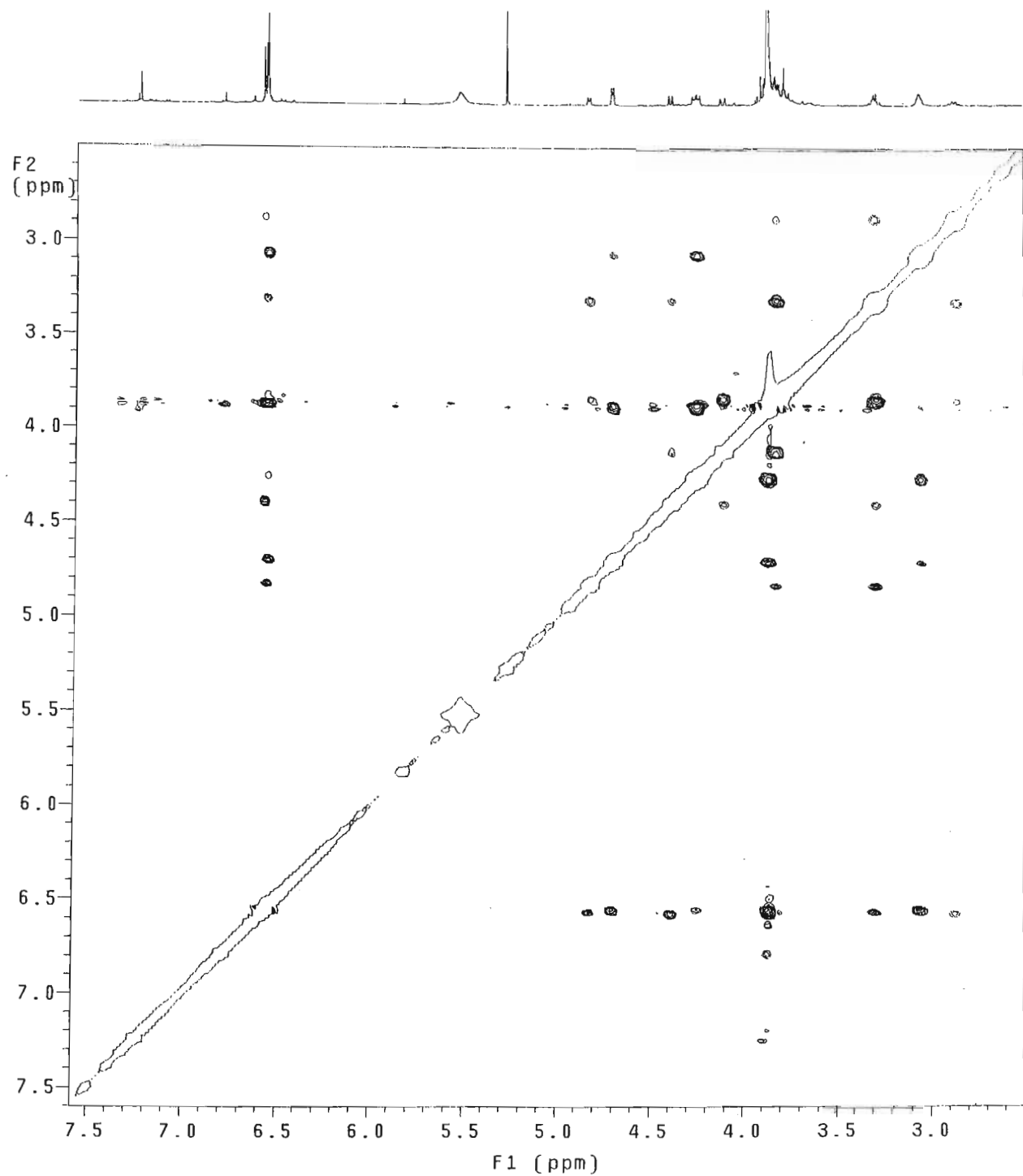
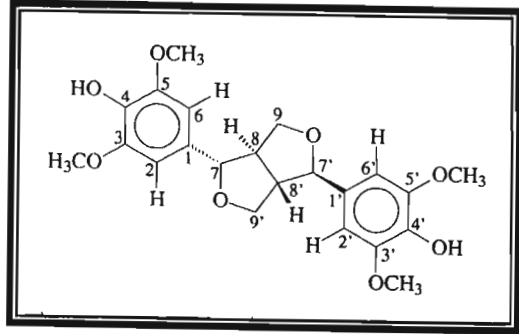


147



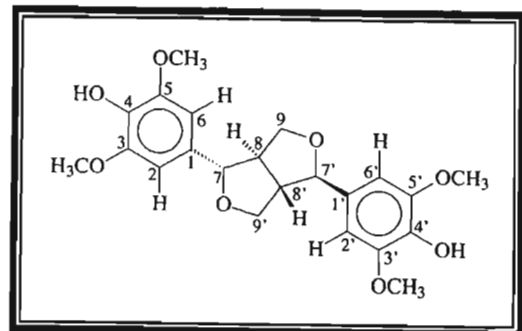
Spectrum 2.8 : HMBC NMR Spectrum of Compound 2, *meso*-syringaresinol

NOESY exp.
mix=1sec
probe=5mmASW
Pulse Sequence: noesy_da

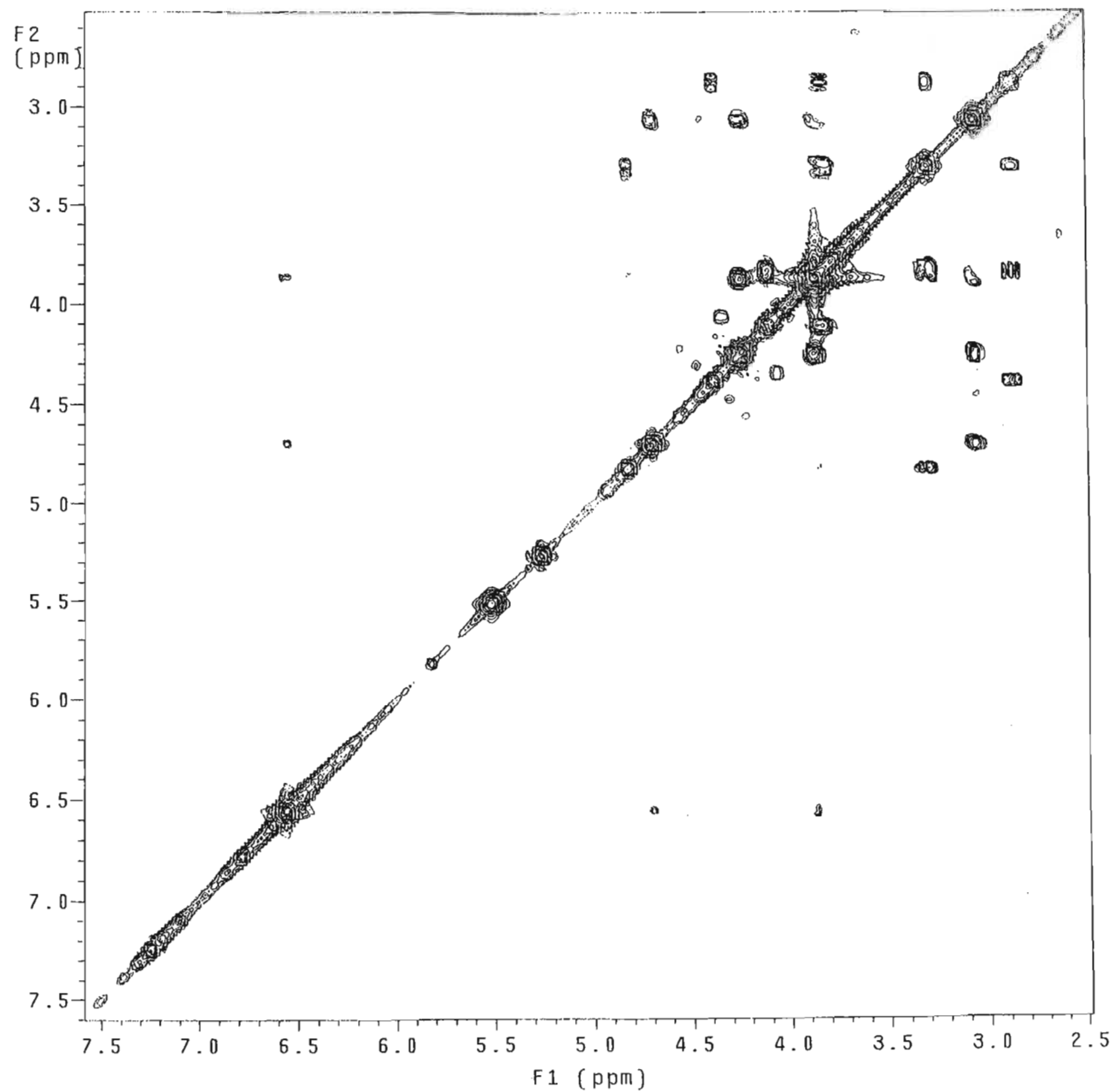


Spectrum 2.9 : NOESY NMR Spectrum of Compound 2, *meso*-syringaresinol

probe=5mmASW
Pulse Sequence: relayh



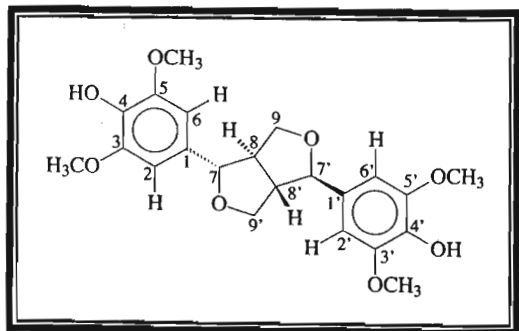
149



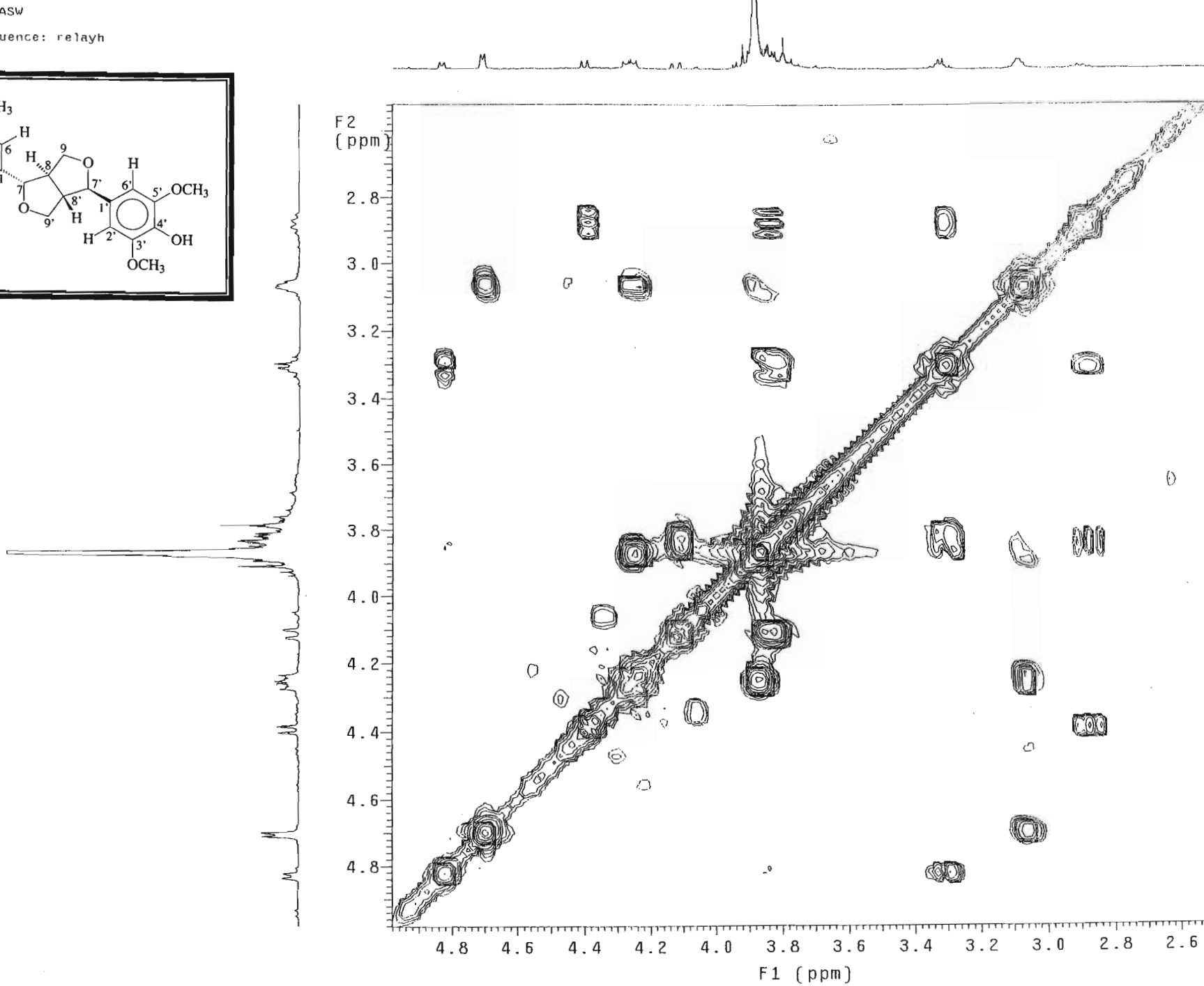
Spectrum 2.10 : COSY NMR Spectrum of Compound 2, *meso*-syringaresinol

probe=5mmASW

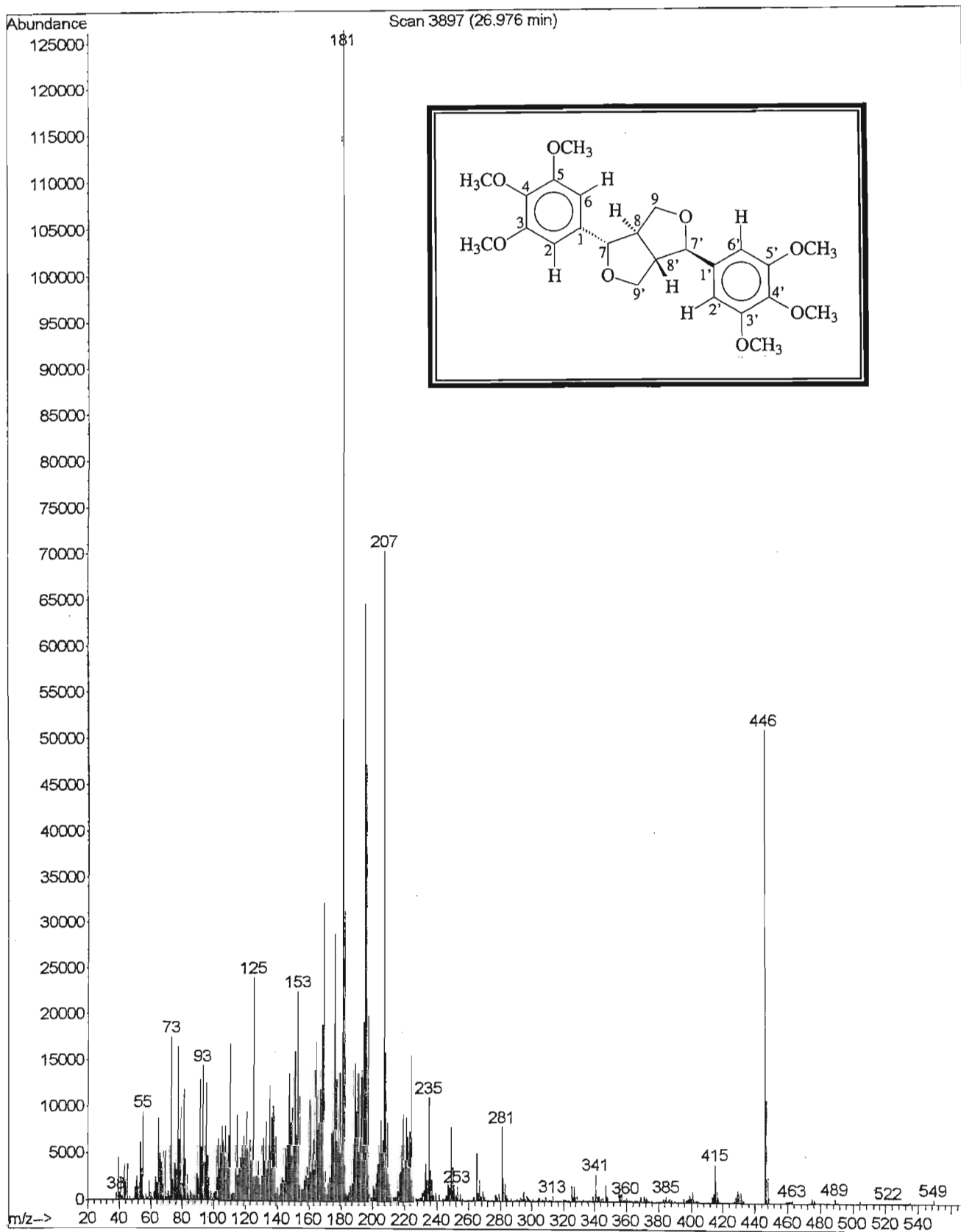
Pulse Sequence: relayh



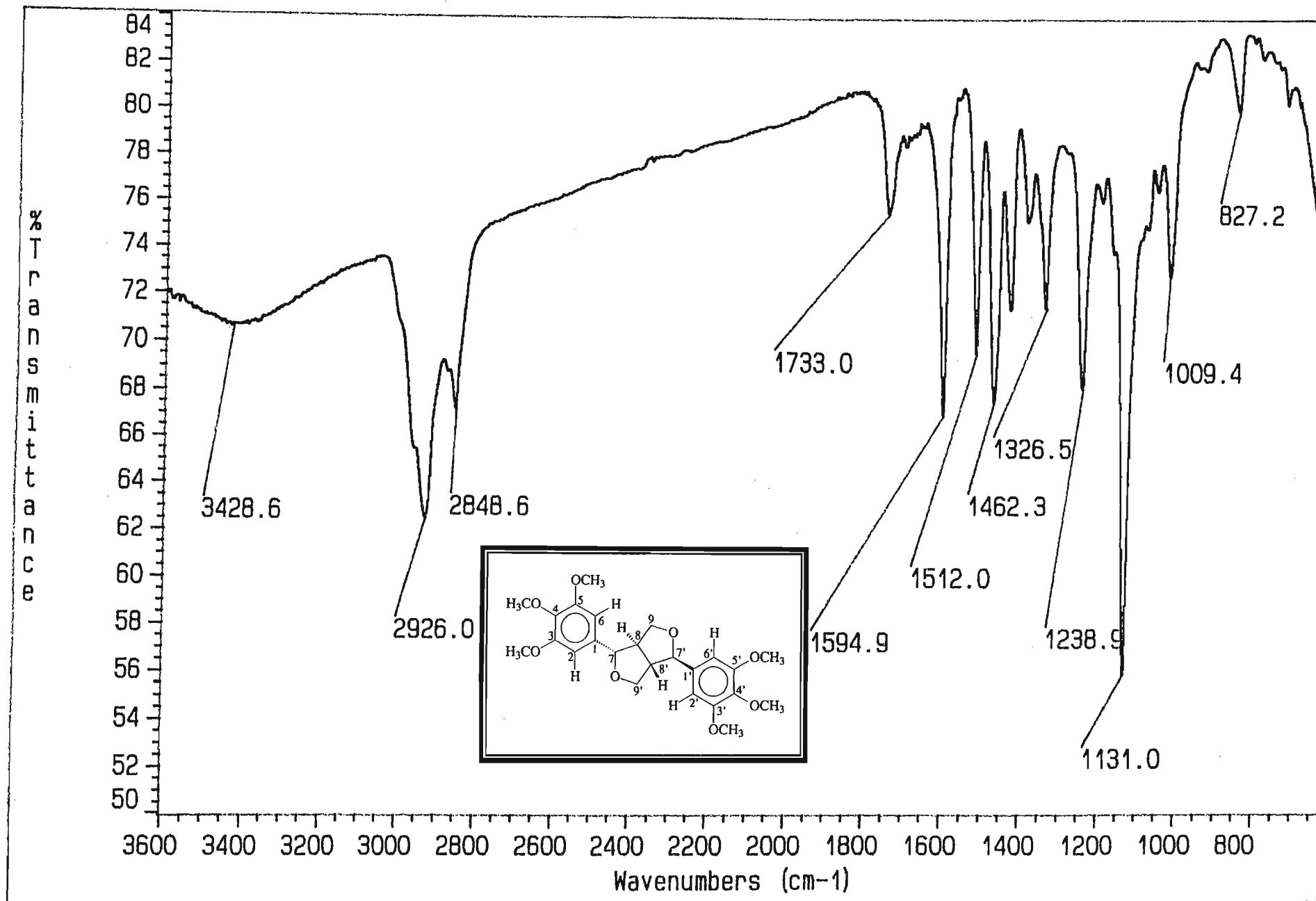
150

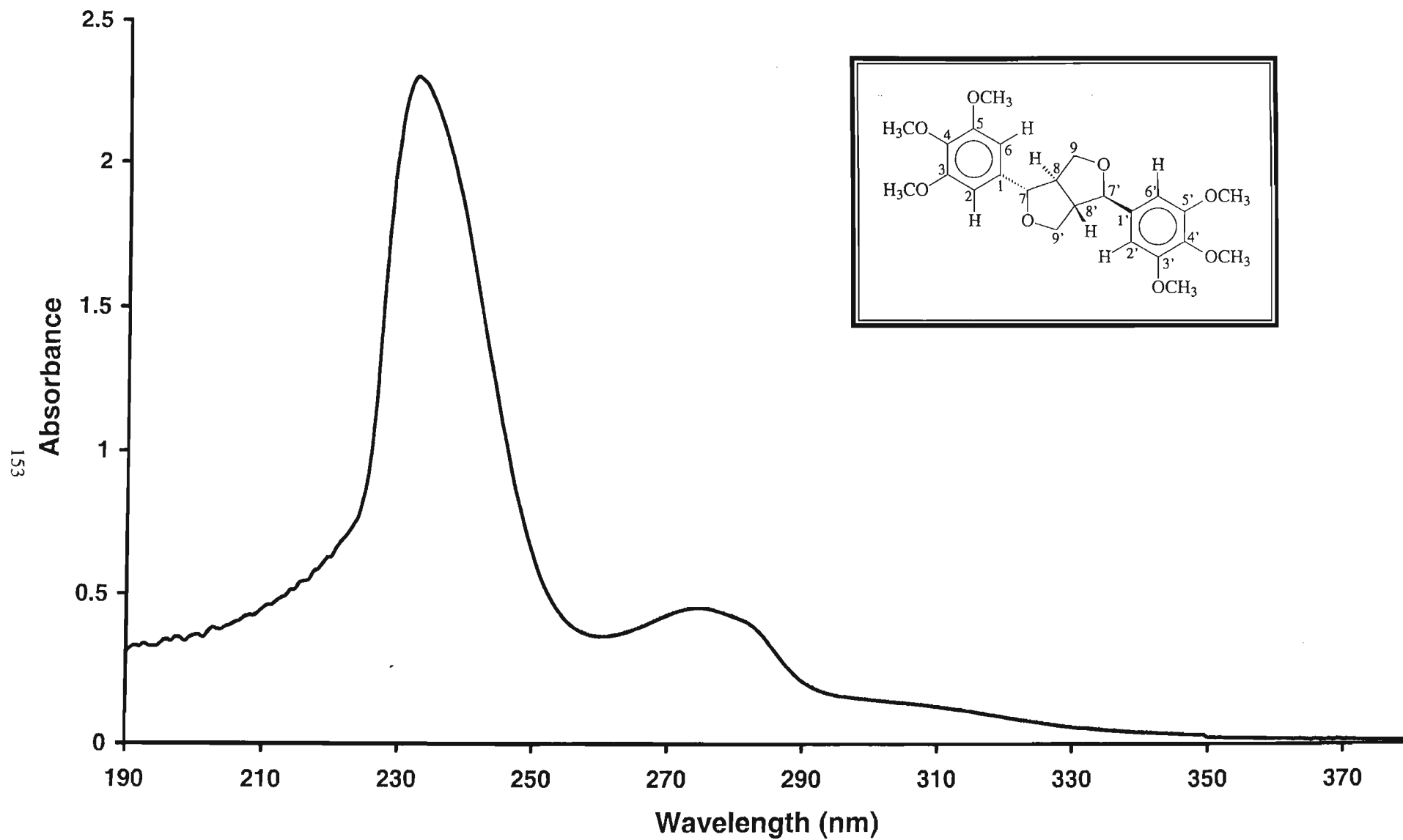


Spectrum 2.11 : Expanded COSY NMR Spectrum of Compound 2, *meso*-syringaresinol

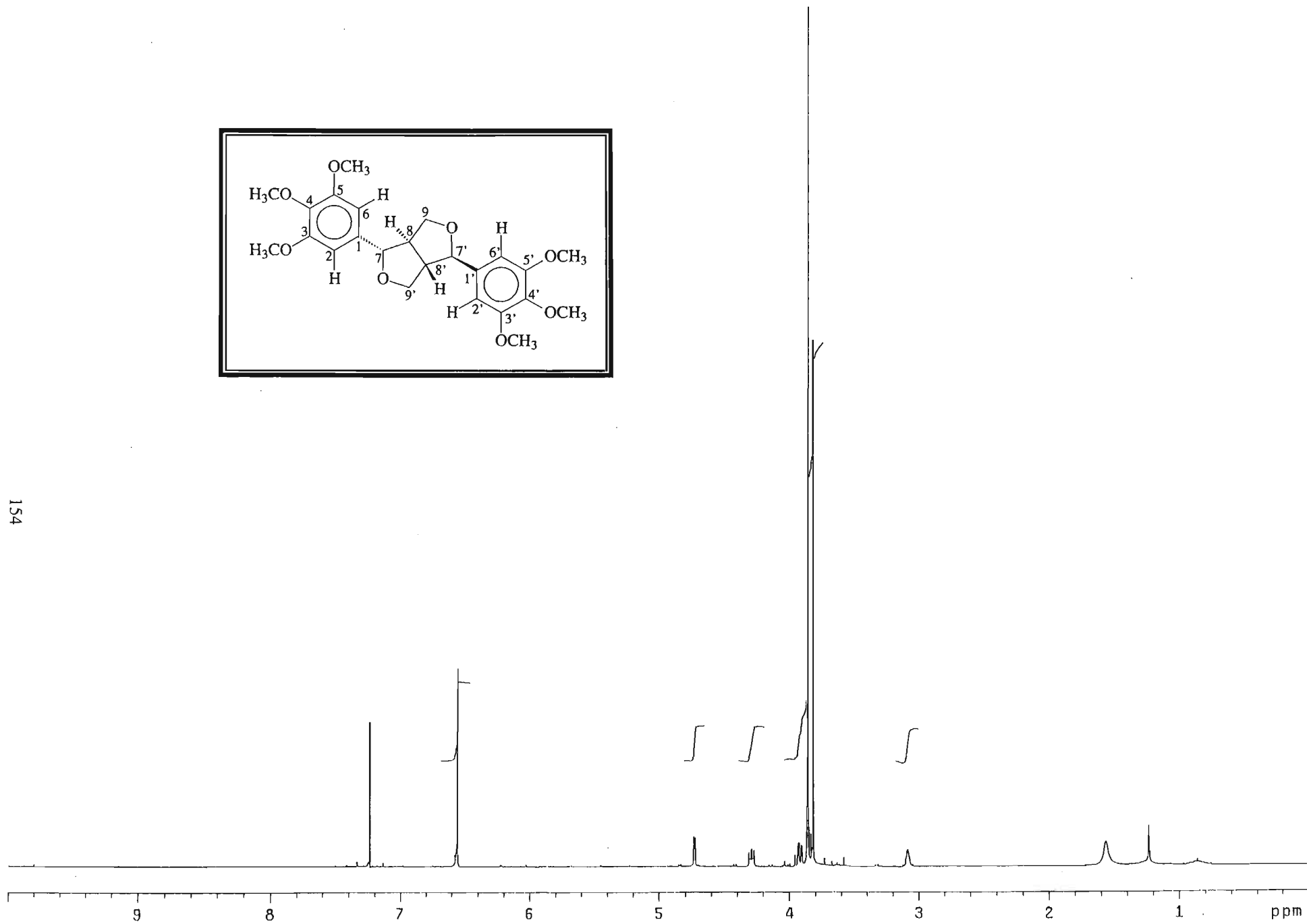
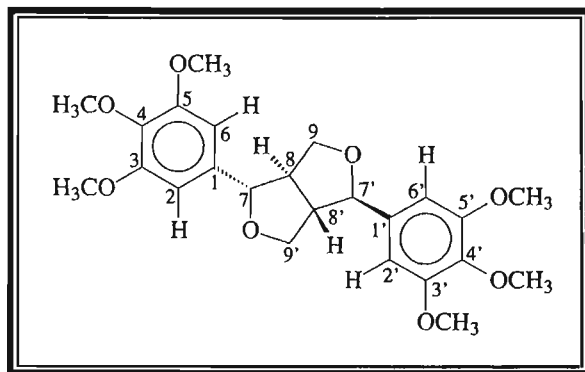


Spectrum 3.1 : Mass Spectrum of Compound 3, *meso*-yangambin

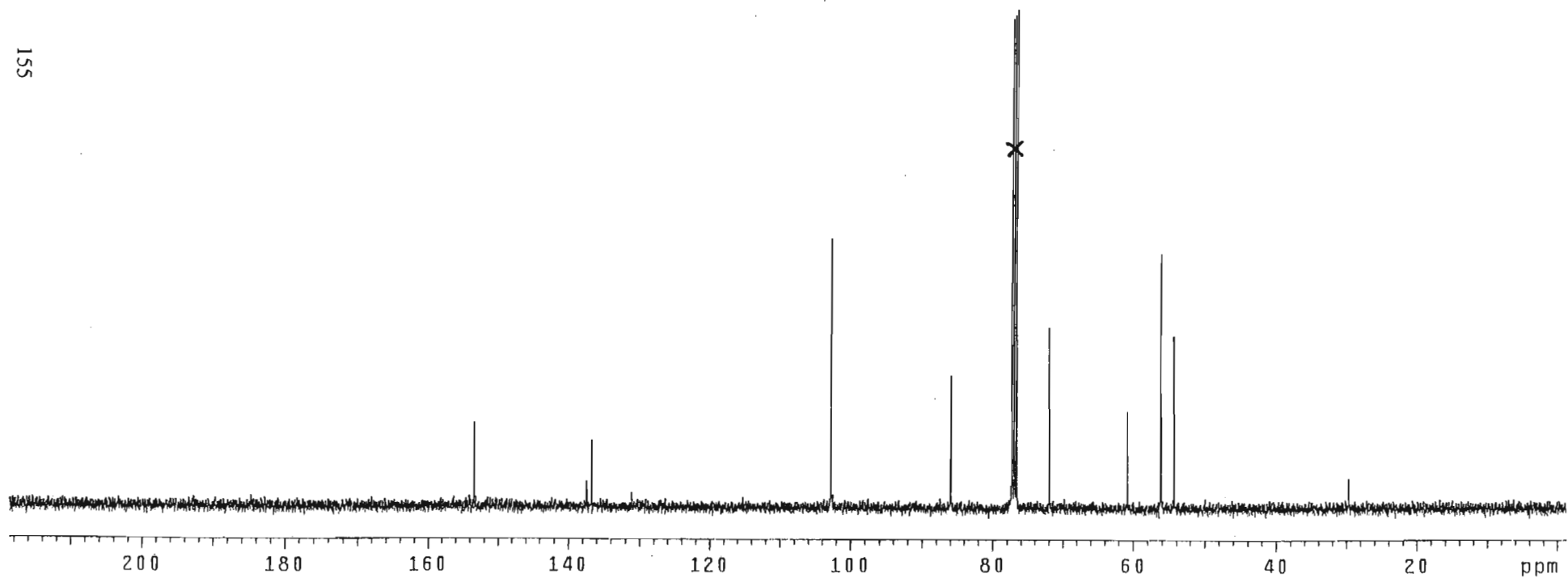
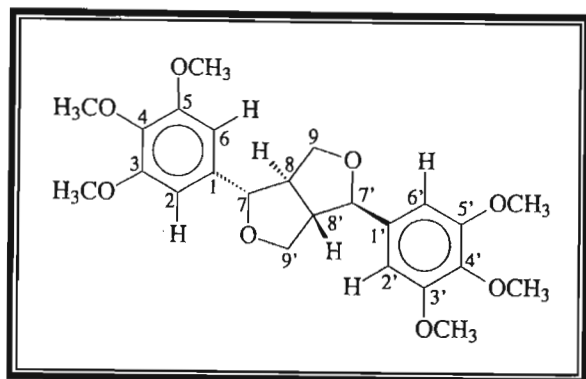
Spectrum 3.2 : Infrared Spectrum of Compound 3, *meso*-yangambin



Spectrum 3.3 : UV Spectrum of Compound 3, *meso*-yangambin



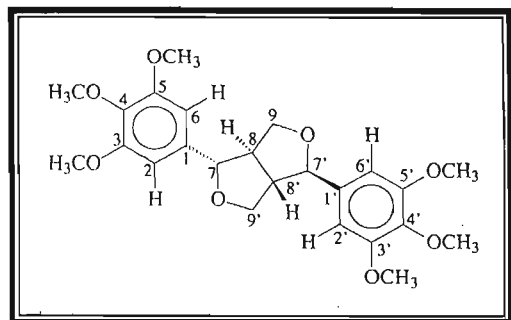
Spectrum 3.4 : ¹H NMR Spectrum of Compound 3, *meso*-yangambin



Spectrum 3.5 : ^{13}C NMR Spectrum of Compound 3, *meso*-yangambin

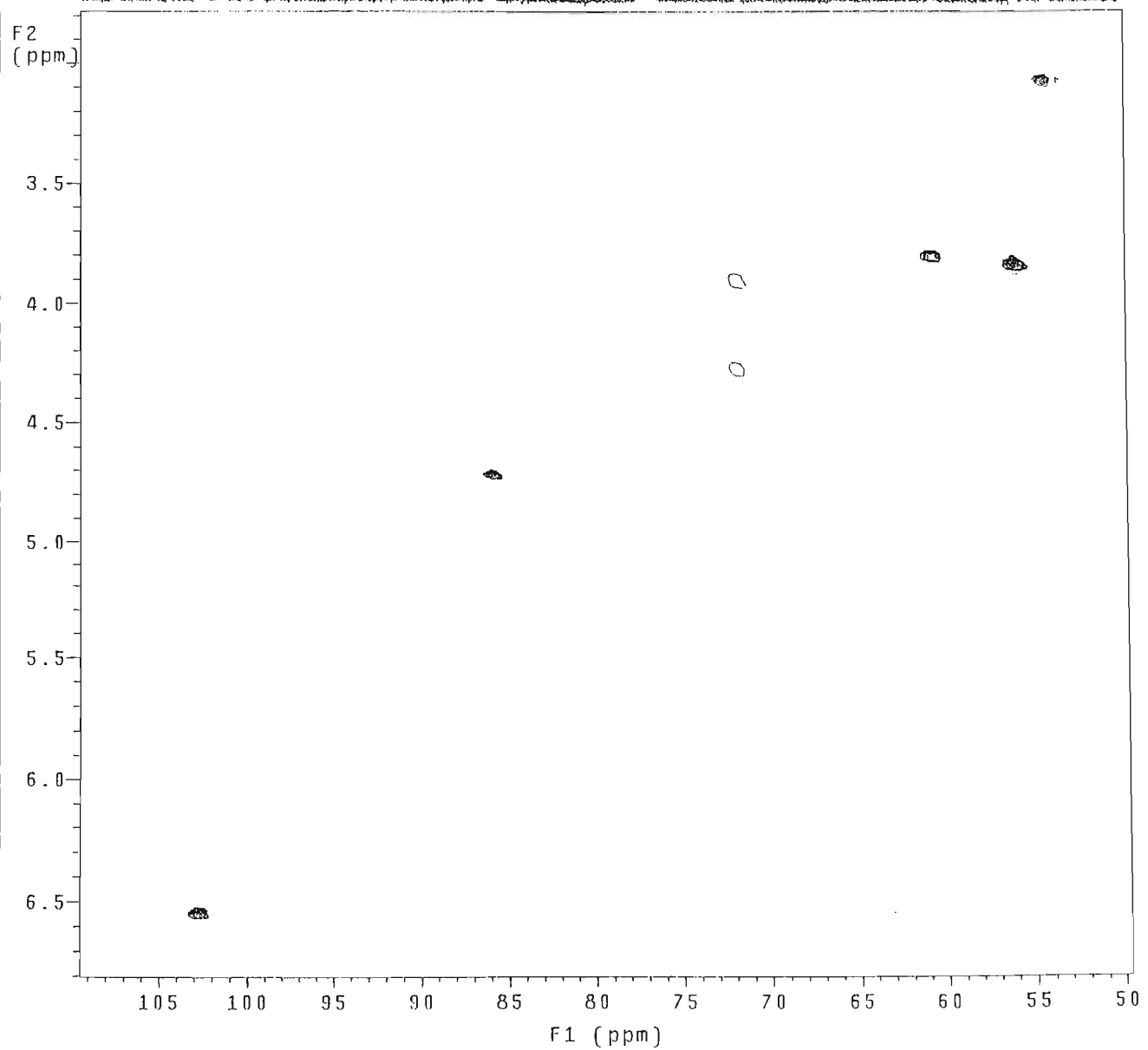
with magic editing
probe=5mmASW

Pulse Sequence: ghsqc_da



156

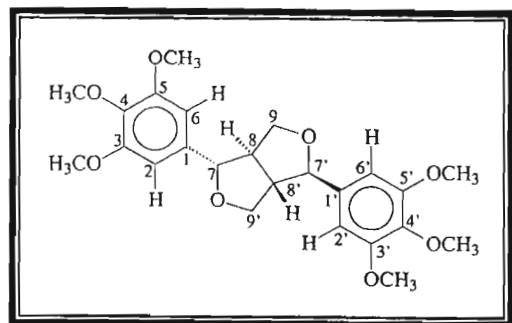
F2
(ppm)



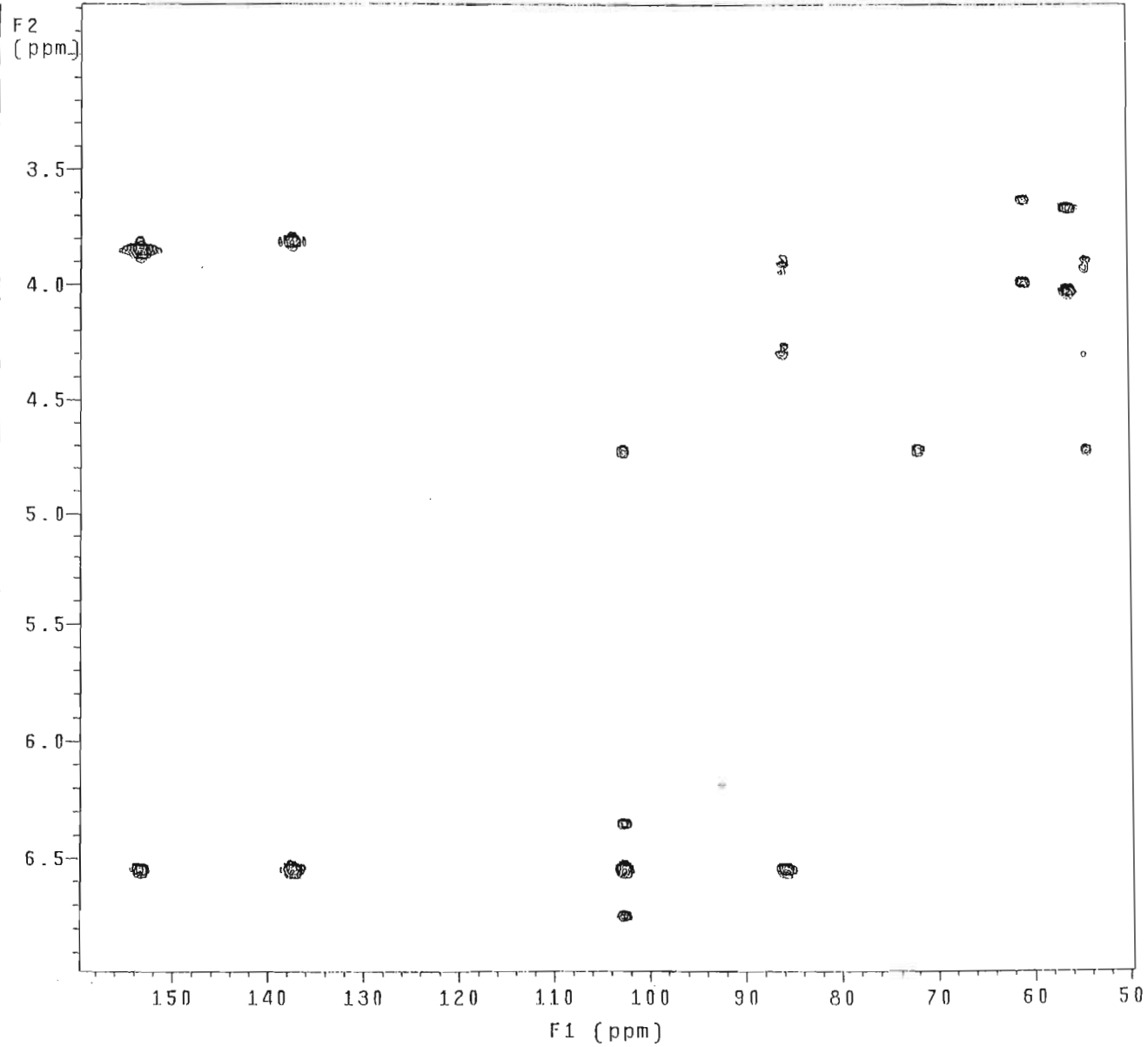
Spectrum 3.6 : HSQC NMR Spectrum of Compound 3, *meso*-yangambin

probe=5mmASW

Pulse Sequence: ghmqc_da

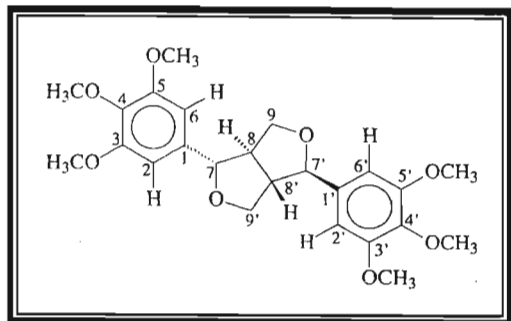


157

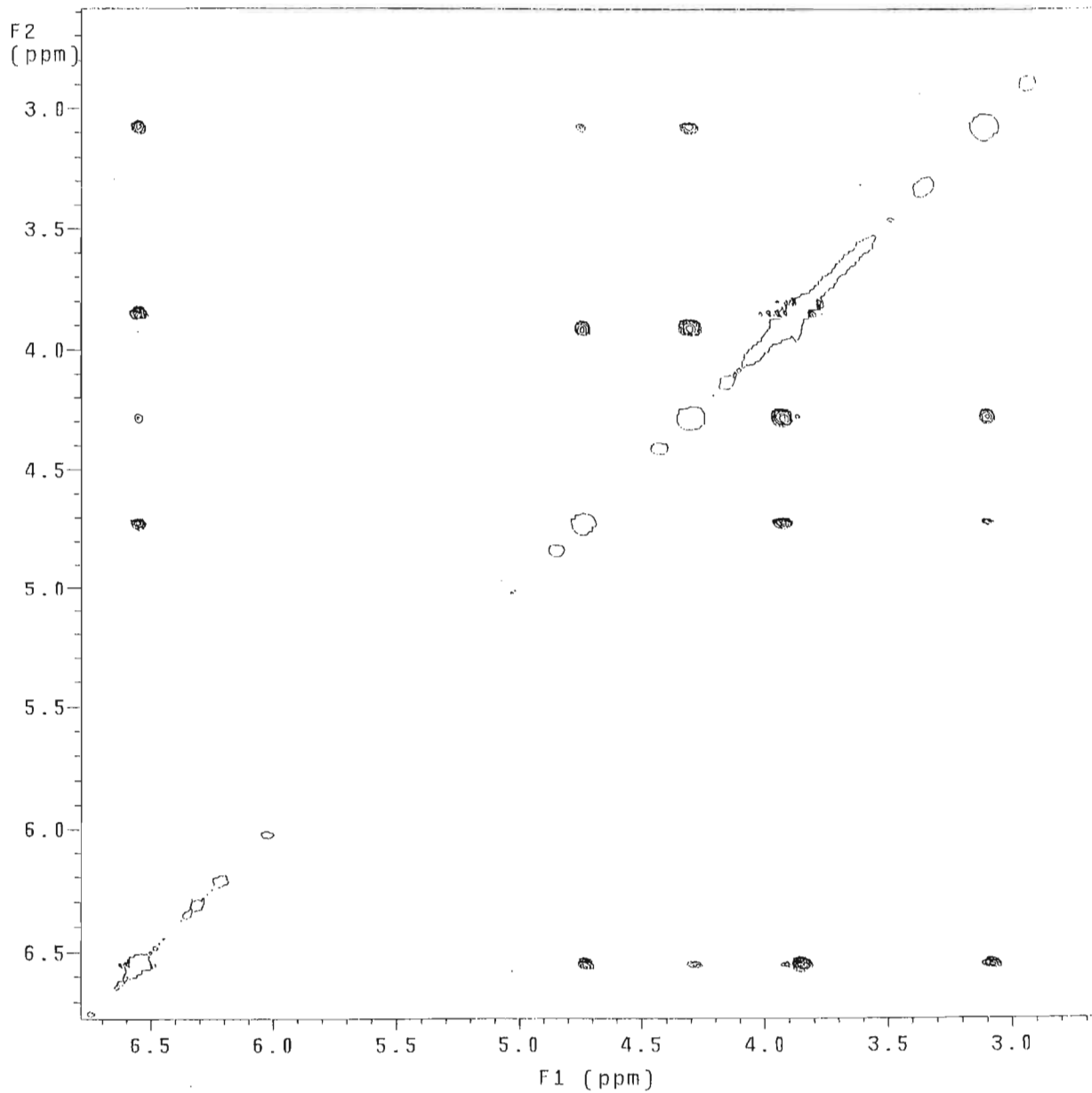


Spectrum 3.7 : HMBC NMR Spectrum of Compound 3, *meso*-yangambin

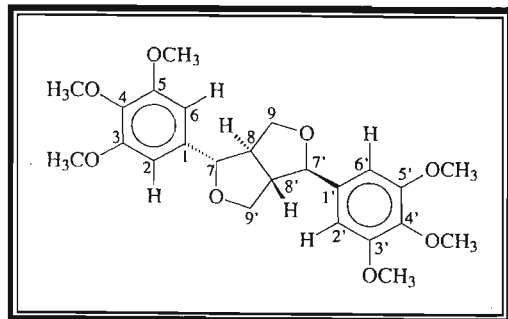
NOESY expt.
mix=1sec
probe=5mmASW
Pulse Sequence: noesy_da



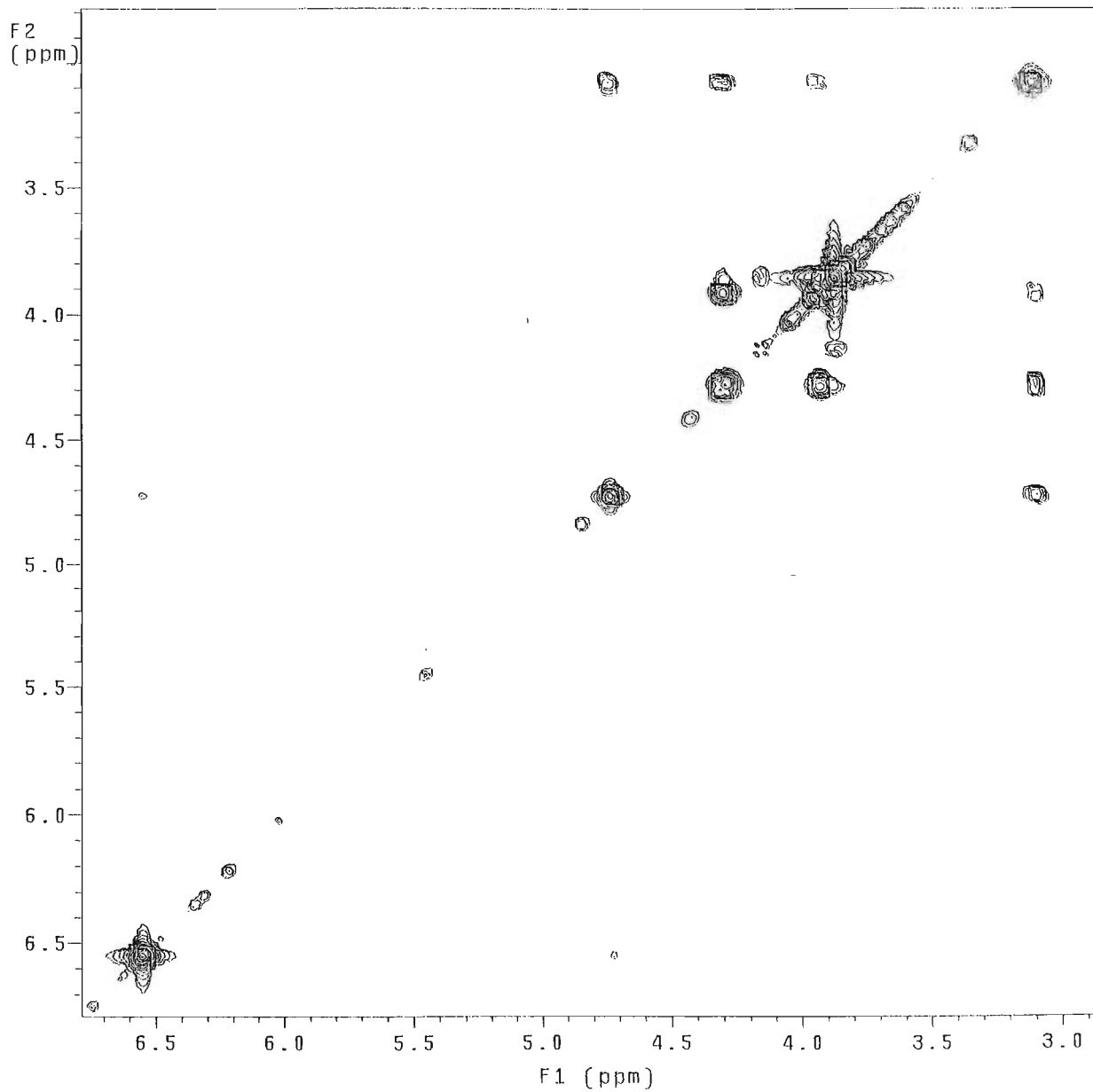
158



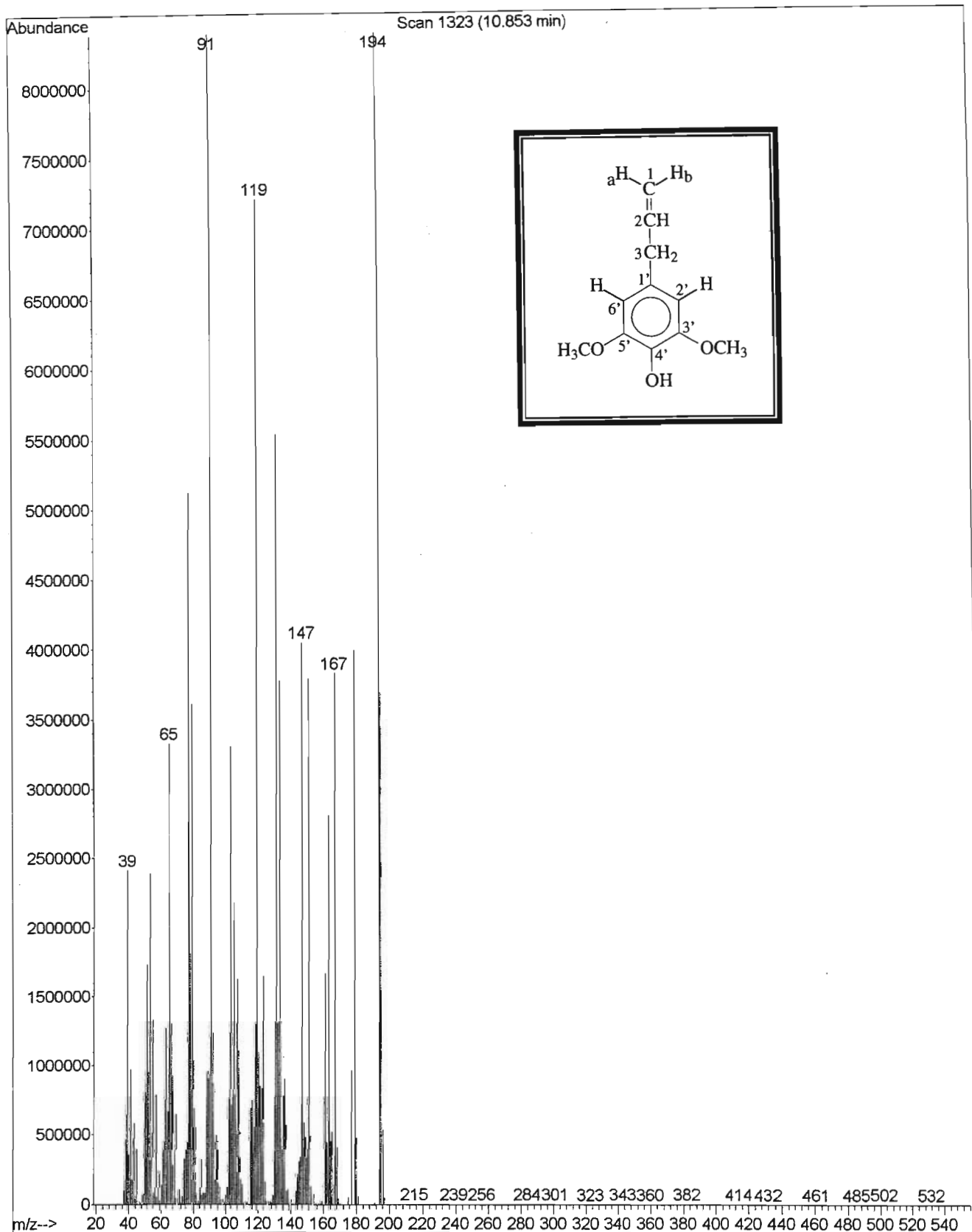
Spectrum 3.8 : NOESY NMR Spectrum of Compound 3, *meso*-yangambin



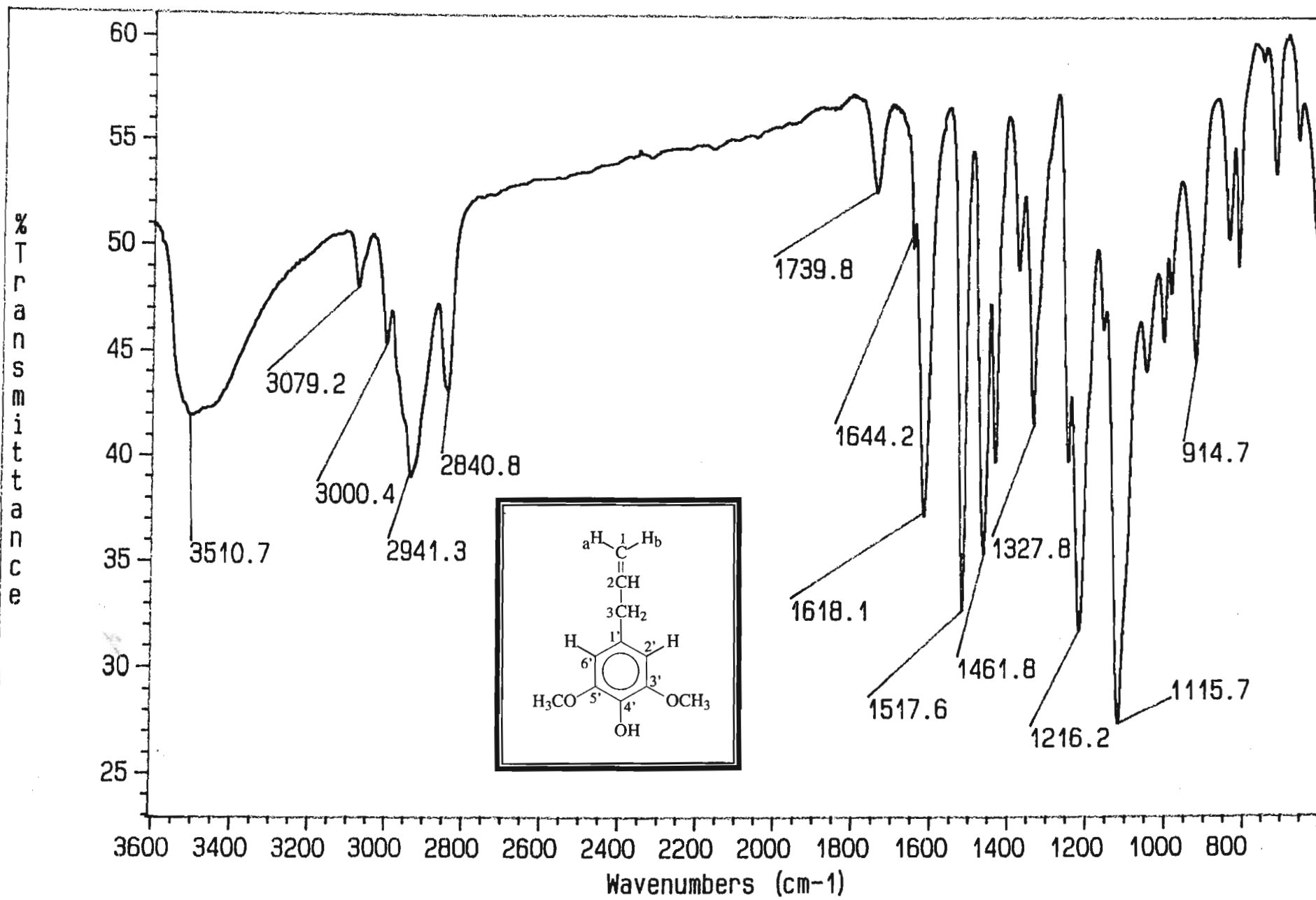
159



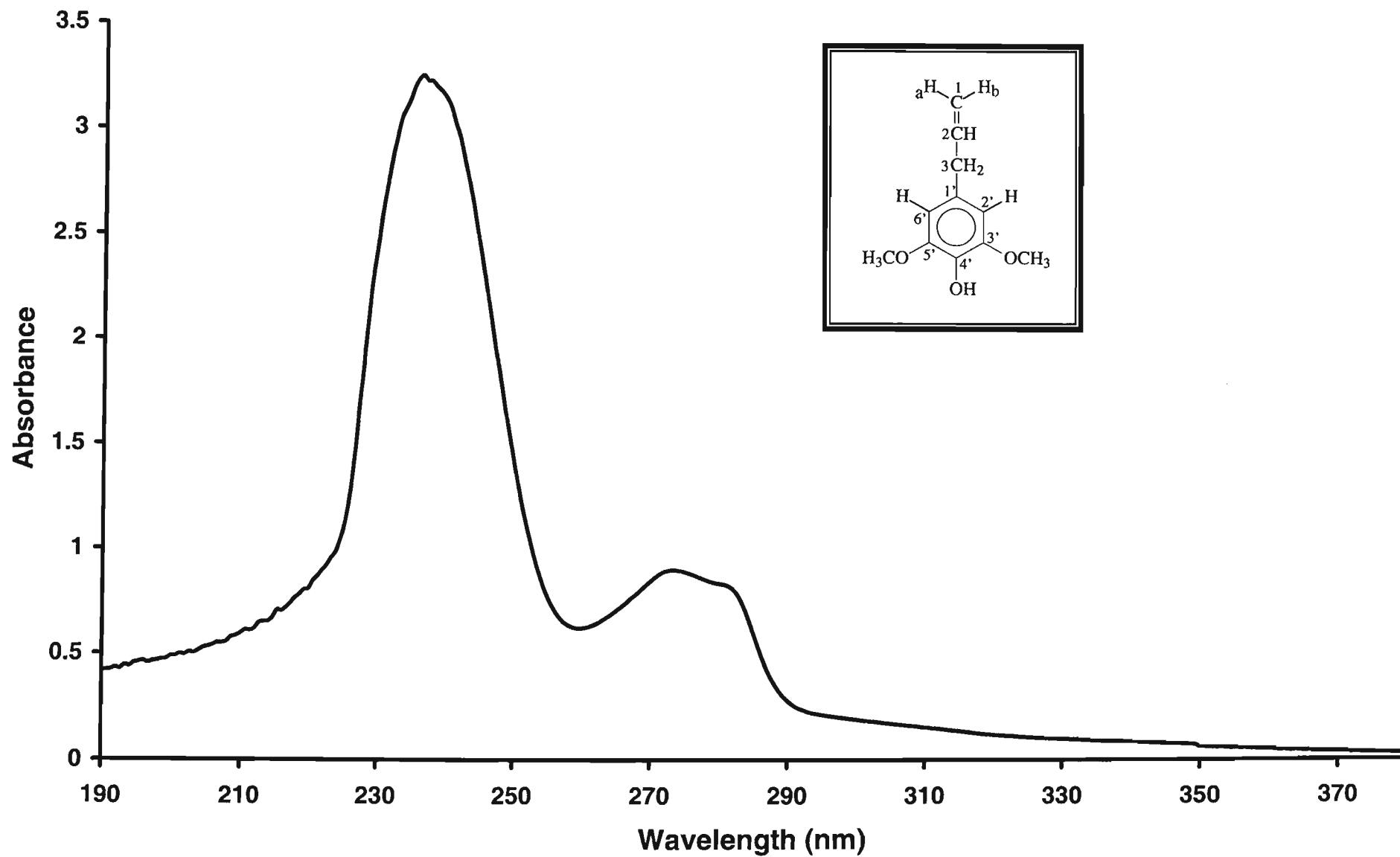
Spectrum 3.9 : COSY NMR Spectrum of Compound 3, *meso*-yangambin



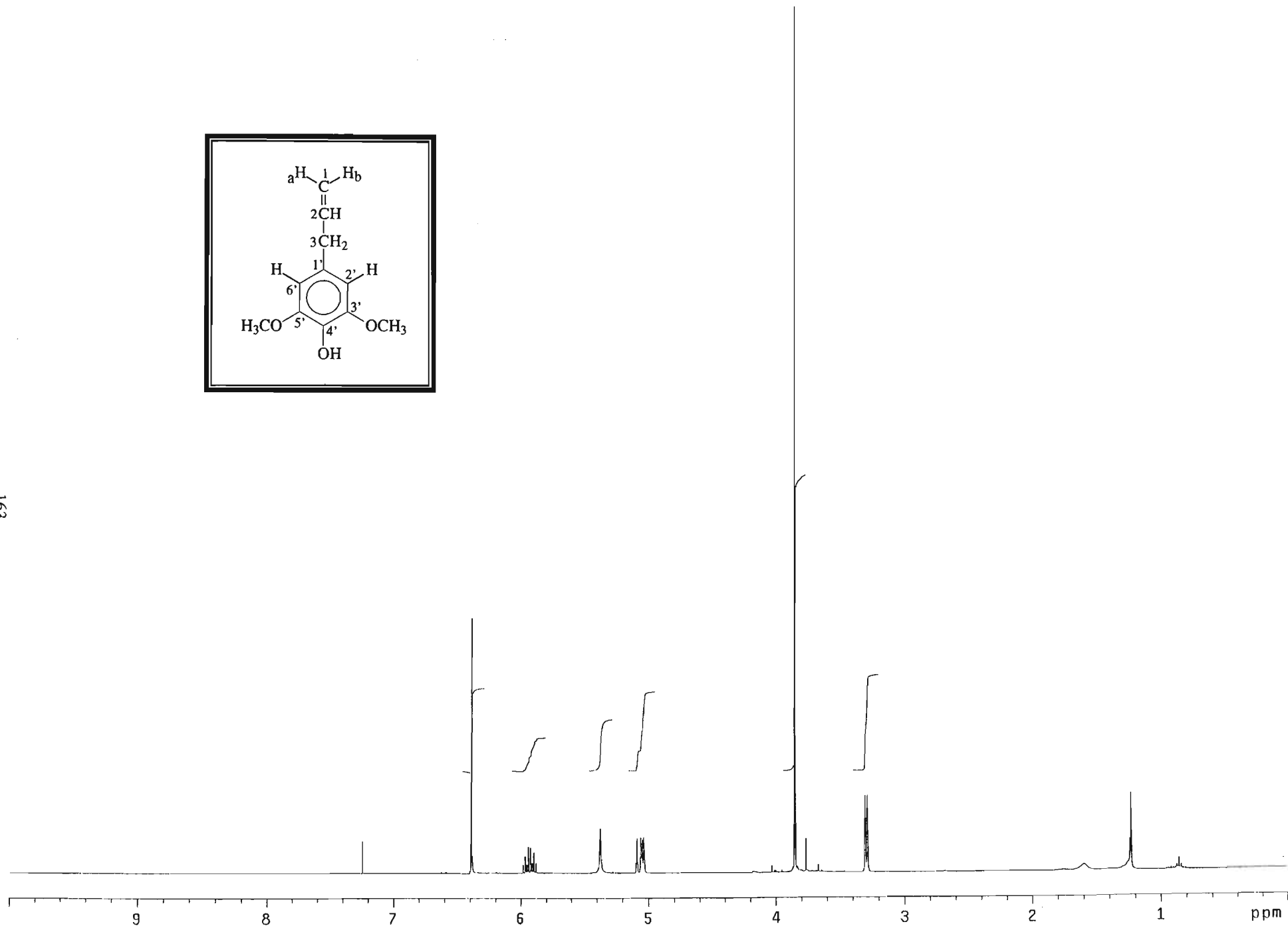
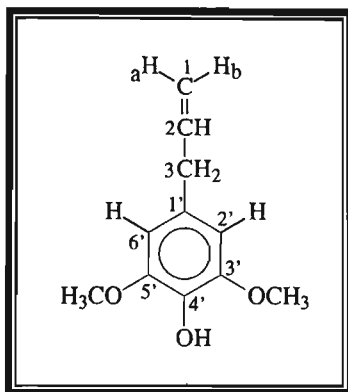
Spectrum 4.1 : Mass Spectrum of Compound 4, methoxyeugenol



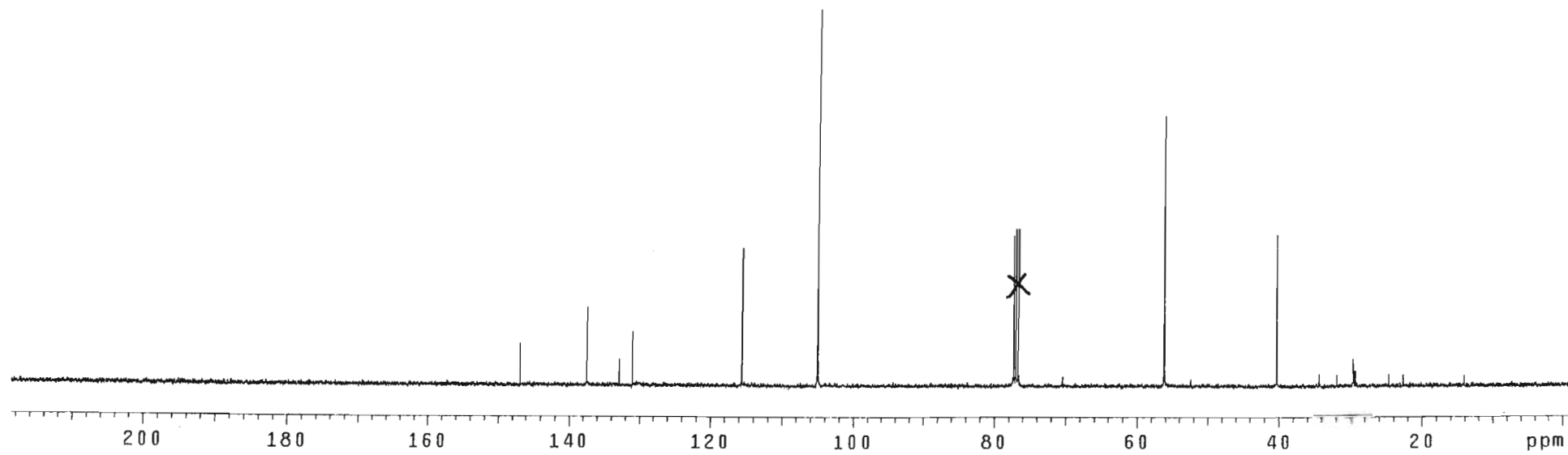
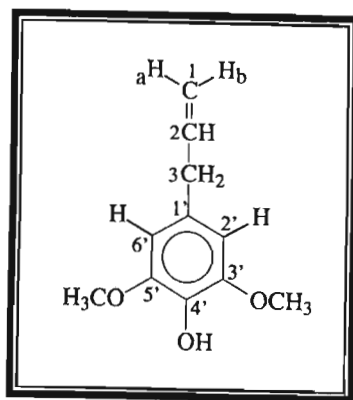
Spectrum 4.2 : Infrared Spectrum of Compound 4, methoxyeugenol



Spectrum 4.3 : UV Spectrum of Compound 4, methoxyeugenol



Spectrum 4.4 : ¹H NMR Spectrum of Compound 4, methoxyeugenol

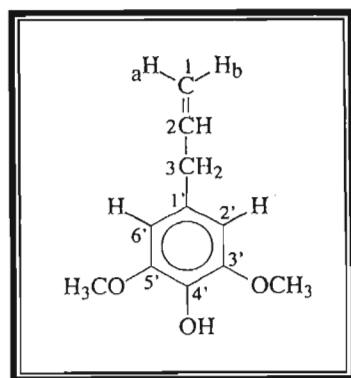


Spectrum 4.5 : ¹³C NMR Spectrum of Compound 4, methoxyeugenol

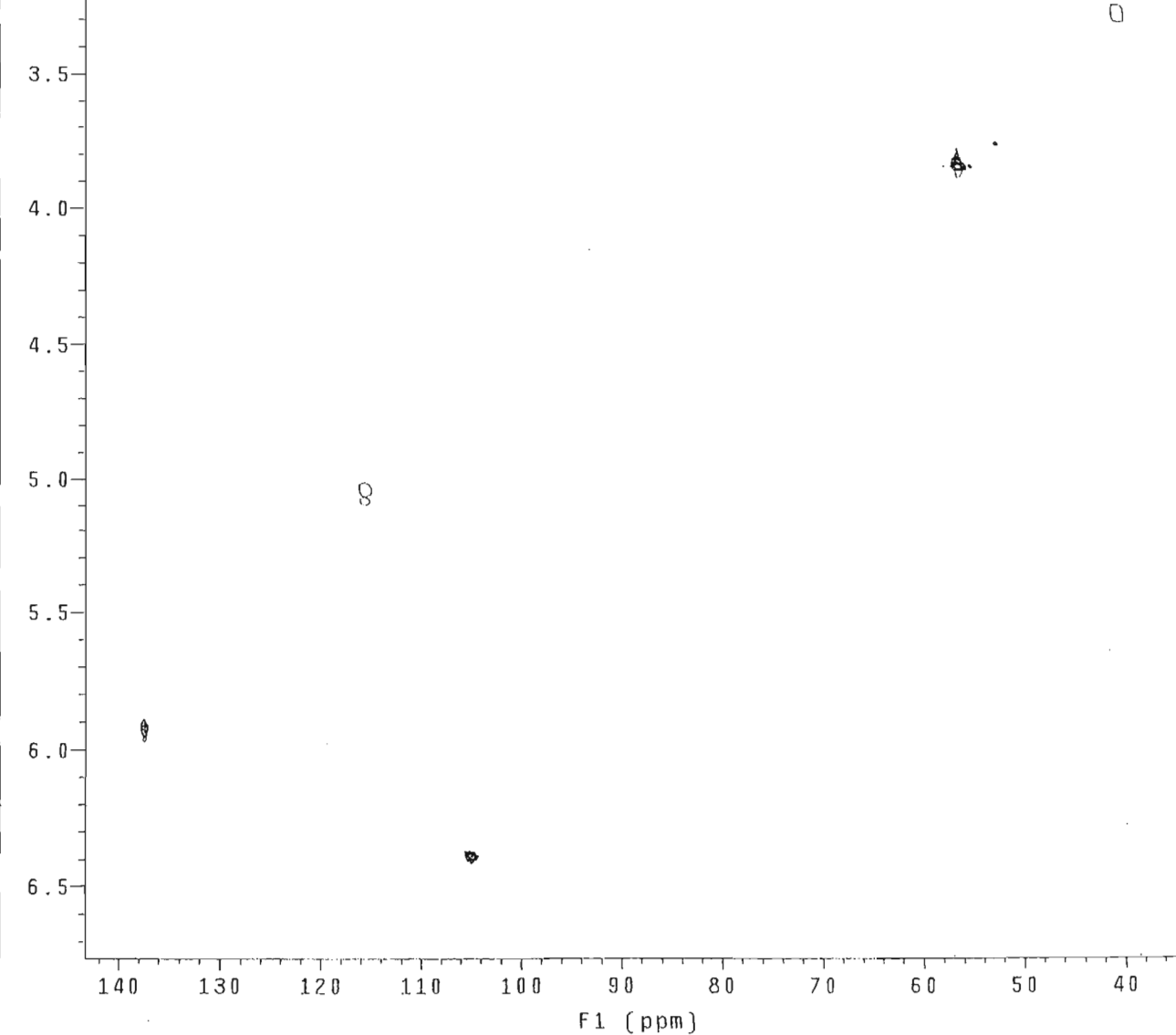
with mult.editing
probe=5mmASW

Pulse Sequence: ghsqc_da

165



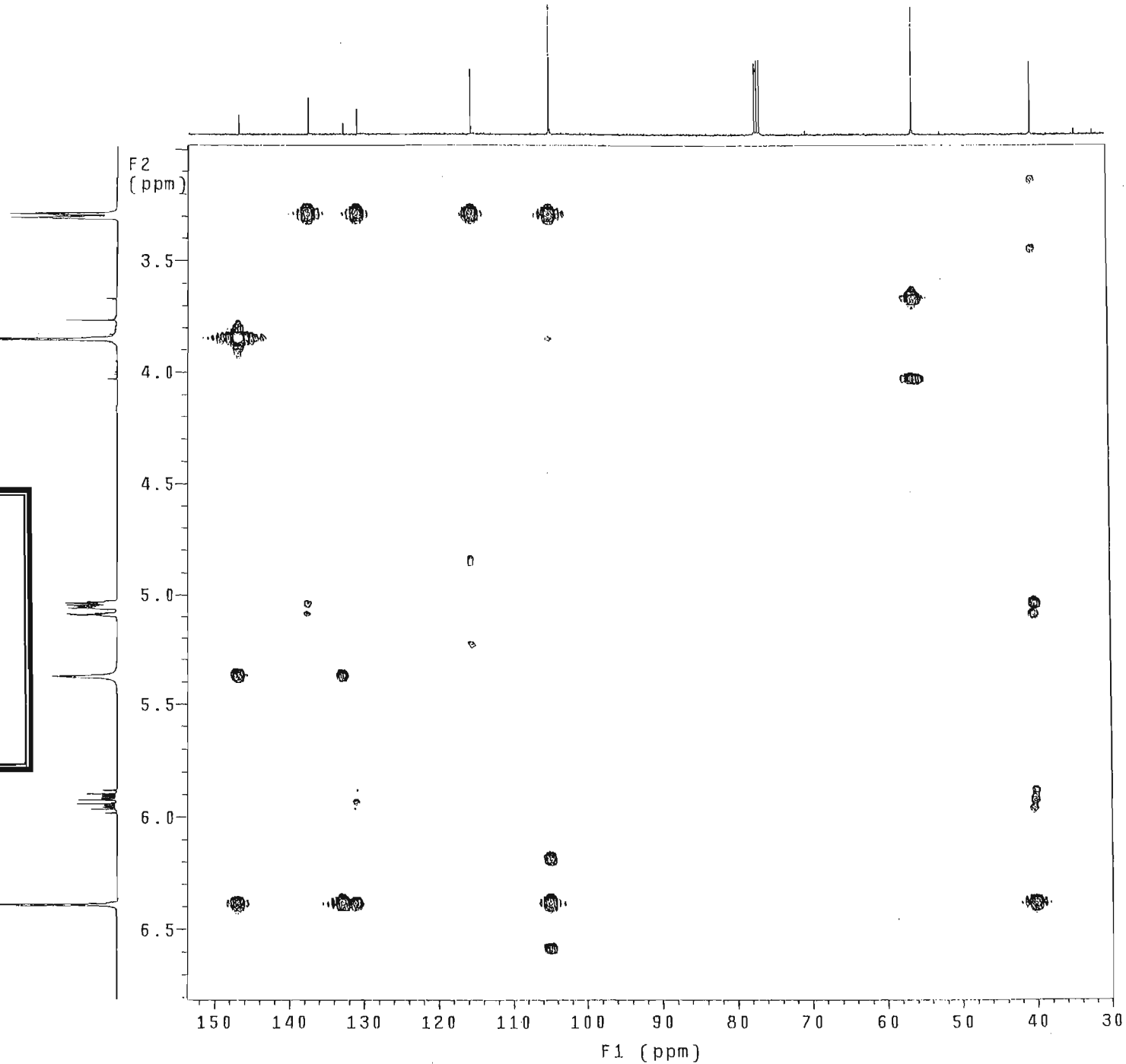
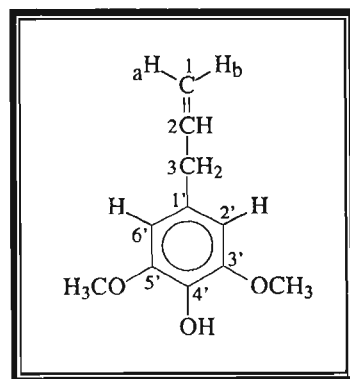
F2
(ppm)



Spectrum 4.6 : HSQC NMR Spectrum of Compound 4, methoxyeugenol

probe=5mmASW
Pulse Sequence: ghmqc_da

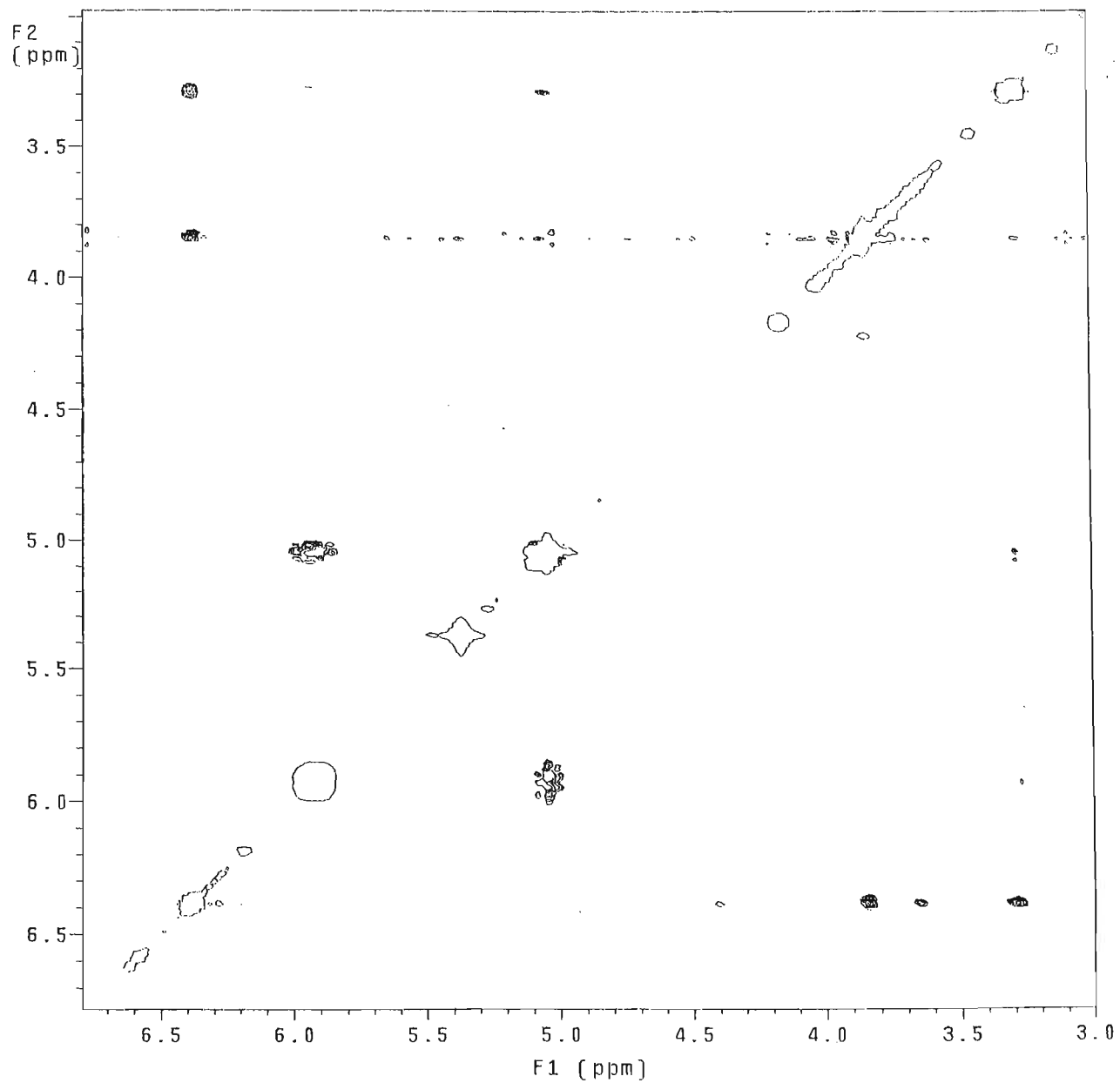
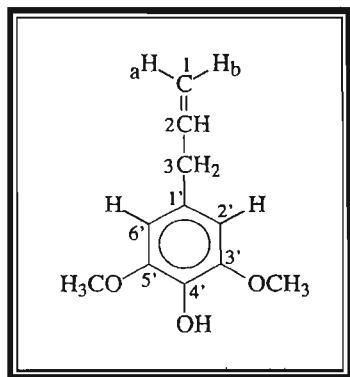
166



Spectrum 4.7 : HMBC NMR Spectrum of Compound 4, methoxyeugenol

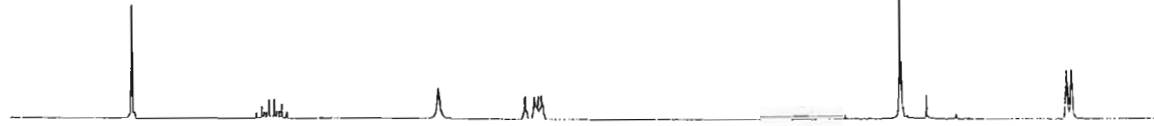
NOESY expt.
mix=1sec
probe=5mmASW
Pulse Sequence: noesy_da

167

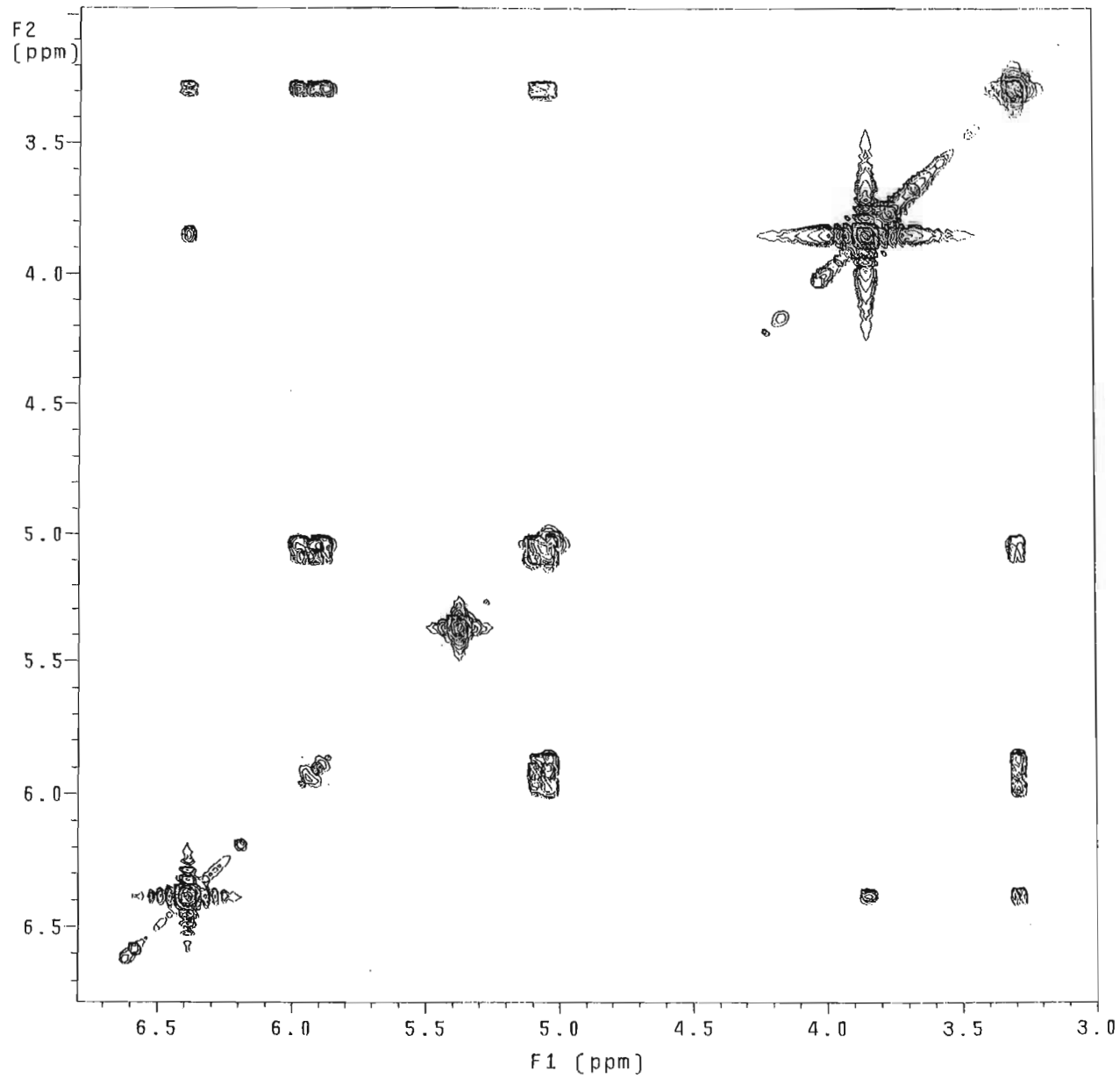
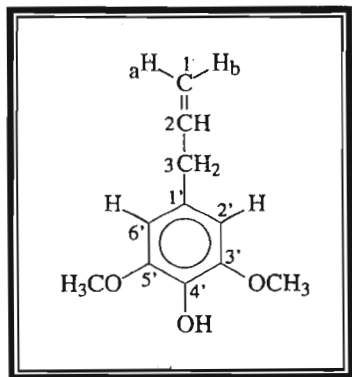


Spectrum 4.8 : NOESY NMR Spectrum of Compound 4, methoxyeugenol

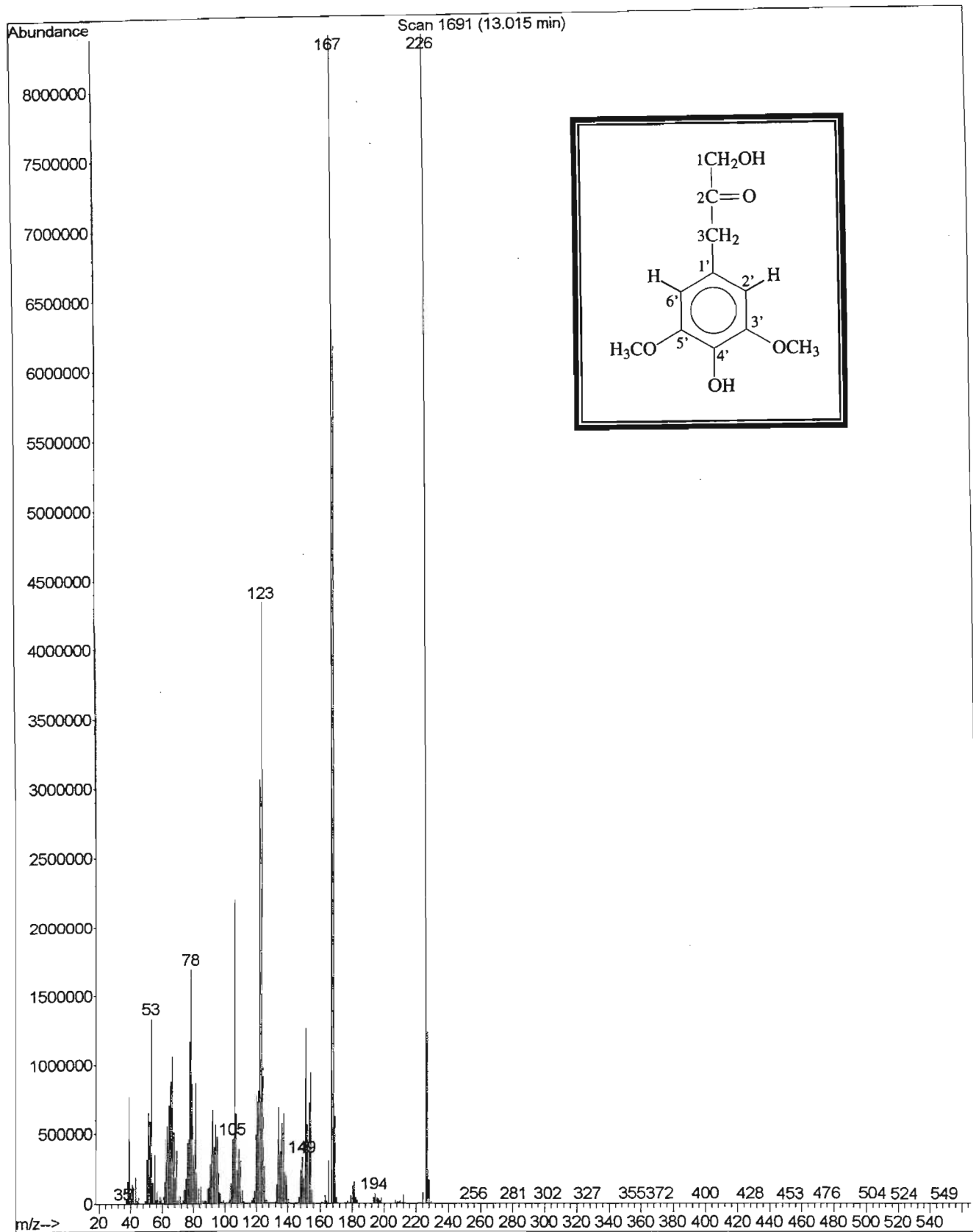
1H Cosy-90
probe=5mmASW
Pulse Sequence: relayh



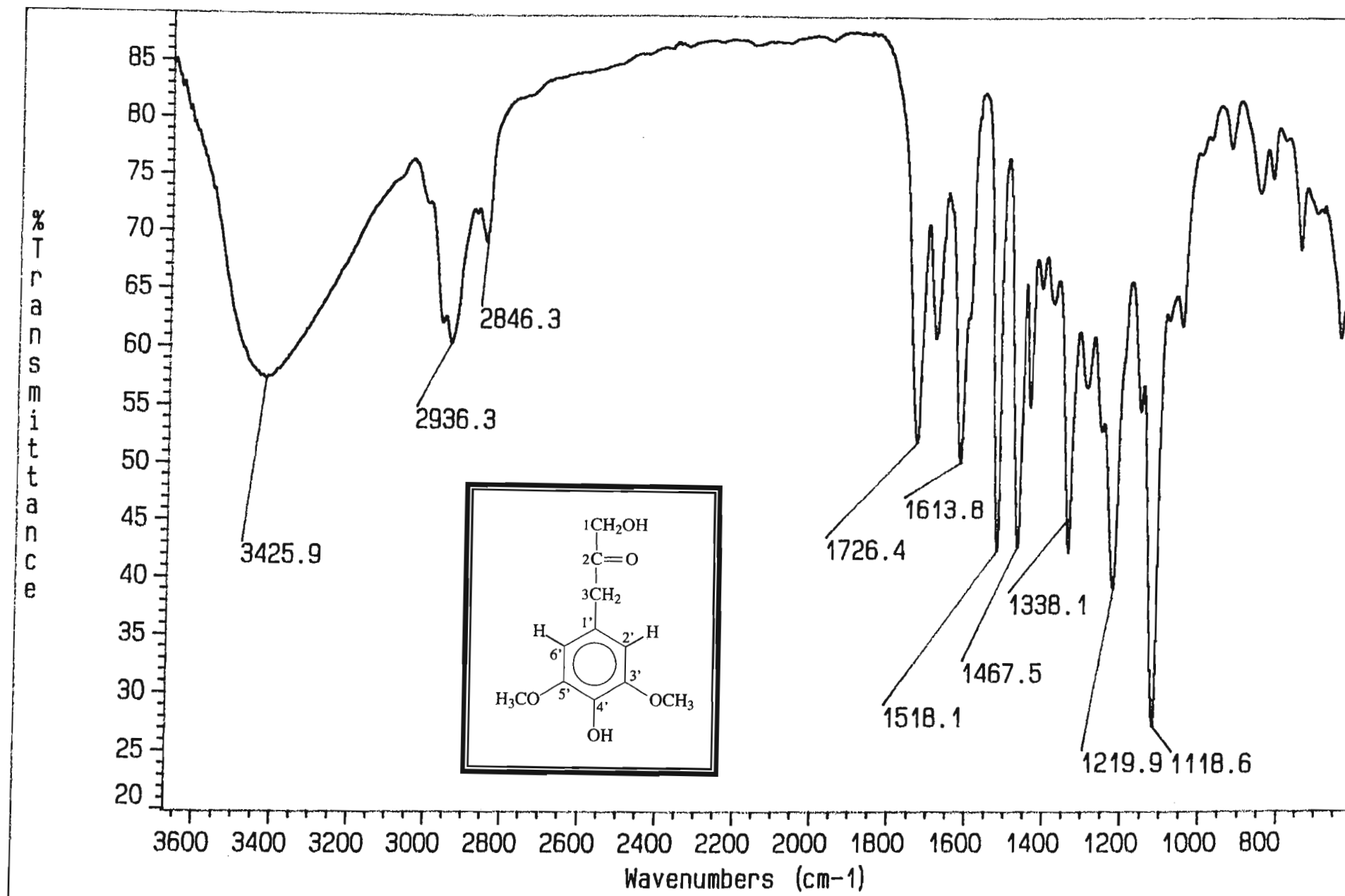
168



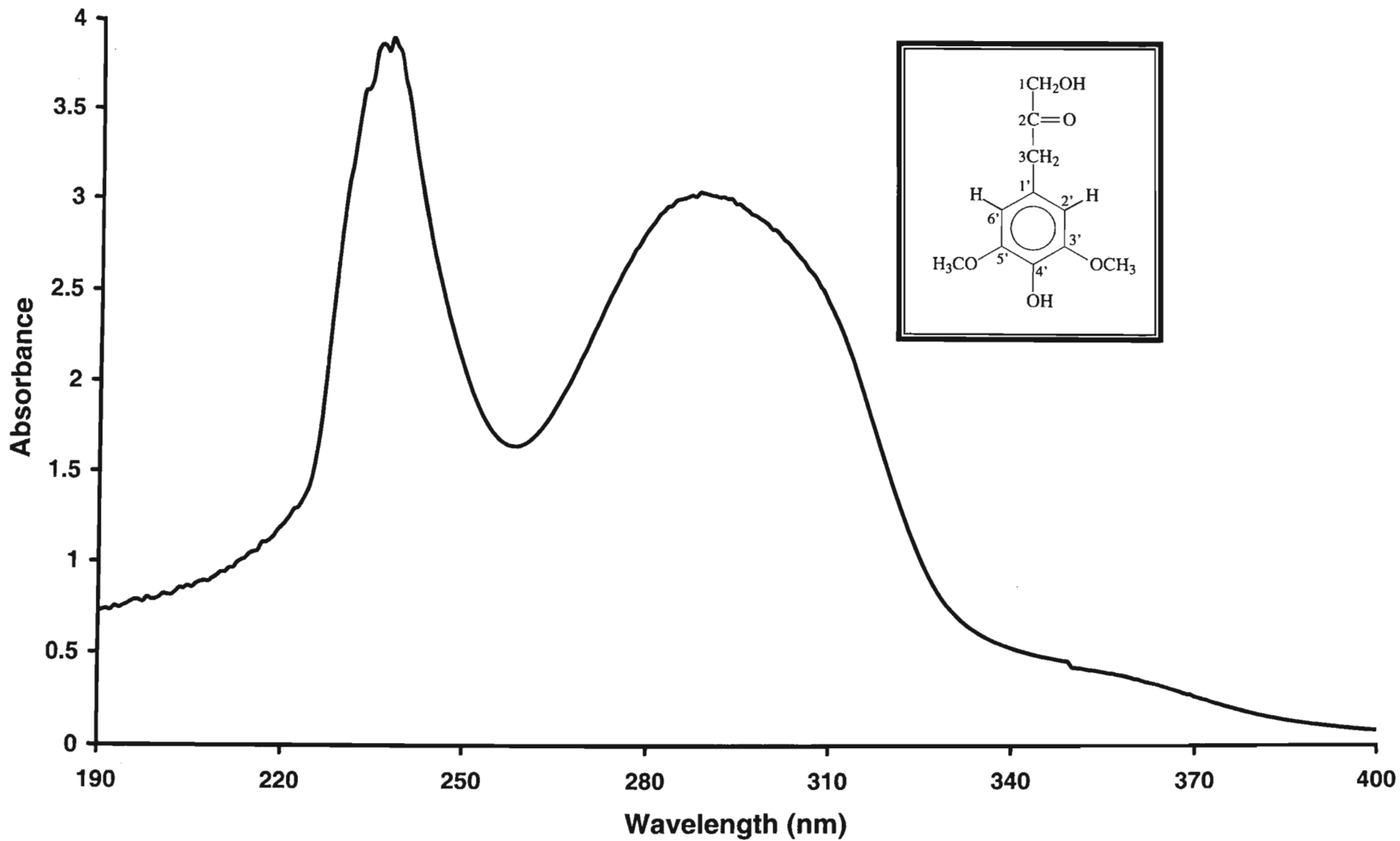
Spectrum 4.9 : COSY NMR Spectrum of Compound 4, methoxyeugenol

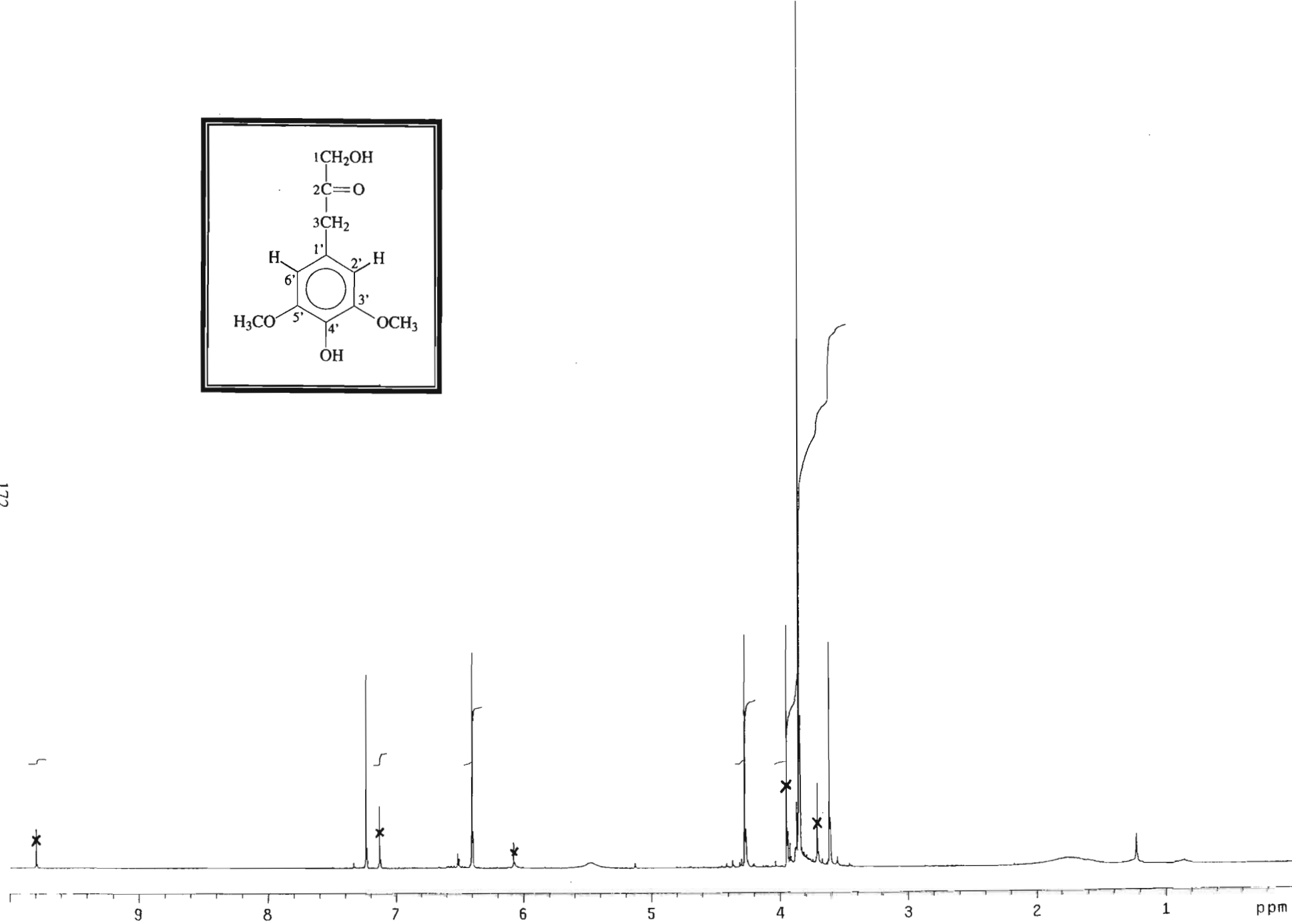
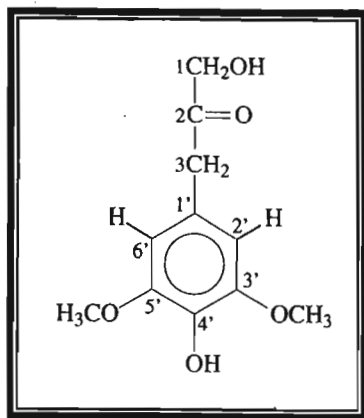


Spectrum 5.1 : Mass Spectrum of Compound 5, β -oxysinapyl alcohol

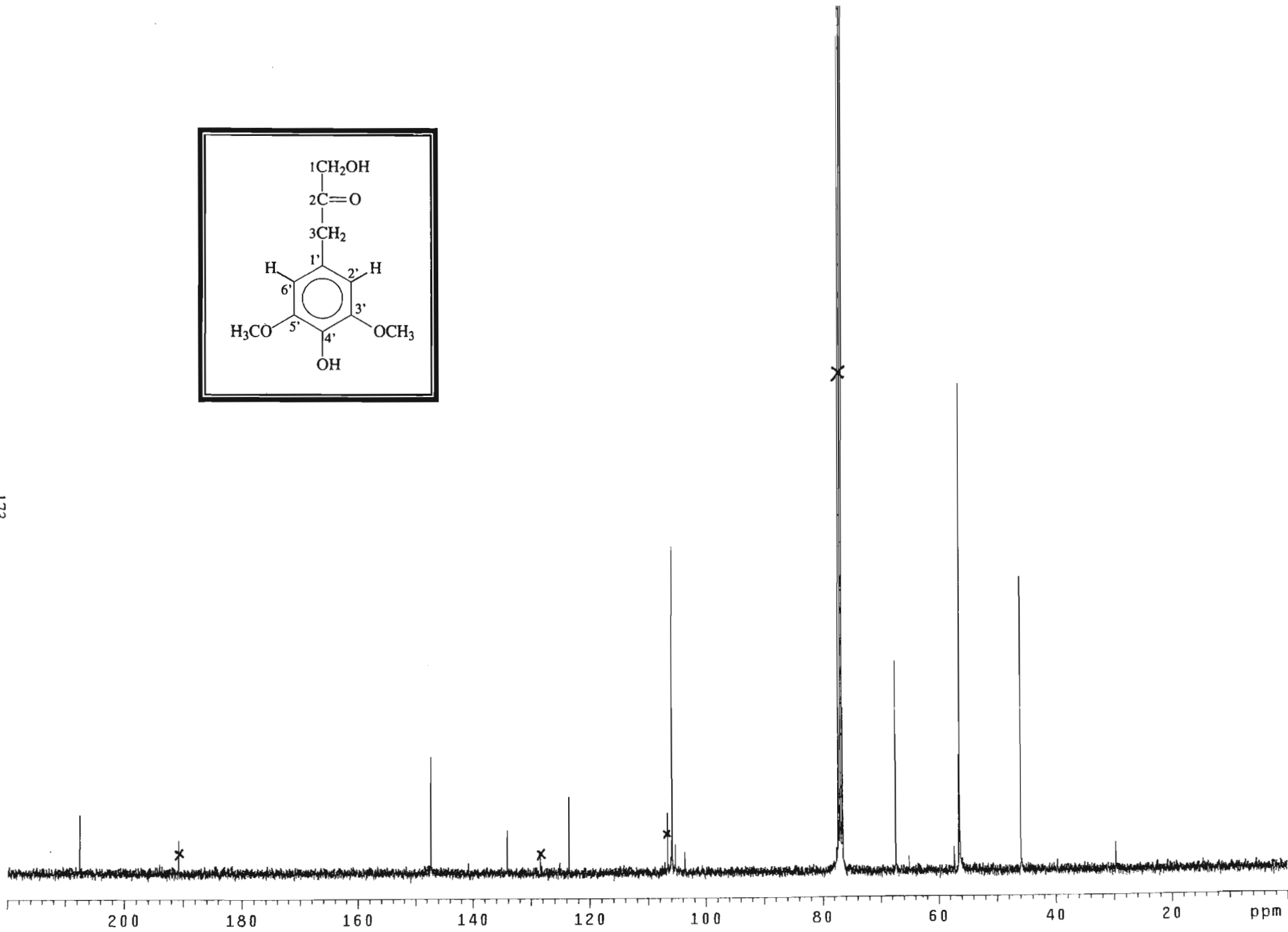
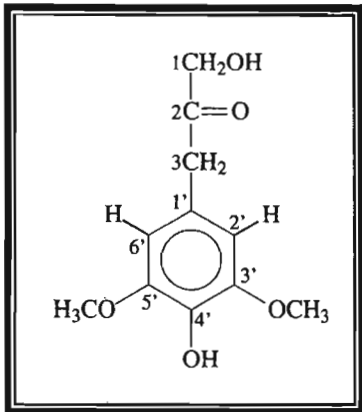


Spectrum 5.2 : Infrared Spectrum of Compound 5, β -oxysinapyl alcohol

Spectrum 5.3 : UV Spectrum of Compound 5, β -oxysinapyl alcohol



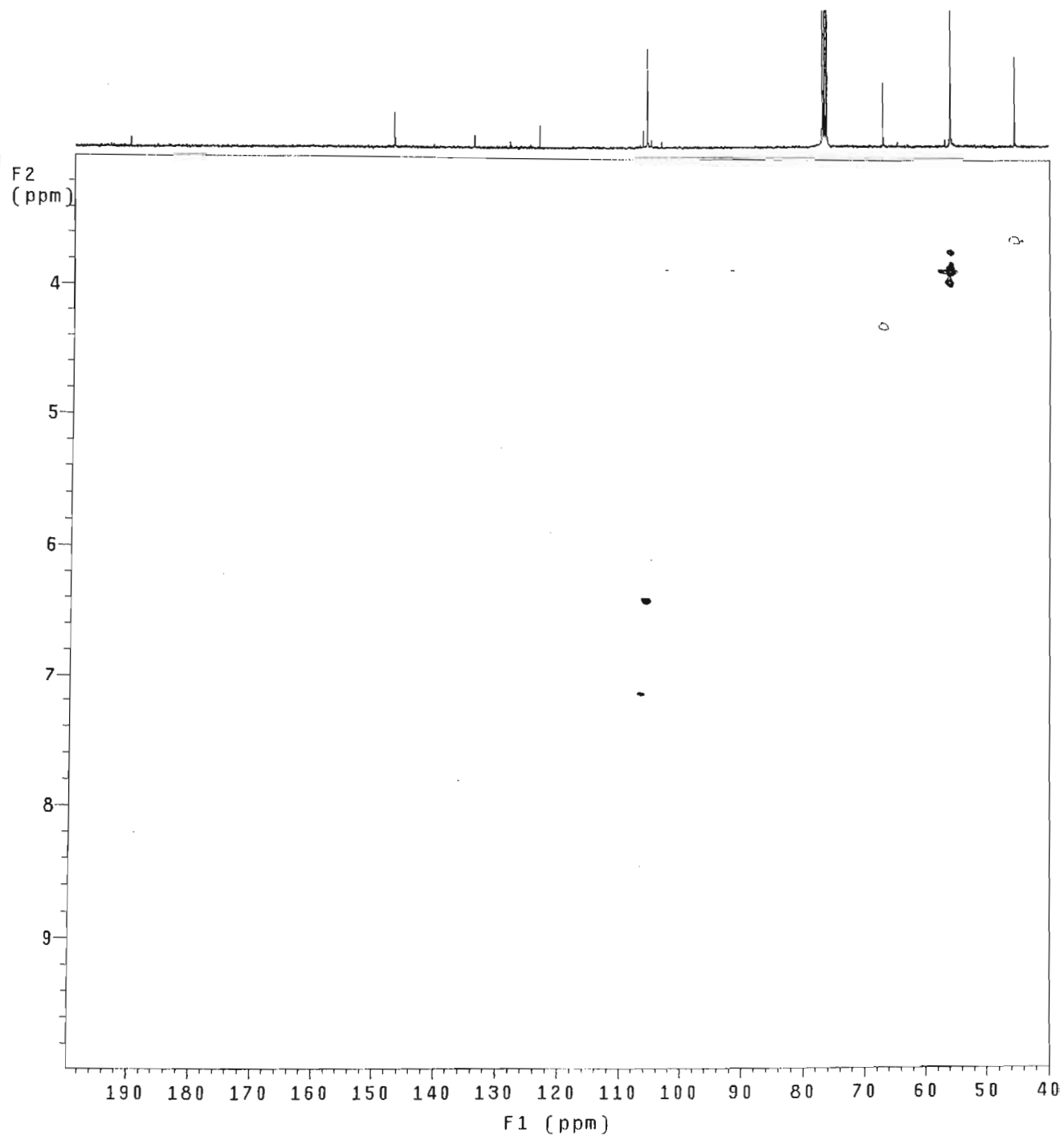
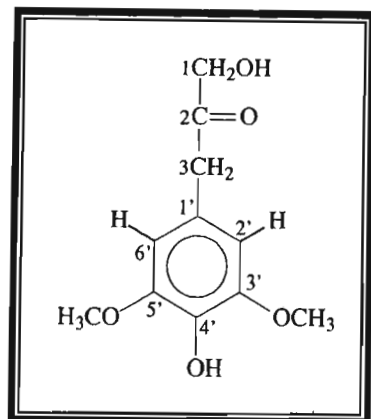
Spectrum 5.4 : ^1H NMR Spectrum of Compound 5, β -oxysinapyl alcohol



Spectrum 5.5 : ¹³C NMR Spectrum of Compound 5, β-oxy sinapyl alcohol

Gradient HSQC expt.
with mult. editing
probe=5mmASW
Pulse Sequence: ghsqc_da

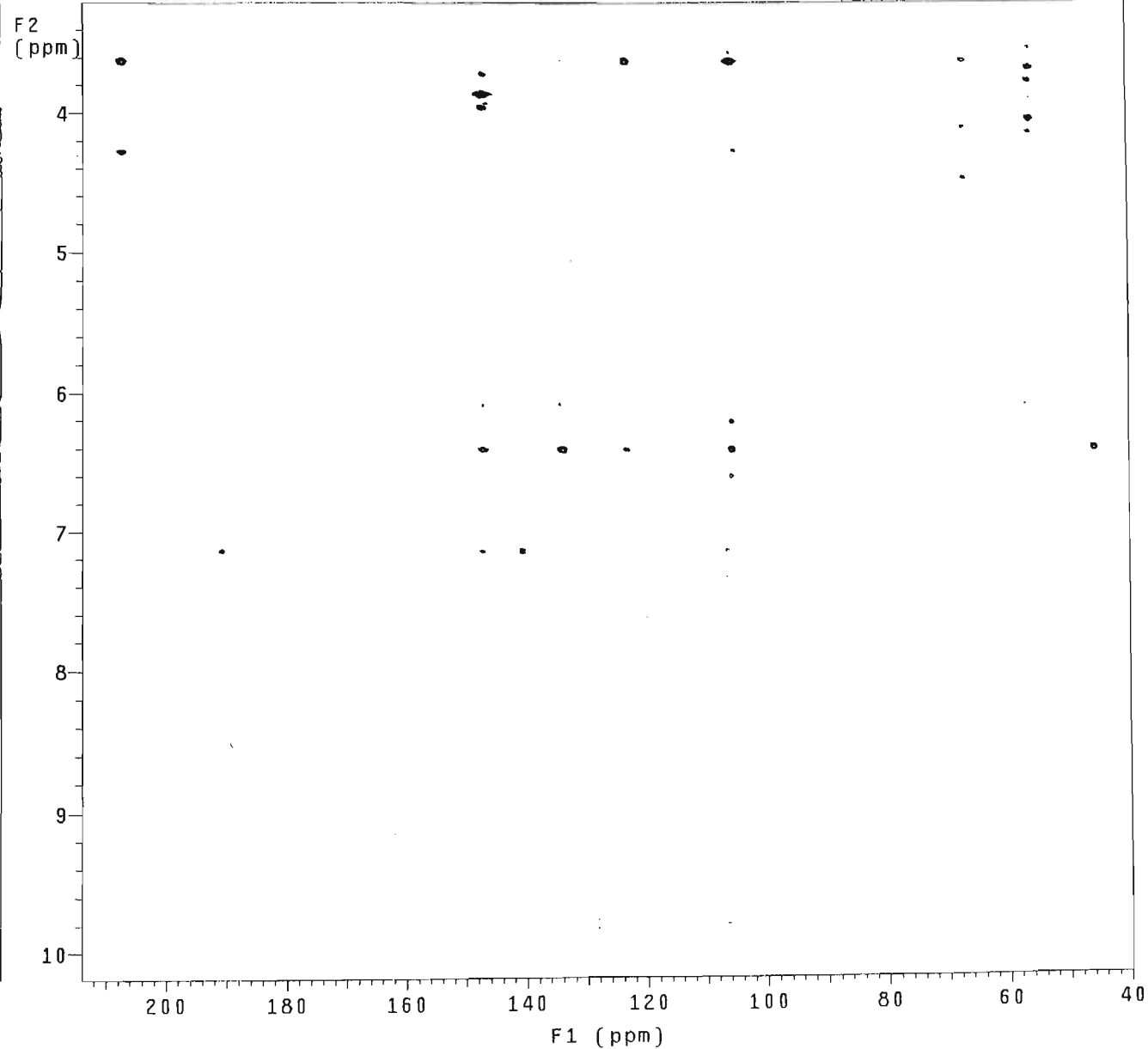
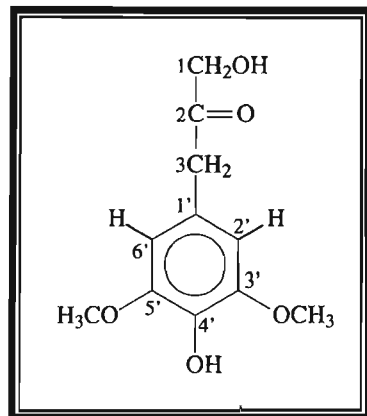
174



Spectrum 5.6 : HSQC NMR Spectrum of Compound 5, β -oxysinapyl alcohol

Gradient HMBC expt.
probe=5mmASW
Pulse Sequence: ghmqc_da

175

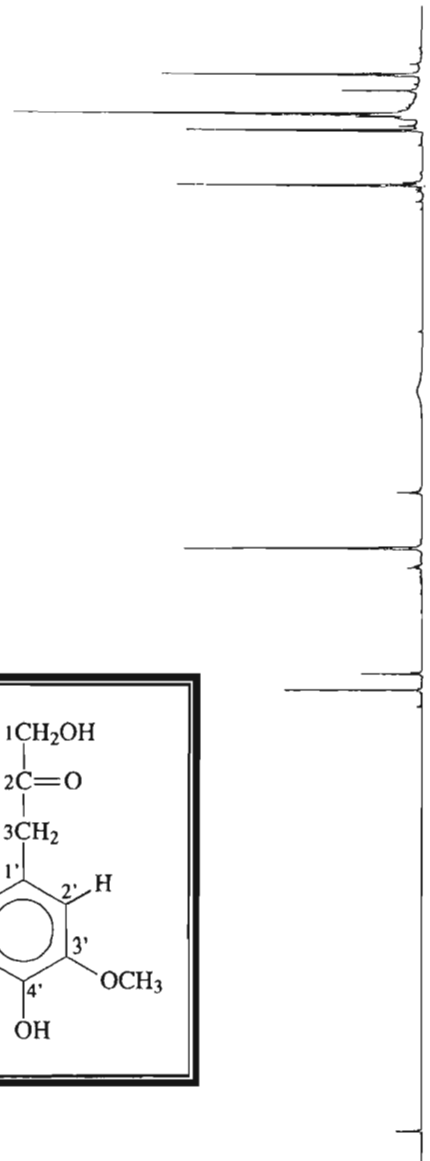
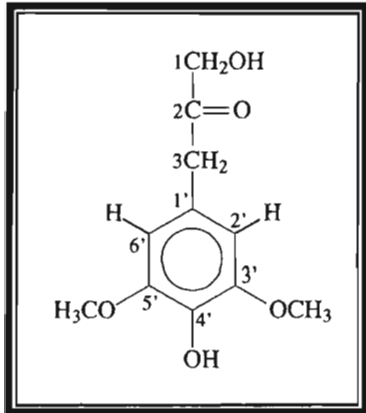


Spectrum 5.7 : HMBC NMR Spectrum of Compound 5, β -oxy sinapyl alcohol

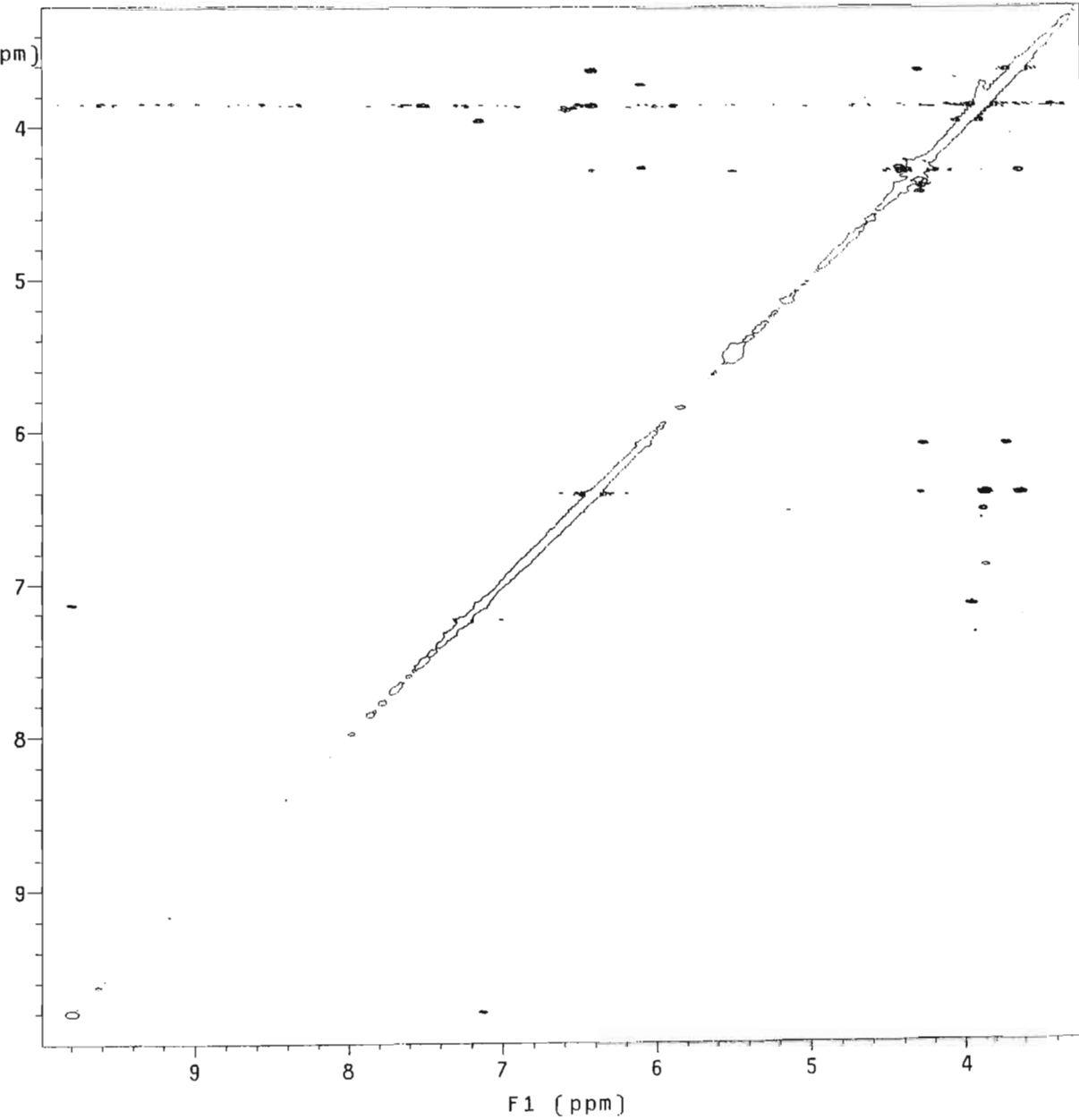
noesy1 exp1.
mix=1sec
probe=5mmASW

Pulse Sequence: noesy_da

176



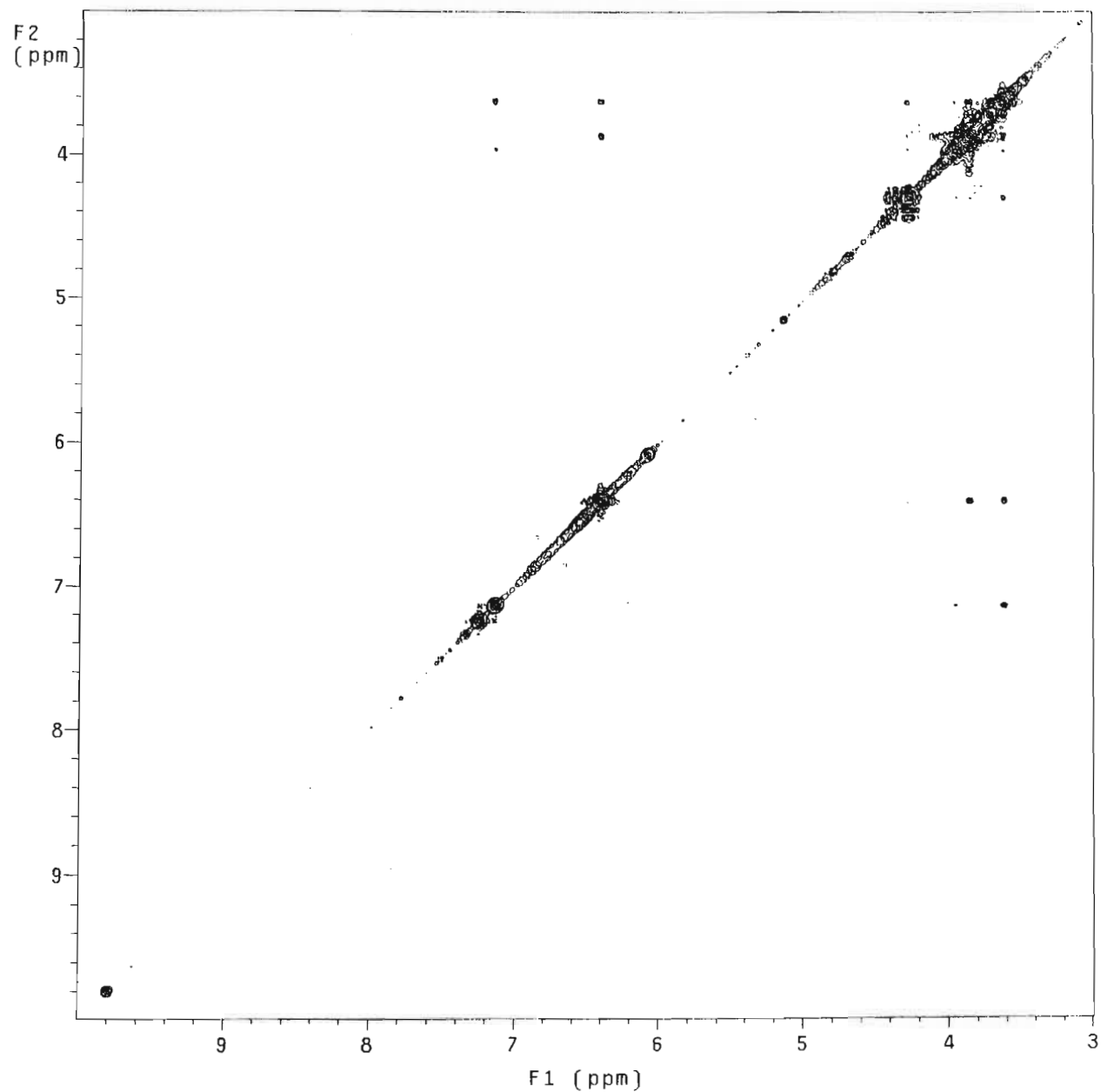
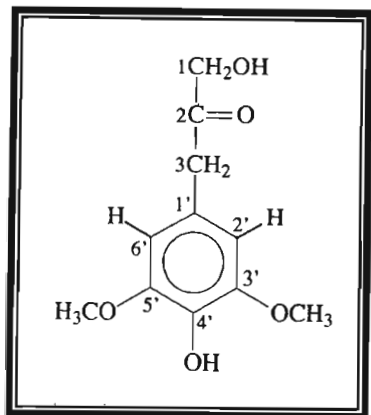
F2
(ppm)



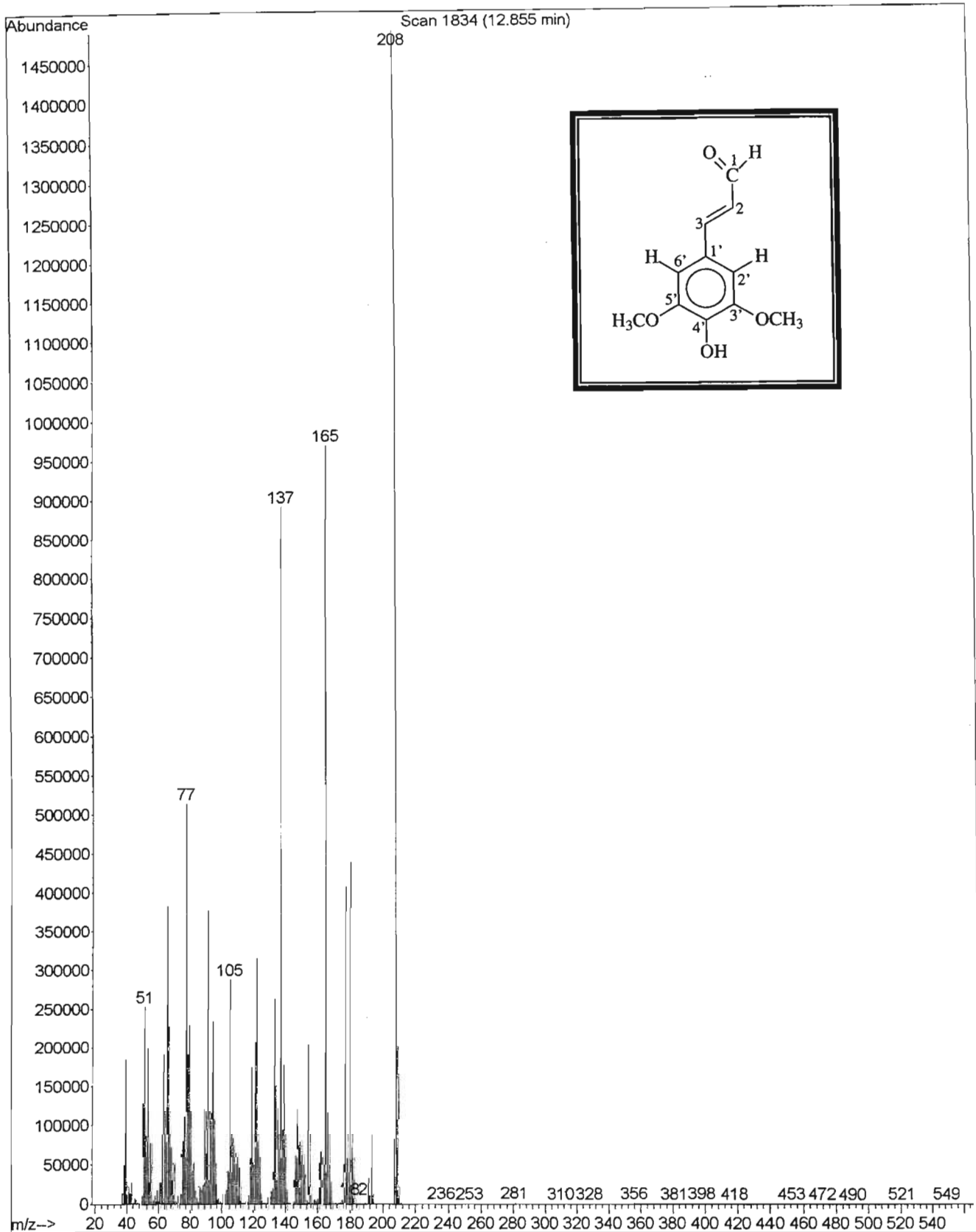
Spectrum 5.8 : NOESY NMR Spectrum of Compound 5, β -oxysinapyl alcohol

1H Cosy-90
probe=5mmASW
Pulse Sequence: relayh

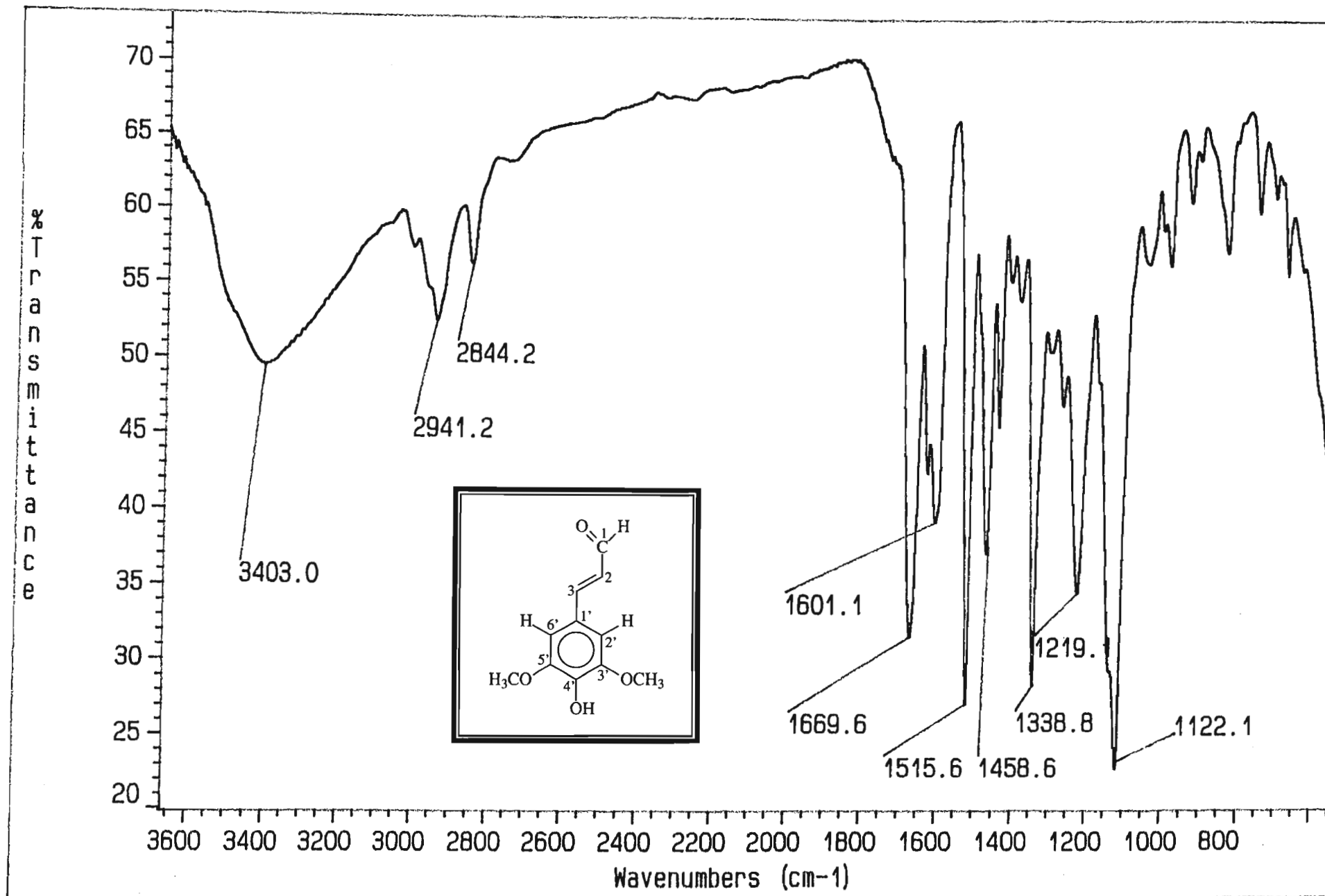
177



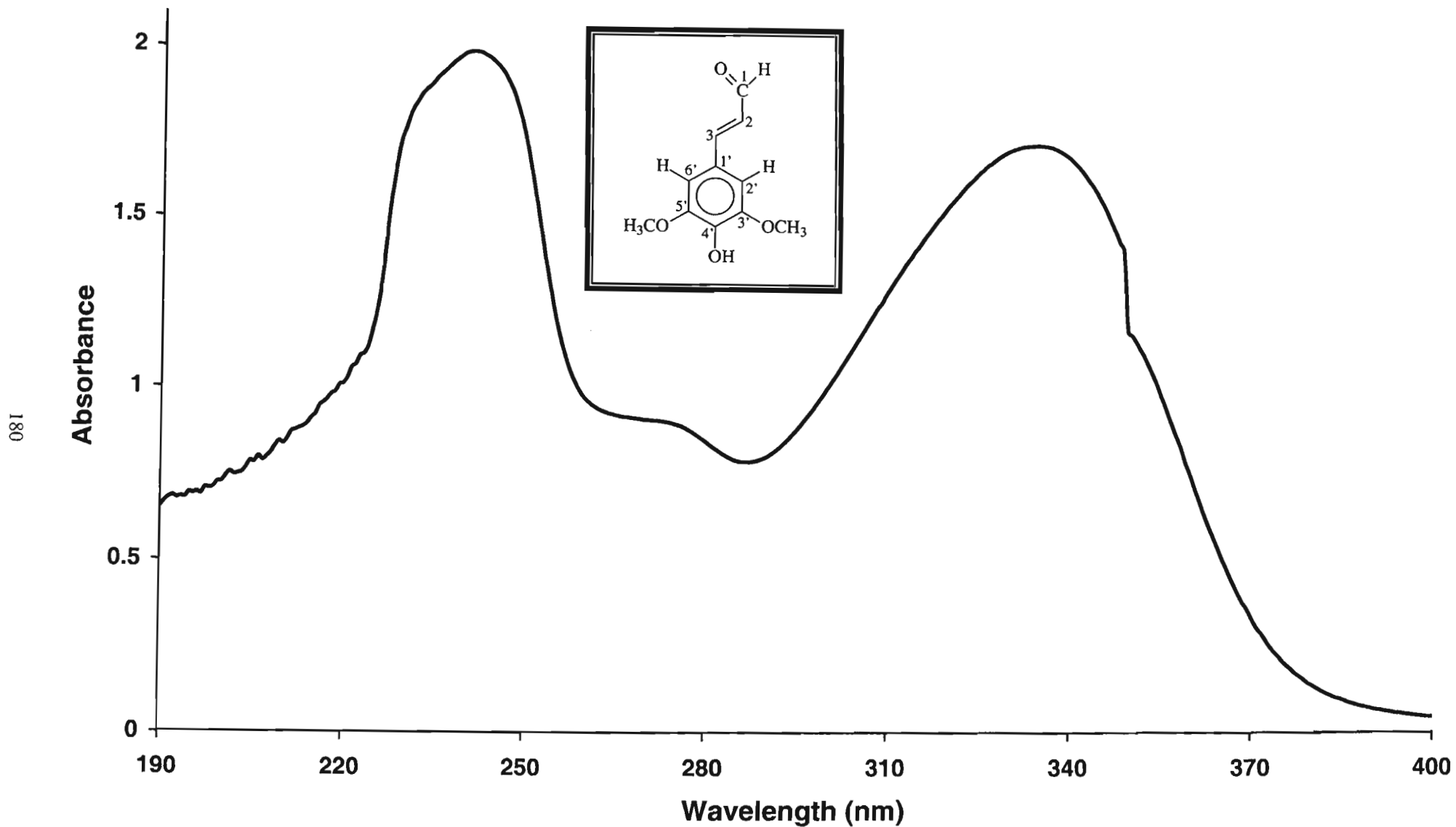
Spectrum 5.9 : COSY NMR Spectrum of Compound 5, β -oxysinapyl alcohol



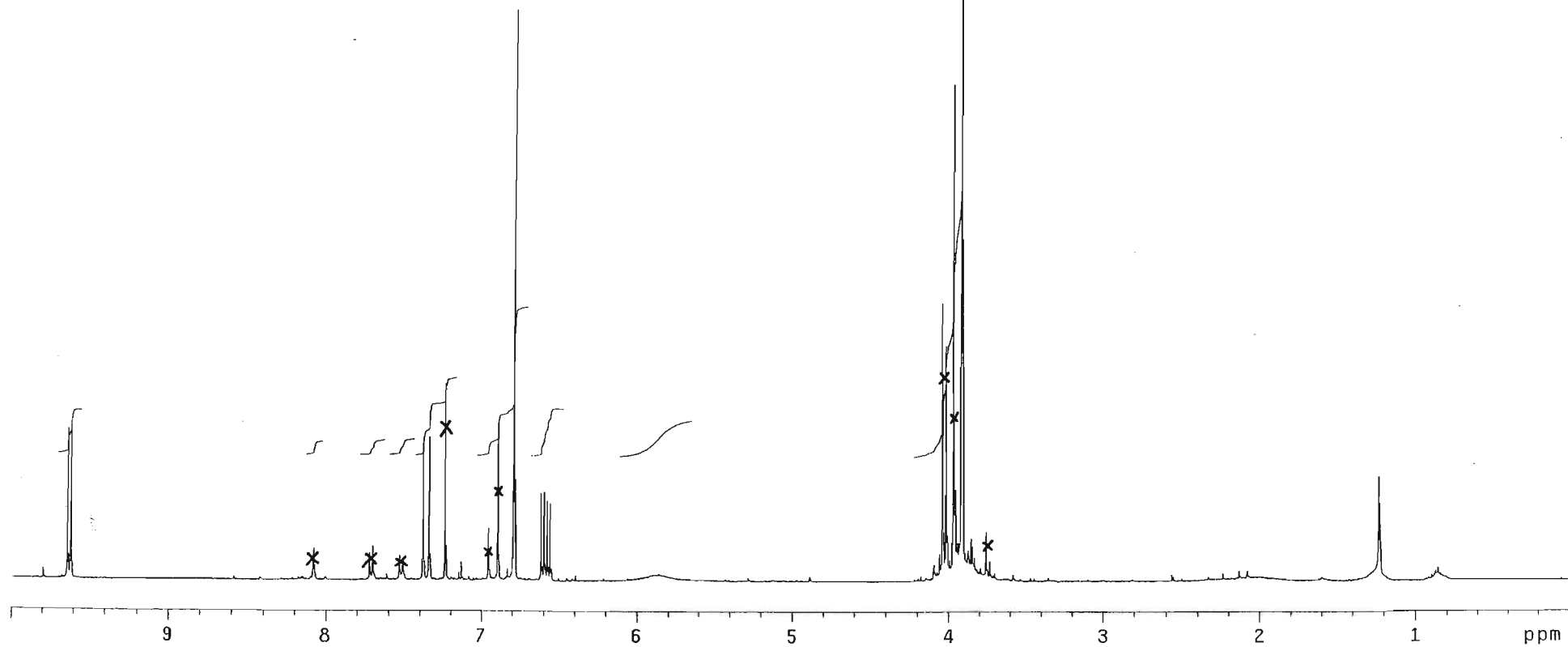
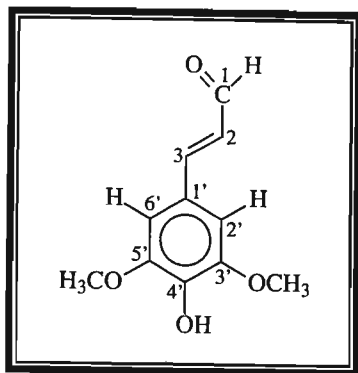
Spectrum 6.1 : Mass Spectrum of Compound 6, sinapyl aldehyde



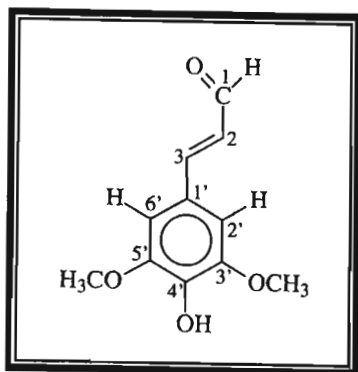
Spectrum 6.2 : Infrared Spectrum of Compound 6, sinapyl aldehyde



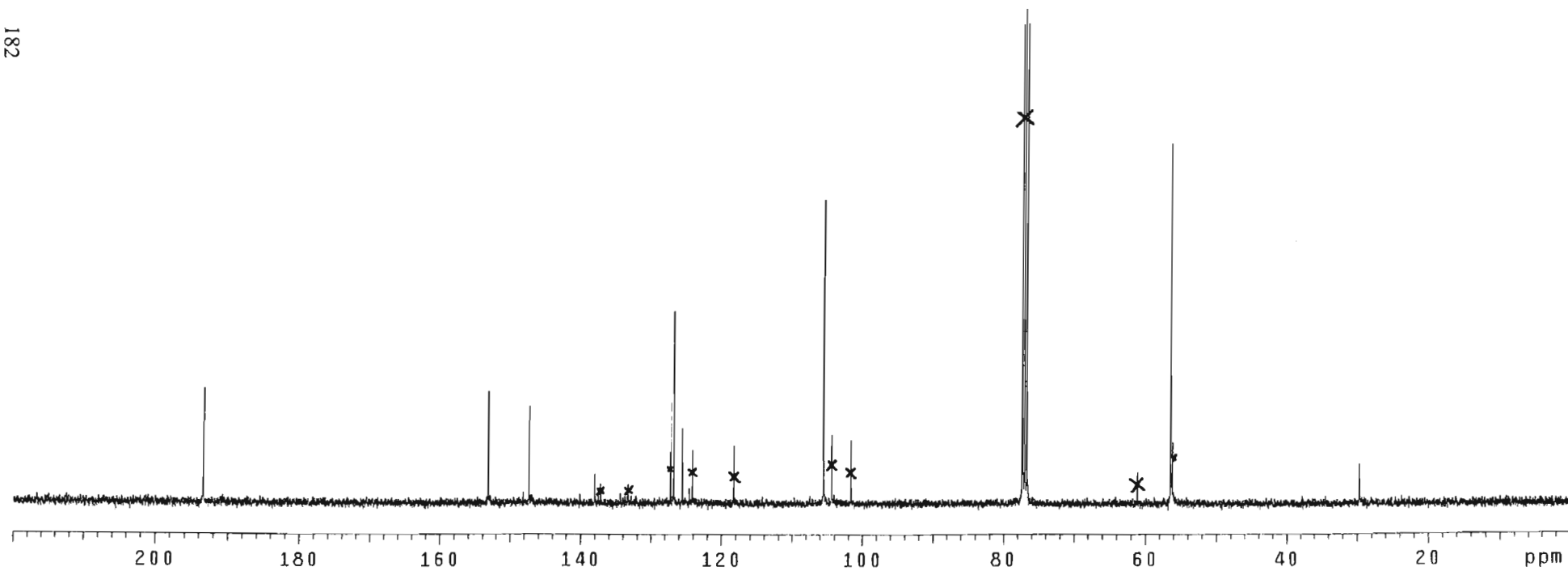
Spectrum 6.3 : UV Spectrum of Compound 6, sinapyl aldehyde



Spectrum 6.4 : ^1H NMR Spectrum of Compound 6, sinapyl aldehyde



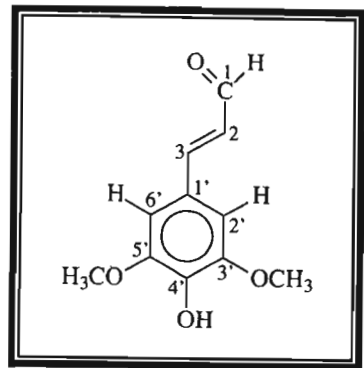
182



Spectrum 6.5 : ¹³C NMR Spectrum of Compound 6, sinapyl aldehyde

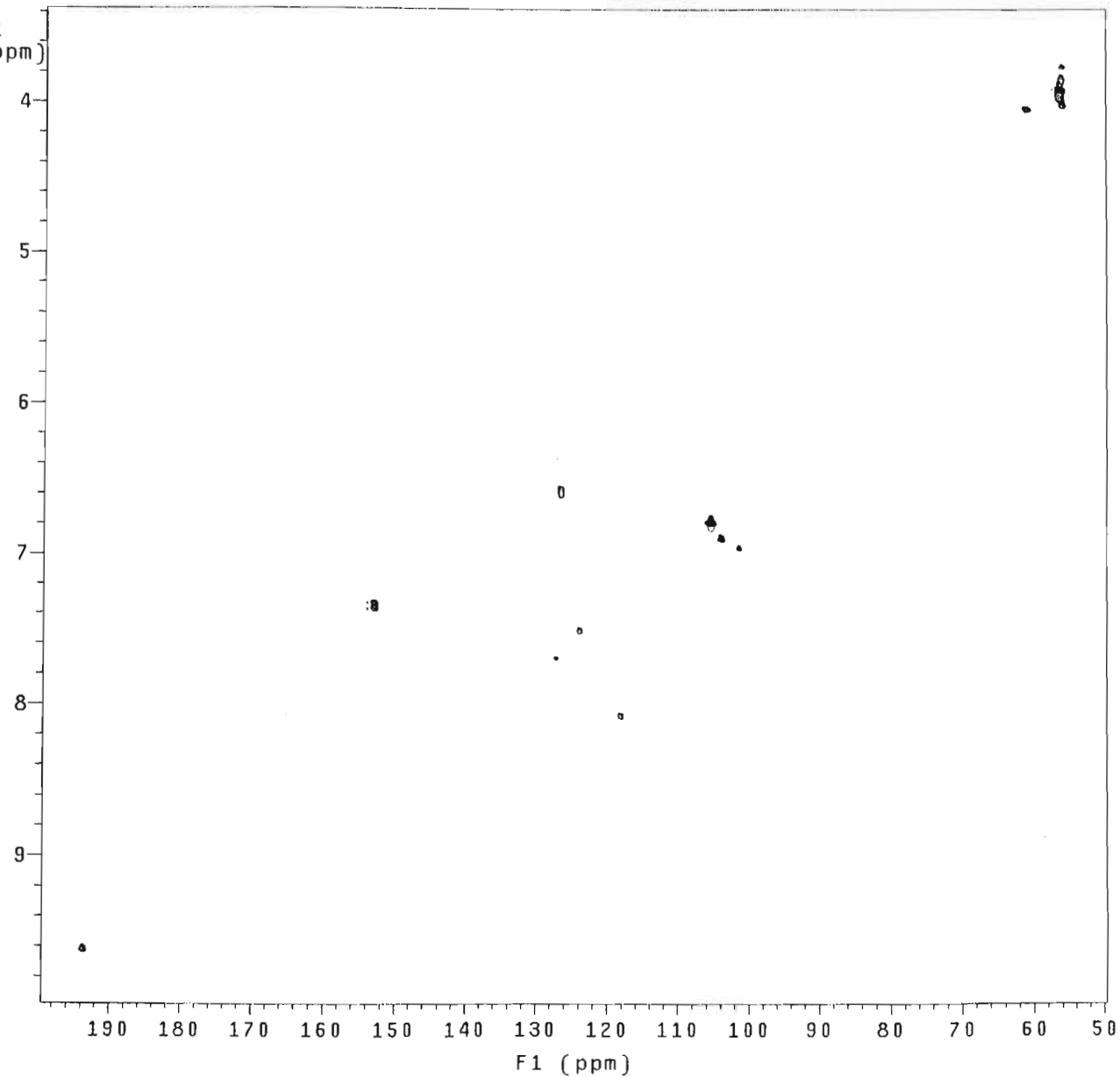
Gradient HSQC expt.
with mult.editing
probe=5mmASW

Pulse Sequence: ghsqc_da



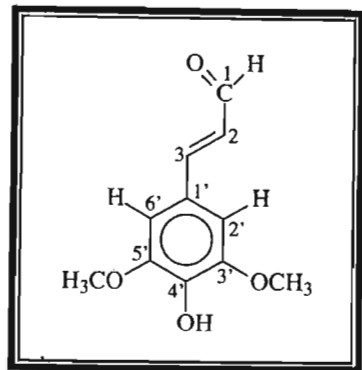
183

F2
(ppm)

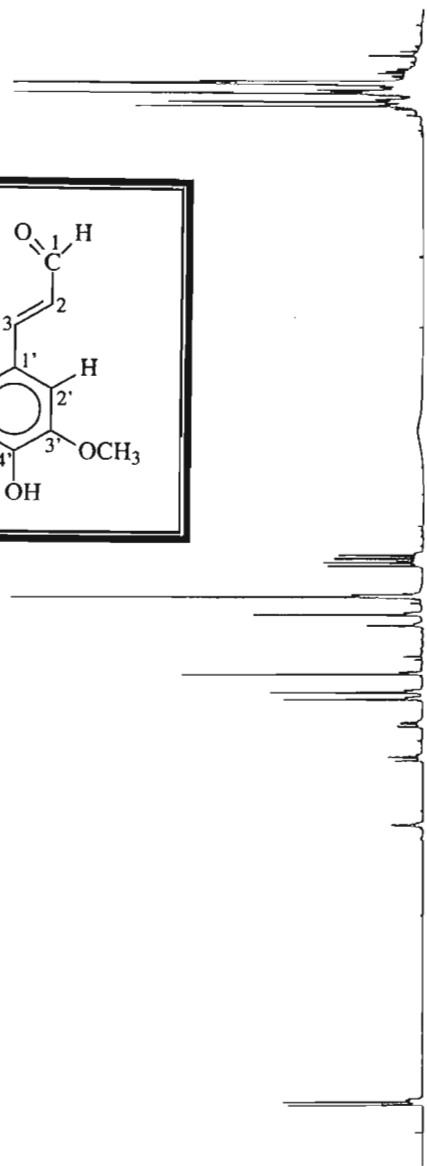


Spectrum 6.6 : HSQC NMR Spectrum of Compound 6. sinanvl aldehyde

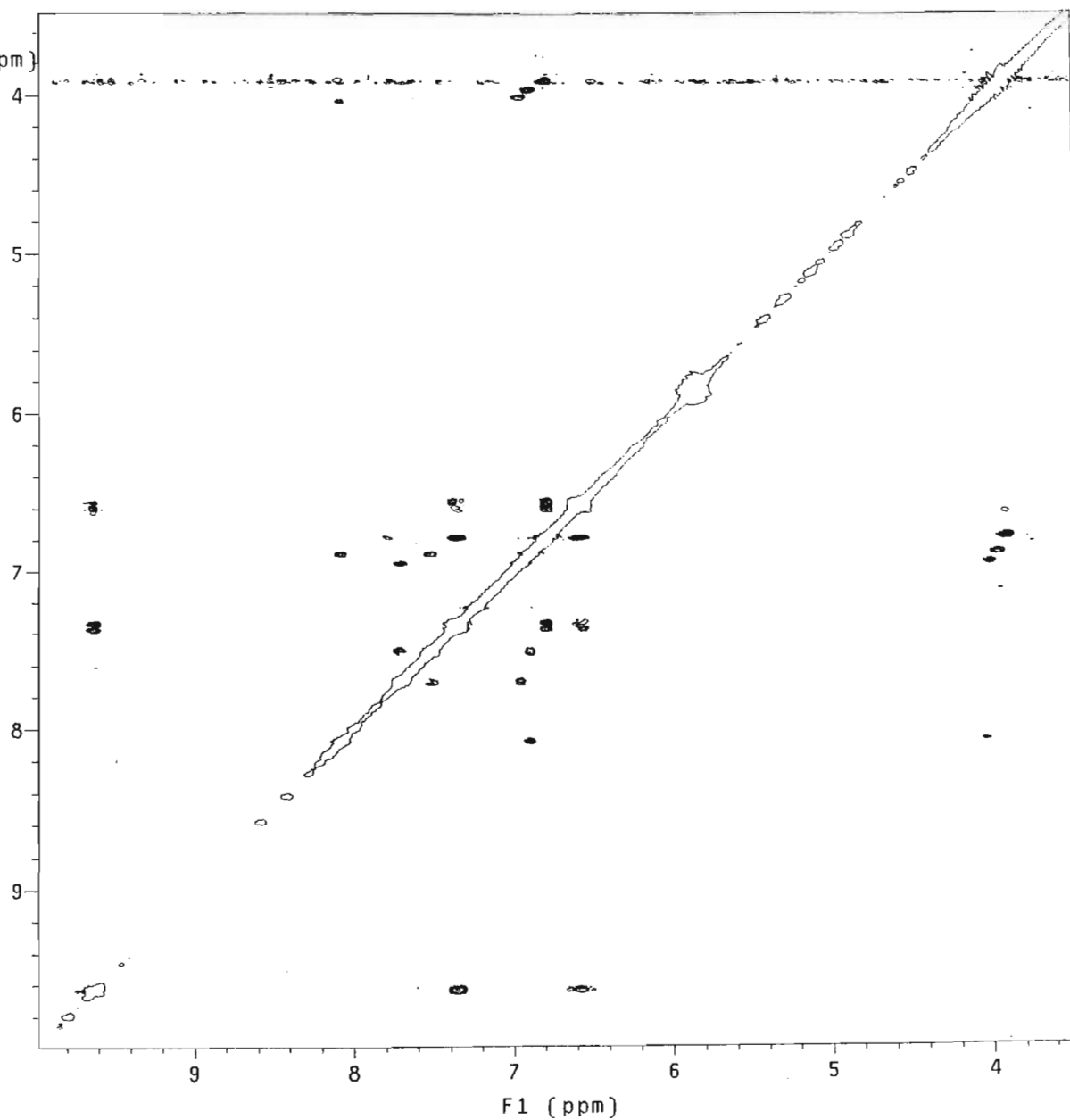
NOCPD1:compound_1 in cdcl3
NOESY expt.
mix=1sec
probe=5mmASW
Pulse Sequence: noesy_da



185

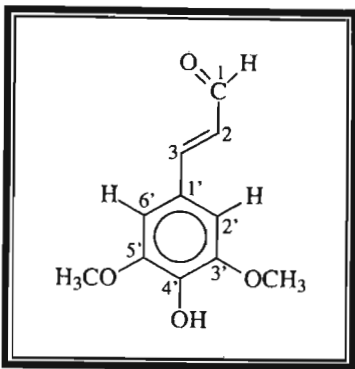


F2
(ppm)



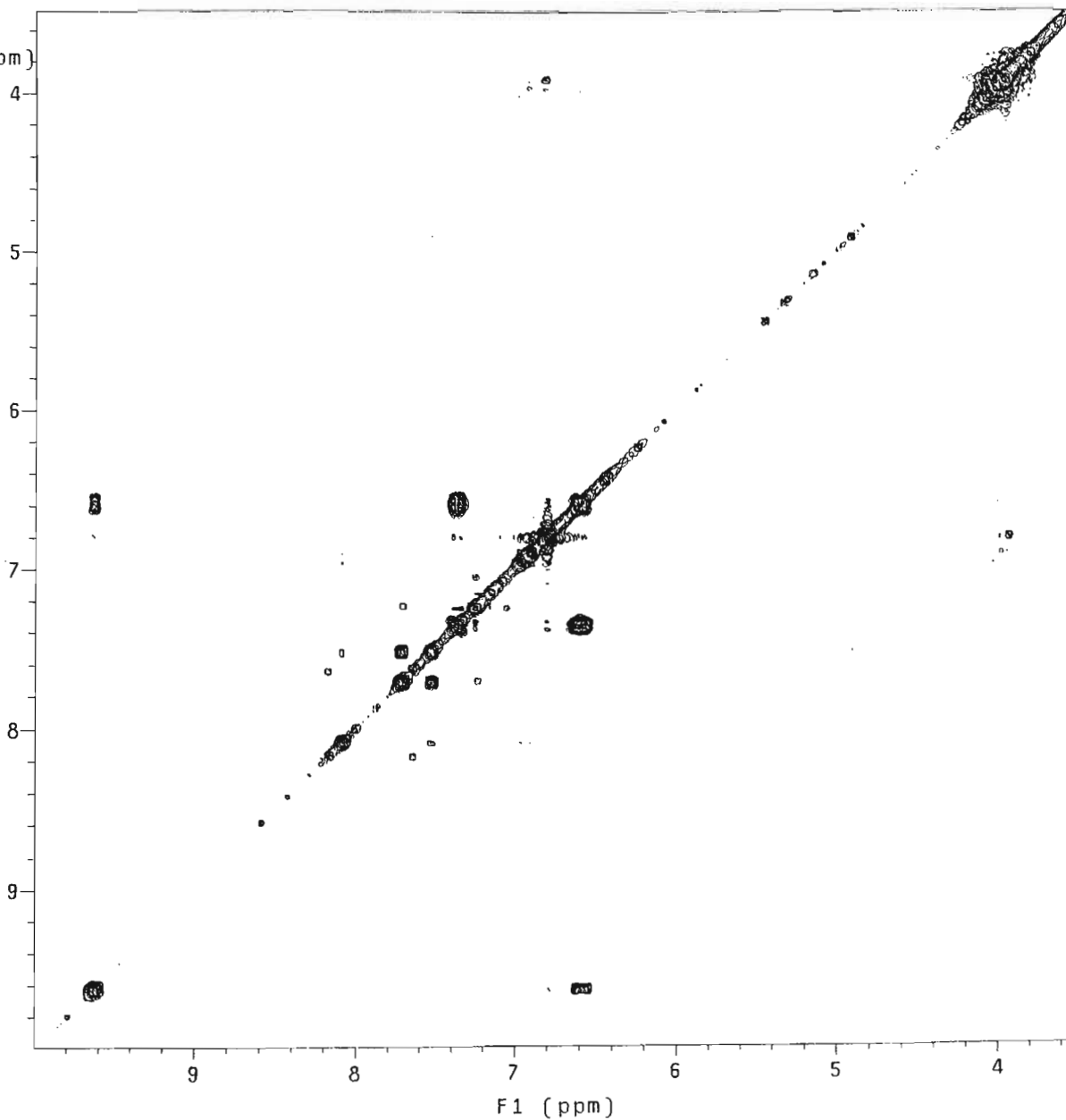
Spectrum 6.8 : NOESY NMR Spectrum of Compound 6. sinanvl aldehyde

¹H Cosy-90
probe=5mmASW
Pulse Sequence: relayh

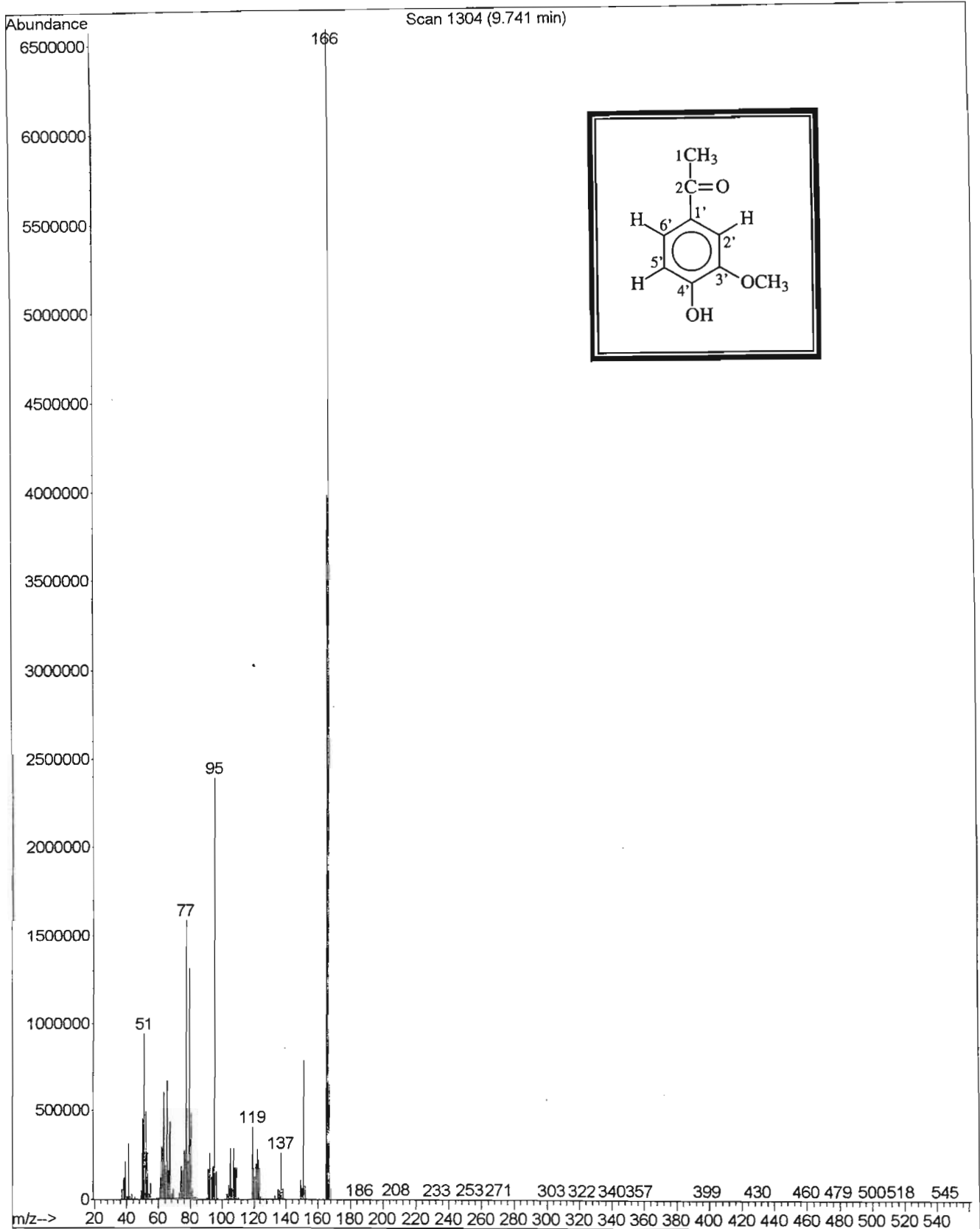


186

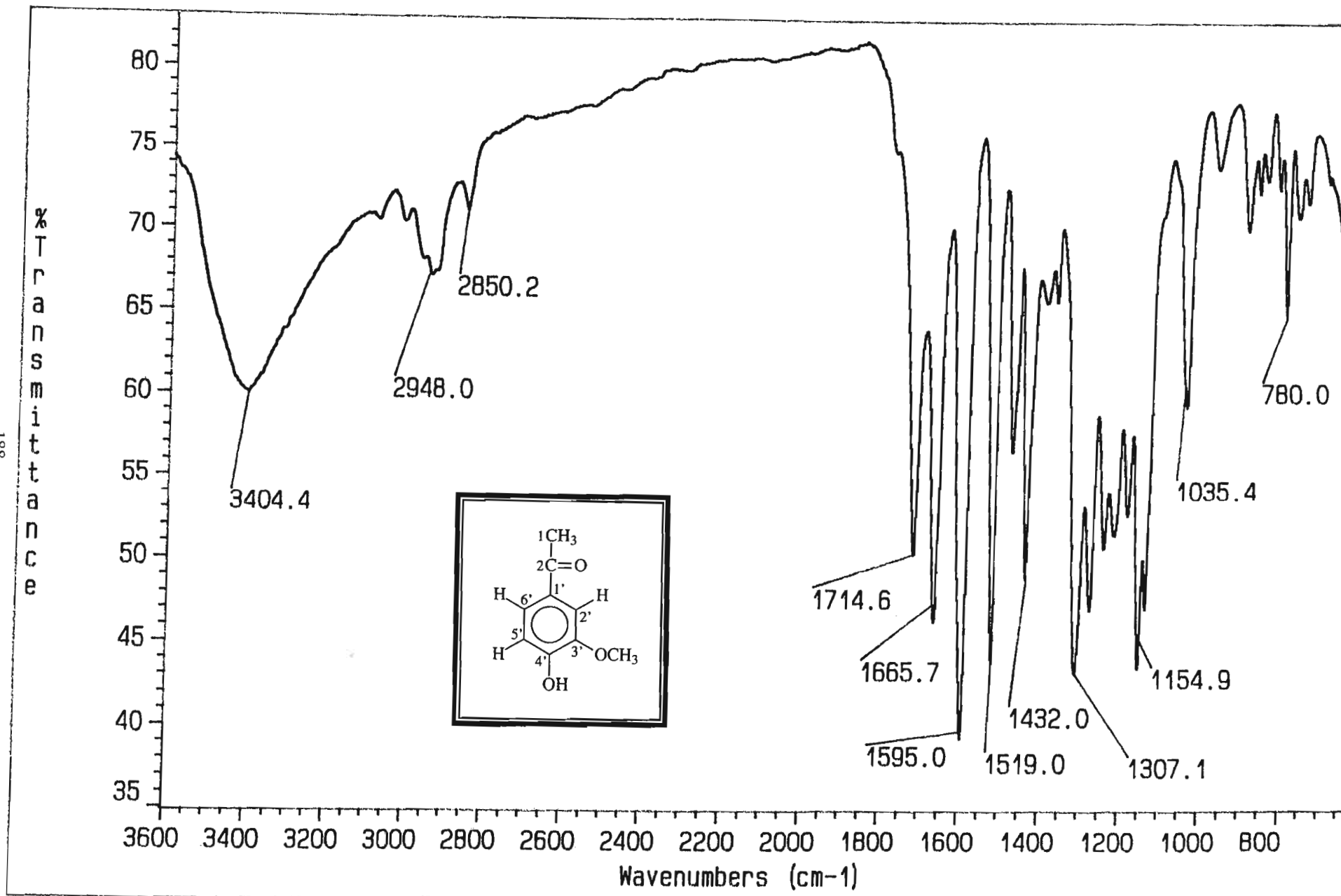
F2
(ppm)



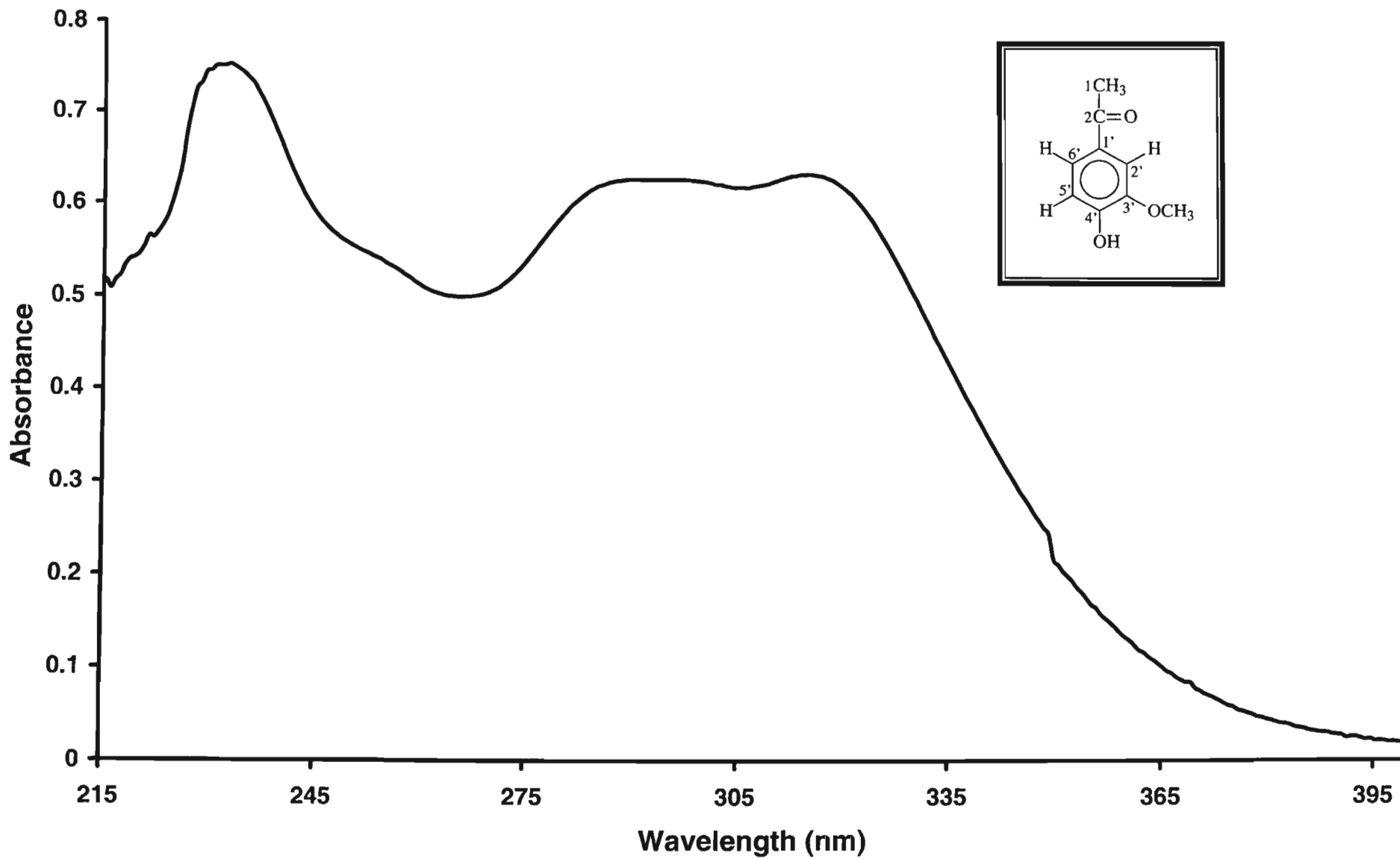
Spectrum 6.9 : COSY NMR Spectrum of Compound 6, sinapyl aldehyde



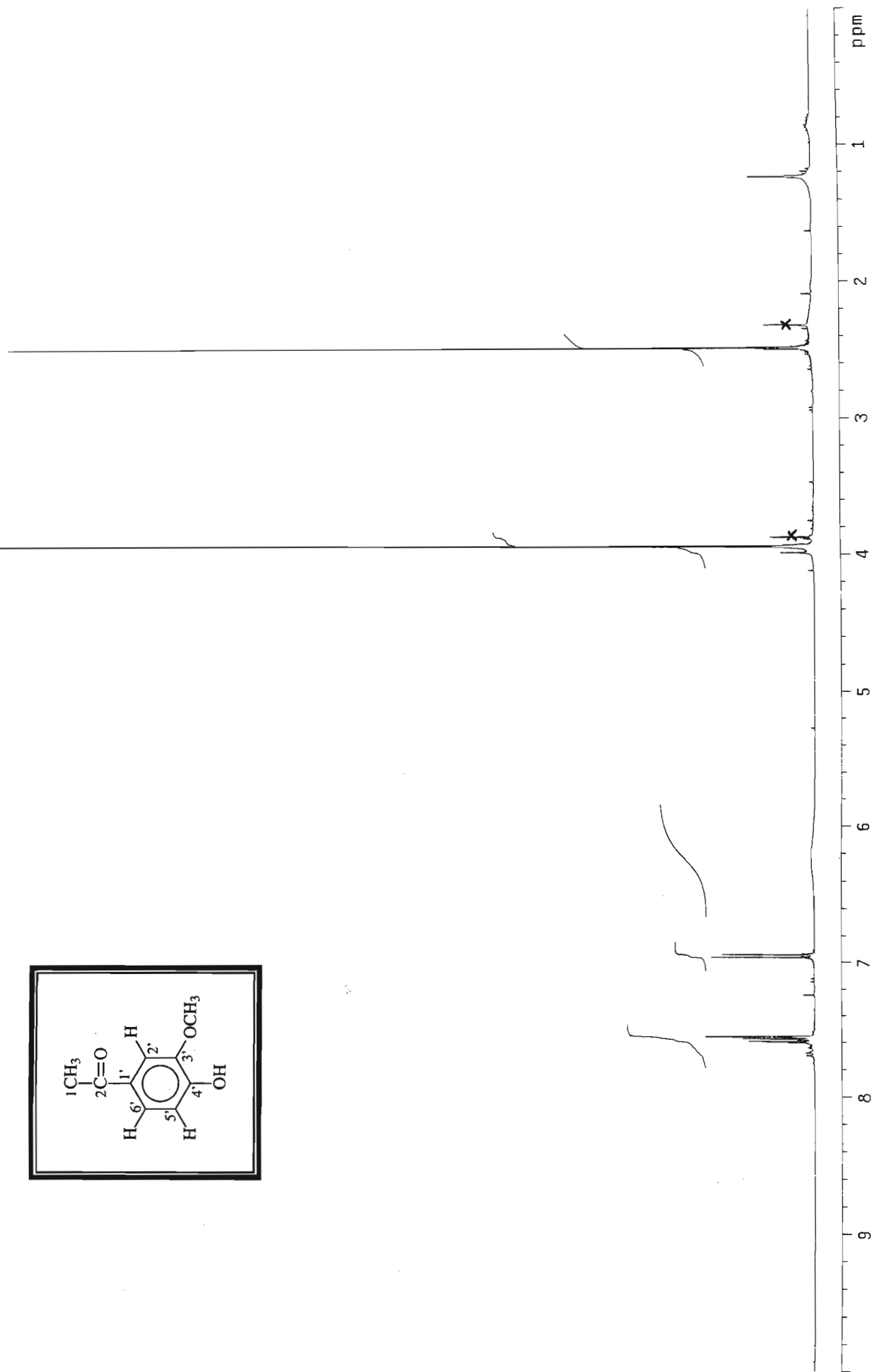
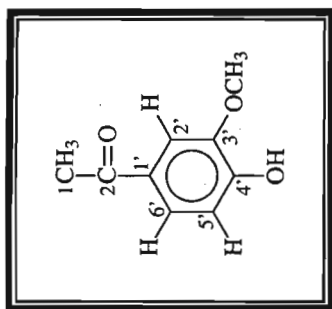
Spectrum 7.1 : Mass Spectrum of Compound 7, acetovanillone



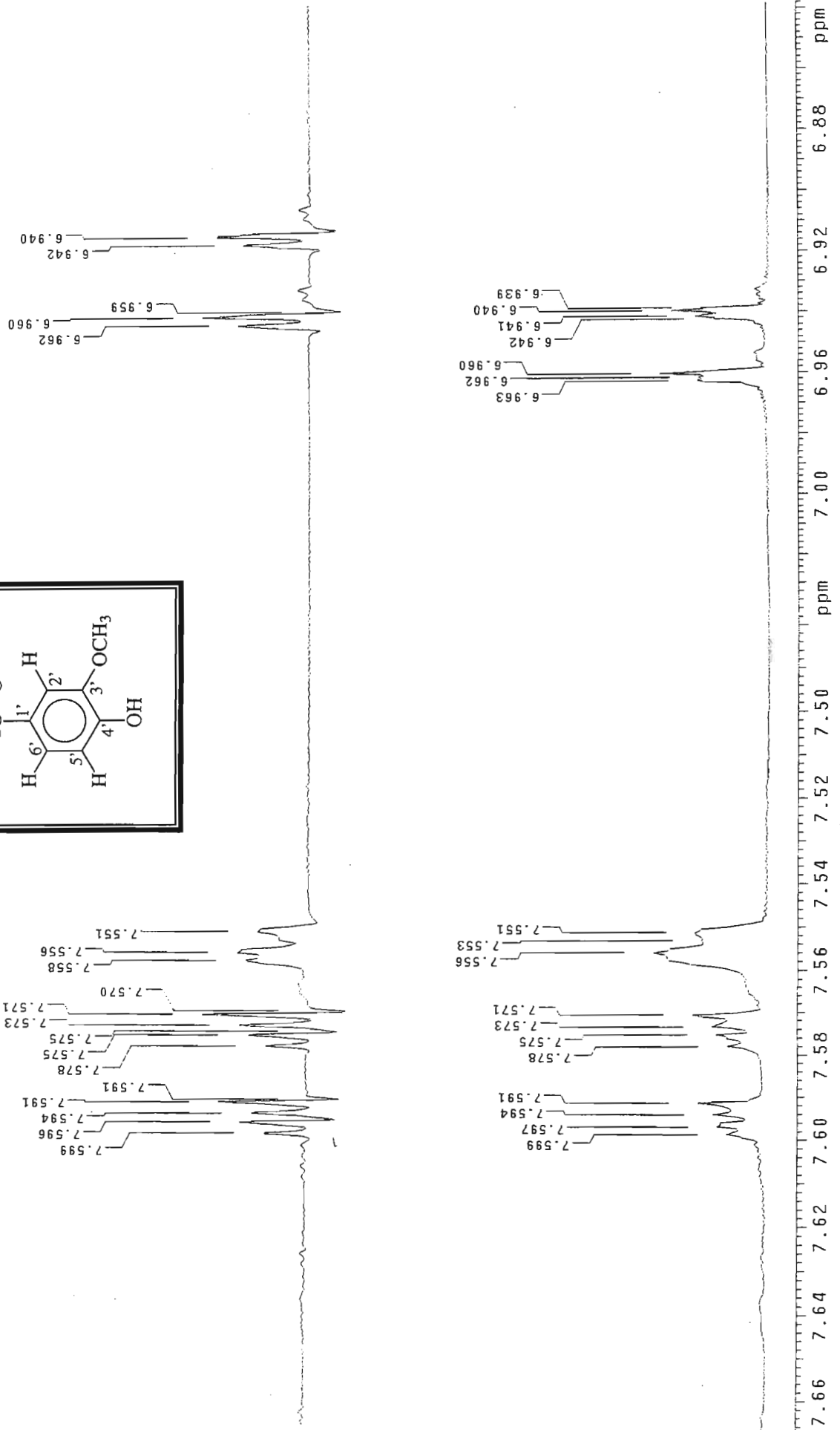
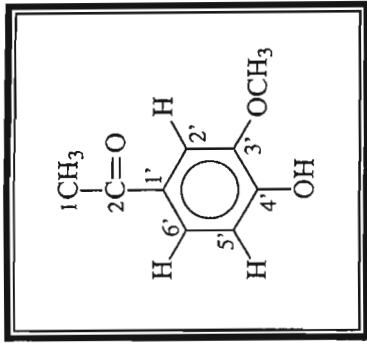
Spectrum 7.2 : Infrared Spectrum of Compound 7, acetovanillone

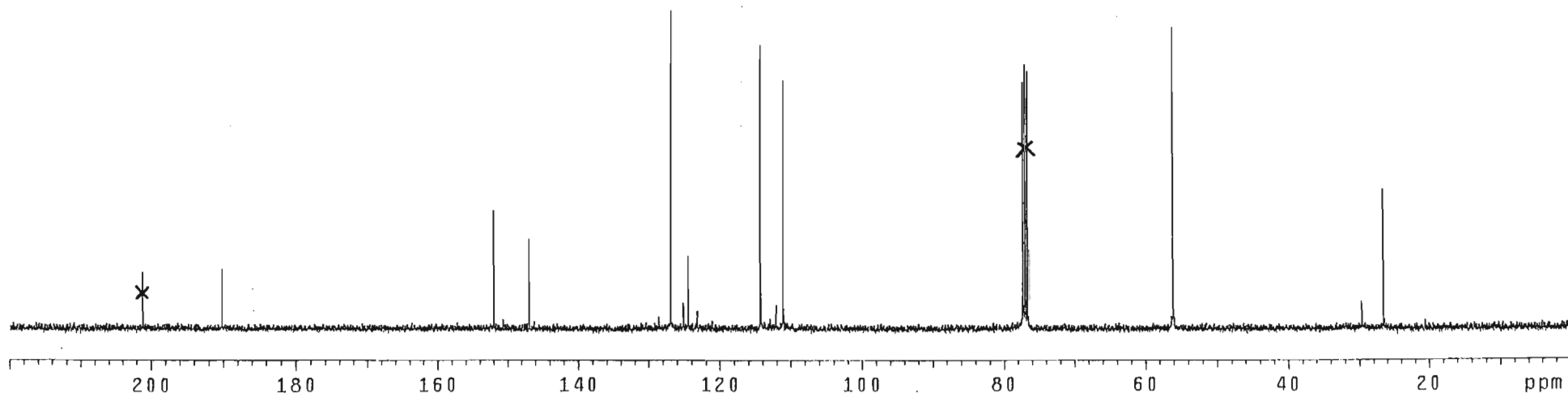
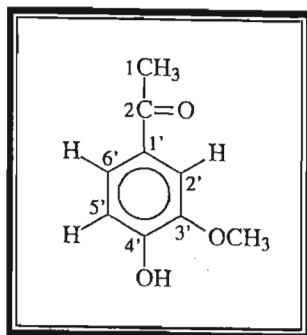


Spectrum 7.3 : UV Spectrum of Compound 7, acetovanillone



Spectrum 7.4 : ¹H NMR Spectrum of Compound 7, acetovanillone



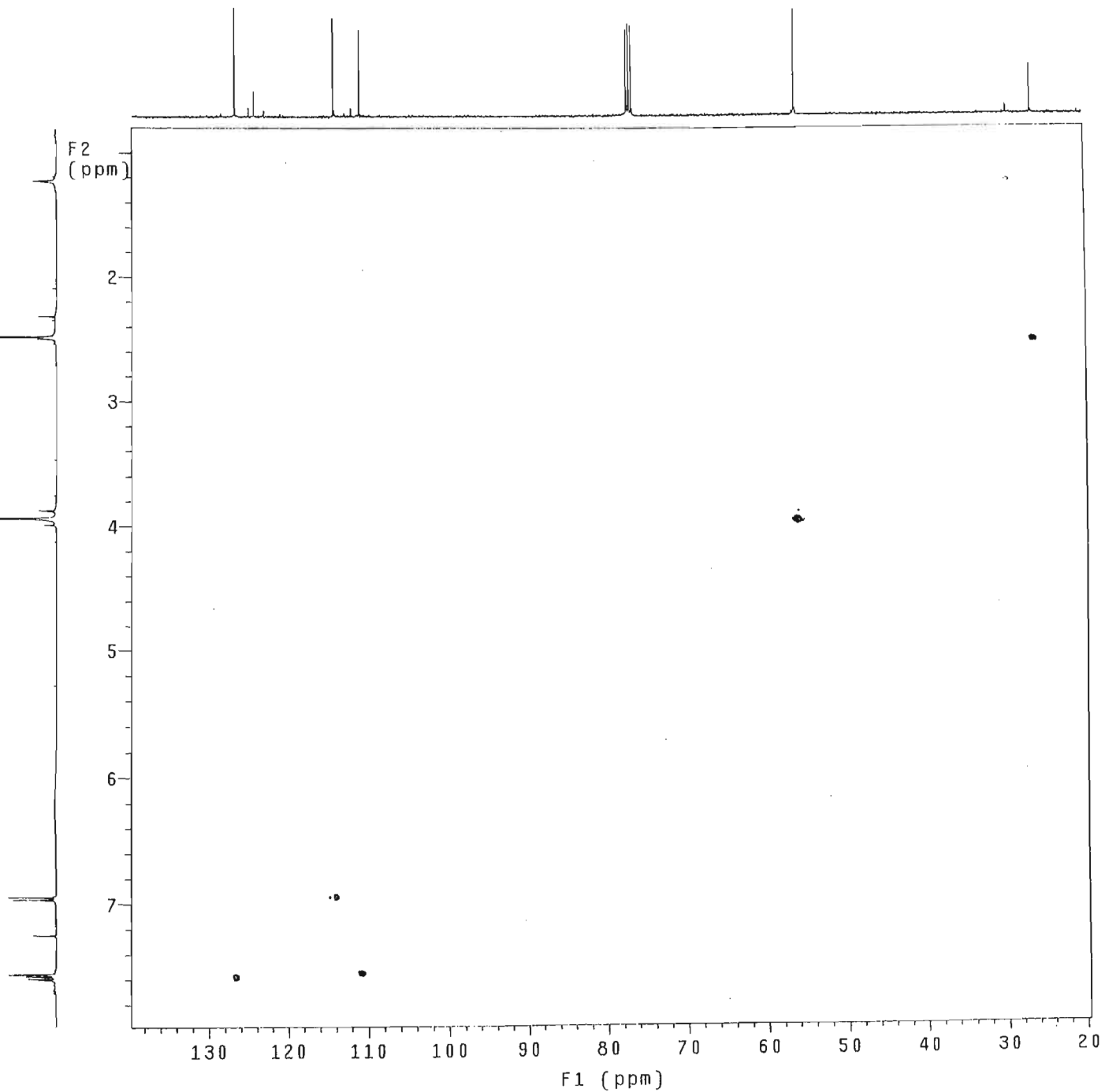
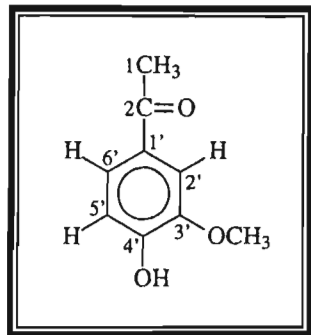


Spectrum 7.6 : ¹³C NMR Spectrum of Compound 7, acetovanillone

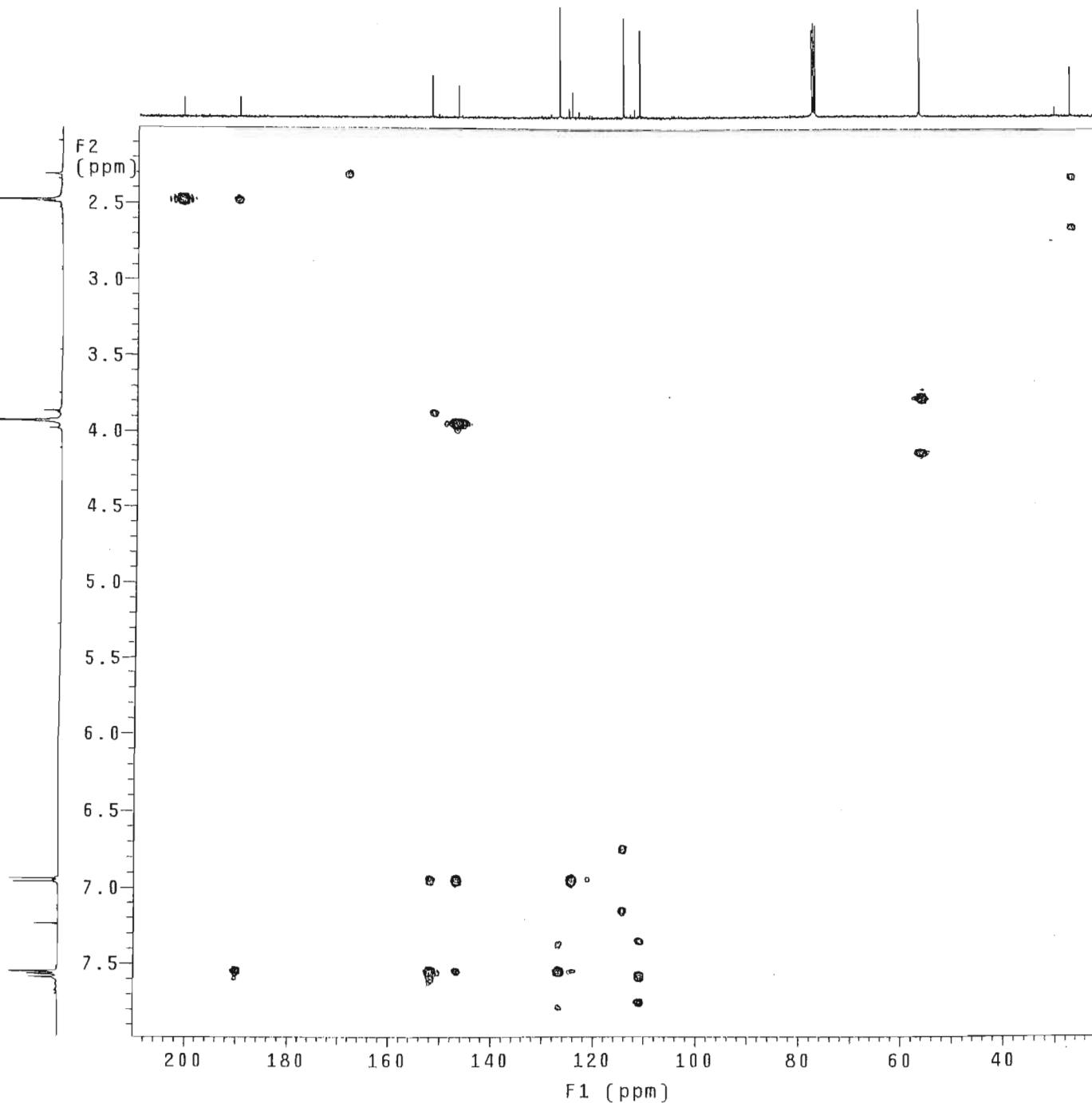
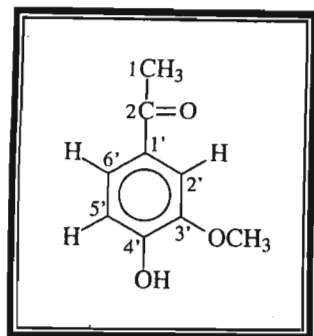
Gradient HSQC expt.
with mult.editing
probe=5mmASW

Pulse Sequence: ghsqc_da

193



Spectrum 7.7 : HSQC NMR Spectrum of Compound 7. acetovanillone

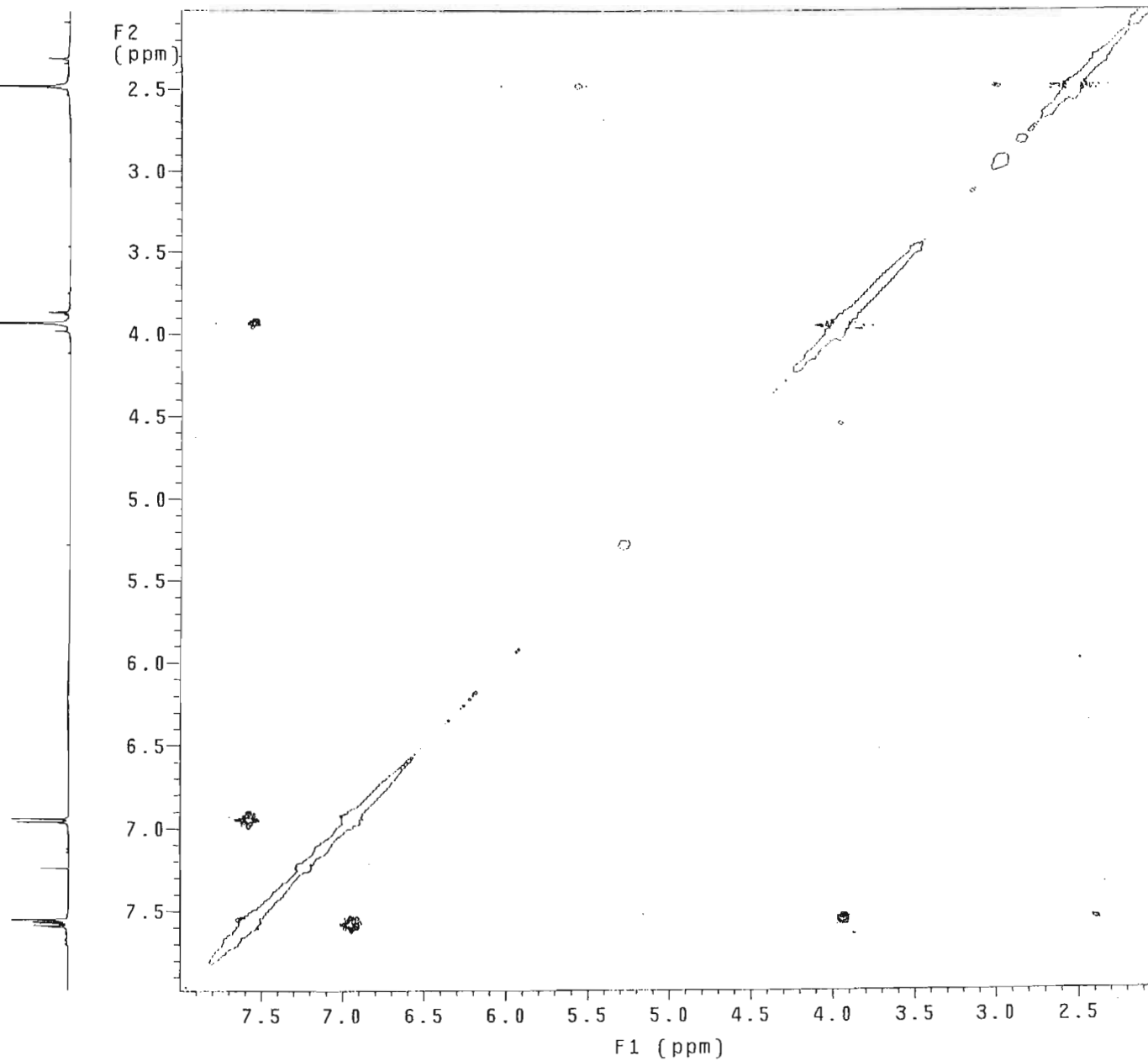
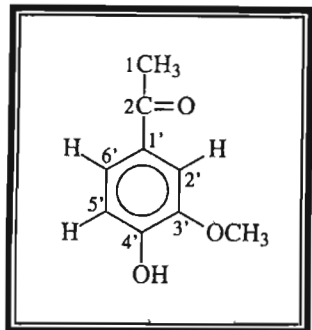


Spectrum 7.8 : HMBC NMR Spectrum of Compound 7, acetovanillone

NOESY expt.
mix=1sec
probe=5mmASW

Pulse Sequence: noesy_da

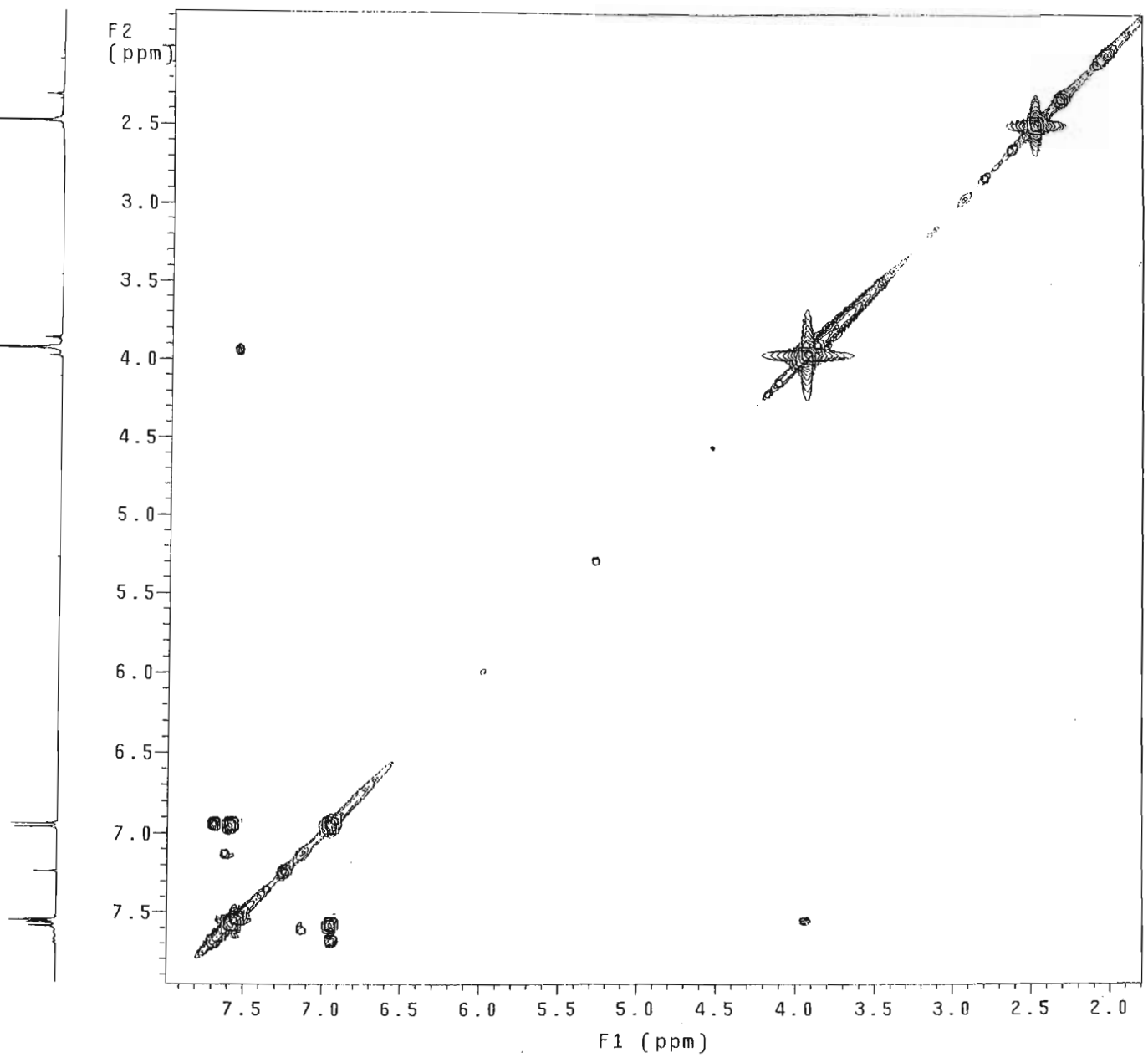
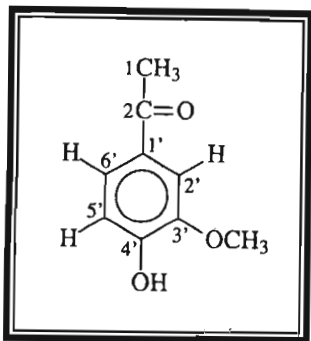
195



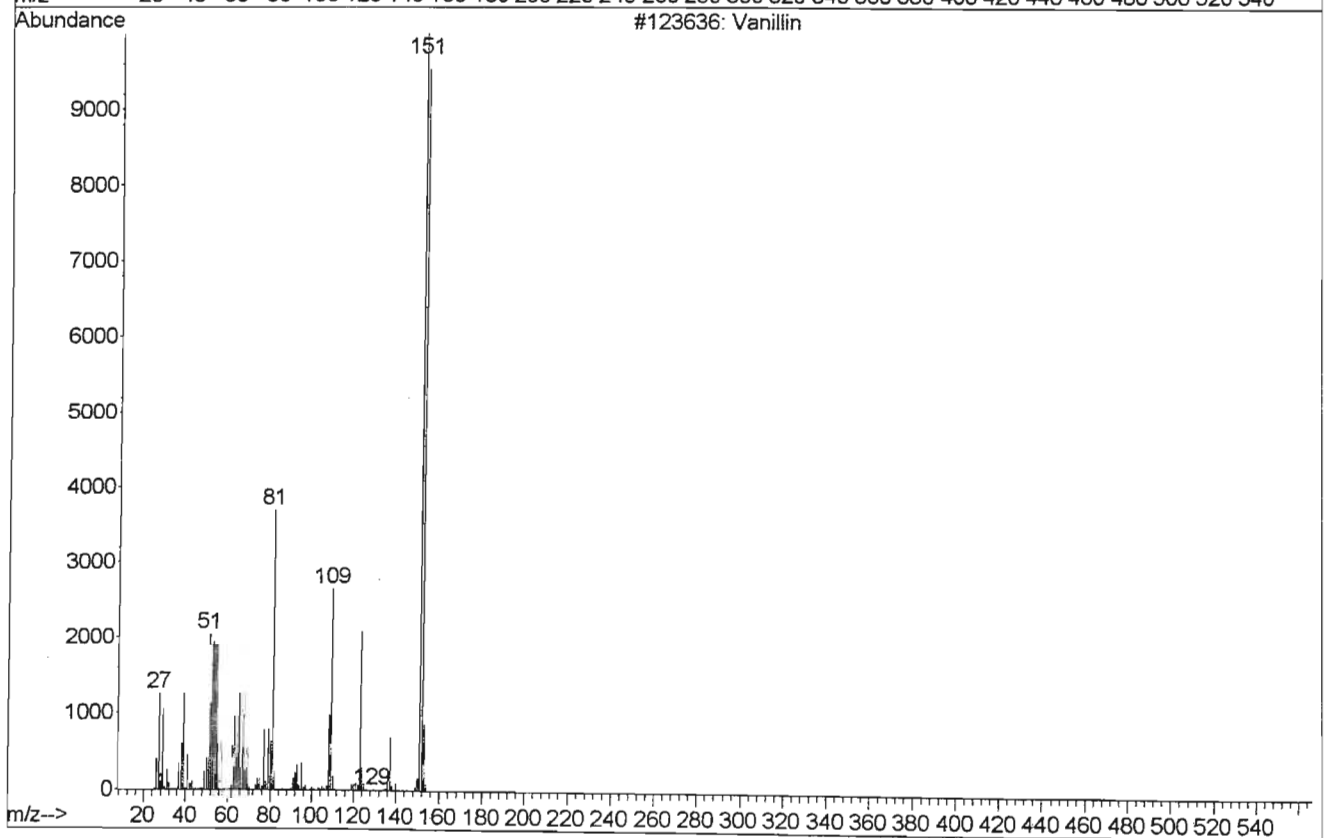
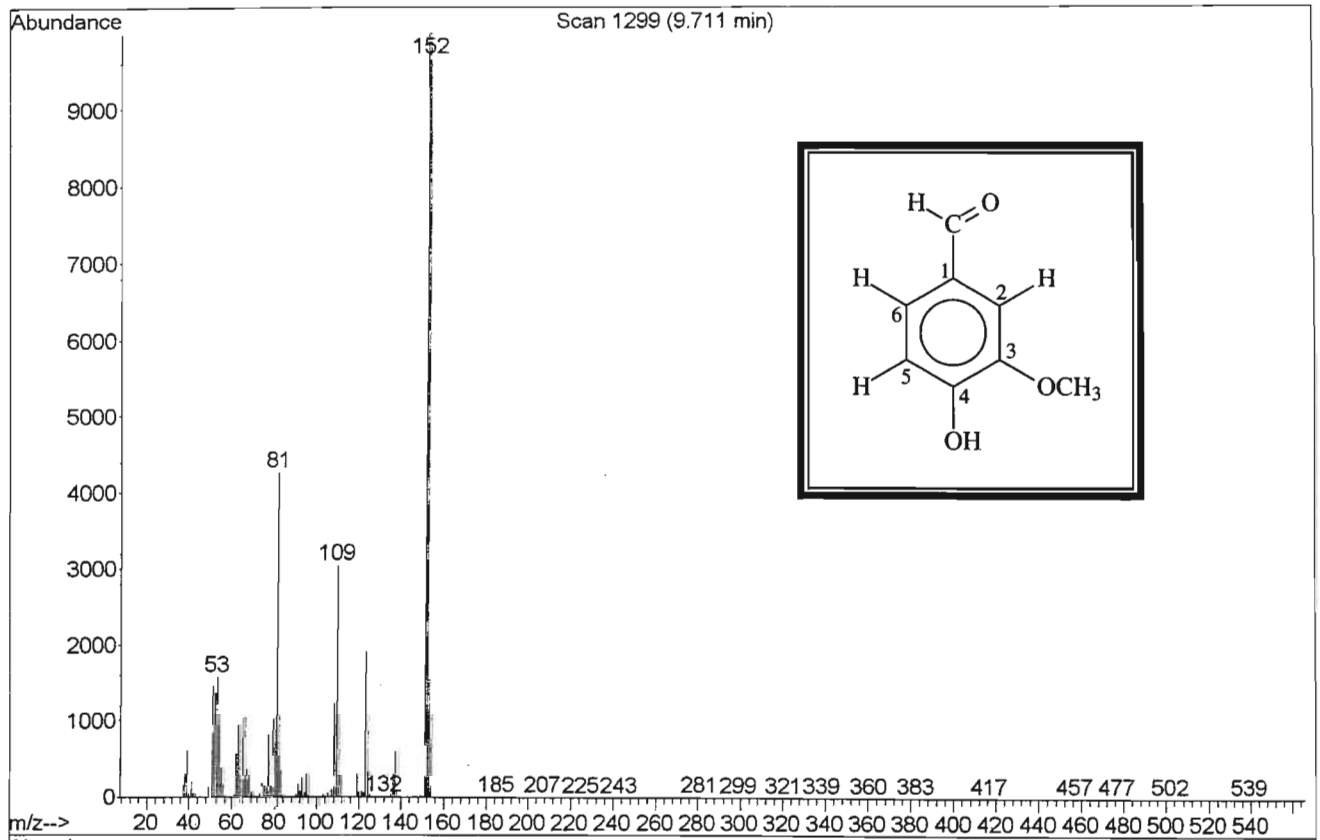
Spectrum 7.9 : NOESY NMR Spectrum of Compound 7. acetovanillone

in cosy-90
probe=5mmASW
Pulse Sequence: relayh

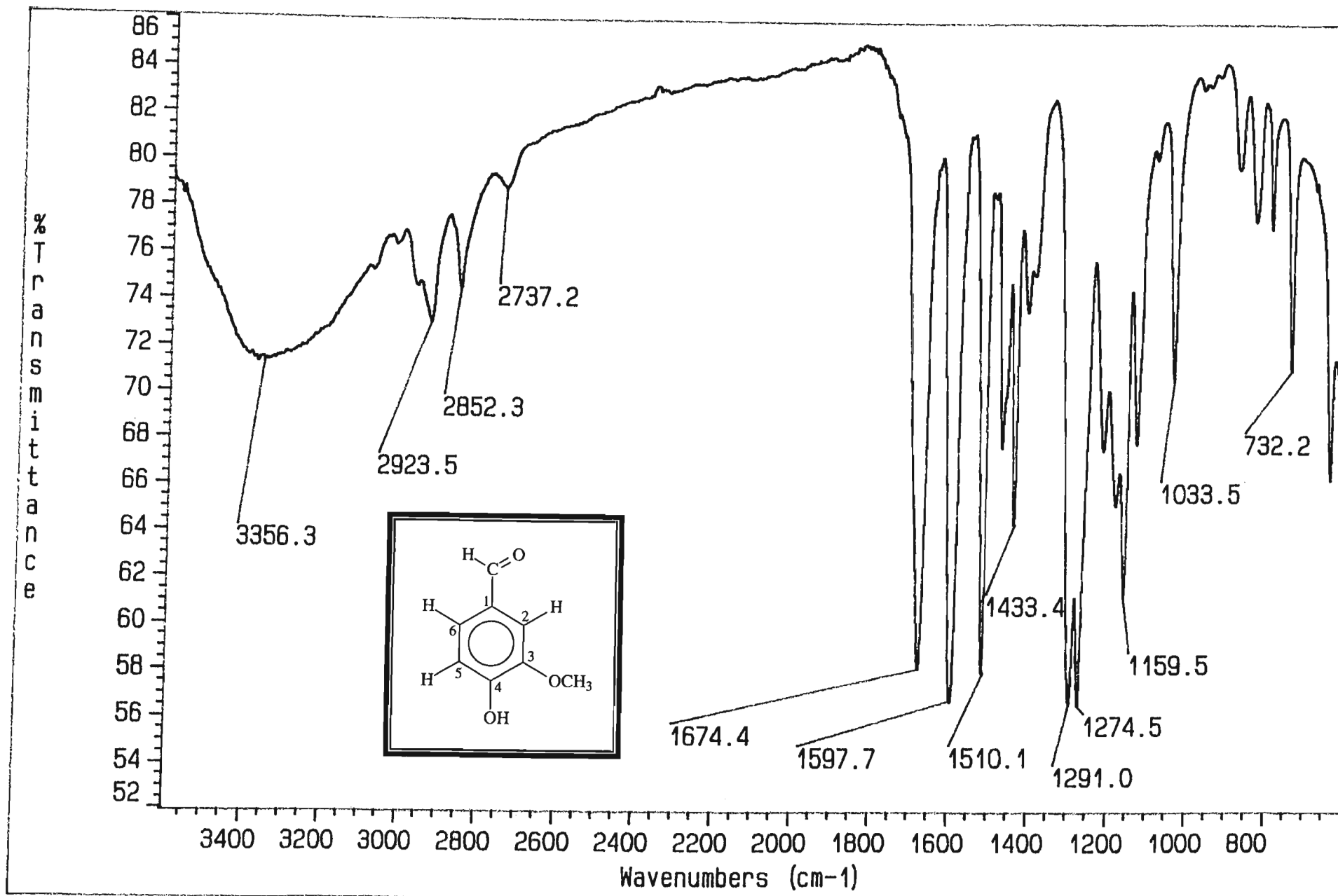
196



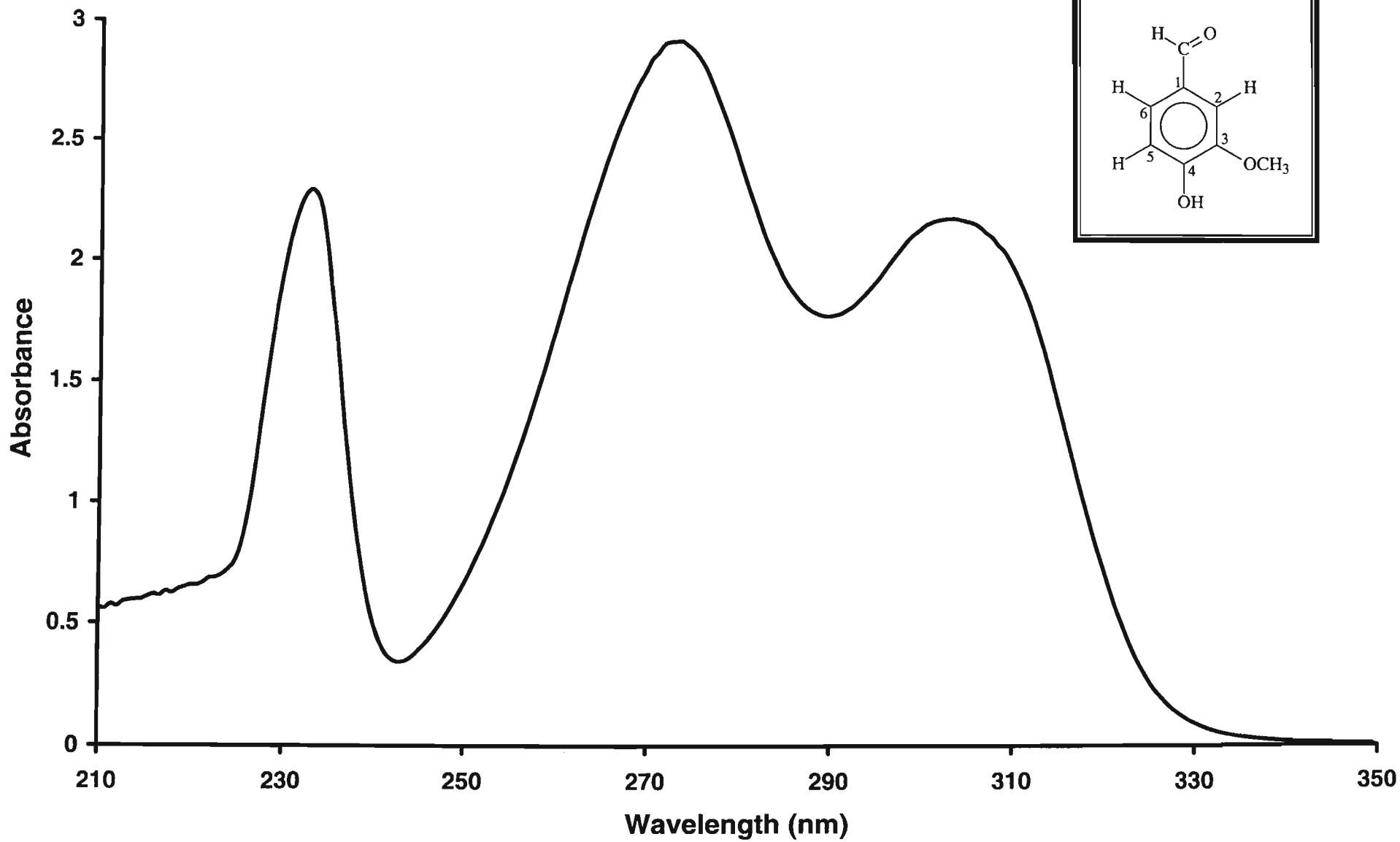
Spectrum 7.10 : COSY NMR Spectrum of Compound 7, acetovanillone



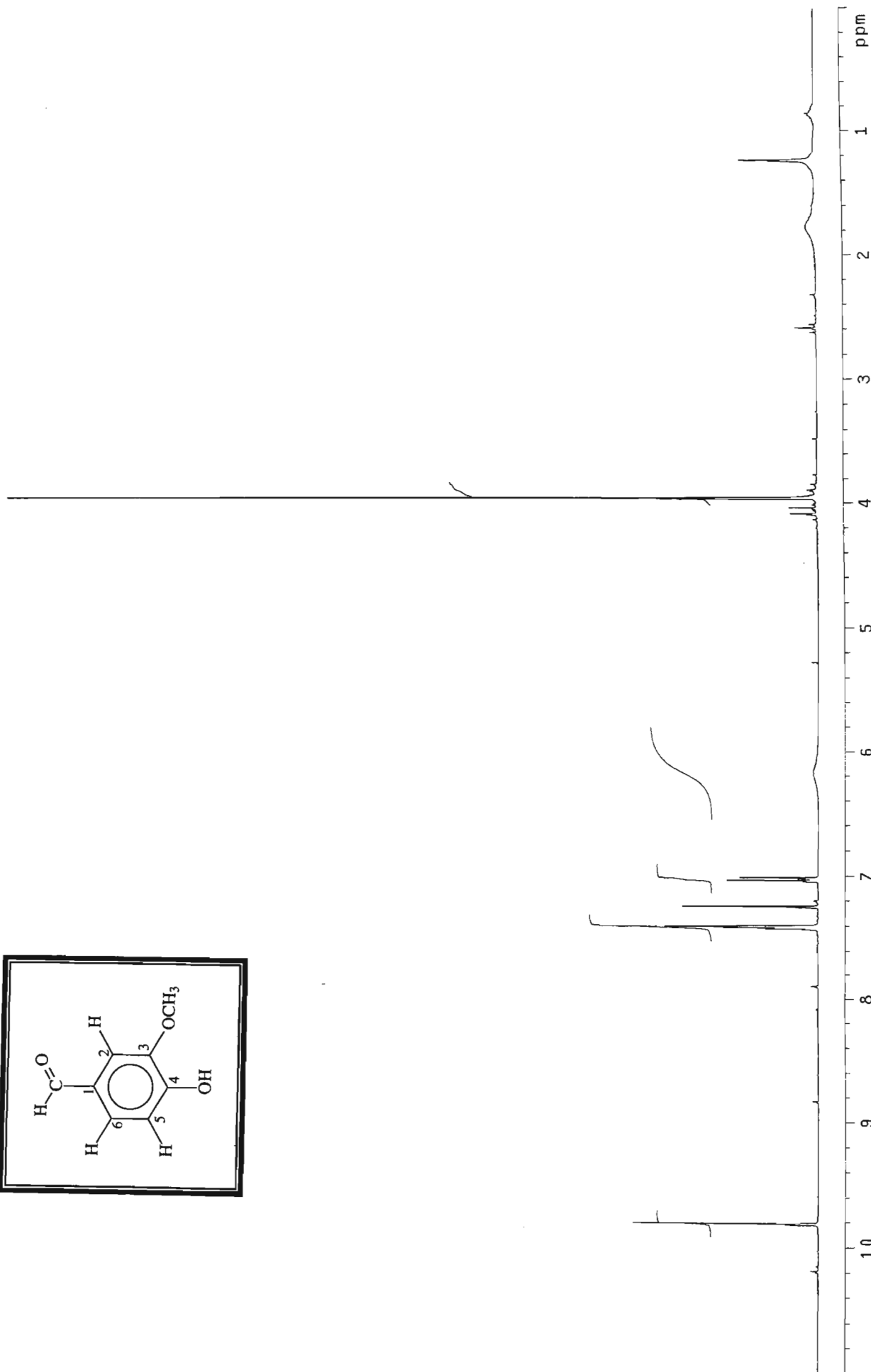
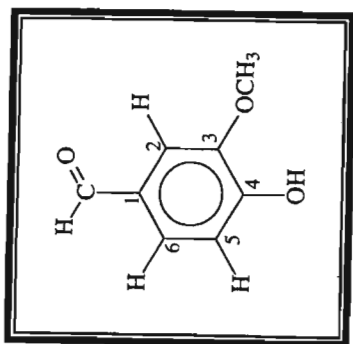
Spectrum 8.1 : Mass Spectrum of Compound 8, vanillin



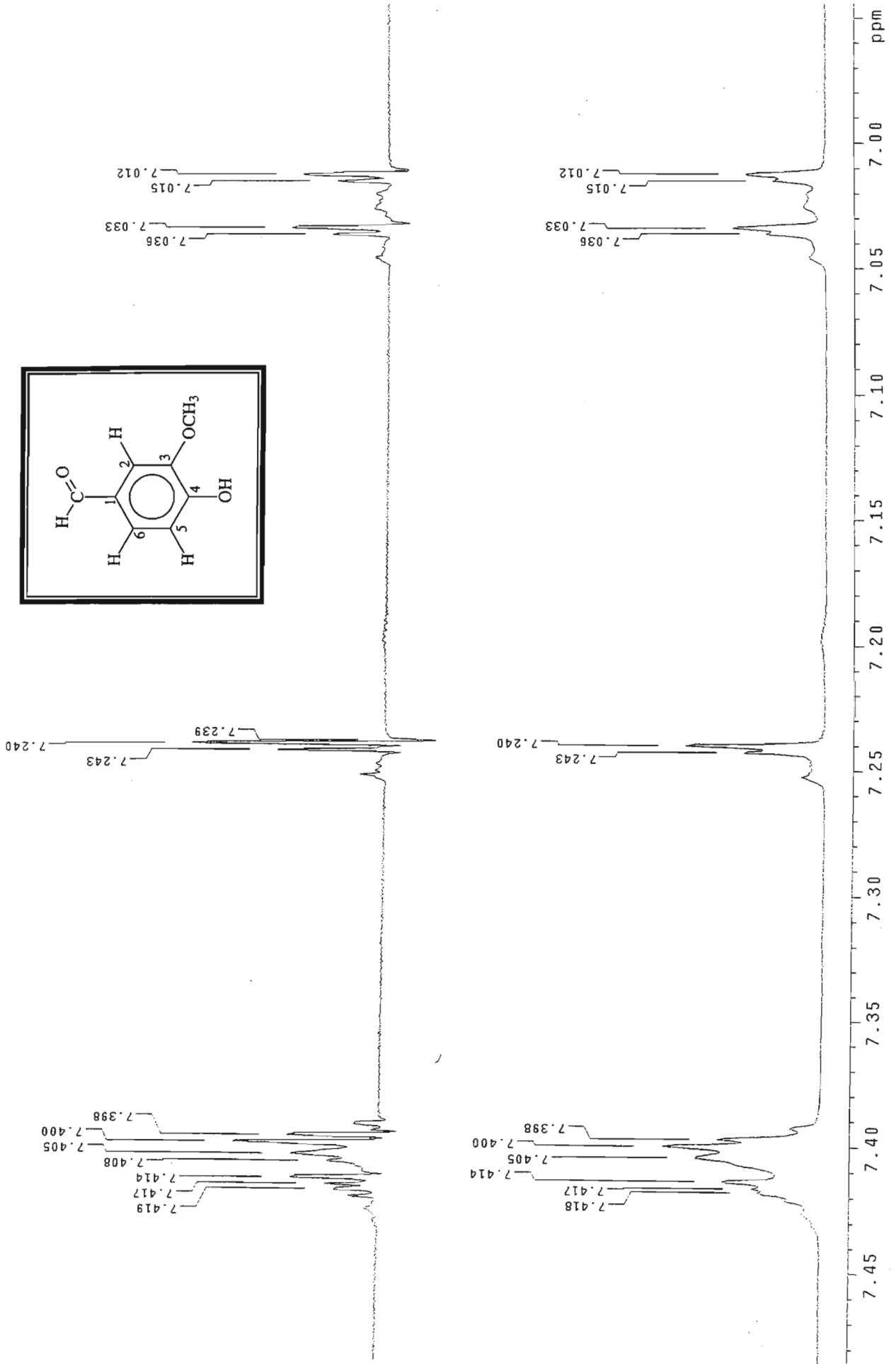
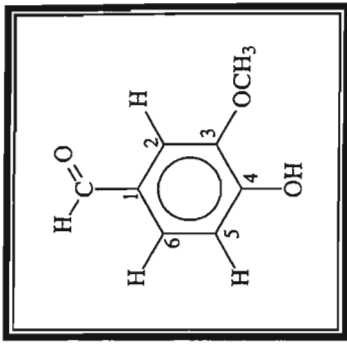
Spectrum 8.2 : Infrared Spectrum of Compound 8, vanillin



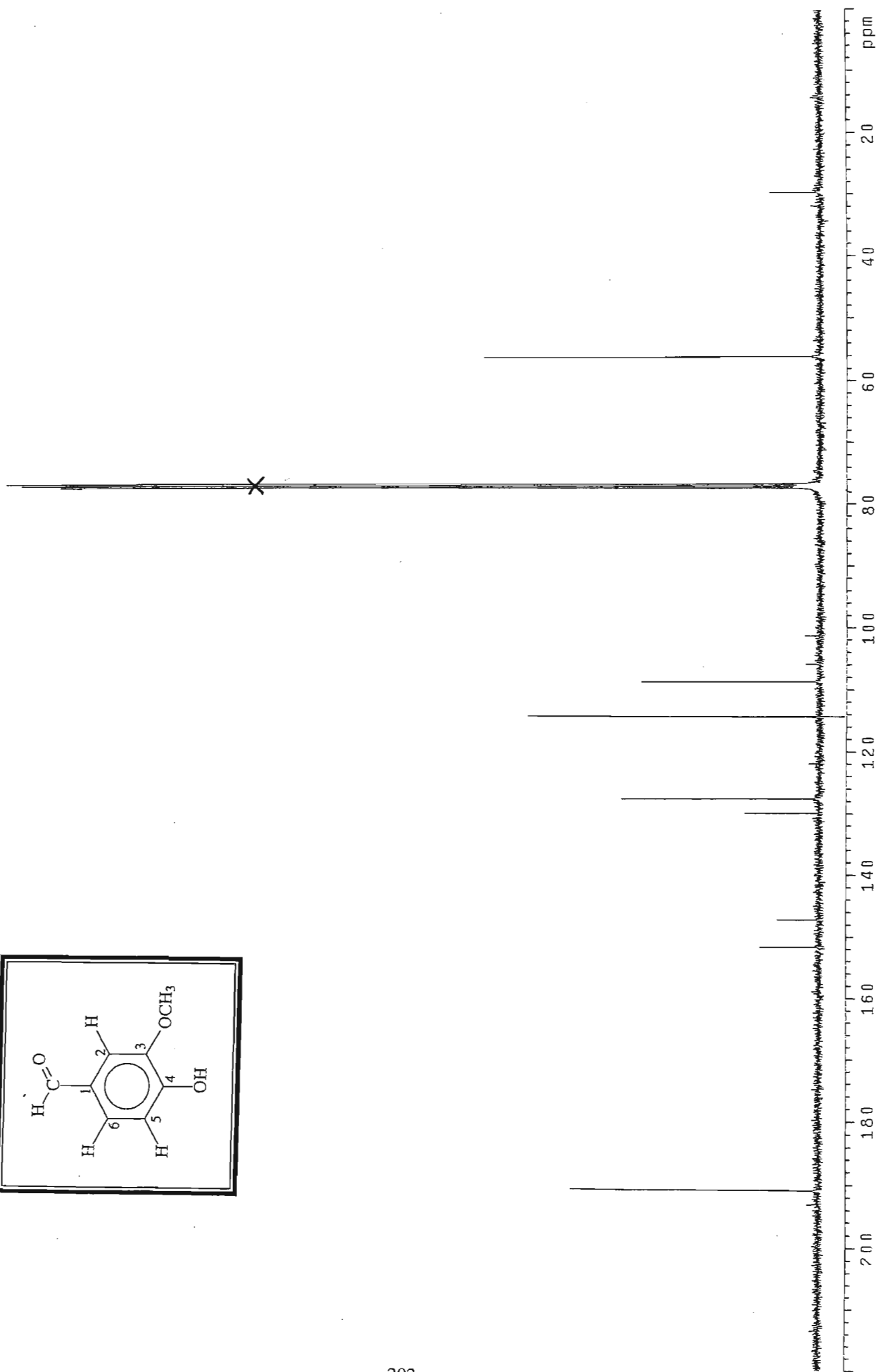
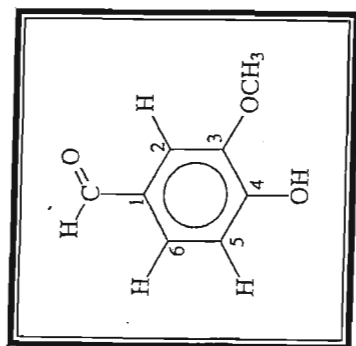
Spectrum 8.3 : UV Spectrum of Compound 8, vanillin



Spectrum 8.4 : ¹H NMR Spectrum of Compound 8, vanillin

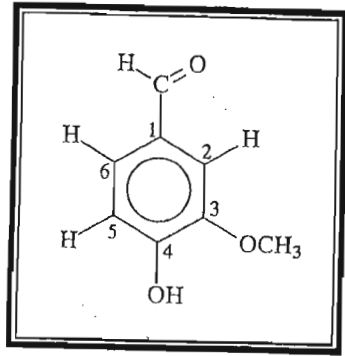


Spectrum 8.5 : Expanded ¹H NMR Spectrum of Compound 8, vanillin

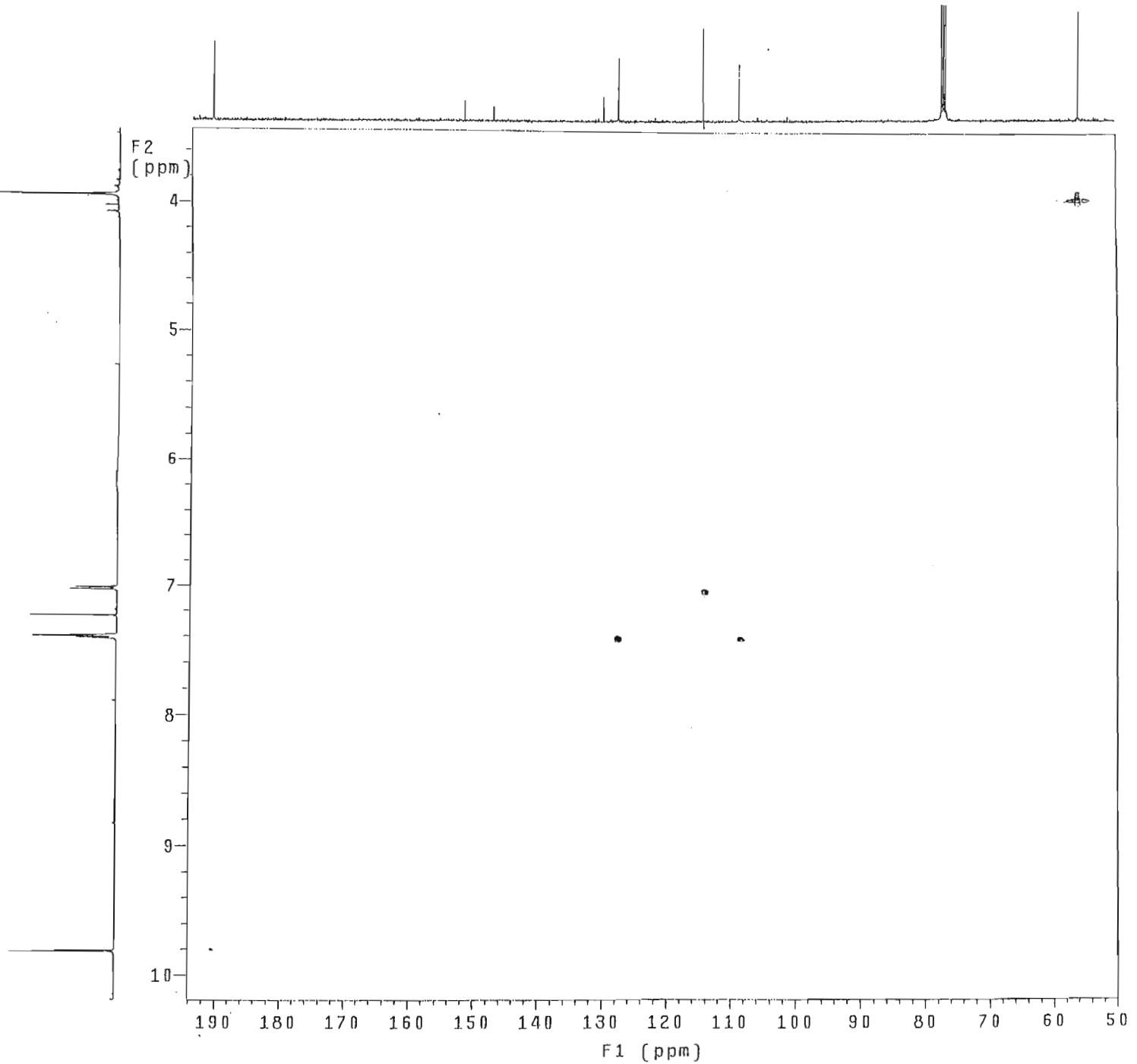


Spectrum 8.6 : ¹³C NMR Spectrum of Compound 8, vanillin

With mult.editing
probe=5mmASW
Pulse Sequence: ghsqc_da



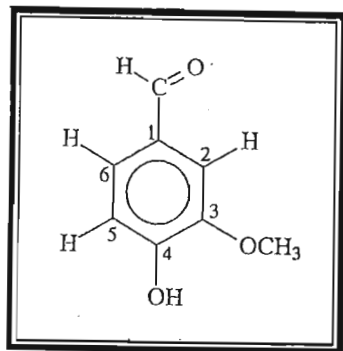
203



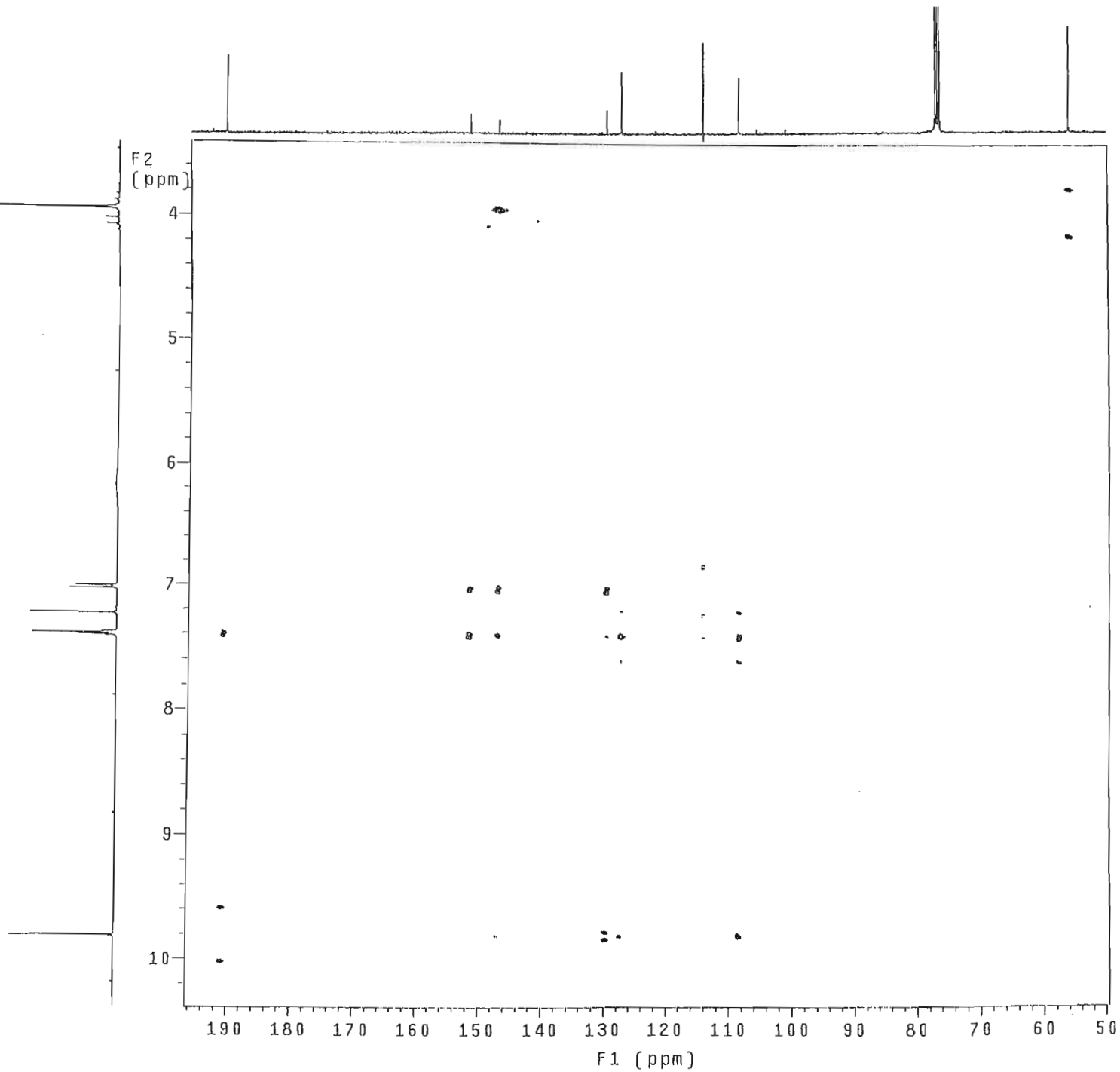
Spectrum 8.7 : HSQC NMR Spectrum of Compound 8, vanillin

Gradient HMBc expt.
probe=5mmASW

Pulse Sequence: ghmqc_da



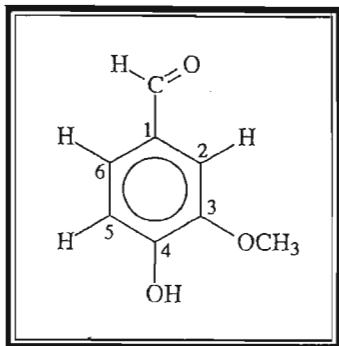
204



Spectrum 8.8 : HMBC NMR Spectrum of Compound 8. vanillin

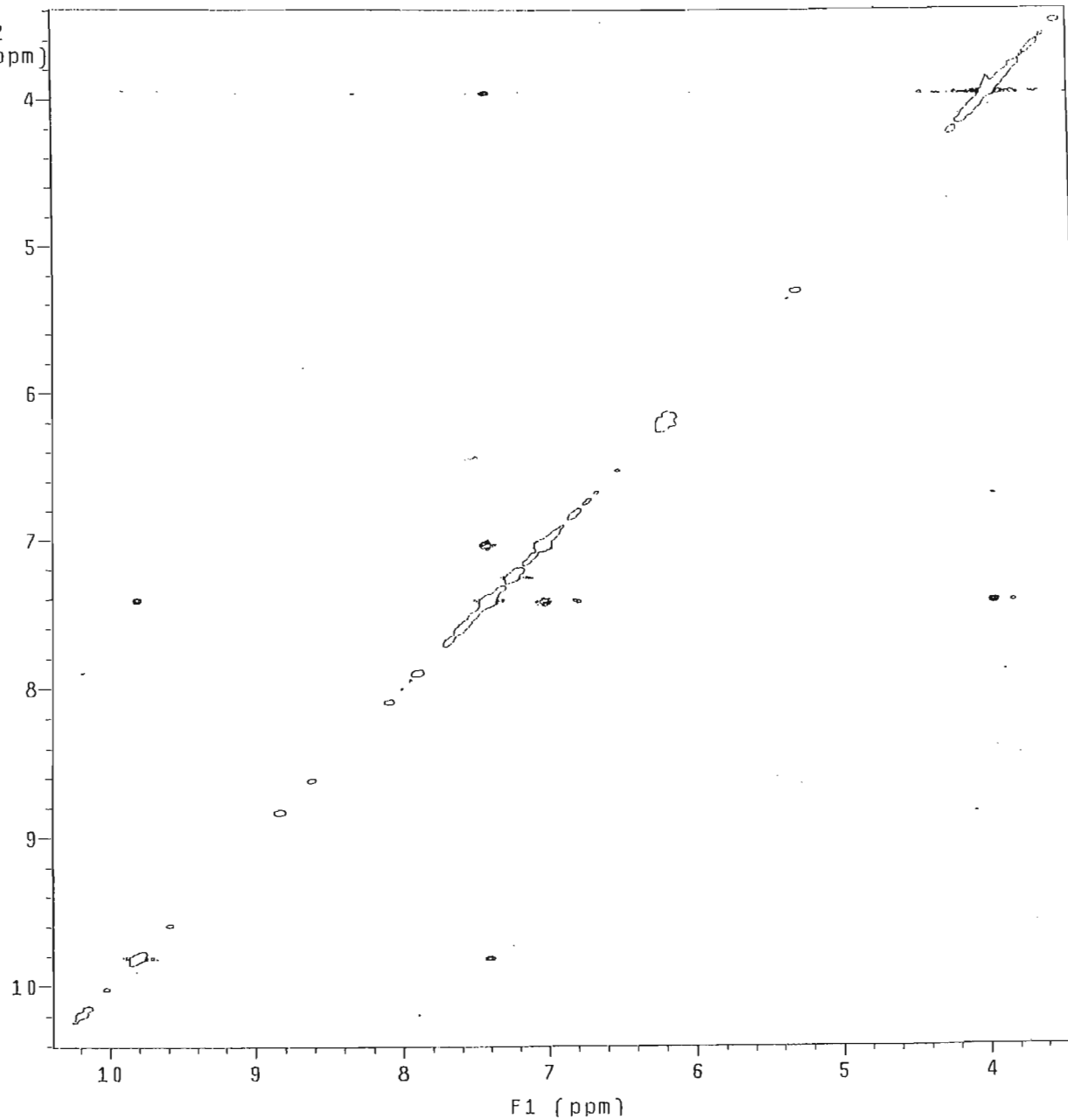
mix=1sec
probe=5mmASW

Pulse Sequence: noesy_da



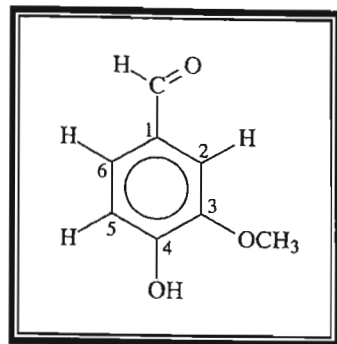
205

F2
(ppm)

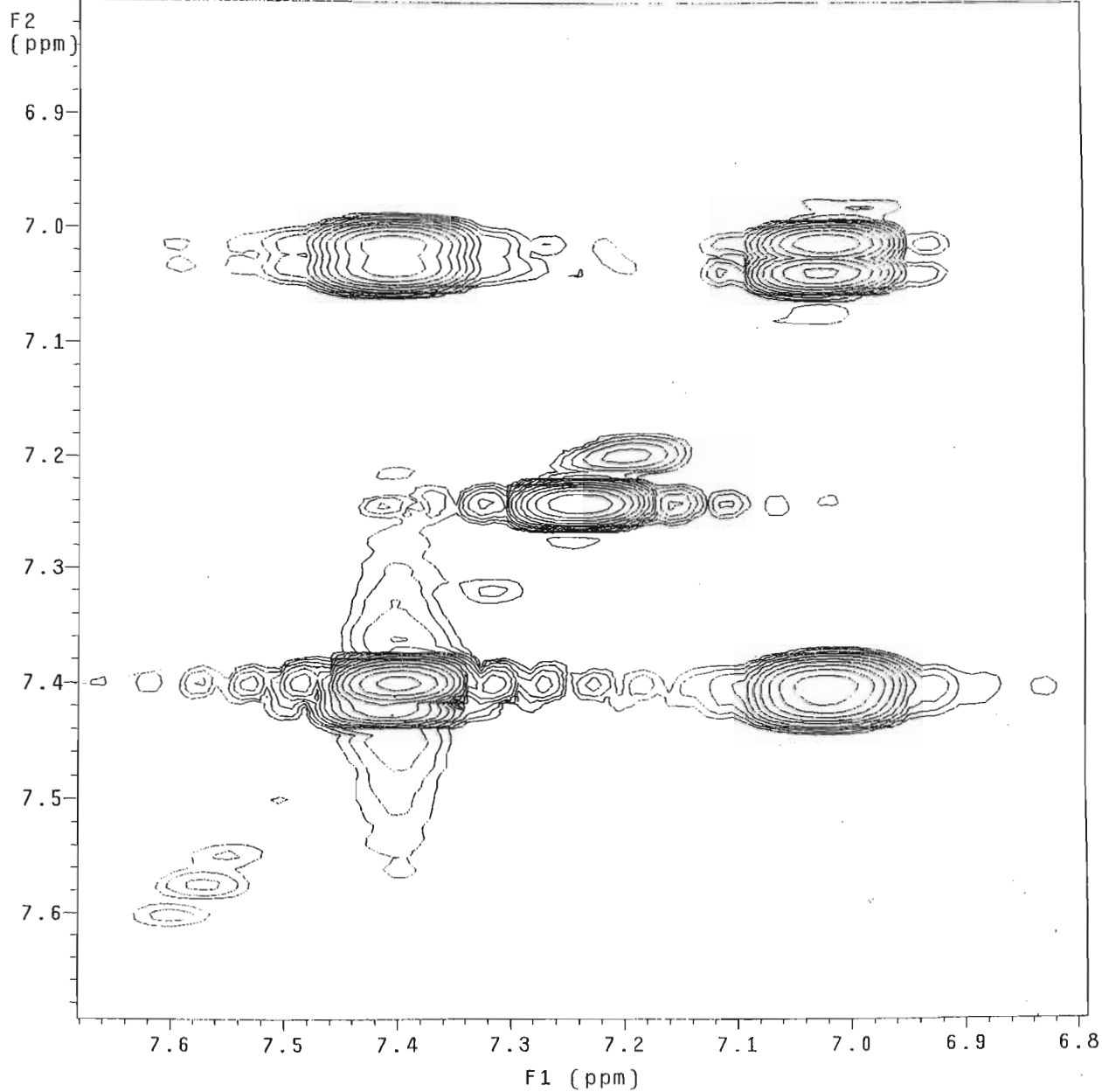
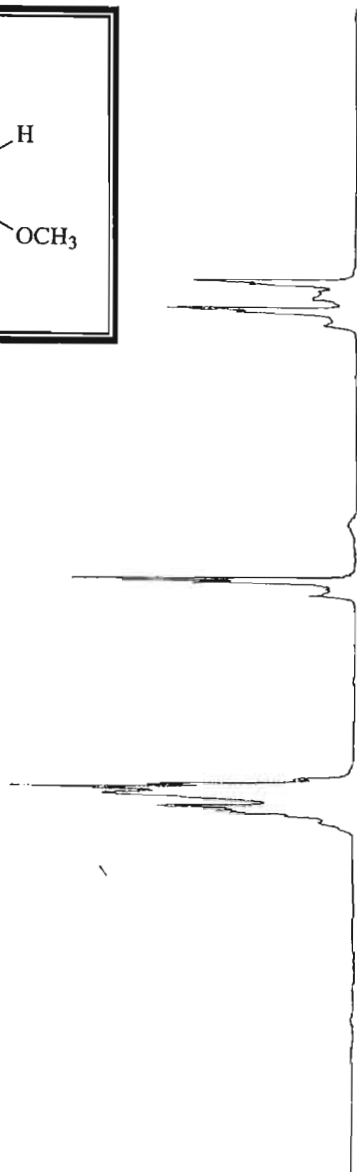


Spectrum 8.9 : NOESY NMR Spectrum of Compound 8, vanillin

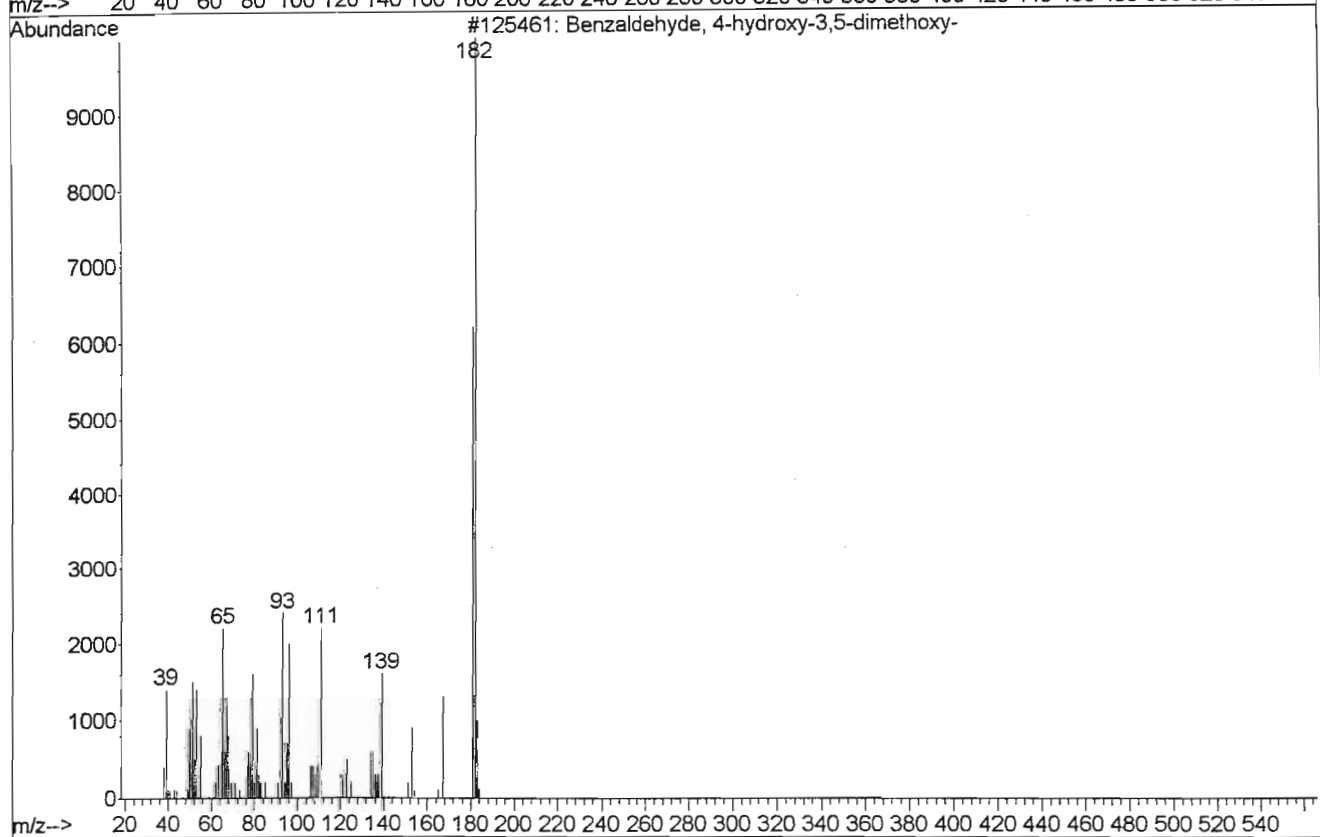
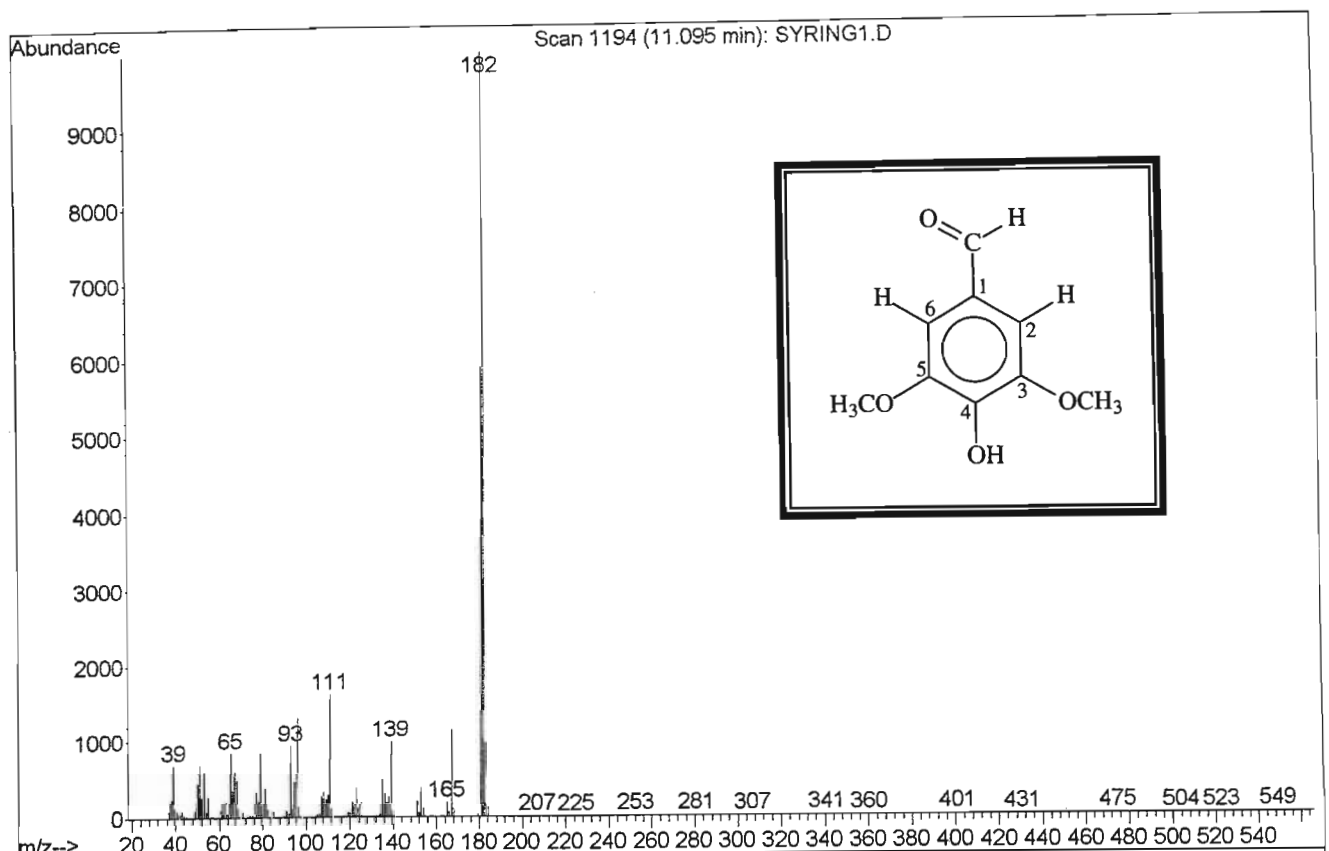
cycpd3.compound_3 in cdc13
1H Cosy-90
probe=5mmASW
Pulse Sequence: relayh



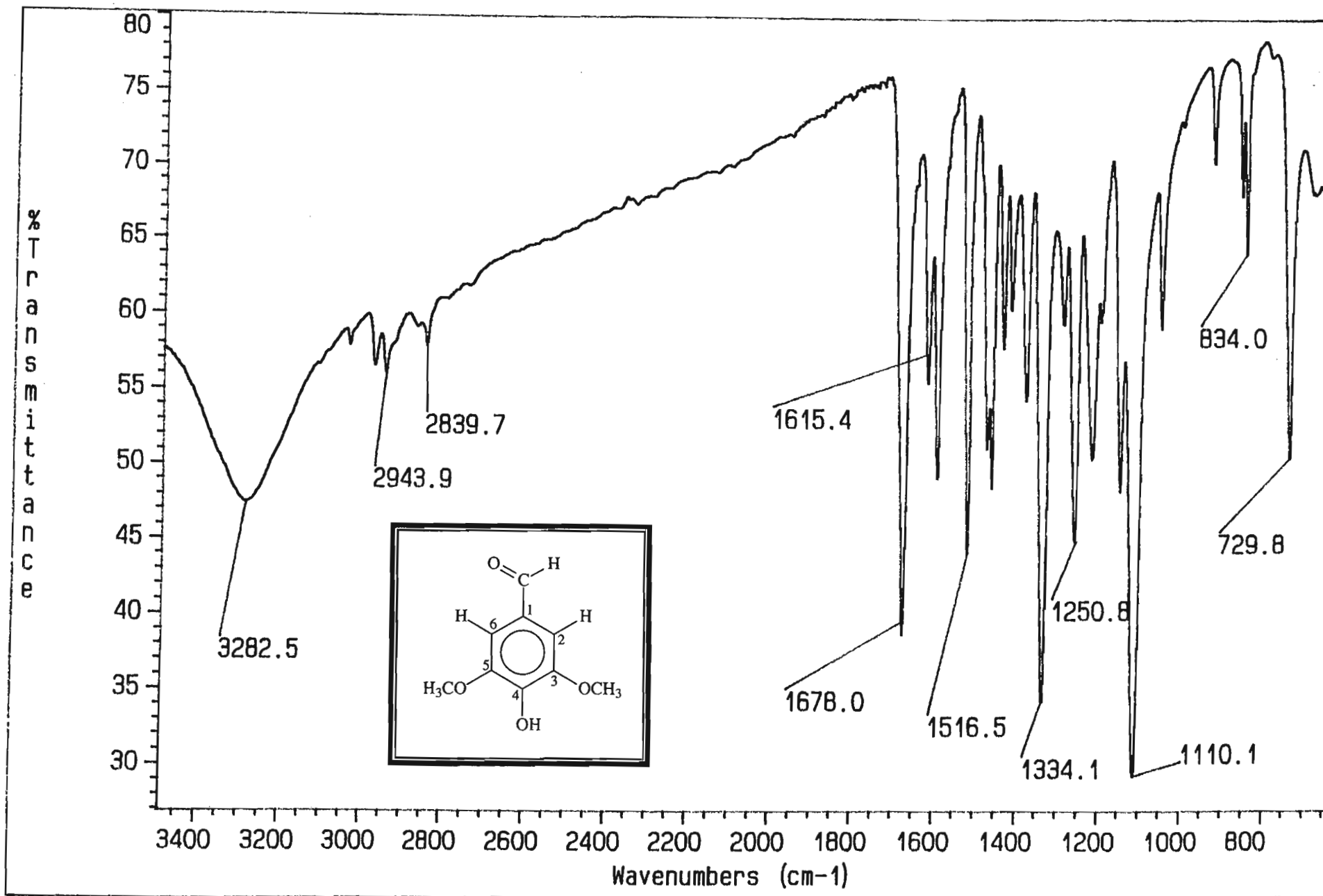
207



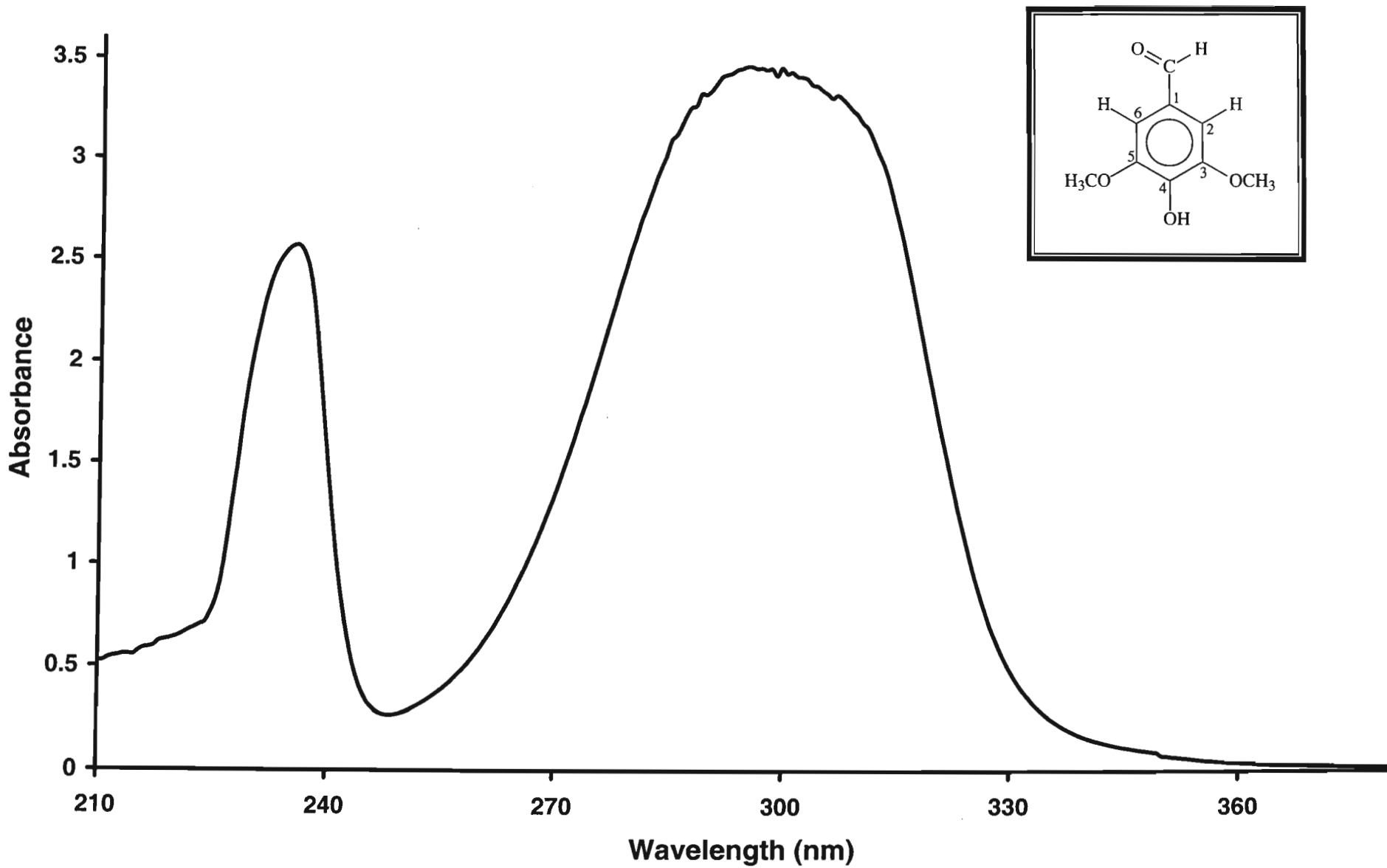
Spectrum 9.11 : Expanded COSY NMR Spectrum of Compound 8 vanillin



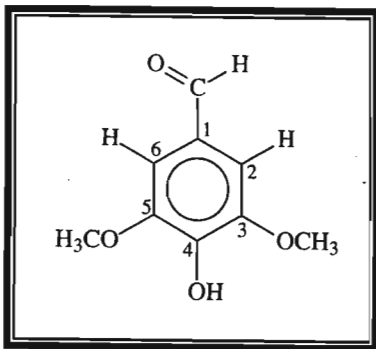
Spectrum 9.1 : Mass Spectrum of Compound 9, syringaldehyde



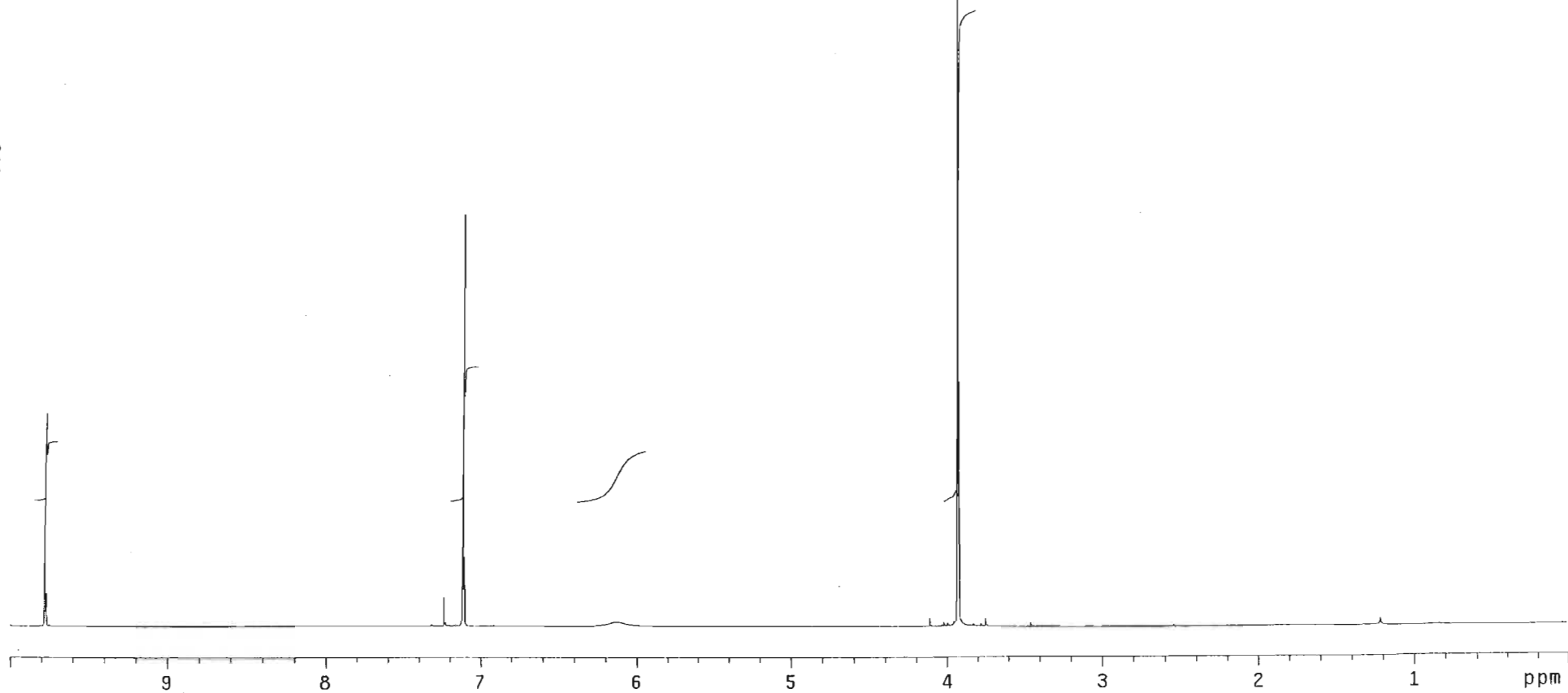
Spectrum 9.2 : Infrared Spectrum of Compound 9, syringaldehyde



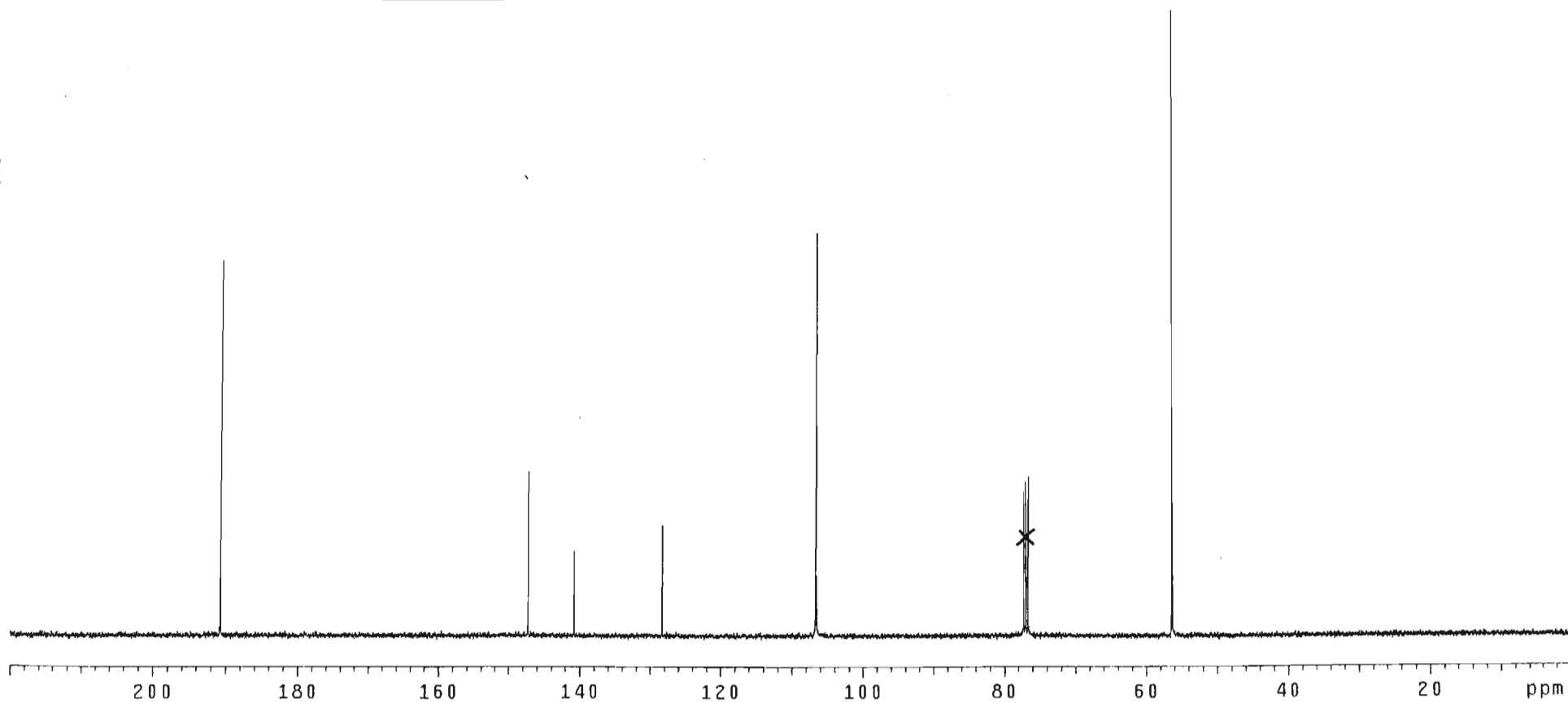
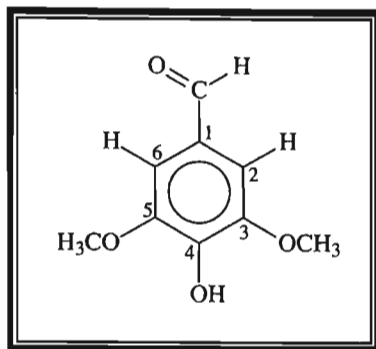
Spectrum 9.3 : UV Spectrum of Compound 9, syringaldehyde



211



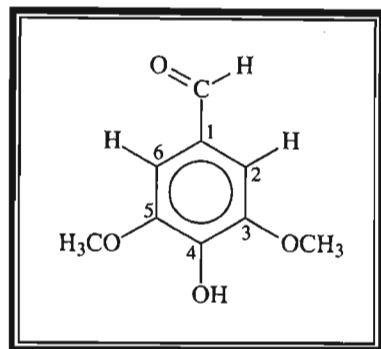
Spectrum 9.4 : ¹H NMR Spectrum of Compound 9, syringaldehyde



Spectrum 9.5 : ^{13}C NMR Spectrum of Compound 9, syringaldehyde

hsqc-compound_9 in cdcl3
Gradient HSQC expt.
with mult.editing
probe=5mmASW

Pulse Sequence: ghsqc_da



F2
(ppm)

4

5

6

7

8

9

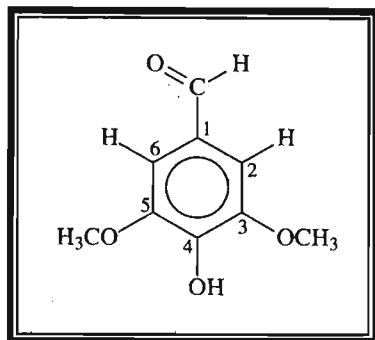
10

190 180 170 160 150 140 130 120 110 100 90 80 70 60 50

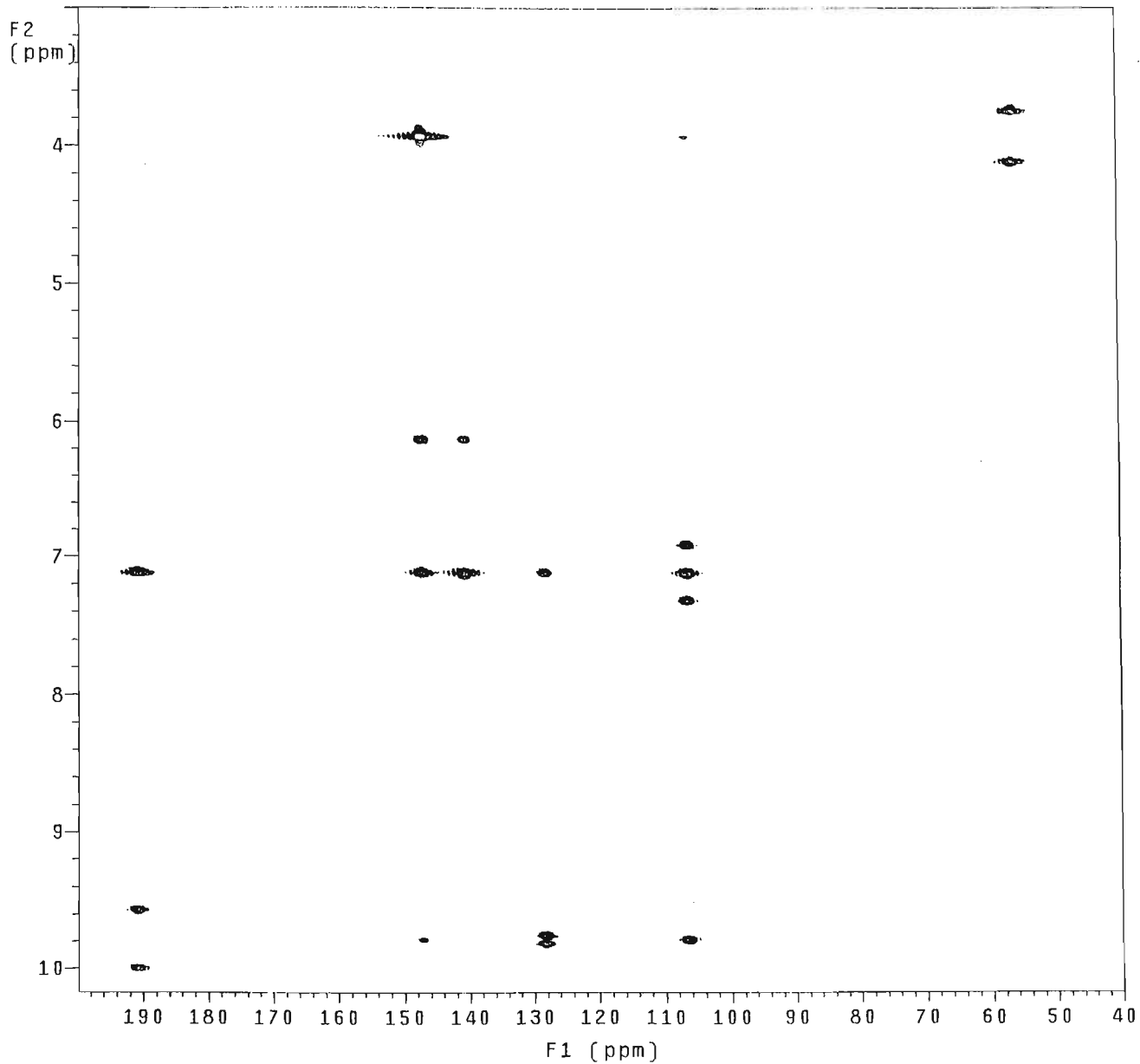
F1 (ppm)

Spectrum 9.6 : HSQC NMR Spectrum of Compound 9, syringaldehyde

Gradient HMBC: expt.
probe=5mmASW
Pulse Sequence: ghmqc_da

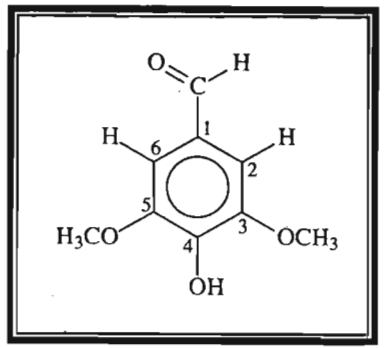


214

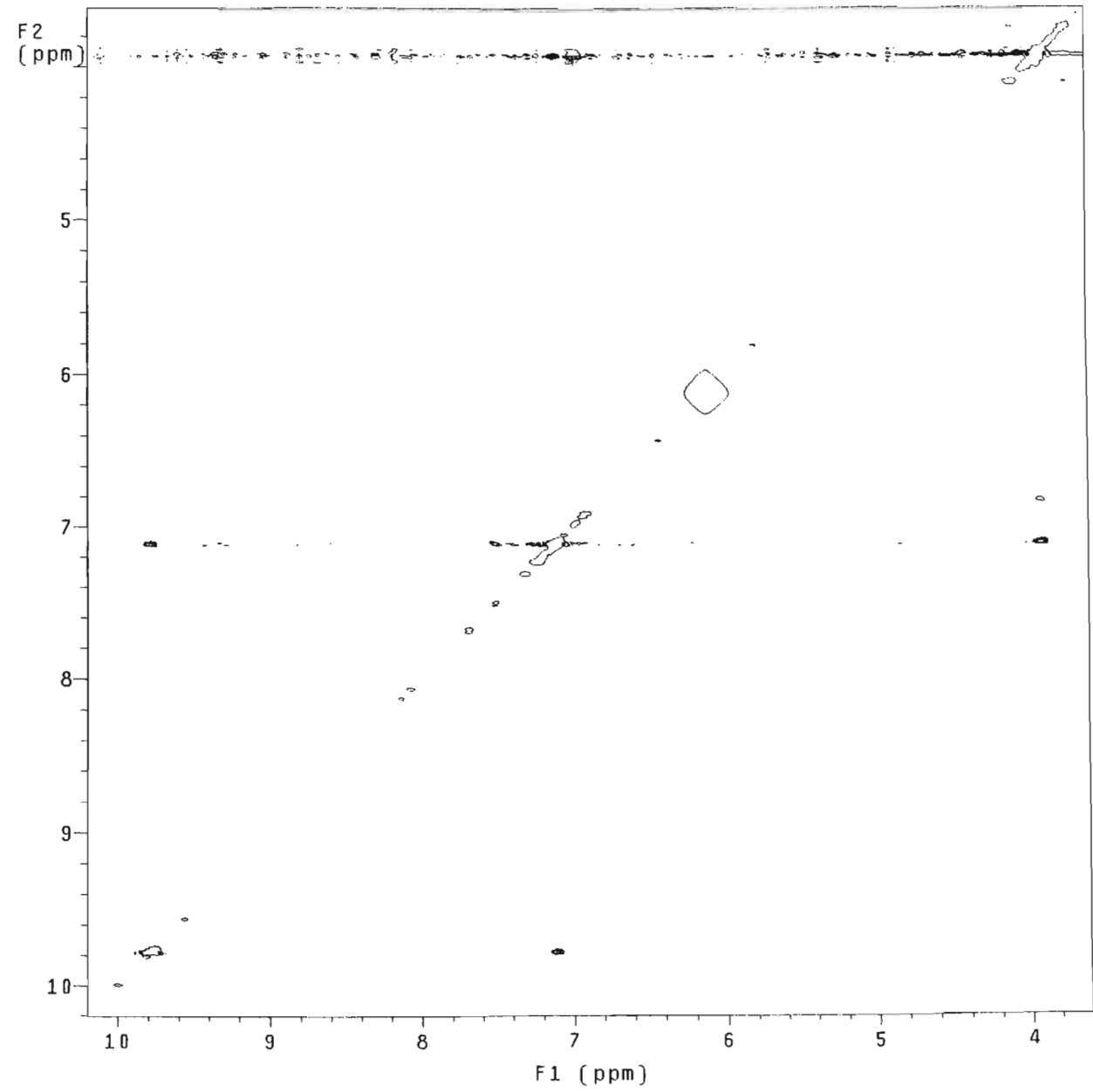


Spectrum 9.7 : HMBC NMR Spectrum of Compound 9, syringaldehyde

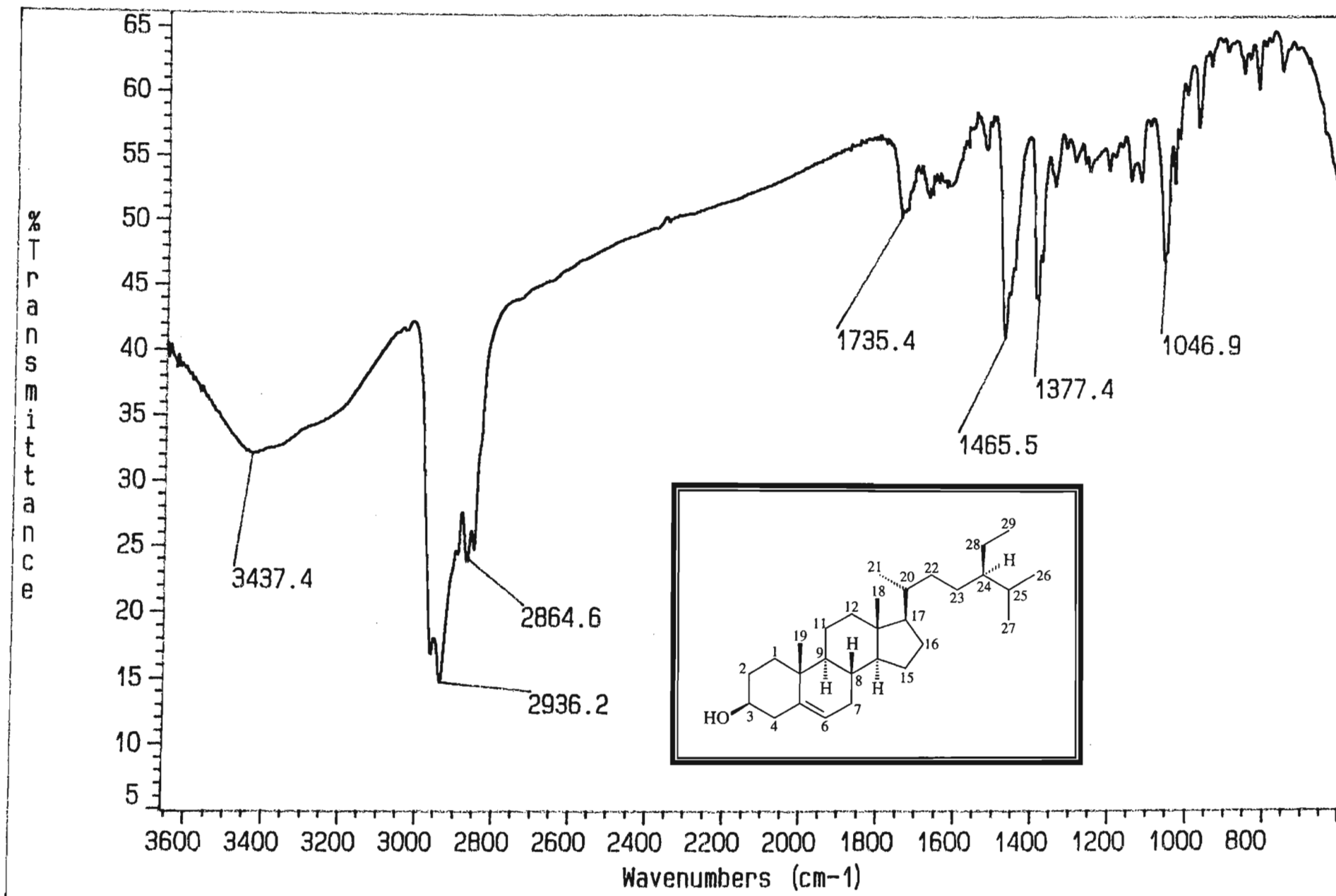
NOESY experiment in CDCl3
NOESY expt.
mix=1sec
probe=5mmASW
Pulse Sequence: noesy_da

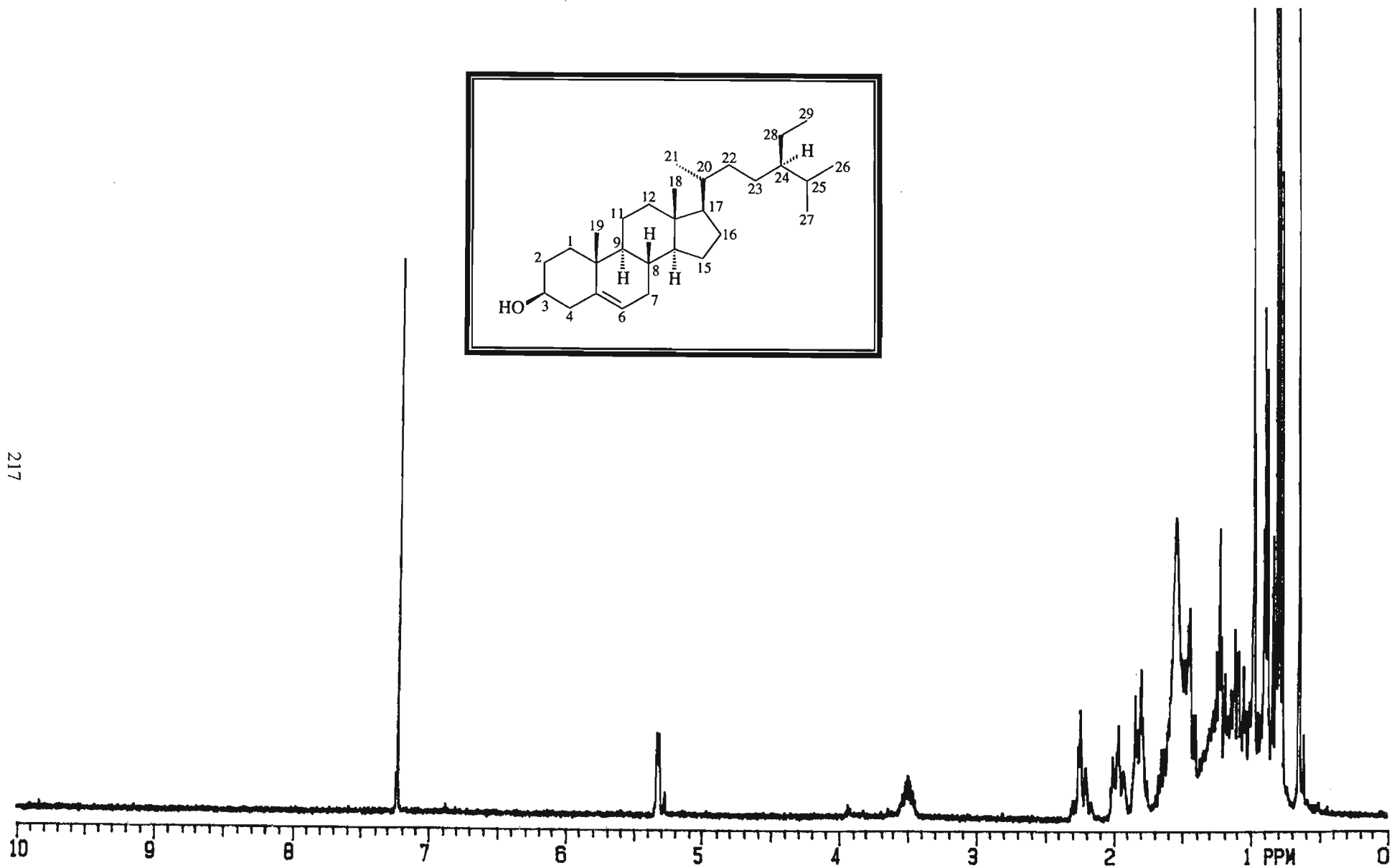


215



Spectrum 9.8 : NOESY NMR Spectrum of Compound 9. svringaldehyde

Spectrum 10.1 : Infrared Spectrum of Compound 10, β -sitosterol

Spectrum 10.2 : ^1H NMR Spectrum of Compound 10, β -sitosterol

APPENDIX B

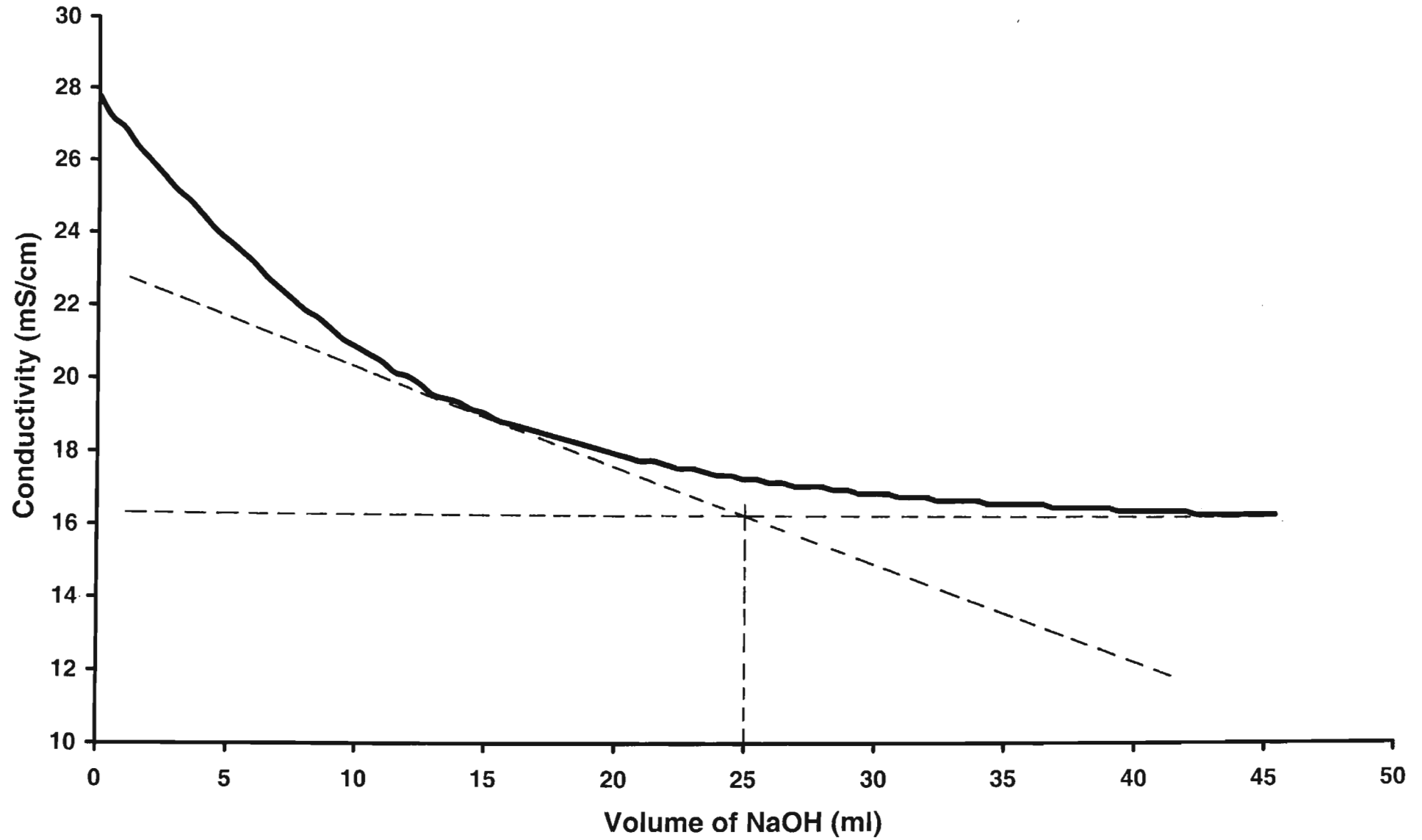
LIST OF DATA IN APPENDIX B

PAGE NO.

| | |
|---|-----|
| Table B1 : Data for the conductometric titration to determine the sulphonic acid content of the calcium spent liquor effluent | 221 |
| Graph B1 : Graph of conductivity (mS/cm) versus volume of NaOH (ml) | 222 |
| Calculations for the sulphonic acid content | 223 |

Table B1: Data for the conductometric titration to determine the sulphonic acid content of the calcium spent liquor effluent

| NaOH (ml) | Conductivity (mS/cm) | NaOH (ml) | Conductivity (mS/cm) |
|-----------|----------------------|-----------|----------------------|
| 0.0 | 27.8 | 22.0 | 17.7 |
| 0.5 | 27.2 | 22.5 | 17.6 |
| 1.0 | 26.9 | 23.0 | 17.6 |
| 1.5 | 26.4 | 23.5 | 17.5 |
| 2.0 | 26.0 | 24.0 | 17.4 |
| 2.5 | 25.6 | 24.5 | 17.4 |
| 3.0 | 25.2 | 25.0 | 17.3 |
| 3.5 | 24.9 | 25.5 | 17.3 |
| 4.0 | 24.5 | 26.0 | 17.2 |
| 4.5 | 24.1 | 26.5 | 17.2 |
| 5.0 | 23.8 | 27.0 | 17.1 |
| 5.5 | 23.5 | 27.5 | 17.1 |
| 6.0 | 23.2 | 28.0 | 17.1 |
| 6.5 | 22.8 | 28.5 | 17.0 |
| 7.0 | 22.5 | 29.0 | 17.0 |
| 7.5 | 22.2 | 29.5 | 16.9 |
| 8.0 | 21.9 | 30.0 | 16.9 |
| 8.5 | 21.7 | 30.5 | 16.9 |
| 9.0 | 21.4 | 31.0 | 16.8 |
| 9.5 | 21.1 | 31.5 | 16.8 |
| 10.0 | 20.9 | 32.0 | 16.8 |
| 10.5 | 20.7 | 32.5 | 16.7 |
| 11.0 | 20.5 | 33.0 | 16.7 |
| 11.5 | 20.2 | 33.5 | 16.7 |
| 12.0 | 20.1 | 34.0 | 16.7 |
| 12.5 | 19.9 | 34.5 | 16.6 |
| 13.0 | 19.6 | 35.0 | 16.6 |
| 13.5 | 19.5 | 35.5 | 16.6 |
| 14.0 | 19.4 | 36.0 | 16.6 |
| 14.5 | 19.2 | 36.5 | 16.6 |
| 15.0 | 19.1 | 37.0 | 16.5 |
| 15.5 | 18.9 | 37.5 | 16.5 |
| 16.0 | 18.8 | 38.0 | 16.5 |
| 16.5 | 18.7 | 38.5 | 16.5 |
| 17.0 | 18.6 | 39.0 | 16.5 |
| 17.5 | 18.5 | 39.5 | 16.4 |
| 18.0 | 18.4 | 40.0 | 16.4 |
| 18.5 | 18.3 | 40.5 | 16.4 |
| 19.0 | 18.2 | 41.0 | 16.4 |
| 19.5 | 18.1 | 41.5 | 16.4 |
| 20.0 | 18.0 | 42.0 | 16.4 |
| 20.5 | 17.9 | 42.5 | 16.3 |
| 21.0 | 17.8 | 43.0 | 16.3 |
| 21.5 | 17.8 | 43.5 | 16.3 |



Graph B1 : Graph of Conductivity (mS/cm) vs Volume of NaOH (ml)

CALCULATIONS FOR THE SULPHONIC ACID CONTENT

Mass of sample used = 50.05 g

Temperature during titration = 22.3°C (start) – 24.4°C

From the graph, the inflection point is approximately 25 ml of NaOH.

$$\begin{aligned}\text{Number of moles of NaOH} &= \text{concentration of NaOH} \times \text{volume of NaOH} \\ &= 0.100 \text{ mol/dm}^3 \times (25 \times 10^{-3}) \text{ dm}^3 \\ &= 0.0025 \text{ moles}\end{aligned}$$

Number of moles of NaOH : number of moles of sulphonic acid groups is 1 : 1, therefore, the number of moles of sulphonic acid groups in the sample = 0.0025 moles.

$$\begin{aligned}\text{Sulphonic acid content} &= 0.0025 \text{ mol} / 50.05 \text{ g} \\ &= 4.995 \times 10^{-5} \text{ mol/g}\end{aligned}$$

A 20 % dodecylamine solution was made by dissolving 20 g of dodecylamine in 100 g of butanol.

Molar mass of dodecylamine = 185.35 g/mol

$$\begin{aligned}\text{The number of moles in 1 g of dodecylamine} &= (1 \text{ g} \times 1 \text{ mol}) / 185.35 \text{ g} \\ &= 5.395 \times 10^{-3} \text{ moles}\end{aligned}$$

There is 4.995×10^{-5} moles of sulphonic acid in 1 g of sample. But equivalent number of moles as dodecylamine is required, that is 5.395×10^{-3} moles.

$$\begin{aligned}\therefore \text{the mass of sample that contains an equivalent number of moles as dodecylamine} &= (5.395 \times 10^{-3} \text{ mol} \times 1 \text{ g}) / 4.995 \times 10^{-5} \text{ mol} \\ &= 108.01 \text{ g}\end{aligned}$$

In order to have an excess of the amine, it was assumed that the sulphonic acid groups in the sample was higher than that shown by the graph, that is, 35 ml instead of 25 ml.

$$\begin{aligned}\text{Thus the sulphonic acid content} &= 0.100 \text{ mol/dm}^3 \times (35 \times 10^{-3}) \text{ dm}^3 / 50.05 \text{ g} \\ &= 6.993 \times 10^{-5} \text{ mol/g}\end{aligned}$$

$$\begin{aligned}\text{From the above calculations, the mass of calcium spent liquor to be used} &= (5.395 \times 10^{-3} \text{ mol} \times 1 \text{ g}) / 6.993 \times 10^{-5} \text{ mol} \\ &= 77.15 \text{ g}\end{aligned}$$

Therefore, 77.15 g of calcium spent liquor was mixed with 100 g of 20 % dodecylamine in butanol solution.